Université d'Ottawa · University of Ottawa

Université d'Ottawa · University of Ottawa

FACULTÉ DE ÉTUDES SUPÉRIEURES ET POSTDOCTORALES

FACULTY OF GRADUATE AND POSTDOCTORAL STUDIES

Jason SZETO

AUTEUR DE LA THÈSE - AUTHOR OF THESIS

Ph.D. (Microbiology)

GRADE - DEGREE

Department of Biochemistry, Microbiology and Immunology

FACULTÉ, ÉCOLE, DÉPARTEMENT - FACULTY, SCHOOL, DEPARTMENT

TITRE DE LA THÈSE - TITLE OF THE THESIS

Splitting Heirs : A Study of the Cell Division Site Determinant MinD from the Coccus *Neisseria gonorrhoeae*

J-A. Dillon

DIRECTEUR DE LA THÈSE - THESIS SUPERVISOR

CO-DIRECTEUR DE LA THÈSE - THESIS CO-SUPERVISOR

EXAMINATEURS DE LA THÈSE - THESIS EXAMINERS

L. Bonen

E. Brown

G. King

M. Kozlowski

J.-M. De Koninck, Ph.D.

LE DOYEN DE LA FACULTÉ DES ÉTUDES SUPÉRIEURES ET POSTDOCTORALES

DEAN OF THE FACULTY OF GRADUATE AND POSTDOCTORAL STUDIES

Splitting heirs: A study of the cell division site determinant MinD from the coccus *Neisseria gonorrhoeae*

A Thesis Presented to

The Faculty of Graduate Studies and Research

of

The University of Ottawa

By

Jason Szeto

In partial fulfillment of requirements

for the degree of Doctor of Philosophy

Department of Biochemistry, Microbiology, and Immunology

Faculty of Medicine

Your file Votre référence
ISBN: 0-494-01770-8
Our file Notre référence
ISBN: 0-494-01770-8

ABSTRACT

Proper cell division site placement in the extensively studied rod *Escherichia coli* (Ec) is determined by the Min proteins. $MinD_{Ec}$ recruits $MinC_{Ec}$ to the membrane to inhibit cell division. $MinE_{Ec}$ restricts $MinC_{Ec}$-$MinD_{Ec}$ activity to cell pole regions by inducing $MinD_{Ec}$ ATPase activity and causing it to dynamically oscillate from end-to-end in *E. coli*. The Dillon laboratory has identified *min* gene homologues in the coccus *Neisseria gonorrhoeae* (Ng) which, unlike *E. coli*, divides along two dimensions. This study investigates the role and identifies functional domains of gonococcal MinD ($MinD_{Ng}$).

MinD is implicated in *Neisseria gonorrhoeae* cell division. Inactivation of $minD_{Ng}$ dramatically disrupted *N. gonorrhoeae* division patterns and reduced cell viability. Overexpression of $MinD_{Ng}$ and $MinC_{Ng}$ together in the gonococcus inhibited cell division, producing grossly enlarged cells. $MinD_{Ng}$ could complement an *E. coli minD* mutant and induced cell division arrest in this organism, provided endogenous *E. coli* MinC was present. GFP-$MinD_{Ng}$ fusions also displayed $MinE_{Ng}$-dependent oscillations within a coiled array in rod-shaped and round mutant *E. coli*.

The self-interaction of $MinD_{Ng}$, as well as $MinD_{Ec}$, was detected using yeast two-hybrid assays, the first report of such interactions. Furthermore, size-exclusion chromatography and analytical ultracentrifugation showed purified $MinD_{Ng}$ to be dimeric. $MinD_{Ng}$ also interacted with both $MinE_{Ng}$ and MinC by yeast two-hybrid experiments.

Structural and sequence alignments implicated a polar region, containing amino acids 92-94, in MinD dimerization. However, mutations to these residues did not eliminate interaction of $MinD_{Ng}$ with itself, MinC, or MinE. Interestingly, this region may have a role in permitting bacterial MinD to respond to MinE stimulation, since mutant GFP-MinD fusions failed to oscillate from pole-to-pole in *E. coli*, despite being distributed uniformly within a coiled array. This was supported by *in vitro* assays, where $MinE_{Ng}$ was unable to stimulate the ATPase activity of mutated $MinD_{Ng}$.

The conserved extreme N-terminus of $MinD_{Ng}$ was also studied and shown to have a role in affecting $MinD_{Ng}$ ATPase activity and localization dynamics. Successive truncation or mutation of this region affected $MinD_{Ng}$ interaction with other Min proteins. Significantly, these alterations resulted in faster GFP-$MinD_{Ng}$ oscillation cycles and increased tendencies to remain in the cytoplasm. Mutant $MinD_{Ng}$ displaying this behaviour possessed hyper-ATPase activities independent of $MinE_{Ng}$.

This is the first study to characterize MinD from a naturally occurring coccus and demonstrates the protein acts as a cell division site determinant in *N. gonorrhoeae* and in *E. coli*. Results from this study were used to generate a model for *N. gonorrhoeae* cell division.

ACKNOWLEDGEMENTS

I would like to give special thanks to my supervisor, Dr. Jo-Anne Dillon, for giving me with an opportunity to work on this project. Throughout my studies she provided me with much appreciated freedom to explore my own ideas...otherwise known as 'fiddling'! I would also like to thank her for always making time for me, as well as her other students, despite her feverishly busy schedule.

I also thank the members of my thesis advisory committee, Dr. John Baenziger, Dr. Sylvia Vidal, and Dr. John Webb, for all their useful comments and advice regarding this project. In addition, I would like to thank Dr. P. de Boer, Case Western Reserve University for providing *E. coli* strains PB103, PB114, and DR105.

I was extremely fortunate to have worked with a great crew in the Dillon laboratory. Rather than just co-workers, they have become a second family to me. Thanks to Sandra for all her helpful advice, both scientific and life-related! Your kindness and generosity will never be forgotten. Franco, you were responsible for 'dragging' me in, and I thank you for guiding me down the pathway to the 'dark side', more commonly known as the 80 year Ph.D. thesis! Thanks to all the 'boys' in the lab (my brothers-in-arms): Nelson, Sudeep, Marc, Pat, and Dan, for making the research environment feel like a play environment. As well, thanks to Susan and Valerie for keeping the remaining sensibility in the boys, including me, from flying out the window. To all the undergraduate 'minions' who allowed me to exercise my supervisory skills (with minimal complaints to the authorities): Sheila, Claude, Mylène, and Yulia; I hope you all learned as much from me as I did from each of you!

In addition, many other former members of the Dillon lab, as well as other graduate students and staff in the department should be acknowledged for making this an unforgettable experience. Hui, André, Tamyo, Neil, the other Jason, Stéphane, Hossein, Cathy, Ann, Lisa, Jennifer, Finola, Isabelle, Madeleine, Placide, Holly, Karine, Tanya, Carol-A

nn, Nicole, Dr. Brown, Dr. Wright, Dr. Dimock, Dr. Filion, and the 'autoclave' ladies, namely Linda and Krystyna.

Gracious thanks go to the Natural Sciences and Engineering Research Council (NSERC), the Canadian Institutes of Health Research (CIHR), and the University of Ottawa for financial support over the course of my graduate studies.

Finally, I would like to thank my 'first' family for their love and support. To my mom, who never quite understood exactly what I was up to, and to my sister, who insisted on telling her co-workers that her little brother "worked with gono..." , I thank you for being there. As well, to all my friends and cousins who drag me out fishing and golfing, so that some level of sanity can be maintained (well, maybe they don't have to 'drag me out'...I'm not made of stone!), I thank you all.

Cheers,

Jason

TABLE OF CONTENTS

LIST OF TABLES

Note: Each chapter contains a list of plasmids that were specific to each study. Chapter 2, Table 2.1 contains all strains that were used in this study, as well as plasmids encoding His-tagged proteins required to raise polyclonal antisera used throughout this study.

Chapter 2

Chapter 3

Chapter 4

Chapter 5

Chapter 6

Chapter 7

Appendix

LIST OF FIGURES

Chapter 1

Chapter 3

Chapter 4

Chapter 7

Chapter 8

Appendix

LIST OF COMMONLY USED ABBREVIATIONS

aa	amino acids
ADP	adenosine 5'-diphosphate
Af	*Archaeoglobus fulgidus*
ATP	adenosine 5'-triphosphate
Bs	*Bacillus subtilis*
CT	C-terminal truncation
dcw	division cell wall cluster
DIC	differential interference contrast
DNA	deoxyribonucleic acid
Ec	*Escherichia coli*
GFP	green fluorescent protein
kb	kilobase
kDa	kilodalton
MTS	membrane targeting sequence
PE	phosphatidylethanolamine
PG	phosphatidylglycerol
Ng	*Neisseria gonorrhoeae*
NT	N-terminal truncation [removal of a designated number of amino acids (or codons) from the N-terminus, and replaced with a start codon]
PCR	polymerase chain reaction
Pf	*Pyrococcus furiosus*
s	seconds
SDS-PAGE	sodium dodecyl sulphate polyacrylamide gel electrophoresis

CHAPTER 1

INTRODUCTION, HYPOTHESIS, AND OBJECTIVES

INTRODUCTION

Cell division, or cytokinesis, is an essential process that permits proper growth, development, and reproduction of all living organisms. In bacteria, this process generally results in the formation of equivalent viable daughter cells that each possess a full genetic complement. In order to achieve this result, proper spatial and temporal coordination must occur between chromosome replication, chromosome segregation, and ultimate septation (Donachie, 1993).

Detailed studies of the mechanisms of bacterial cell division are relatively new in comparison to that of eukaryotic cells. Since the discovery that a crucial bacterial cell division protein, FtsZ, formed a ring-like structure at midcell in *Escherichia coli* (Bi and Lutkenhaus, 1991), molecular studies have substantially advanced the identification of many of the components required for successful bacterial cytokinesis. Almost all of our present knowledge of this event has been acquired from studying rod-shaped bacteria (bacilli), such as *E. coli* and *Bacillus subtilis*, which, under normal conditions, will divide at the middle of the cell to form two equally sized progeny.

Prior to the actual division event, the proper cytokinetic site at midcell must be chosen in order to ensure the production of equivalent daughter cells. It is now recognized that bacteria can possess quite elaborate mechanisms to specify the placement of septation sites. In *E. coli*, the Min system relies on the dynamic localization and interaction of MinC, MinD, and MinE proteins in order to achieve proper midcell division. However, many species of bacteria are not rod-shaped, and exhibit round, spiral, and asymmetric morphologies instead. Whether the strategies used to address cytokinesis in bacilli can be applied to these other organisms is not known. The present study is the first to characterize the cell division site-determinant MinD from a naturally occuring round bacterium, or coccus, using *Neisseria gonorrhoeae* as a model organism.

In the first section of the Introduction, an overview of bacterial cell division and the key components of the cytokinetic and chromosome segregation machinery will be described using the two most commonly studied organisms, *E. coli* and *B. subtilis*, as examples. In particular, the cell

division components of *E. coli* will be reviewed more extensively, as it is a Gram-negative organism like *N. gonorrhoeae*. The second section will discuss how the placement of cell division sites is regulated in rod-shaped bacteria by the Min proteins. The final section of the Introduction will describe the coccus *N. gonorrhoeae* and the current state of knowledge in gonococcal cell division.

1.1. Bacterial cell division

1.1.1. The division cell wall (*dcw*) cluster of genes

Bacterial cell division has been most extensively studied in the Gram-negative rod *E. coli.* In this organism, a cluster of 16 genes directly involved in cell division or cell wall biosynthesis has been identified: *mraZ, mraW, ftsL, ftsI (pbp3), murE, murF, murD, ftsW, murG, murC, ddl, ftsQ, ftsA, ftsZ,* and *envA.* The genes within this division cell wall (*dcw*) cluster are organized as an operon with transcription proceeding in the same direction (Ayala *et al.*, 1994). Several promoters have been identified within the *E. coli dcw* cluster; however, the main promoter seems to be the one located upstream of *mraZ* (Mengin-Lecreulx *et al.*, 1998) which drives co-transcription of all *dcw* genes, ending at the single transcriptional terminator identified downstream of *envA* (Lutkenhaus and Addinall, 1996). The remaining promoters are likely involved in regulating different expression levels of individual genes (Lutkenhaus and Addinall, 1996; Vicente *et al.*, 1998).

Such *dcw* clusters have also been identified in many other bacteria, including *B. subtilis* (Henriques *et al.*, 1992; Daniel *et al.,* 1996), *Haemophilus influenzae* (Fleischmann *et al.*, 1995), *Staphylococcus aureus* (Pucci *et al.*, 1997), *Streptococcus* species (Massidda *et al.*, 1998), and *N. gonorrhoeae* (Dillon laboratory; Francis *et al.*, 2000). While not all bacteria possess the same *dcw* gene homologues, the order of gene arrangement is generally conserved (Vicente *et al.*, 1998).

The following sections review some of the key proteins encoded by the *dcw* cluster which are directly involved in the formation of the bacterial division apparatus. Other proteins, not encoded in the *dcw* cluster, but which are also recruited to the cytokinetic apparatus, are described as well.

1.1.2. The essential cell division protein FtsZ

The actual physical process of bacterial cell division can be divided into several key steps: a) assembly of the cytokinetic apparatus at a specified division site; b) anchoring of the division machinery to the membrane; and c) synthesis of cell wall and cell envelope material to ultimately divide a cell (Errington *et al.*, 2003). Probably the most important bacterial cell division protein is the

highly conserved GTPase FtsZ, which is found in almost all eubacteria (with *Chlamydia trachomatis* being an exception; Stephens *et al.*, 1998), in Archaea, in chloroplasts, and in mitochondria (Addinall and Holland, 2002).

Green fluorescent protein (GFP) fusions to FtsZ, as well as immunostaining with FtsZ antibodies, have shown that the protein localizes as a distinct ring-like structure (Z-ring) associated with the normal midcell division plane in *E. coli* (Figure 1.1A) (Ma *et al.*, 1996; Addinall and Holland, 2002). FtsZ proteins also exhibit cross-species functionality, and it has observed that expression of a GFP fusion to *N. gonorrhoeae* FtsZ localized to the *E. coli* midcell as well (Figure 1.1B) (Salimnia *et al.*, 2000). Z-ring cytoskeleton formation appears to originate at a single nucleation point and progresses bidirectionally until a closed ring is formed (Sun and Margolin, 1998). This process is completed within one minute of initiation in *E. coli* cells (Addinall *et al.*, 1997). As cell division proceeds, the Z-ring contracts while remaining at the leading edge of the developing septum between two daughter cells (Bi and Lutkenhaus, 1991). This suggests that the Z-ring is, or is part of, a contractile motor that helps drive septation (Lutkenhaus and Addinall, 1997).

While reduced FtsZ levels result in fewer division events, two distinct *E. coli* phenotypes are observed upon its overexpression. A two- to seven-fold increase in FtsZ produces a 'minicell' phenotype in *E. coli* characterized by septation at the cell ends (cell poles), resulting in round minicells, in addition to septation at the normal midcell region. At higher expression levels, a block in cell division occurs, giving rise to long filamentous cells (Ward and Lutkenhaus, 1985). It is estimated that there are approximately 15,000 FtsZ molecules in an *E. coli* cell (Lu *et al.*, 1998), sufficient to form a cytoskeleton that encircles the cell midpoint several times over (Bramhill, 1997). However, recent fluorescence recovery after photobleaching (FRAP) studies in *E. coli* have indicated that only about 30 % of total FtsZ is found in the Z-ring at any particular time, with the remaining protein engaged in rapid dynamic exchange between the ring and the cytoplasm (Stricker *et al.*, 2002).

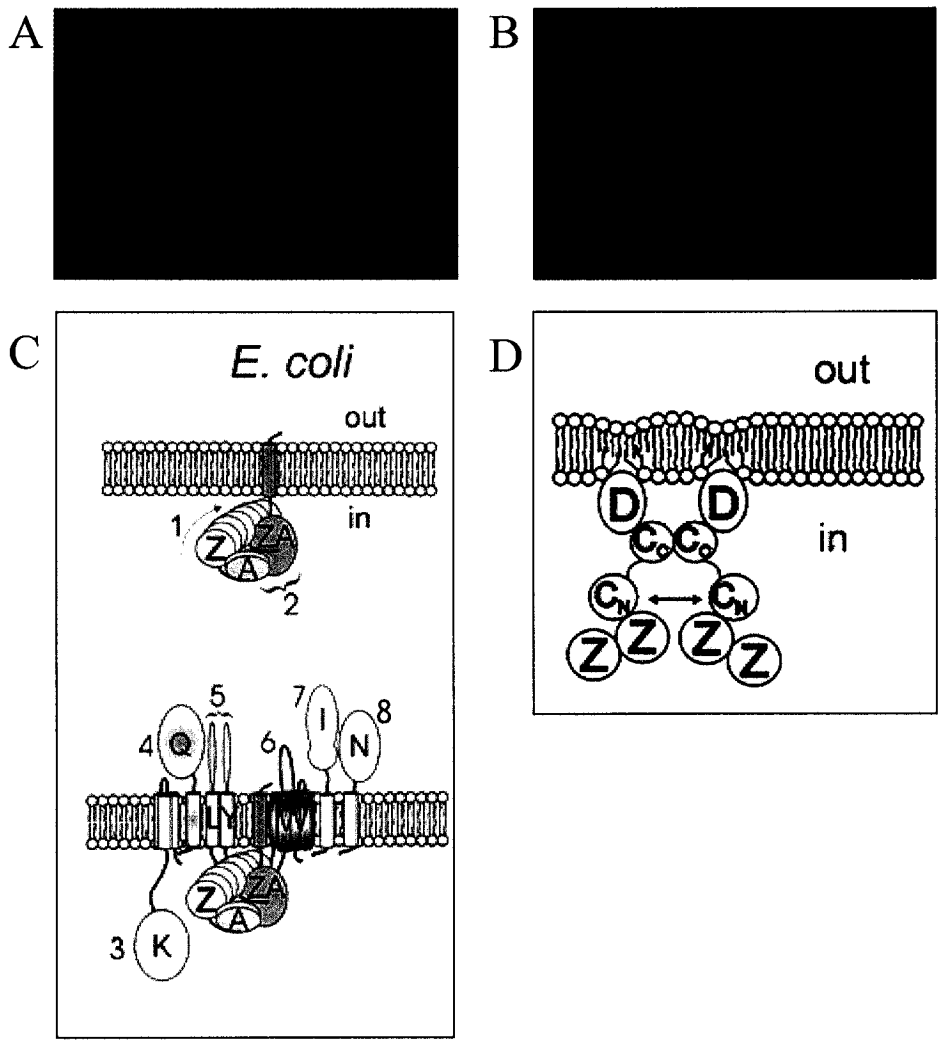

Figure 1.1. Cell division in the rod *E. coli*. (A) *E. coli* stained with anti-FtsZ antisera show FtsZ localization at the middle of each cell [reprinted with permission from Elsevier (Addinall and Holland, 2002)]. (B) Expression of GFP-fusion to *N. gonorrhoeae* FtsZ protein in *E. coli* also results in midcell localization of fluorescent fusion protein (Dillon laboratory). (C) Assembly of cytokinetic proteins at the *E. coli* cell division site. Numbers indicate the general order to which proteins are recruited to the division site. FtsZ (Z) initiates polymerization at the division site and may be stabilized by FtsA (A) and ZipA (ZA). ZipA may act as a membrane anchor for FtsZ. Proteins subsequently recruited to the septal FtsZ-ring include FtsK (K), FtsQ (Q), FtsL (L) and YgbQ (Y), FtsW (W), FtsI (I), and FtsN (N) [reprinted with permission from the American Society for Microbiology (Errington *et al.*, 2003)]. (D) MinD is proposed to direct MinC to its target, FtsZ, at impending septation sites along the inner cell membrane. The N-terminus of *E. coli* MinC inhibits FtsZ polymerization, while the C-terminus is involved in self-association and interaction with MinD (Hu and Lutkenhaus, 2000; Szeto *et al.*, 2001b) (Figure obtained from Errington *et al.*, 2003).

Crystallographic studies of FtsZ from the Archaea *Methanococcus jannaschii* have shown that it bears a remarkable structural resemblance to eukaryotic tubulin, despite overall sequence dissimilarities (Löwe and Amos, 1998). Like tubulin, FtsZ is able to polymerize in a GTP-dependent manner. *In vitro* studies have shown that FtsZ-GTP is able to assemble into several structures, including protofilaments and sheets (Löwe and Amos, 1999), while the hydrolysis of GTP or addition of GDP promotes FtsZ disassembly and/or formation of curved protofilaments and tubes (Mukherjee and Lutkenhaus, 1998; Lu *et al.*, 2000).

The actual arrangement of FtsZ subunits within the Z-ring and the mechanism of its constriction *in vivo* are currently not known. In one model, the Z-ring is proposed to be formed from short, overlapping filaments of FtsZ that slide along each other by means of an unidentified motor protein, leading to Z-ring constriction (Bramhill, 1997). Another model suggests that Z-ring constriction occurs by depolymerization of FtsZ subunits from one, or both, end(s) of an FtsZ polymer (Bramhill, 1997). A third model proposes that bending or curving of FtsZ filaments due to GTP hydrolysis may result in Z-ring constriction (Lu *et al.*, 2000). FtsZ does not possess any defined membrane spanning sequence (Errington *et al.* 2003), hence each model requires that the FtsZ cytoskeleton be anchored to the membrane by another partner in order to exert its constrictive effects (Bramhill, 1997); however, such an anchor has yet to clearly identified.

Aside from its proposed 'contractile' role during septation, the FtsZ ring is believed to serve as a scaffold to which other cell division proteins are recruited. Thus far, all other cell division proteins seem to require the presence of the Z-ring for their successful recruitment to the division site (Errington *et al.*, 2003). In addition, there is a specific sequence in which downstream cell division proteins appear. Each protein depends on the previous protein in order to be properly localized to the *E. coli* cytokinetic ring in the following order: FtsA and ZipA, FtsK, FtsQ, FtsL and YgbQ, FtsW, FtsI, and FtsN (Errington *et al.*, 2003) (Figure 1.1 C).

1.1.3. FtsA, ZipA and Z-ring stabilization

The next proteins to associate with the cytokinetic Z-ring are FtsA and ZipA. Z-rings are capable of forming in the presence of either FtsA or ZipA, but not when both proteins are absent (Pichoff and Lutkenhaus, 2002). In turn, both proteins require FtsZ for their localization to the division plane, however they do so independently of each other (Hale and de Boer, 1997; Hale and de Boer, 1999; Pichoff and Lutkenhaus, 2002).

FtsA is an ATP-binding protein that belongs to the actin/hsp70/sugar kinase superfamily (Sánchez *et al.*, 1994, Feucht *et al.*, 2001) and the crystal structure of FtsA from the thermophilic bacterium *Thermotoga maritima* shows that it is structurally homologous to actin (van den Ent and Löwe, 2000). FtsA co-localizes as a ring with FtsZ at division sites (Ma *et al.*, 1996). In *E. coli*, overexpression of FtsA will arrest cell division (Wang and Gayda, 1990); however, increasing FtsZ levels can counteract this effect (Dai and Lutkenhaus, 1992). This suggests that the ratio of FtsZ to FtsA (normally ~100:1) is required for proper cell division to occur (Dai and Lutkenhaus, 1992). No defined role for FtsA in cytokinesis has been established; however, it may play a role in cross-linking and stabilizing Z-ring polymers and/or recruiting other cell division proteins (Errington *et al.*, 2003).

ZipA (Z-interacting protein A) is an inner membrane protein containing an N-terminal membrane domain, and a C-terminal cytoplasmic domain (Ohashi *et al.*, 2002). Currently, ZipA is the leading candidate for the FtsZ membrane anchor (Erickson, 2001). ZipA is recruited to the division site by FtsZ (Hale *et al.*, 1999; Liu *et al.*, 1999), with both proteins interacting at their C-termini (Hale *et al.*, 1997; Hale *et al.*, 2000; Haney *et al.*, 2001). *In vitro* experiments have shown that ZipA stabilizes (RayChaudhuri, 1999) and induces bundling of FtsZ polymers (Hale *et al.*, 2000).

FtsZ polymerization is also prevented by certain proteins. The general cell division inhibitor MinC, part of the Min system in *E. coli* (de Boer *et al.*, 1989), has been shown to interact with and dissassemble FtsZ polymers *in vitro* (Hu and Lutkenhaus, 2000). Furthermore, overexpression of MinC in *E. coli* will lead to a filamentous phenotype, indicative of cell division arrest (de Boer *et al.*, 1992). Hence, it is proposed that MinC can regulate cell division events at the membrane *in vivo* by

inhibiting FtsZ-ring formation, and thus subsequent recruitment of other downstream cytokinetic proteins (Bi and Lutkenhaus, 1993; Hu *et al.*, 1999) (Figure 1.1 D). More detailed description of MinC and the Min system can be found in Section 1.3.2. of the Introduction.

There are several other proteins, not necessarily found in *E. coli*, which may also contribute to Z-ring stability. In the Gram-positive rod *B. subtilis*, two proteins, EzrA and ZapA, also seem to be involved in maintaining Z-ring integrity. The recently described ZapA (Z-ring associated protein A) is distributed more widely than ZipA, and orthologs are found in *B. subtilis* and in *E. coli* (Gueiros-Filho and Losick, 2002). Like ZipA, ZapA localizes to the *B. subtilis* Z-ring at an early stage in cell division and this localization is dependent upon FtsZ. *In vitro*, ZapA can also bind FtsZ and stimulate FtsZ-GTP protofilament bundling into branched networks; therefore, ZapA likely plays a role in Z-ring stability (Gueiros-Filho and Losick, 2002).

In *B. subtilis*, deletion of *erzA* lowers the critical concentration of FtsZ needed to form Z-rings and results in the formation of multiple Z-rings distributed along the length of the cylindrical cell (Levin *et al.*, 1999). These results suggest that *ezrA* may have the opposite function of ZipA from *E. coli*, and acts to promote Z-ring depolymerization. Hence, bacterial cell division proteins such as FtsA, ZipA, ZapA, and EzrA, appear to be involved in FtsZ polymer stabilization/destabilization. The actions of these proteins may also account for the dynamic remodeling of the Z-ring observed with the continuous exchange of FtsZ subunits between Z-polymers and the cytoplasmic pool (Gueiros-Filho and Losick, 2002; Stricker *et al.*, 2002; Margolin, 2003).

1.1.4. FtsN, FtsL, YgbQ, and FtsQ

Comparatively little is known about FtsN, FtsL, YgbQ, and FtsQ transmembrane proteins relative to the other members of the cytokinetic ring. The *ftsQ* gene is commonly found directly upstream of *ftsA* and *ftsZ* in the *dcw* gene cluster in many bacteria (Errington *et al.*, 2003). FtsQ is a low copy number protein in *E. coli* (~20 copies/cell; Carson *et al.*, 1991) and contains a short N-terminal cytoplasmic domain, a transmembrane region, and a periplasmic domain; however, only the

periplasmic domain is required for localizing to the septum (Chen *et al*, 1999). Although essential for cell division, the role of FtsQ in bacterial cytokinesis is not known (Chen *et al*, 1999; Errington *et al.*, 2003).

FtsL is present in low abundance in *E. coli* (20-40 copies/cell) and contains a coiled-coil motif in its periplasmic domain implicated in homodimerization and localization to the division site (Guzman *et al*, 1992; Ghigo *et al.*, 2000). Since FtsL has no apparent catalytic domains, it is proposed to have a structural role in cell division (Ghigo *et al.*, 2000). Another protein, YgbQ, has recently been shown to localize to the division site with FtsL. Both proteins required one another for this localization, and it is proposed that they interact through a coiled-coil structure (Buddelmeijer *et al.*, 2002).

FtsN carries a short N-terminal cytoplasmic domain, a single transmembrane region, and a large periplasmic domain that is responsible for targetting to the septal ring (Addinall *et al.*, 1997). FtsN has some similarity to cell wall amidases and may play a role in degrading cell wall material required during the constriction process of cytokinesis (Errington *et al.*, 2003).

1.1.5. Cell wall synthesis at the division site: FtsI and FtsW

In order to physically separate two future daughter cells, new peptidoglycan (murein) must be incorporated at the division site. The gene *ftsI* encodes penicillin-binding protein 3 (PBP-3 or FtsI), a transpeptidase that catalyzes the addition of new cell wall material, in the form of glycan strands, to septation sites (Bramhill, 1997). A related protein, PBP-2, is involved in the addition of peptidoglycan strands to the lateral cell wall, and hence for cell elongation and growth (Errington *et al.*, 2003).

FtsI contains an N-terminal transmembrane region and a larger C-terminal domain containing the catalytic motifs common to other PBPs (Goffin and Ghuysen, 1998). This protein is proposed to form part of a murein-synthesizing complex that adds glycan strands in such a way that a constriction forms at the site of division. A "three-for-one" model for glycan strand insertion has been proposed to

account for the sharp inward growth of murein observed during cell division (Höltje, 1998). In general, the model suggests that three crosslinked strands of new glycan are brought to an existing murein 'docking' strand at a designated cell division site. The FtsI-containing complex incorporates these crosslinked strands underneath the single docking strand so that the latter is 'straddled' by the new strands. The murein-synthesizing complex also bears lytic transglycosylase and endopeptidase activity, and can degrade the old docking strand (Bramhill, 1997). In essence, the three new glycan strands (murein triplets) underneath the docking strand will form the basis for murein constriction. The addition of more murein triplets to the apex of the constriction, coupled with the inward pull of the membrane, driven by the anchored Z-ring, is proposed to result in cell constriction and the formation of two cells (Höltje, 1998).

FtsW contains 10 membrane spanning regions (Lara and Ayala, 2002), and its presence is always correlated with that of FtsI, suggesting a link in their functions (Errington *et al.*, 2003). Interestingly, FtsW has high homology to RodA, a shape-determinant in *E. coli* (Bramhill, 1997). RodA is one of several proteins implicated in maintaining the rod-shape typically found in *E. coli*, and abrogation of this gene results in round *E. coli* cells (Begg *et al.*, 1986). Studies investigating murein synthesis in temperature sensitive *rodA E. coli* cells have shown that murein synthesis directed towards cell elongation is affected upon *rodA* impairment (de Pedro *et al.*, 2001). Due to their similarities, it has been proposed that FtsW and RodA act as translocation proteins that shuttle murein precursors to their corresponding PBPs, namely PBP-3 (cell division) and PBP-2 (cell elongation), respectively (Höltje, 1998).

1.1.6. FtsK

FtsK is a multi-role protein and has two distinct functions mediated by its N-terminal membrane domain and its C-terminal cytoplasmic domain. The first domain is involved in cell division, as cells encoding only the N-terminal domain of FtsK are still able to divide (Liu *et al.*, 1998). In addition, while a deletion of *ftsK* inhibits *E. coli* cell division, a corresponding

overexpression of the FtsK N-terminus can reverse cell division arrest (Draper *et al.*, 1998). The formation of smooth filaments (without any signs of constriction) in *ftsK* mutants (Wang and Lutkenhaus, 1998) and the dependence on FtsK for FtsQ, FtsL, and FtsI localization (Chen and Beckwith, 2001) supports the notion that the protein is required at an early stage in cytokinesis.

FtsK is a member of the SpoIIIE family of DNA translocases and its C-terminal domain contains an ATP-binding site that functions in chromosome partitioning, or the movement of replicated bacterial chromosomes through the closing septum (see below for an overview of chromosome segregation). The protein has been shown to use an ATP-dependent mechanism to actively push DNA through the septum (Aussel *et al.*, 2002). *E. coli* lacking the C-terminus of FtsK exhibit defective chromosome segregation (Liu *et al.*, 1998). Hence, FtsK also plays an essential role late in the cytokinetic process, and provides an intimate link between cell division and chromosome segregation.

Cell division must ensure that progeny cells each receive complete chromosomal material; however, chromosome replication can often lead to the formation of circular dimers of daughter chromosomes formed by odd numbers of recombination events (Draper and Gober, 2002). FtsK functions to resolve such dimers prior to their segregation into daughter cells. Resolution is achieved by a recombination event mediated through a 28 base pair sequence, termed *dif*, that is found in each daughter chromosome near the replication terminus (Kuempel *et al.*, 1991). The C-terminus of FtsK is believed to activate the XerC and XerD DNA resolvases that will catalyze dimer resolution at *dif* sites and produce separate, uncatenated chromosomes (Aussel *et al.*, 2002). Since FtsK is localized to the septum, the resolution of chromosome dimers is ensured prior to full septum closure (Draper and Gober, 2002).

1.2. Bacterial chromosome segregation

In most cases, the bacterial chromosome is circular and DNA replication is initiated at a single origin of replication (*oriC*) and proceeds bidirectionally towards a terminus located approximately opposite of *oriC* (Draper and Gober, 2002). Successful DNA replication, followed by the complete distribution of chromosomes to each daughter cell during cytokinesis, is paramount to the production of viable cells. One model of chromosome segregation proposes that newly replicated chromosomes are attached to the inner membrane at midcell and that cell elongation occurring prior to cell division would provide the motive force needed to equally distribute chromosomal material to each offspring cell (Jacob *et al.*, 1963). A more contemporary 'transertion-mediated' segration model has been proposed, whereby newly replicated DNA is linked to the membrane by virtue of coupled transcription, translation, and translocation of membrane proteins, creating bidirectionality in chromosome segregation in the predivisional cell (Woldringh, 2002).

1.2.1. Intracellular migration of the chromosomal origin of replication

Recent advances in intracellular localization and biochemical techniques have challenged the above proposals. By introducing *lac* operator sites near *oriC*, the position of the replication origin could be tracked in *E. coli* and in *B. subtilis* cells that encoded GFP-fusions to the *lac* repressor (LacI-GFP) (Gordon *et al.*, 1997; Webb *et al.*, 1997; Webb *et al.*, 1998). These and other studies have shown that *oriC*s exhibit dynamic movement throughout the cell cycle.

In cells undergoing rapid growth and DNA replication, two copies of GFP-labeled *oriC* were observed positioned at opposite cell poles. These labeled *oriC*s migrated towards the cell center prior to re-initiating DNA replication. After replication, four origins were observed in a single cell, with one of the origins from each chromosome moving to the cell pole while the other remained near midcell. Hence, two chromosomal DNA masses (nucleoids) were situated at the one- and three-quarter positions of the predivisional cell (Hiraga *et al.*, 1990). Cell division and septum formation

then proceeds, resulting in daughter cells that each have *oriC* regions at their cell poles (Webb *et al.*, 1998; Draper and Gober; 2002).

Since the *oriC* regions could move irrespective of cell elongation, it was unlikely that simple lateral cell envelope growth was responsible for their migration (Sharpe and Errington, 1998; Webb *et al.*, 1998; Draper and Gober; 2002). Furthermore, since the measured rate of *oriC* movement in *B. subtilis* (0.17 mm/min) was greater than that of cell elongation (0.011-0.025 mm/min), it argued against the chromosome segregation model based on simple nucleoid/membrane association (Webb *et al.*, 1998).

1.2.2. The extrusion-capture model of chromosome partitioning

What drives the migration of bulk chromosomal material towards cell pole regions in the predivisional cell? Recently, it was shown that the DNA replication complex, or replisome, is located at a relatively fixed site at midcell in *B. subtilis* (Lemon and Grossman, 1998). Experiments using [^{3}H] thymidine to localize newly duplicated DNA in *E. coli* have also indicated that DNA replication occurs at a midcell site (Koppes *et al*, 1999). Thus, it is proposed that a spooling effect caused by the movement of replicating DNA through a *stationary* replisome may provide some of the necessary motive force needed for chromosome segregation (Lemon and Grossman, 1998; Lemon and Grossman, 2000; Lemon and Grossman, 2001).

The 'push' imparted on nascent chromosomes by the replisome may also be aided by corresponding 'pulls' caused by DNA condensation proteins, such as MukB (from *E. coli*) or Smc (structural maintenance of chromosomes) in *B. subtilis* (Draper and Gober, 2002). Both proteins belong to a large SMC family of proteins involved in DNA repair, condensation, and segregation (Draper and Gober, 2002). MukB is an ATP-binding protein that exhibits ATPase activity in the presence of DNA (Niki *et al.*, 1991; Niki *et al.*, 1992). Both MukB and Smc are large proteins (176 kDa and 135 kDa, respectively) and electron microscopy has shown each to exist in homodimeric

arrangements characterized by two globular domains linked by a flexible coiled-coil domain that allows significant changes in conformation (Niki *et al.*, 1992; Melby *et al.*, 1998).

Mutations in *E. coli mukB* produced a significant proportion of cells bearing improperly segregated chromosomes, including DNA masses of varying size and location (Niki *et al.*, 1991). Null mutations in *B. subtilis* Smc also affected chromosome segregation (Britton *et al.*, 1998; Moriya *et al.*, 1998).

While MukB localizes to the nucleoid, Smc localizes to both nucleoid and adjacent polar regions (Britton *et al.*, 1998; Graumann *et al.*, 1998). It is proposed that these DNA condensation proteins may disassemble from DNA prior to its replication and reassemble onto the nascent chromosomes to provide the additional tension required to direct chromosome movement away from midcell (Lemon and Grossman, 2001).

As replication is completed, two interlinked chromosomal DNA circles result, which are decatenated by topoisomerase IV. Any chromosome dimers that may have also formed, due to odd numbers of recombination events, are resolved by FtsK (already recruited to the constricting midcell division ring) and the XerCD recombinases (Lemon and Grossman, 2001; Donachie 2001). Remaining DNA is finally translocated by FtsK to their respective daughter cell compartments before septum closure (Aussel *et al.*, 2002). Hence, the combined motive force provided by a stationary replisome and DNA organizing molecules have led to this current 'extrusion-capture' model of chromosome partitioning (Lemon and Grossman, 2001; Draper and Gober, 2002). However, it is still possible that co-transcription/translation of proteins coupled to the membrane may also play some role in active chrosomome partitioning (Lemon and Grossman, 2001).

1.2.3. Par proteins and their involvement in chromosome partitioning

Eukaryotic sister chromosomes are separated by the actions of a mitotic spindle apparatus originating from each end of the dividing cell. The spindle appartus is attached to chromosomal centromere regions through protein structures termed kinetochores (Nanninga, 2001). The possibility

that bacteria possess a functionally equivalent apparatus has been raised with several nucleoid associated proteins, including members of the Par protein family, which may help direct the movement of nascent chromosomal origins towards the cell poles (Draper and Gober, 2002).

Par proteins were first studied in the *E. coli* low-copy number plasmids P1 and F, where they are involved in efficient plasmid partitioning between daughter cells (Gerdes *et al.*, 2000). Plasmid P1 encodes ParA and ParB proteins. ParB binds co-operatively to a *parS* DNA site on the plasmid, and also interacts with the ATPase ParA (Gerdes *et al.*, 2000). ParA itself is membrane associated and may tether the ParB-*parS* complex to specific cellular locations (Lin and Mallavia, 1998).

Many bacteria possess chromosomal homologues of these plasmid-borne *par* genes, including *B. subtilis* [Soj, ParA homologue; SpoOJ, ParB homologue] and *Caulobacter crescentus* (Draper and Gober, 2002); however *E. coli* lacks any such genes (Lemon and Grossman, 2001). Like plasmid P1, the *B. subtilis* chromosome also possesses several *parS* sites near its *oriC* and localization experiments have revealed that SpoOJ binds to these sites and localizes to the cell poles (Lewis and Errington, 1997). In contrast, Soj undergoes dynamic SpoOJ-dependent movement that has been described as 'internucleoid jumping', involving its apparent assembly into a single, large nucleoid-associated patch, followed by dynamic movement of the Soj patch onto an adjacent nucleoid. Such movement occurred on a timescale of minutes (Marston and Errington, 1999a). Others have observed than Soj movement is more of a pole-to-pole pattern, rather than nucleoid-to-nucleoid (Quisel *et al.*, 1999). The intracellular jumping of Soj, and the binding of SpoOJ to *parS* regions near *oriC*, has led to the proposal that Par systems may act to direct *oriC* to cell pole regions during chromosome partitioning, possibly comparable to the eukaryotic centromeric system (Gordon and Wright, 2000; Bignell and Thomas, 2001; Draper and Gober, 2002).

Another possible candidate for restricting nascent chromosomes to cell polar regions is the recently described *B. subtilis* RacA protein (Ben-Yehuda *et al.*, 2003). Analysis of RacA revealed a putative helix-turn-helix DNA binding motif and RacA-GFP fusions were colocalized with the nucleoid, particularly around the origin region. However, the protein was also strongly associated

with the cell poles, prompting the proposal that RacA may form a chromosomal anchor (Ben-Yehuda *et al.*, 2003). RacA may be tethered to the cell poles by DivIVA, another protein normally found *B. subtilis* cell poles. Hence, RacA may be a kinetochore-like protein that is attached to both cell poles and that binds to a centromere-like region in newly replicated *B.subtilis* chromosomes which anchors them to the cell poles (Ben-Yehuda *et al.*, 2003).

1.3. Spatial regulation of the cell division site

In general, rod-shaped cells divide at midcell to produce viable bacterial cells that each contain a full genetic complement. However, before cell division is even initiated, the correct site for cell division must be determined. Currently, there are two proposed mechanisms of toporegulating bacterial division sites: nucleoid occlusion and the Min protein system. Little is known about the molecular details responsible of the first mechanism in comparison to the second; hence, a brief discussion of nucleoid occlusion will be followed by a more detailed review of Min proteins.

1.3.1. Nucleoid occlusion model

The nucleoid occlusion model states that cell division generally occurs in regions devoid of nucleoid masses, such as the space between newly separated chromosomes (Mulder *et al.*, 1989; Woldringh *et al.*, 1990) (Figure 1.2). In this way, the predivisional cell ensures that its progeny will each receive a complete chromosome. This model was developed through the observation that visible cytokinesis in *E. coli* does not occur over regions occupied by a nucleoid mass (Woldringh *et al.*, 1991). This was further supported by FtsZ localization studies showing that Z-rings usually do not form over nucleoids (Yu and Margolin, 1999; Sun and Margolin, 2001). In addition, mutant cells with non-replicating nucleoids still display preferential Z-ring formation over nucleoid free regions (Gullbrand and Nordstrom, 2000; Sun and Margolin, 2001).

The compactness of the nucleoid itself may play a role in preventing Z-ring assembly. In wild-type *E. coli*, Z-ring formation coincides with the termination of DNA replication, a time when most of the chromosomal mass has been cleared away from midcell (Den Blaauwen *et al.*, 1999). In *E. coli* that cannot resolve chromosome dimers (due to mutations in *dif*, *xerC*, and *xerD*), cell division can occur on top of unresolved dimer chromosomes, resulting in a guillotining effect on the DNA. In this case, it is proposed that the remaining unresolved DNA at the midcell is ineffective at imparting nucleoid occlusion, thus permitting complete cell division (Hendricks *et al.*, 2000). Moreover, inactivation of the DNA condensation protein MukB in *E. coli* produces decondensed chromosomes

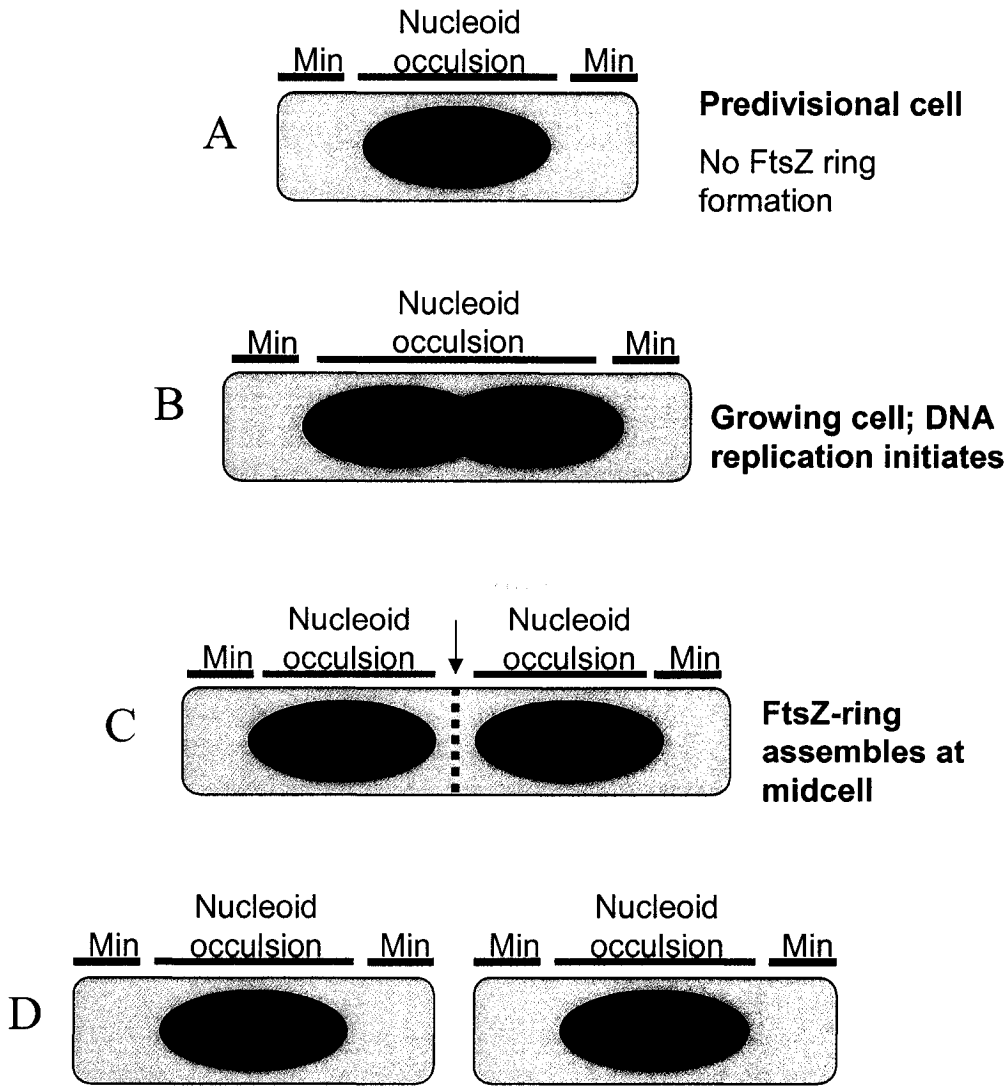

Figure 1.2. Nucleoid occlusion and the Min protein system act to toporegulate cell division in *E. coli*. (A-B) In the predivisional cell, the nucleoid mass (black oval) prevents FtsZ ring formation throughout the central region of the cell (red bar). The Min system acts to prevent FtsZ ring formation at cell pole regions (black bars). (C) As DNA replication terminates, a nucleoid-free zone between each daughter chromosome is formed. The lack of nucleoid occlusion in this central region allows FtsZ polymerization to proceed (dotted line). The Min system continues to inhibit cell division at cell pole regions. (D) Cell division is completed and nucleoid occlusion and the Min system are re-established in each daughter cell.

over which FtsZ ring assembly can occur, further suggesting that the compactness of the nucleoid plays a role in regulating Z-ring formation (Yu *et al.*, 2001).

Although a defined mechanism of nucleoid occlusion has not been elucidated, one recent proposal attempts to link the transertion-mediated model of chromosome segregation with nucleoid occlusion (Woldringh, 2002). It is proposed that the coupled transcription, translation, and translocation of membrane proteins from nascent DNA creates a crowded condition around the nucleoid that prevents FtsZ assembly. This inhibition may be suppressed towards the end of DNA replication by virtue of a decreased number of expressed genes in the chromosomal terminus region. Since the terminus is localized to the midcell at a late stage in the DNA replication cycle, Z-ring assembly at this 'spatially-free' site can proceed (Woldringh, 2002; Zaritsky and Woldringh, 2003). Interestingly, in outgrowing *B. subtilis* spores grown under thymineless conditions that prevented DNA replication, it was found that Z-ring assembly could still occur over the still compact nucleoid mass, which argues against the idea of nucleoid occlusion, at least in this gram-positive rod (Regamey *et al.*, 2000)

1.3.2. The Min system of cell division site determination

1.3.3. The *min* genes

Although the mechanism of nucleoid occlusion remains unclear, cell division toporegulation by Min proteins in bacilli is significantly better elucidated. The *min* genes were first identified by characterizing *E. coli* cells that displayed a 'minicell' phenotype due to mutations at a locus termed the *minB* (*min*icell) operon, containing *minC*, *minD*, and *minE* genes (Davie *et al.*, 1984; de Boer *et al.*, 1988; de Boer *et al.*, 1989). Such mutants displayed cell division at their cell poles, in addition to cytokinesis at the normal midcell site, resulting in a population consisting of round chromosomeless minicells, normal sized cells, and filamentous cells of varying lengths (Adler *et al.*, 1967; de Boer *et al.*, 1988; de Boer *et al.*, 1989). Although minicells are not viable, normal midcell division occurs in sufficient numbers of *min* mutant cells to maintain the population (Margolin, 2001a).

Cytokinesis in cells lacking the *min* genes will still occur between nucleoid masses, indicating that nucleoid occlusion functions independently of the Min proteins (Yu and Margolin, 1999; Margolin, 2001a). In cells lacking both normal chromosome segregation and Min proteins, clusters of closely spaced FtsZ rings are observed within the nucleoid free regions of these filamentous cells, suggesting roles for both the nucleoid and Min proteins in Z-ring localization. In addition, these studies revealed the potential for Z-ring formation at *all* positions along the length of the *E. coli* rod (Yu and Margolin, 1999). Hence, while nucleoid occlusion seems to prevent untimely Z-ring formation over unsegregated nucleoids, the Min system appears to act by inhibiting cell division at the cell poles (Figure 1.2). The overall result is the restriction of cell division to the proper midcell site upon completion of chromosome replication (Margolin, 2001a).

1.3.4. MinC

E. coli MinC ($MinC_{Ec}$; ~25 kDa) acts as a general cell division inhibitor. Overexpression of $MinC_{Ec}$ in wild-type cells leads to the formation of long filaments, a hallmark of cell division inhibition, while the loss of $MinC_{Ec}$ produces a minicell phenotype (de Boer *et al.*, 1989). In *E. coli* lacking all its chromosomal *min* genes, the overexpression of both $MinC_{Ec}$ and $MinD_{Ec}$ in the absence of $MinE_{Ec}$ could induce total cell division arrest, causing a long filamentous morphology. This suggested that $MinC_{Ec}$ and $MinD_{Ec}$ form a division inhibitor that acts throughout the length of the cell (de Boer *et al.*, 1989). Further studies showed that a >25-fold increase in the levels of $MinC_{Ec}$ alone will inhibit *E. coli* cytokinesis (de Boer *et al.*, 1992). The requirement for such a large increase in MinC to arrest cell division suggested that MinD may function to augment MinC activity (de Boer *et al.*, 1992).

$MinC_{Ec}$ [231 amino acids (aa) long] consists of two distinct domains, with the N-terminus comprising amino acids 1-99 and the C-terminus formed by residues 125-231, both joined by a linker region (Hu and Lutkenhaus, 2000). Size exclusion chromatography has shown $MinC_{Ec}$ to be a dimer (Hu and Lutkenhaus, 2000; Szeto *et al.*, 2001b), while yeast two-hybrid studies have detected a strong

interaction between $MinC_{Ec}$ and $MinD_{Ec}$ (Huang *et al.*, 1996). Using far-UV circular dichroism the $MinC_{Ec}$ C-terminus has been shown to contain predominantly β-sheet secondary structure (Szeto *et al.*, 2001b). Furthermore, the $MinC_{Ec}$ C-terminus has been implicated in the self-association of the protein and in its interaction with $MinD_{Ec}$ (Hu and Lutkenhaus, 2000; Szeto *et al.*, 2001b).

The crystal structure of MinC from the thermophilic bacterium *Thermotoga maritima* (Tm) has been elucidated, showing the protein existing as four $MinC_{Tm}$ molecules arranged as two dimers (Cordell *et al.*, 2001). Similar to *E. coli* MinC, each $MinC_{Tm}$ monomer contains two domains. The N-terminus is composed of two α-helices and five β-strands, while the C-terminus consists of a right-handed β-helix that forms a triangular barrel-like structure with three surfaces, designated A, B, and, C (Cordell *et al.*, 2001). The dimerization interface of $MinC_{Tm}$ appears to lie on the hydrophobic A surface (Cordell *et al.*, 2001).

Using biosensor technology, a purified MalE-$MinC_{Ec}$ fusion was shown to interact with FtsZ (Hu *et al.*, 1999). Furthermore, FtsZ polymers are disassembled in the presence of MalE-$MinC_{Ec}$; however, $MinC_{Ec}$ disassembles FtsZ polymers by a mechanism that does not involve modifying FtsZ GTPase activity, in contrast to another characterized FtsZ inhibitor, SulA (Hu *et al.*, 1999). *In vitro*, the N-terminus of $MinC_{Ec}$ has been shown to be sufficient to inhibit FtsZ polymerization, and overexpression of a MalE-$MinC_{Ec}$ fusion encoding only the first 115 residues of MinC in *E. coli* can inhibit cell division (Hu and Lutkenhaus, 2000).

1.3.5. MinD

Of the three Min proteins, MinD is the most ubiquitously distributed (Ramirez-Arcos *et al.*, 2001a) and is the most conserved bacterial protein involved in cell division, aside from FtsZ (Sakai *et al.*, 2001). This protein has a conserved ATP-binding site and is part of the ParA subfamily of proteins, which includes proteins involved in DNA segregation (de Boer *et al.*, 1991; Lutkenhaus and Sundaramoorthy, 2003).

In *E. coli* (Ec), the presence of $MinD_{Ec}$ (270 residues; ~30 kDa) greatly reduces the amount of $MinC_{Ec}$ required to induce cell filamentation; hence, $MinD_{Ec}$ has been termed an activator of $MinC_{Ec}$ (de Boer *et al.*, 1992). In contrast, overexpression of $MinD_{Ec}$ does not block *E. coli* cell division in the absence of $MinC_{Ec}$ (de Boer *et al.*, 1992). *E. coli* that lack functional $MinD_{Ec}$ exhibit a classic minicell phenotype and experience cell division at polar sites, in addition to the cell center (de Boer *et al.*, 1988). Immunoelectron microscopy localized MinD to the inner cell membrane of *E. coli* (de Boer *et al.*, 1991), consistent with initial proposals that the protein may act at the cell envelope (with $MinC_{Ec}$) to block cell division (de Boer *et al.*, 1989).

MinD proteins contain what is classified as a 'deviant' Walker A ATP-binding motif (P-loop) at its N-terminus (aa 10-17 in *E. coli* MinD) (de Boer *et al.*, 1991; Lutkenhaus and Sundaramoorthy, 2003) (Figure 1.3 A, B; green and blue residues). Classic Walker A motifs have a GXXGXGK[T/S] sequence (where X is any amino acid), while the deviant consensus sequence is X**K**GGXXK[T/S] and includes a signature lysine (bold) found in MinD proteins (Koonin, 1993; Lutkenhaus and Sundaramoorthy, 2003) (Figure 1.3 A, B; black arrow). Purified $MinD_{Ec}$ can bind ATP (de Boer *et al.*, 1991) and dimerizes in the presence of this nucleotide (Hu *et al.*, 2003). By itself, $MinD_{Ec}$ has relatively weak ATPase activity, and point mutations within the Walker A motif (e.g. K16Q) abolished the ability of the protein to activate $MinC_{Ec}$-mediated division inhibition in *E. coli*, thus indicating a role for ATP in this process (de Boer *et al.*, 1991) (K16 residue of a MinD homologue from *Archaeoglobus fulgidus* is shown as blue residue in Figure 1.3 A, B).

The crystal structures of several MinD homologues have been elucidated from the Archaeal organisms *A. fulgidus* (Af), *Pyrococcus furiosus* (Pf), and *P. horikoshii* (Ph). While all structures consisted of monomeric protein, they were obtained bound to ADP ($MinD_{Pf}$ and $MinD_{Ph}$) (Hayashi *et al.*, 2001; Sakai *et al.*, 2001); to an ATP analogue, AMPPCP ($MinD_{Pf}$) (Hayashi *et al.*, 2001); or in the absence of nucleotide ($MinD_{Af}$) (Cordell and Löwe, 2001). All proteins consisted of a curved β-sheet formed of seven parallel, and one antiparallel, β-strands (Figure 1.3 A, B; orange residues). In

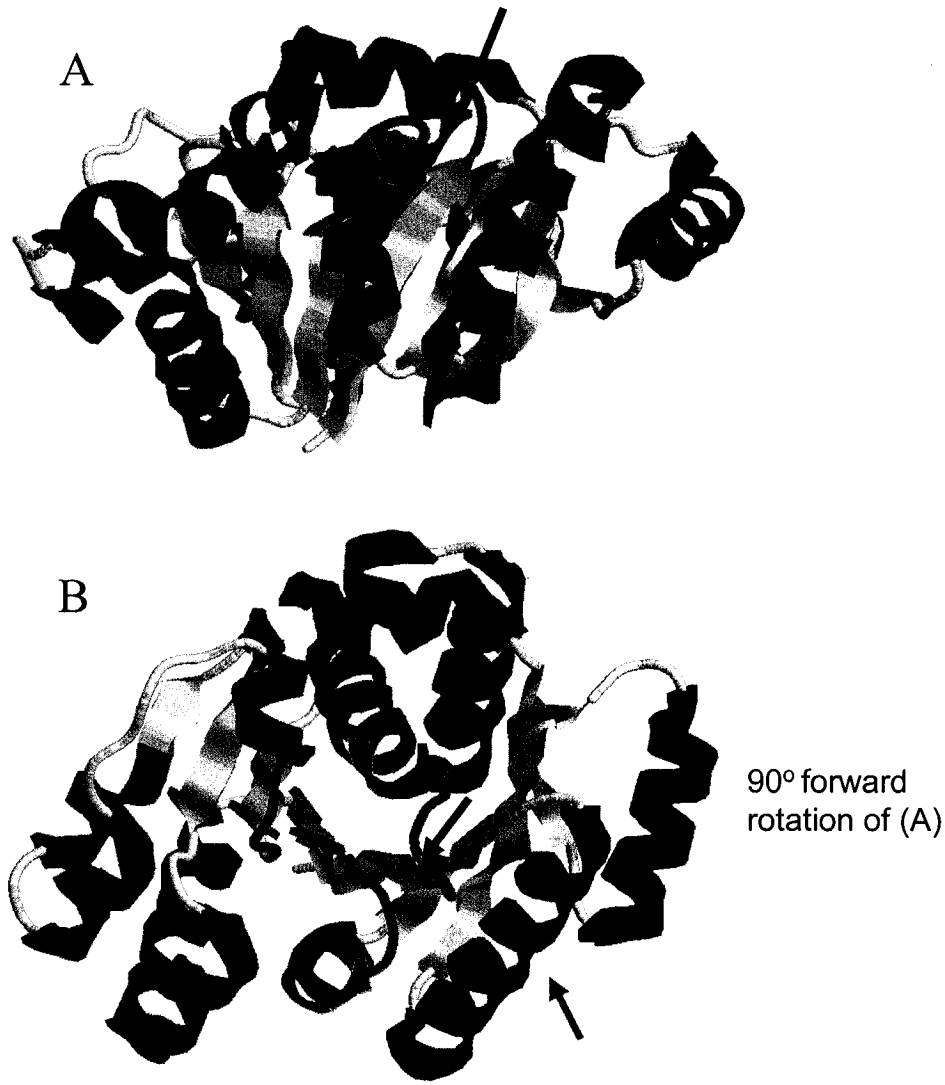

Figure 1.3. Crystal structure of MinD from *Archaeoglobus fulgidus* (Cordell and Löwe, 2001). (A, B) MinD consists a curved β-sheet formed of seven parallel and one antiparallel β-strands (orange residues) surrounded by a network of 11 α-helices (red residues). Residues forming the Walker A ATP-binding motif are shown in green and blue. Blue residue represents residue K16. Signature lysine in this ATP-binding motif is indicated with a black arrow. Purple and cyan residues indicate position of switch I and switch II sites, respectively. The MinD α-7 helix is indicated with a green arrow. (B) depicts a 90° forward rotation of (A).

turn, this centralized β-sheet is surrounded by a network of 11 α-helices (Cordell and Löwe, 2001; Hayashi *et al.*, 2001; Sakai *et al.*, 2001) (Figure 1.3 A, B; red residues). Structurally, the solved MinD proteins most closely resemble the monomeric subunits that form dimeric nitrogenase iron proteins (NIPs) (Cordell and Löwe, 2001; Hayashi *et al.*, 2001; Sakai *et al.*, 2001), such as NifH that are involved in nitrogen fixation (Schindelin *et al.*, 1997).

The NifH dimer interface includes the ATP binding sites of each monomer, such that a nucleotide sandwich is formed (Schindelin *et al.*, 1997). NifH also contains a deviant Walker A motif, and its signature lysine has been shown to contact the nucleotide that is bound by the opposite monomer. This is proposed to stabilize the negative charges of ATP, permitting efficient ATP hydrolysis (Schindelin *et al.*, 1997). Like NifH, MinD proteins also contain switch I and switch II sites (Cordell and Löwe, 2001; Sakai *et al.*, 2001) [Figure 1.3 A, B; purple residues (switch I) and cyan residues (switch II); see also Figure 3.1], which have been implicated in nucleotide dependent conformational changes in other proteins (Vale, 1996). Using dimeric NifH as a template, a model for dimeric Archael MinD has been generated (Hu and Lutkenhaus, 2003). It was shown that the modeled MinD dimer could also have intermonomer contacts between the signature lysine of one monomer and the ATP molecule of the opposite monomer, suggesting that dimerization may be important for aiding MinD ATPase activity, similar to NifH (Lutkenhaus and Sundaramoorthy, 2003).

1.3.6. MinE

MinE is the smallest of the three Min proteins (88 residues, ~10 kDa). In contrast to $MinC_{Ec}$ and $MinD_{Ec}$, the overexpression of $MinE_{Ec}$ in wild-type *E. coli* cells resulted in a minicell phenotype, not filamentous cells. Furthermore, minicells are also formed when all three Min proteins are overexpressed simultaneously, showing the epistatic effects of $MinE_{Ec}$ over $MinC_{Ec}$ and $MinD_{Ec}$ (de Boer *et al.*, 1989). Using the yeast two-hybrid system, an interaction between $MinE_{Ec}$ and $MinD_{Ec}$ was detected, as well as the ability of $MinE_{Ec}$ to disrupt $MinC_{Ec}$-$MinD_{Ec}$ association (Huang *et al.*, 1996). The ability of MinE to suppress the MinCD division block at polar and midcell sites suggested

two roles for the protein: 1) to impart topological specificity to the MinCD complex and, 2) to inhibit MinCD activity (de Boer *et al.*, 1989; Pichoff *et al.*, 1995, Zhao *et al.*, 1995).

Separate domains in $MinE_{Ec}$ seem to be responsible for these functions. Deletion analyses have shown that the N-terminal amino acids 1-22 of $MinE_{Ec}$ contain an 'anti-MinCD' domain that interacts with $MinD_{Ec}$ (Zhao *et al.*, 1995), while the remaining residues (aa 23-88) contain the topological specificity domain (TSD) that is responsible for restricting MinCD division inhibition to the cell pole regions (Pichoff *et al.*, 1995; Zhao *et al.*, 1995; King *et al.*, 1999). Nuclear magnetic resonance (NMR) analysis of the N-terminal anti-MinCD domain of $MinE_{Ec}$ revealed it to be a peptide region that can rapidly convert between randomly coiled and α-helical conformations, with the latter being a possible interacting surface with $MinD_{Ec}$ (King *et al.*, 1999). The N-terminal domain of $MinE_{Ec}$ (aa 6-35) is predicted to form an α-helix, with one face containing residues that are involved in interaction with $MinD_{Ec}$, as determined by yeast two-hybrid studies (King *et al.*, 1999; Ma *et al.*, 2003). The coiled-coil nature of this region has led to the proposal that the N-terminus of $MinE_{Ec}$ interacts with a complementary helix in $MinD_{Ec}$ (Ma *et al.*, 2003).

Using yeast two hybrid studies and gel-filtration analyses, $MinE_{Ec}$ has also been shown to be dimeric, with residues 36-62 of the TSD likely involved in protein self-association (Pichoff *et al.*, 1995). Analytical ultracentrifugation of a peptide comprised of $MinE_{Ec}$ residues 31-88 also showed it was dimeric (King *et al.*, 1999). NMR studies have further confirmed the self-association of the $MinE_{Ec}$ TSD (King *et al.*, 2000). Each TSD contains a long α-helix and dimerization seems to occur by extensive hydrophobic interactions between the α-helices of each TSD monomer, forming an antiparallel coiled-coil. Two β-strands from each TSD also form a four stranded beta-sheet against which the coiled-coil packs to form a hydrophobic sandwich (King *et al.*, 2000).

1.3.7. Min protein localization in *Escherichia coli*

The detailed localization of GFP fusions to *E. coli* Min proteins have greatly advanced the study of Min protein function in this organism. Using a GFP-fusion to the N-terminus of $MinD_{Ec}$ (GFP-$MinD_{Ec}$), several groups have demonstrated that the protein exhibits a rapid, $MinE_{Ec}$-dependent, pole-to-pole oscillation in rod-shaped *E. coli* (Figure 1.4 A) (Raskin and de Boer, 1999a; Rowland *et al.*, 2000). This dynamic localization is characterized by the progressive assembly of GFP-$MinD_{Ng}$ along the inner membrane, from the pole towards midcell, to form a tube-like structure that dwells for a short period of time (~10 seconds) at one cell half before disassembling and reforming at the opposite cell pole (Figure 1.4 A) (Raskin and de Boer, 1999a; Rowland *et al.*, 2000). The period of oscillation of GFP-$MinD_{Ec}$ (defined by the time required for fluorescent signal to leave one cell pole, migrate to the other and back) was approximately 50 seconds and was dependent only upon $MinE_{Ec}$ and not $MinC_{Ec}$ (Raskin and de Boer, 1999a). In the absence of $MinE_{Ec}$, GFP-$MinD_{Ec}$ localized along the entire cell periphery without evidence of pole-to-pole movement (Raskin and de Boer, 1999a; Rowland *et al.*, 2000).

Recently, quantitiative immunoblotting indicated that there are approximately 1400 and 2000 molecules of $MinE_{Ec}$ and $MinD_{Ec}$ in an *E. coli* cell (Shih *et al.*, 2002). Increasing the ratio of GFP-$MinD_{Ec}$/$MinE_{Ec}$ appears to increase the dwell time within each cell pole, and hence the oscillation period, of the fusion protein (Raskin and de Boer, 1999a). This increased period was accompanied by minicell formation, suggesting that a certain minimum oscillation frequency, mediated by a proper $MinD_{Ec}$/$MinE_{Ec}$ ratio, is required to maintain correct midcell division in rod-shaped *E. coli* (Raskin and de Boer, 1999a).

Recently, using deconvolution and three-dimensional imaging of *E. coli*, Shih *et al.* (2003) observed that the GFP-$MinD_{Ec}$ 'tube' is actually organized into one or two helical, or coiled, structures that wind around the inner membrane of the cylindrical cell, suggesting the existence of a possible Min cytoskeletal apparatus (Figure 1.4 B). The appearance of these coils is $MinE_{Ec}$-dependent and they are not restricted to polar regions. Interestingly, a faint coiled structure remains in

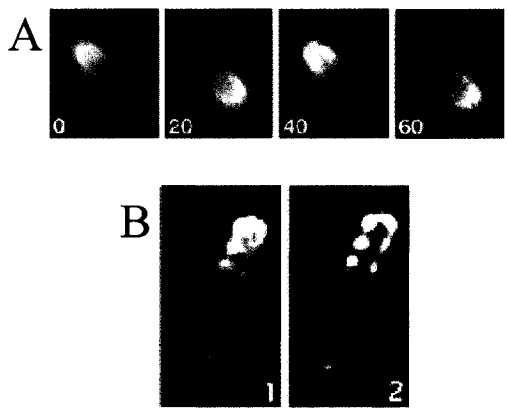

Figure 1.4. Localization of GFP-MinD$_{Ec}$ in *E. coli*. (A) GFP-MinD$_{Ec}$ exhibits pole-to-pole movement in rod-shaped *E. coli*. Timepoints are indicated in seconds in each panel (image from Raskin and de Boer, 1999a). (B) Image deconvolution shows GFP-MinD$_{Ec}$ localizing as a coiled-structure in *E. coli*. Note the majority of fluorescent signal at one half of the cell and a residual coiled array at the other. Image 1 is raw image, image 2 shows deconvolution of image 1 [Reprinted with permission from the National Academy of Sciences, USA (Shih *et al.*, 2003)].

one cell pole after the majority of GFP-$MinD_{Ec}$ has localized as a coiled array in the opposite cell half (Figure 1.4 B) (Shih *et al.*, 2003). Hence, it would appear that this helical array(s) is extended throughout the length of the cell. The apparent oscillatory movement of GFP-$MinD_{Ec}$ is attributed to a dynamic shift in fusion protein concentration along the coiled array from one cell pole to the other (Shih *et al.*, 2003).

Similar to GFP-$MinD_{Ec}$, a GFP-$MinC_{Ec}$ fusion also displayed periodic membrane-associated pole-to-pole movement in *E. coli* (Hu and Lutkenhaus, 1999; Raskin and de Boer, 1999b). This oscillation pattern was dependent upon both $MinD_{Ec}$ and $MinE_{Ec}$, and the period of oscillation was ~40-50 seconds, comparable to that observed with GFP-$MinD_{Ec}$ (Hu and Lutkenhaus, 1999; Raskin and de Boer, 1999b). In the absence of $MinE_{Ec}$, GFP-$MinC_{Ec}$ would be localized along the entire inner cell periphery, provided that $MinD_{Ec}$ was present (Hu and Lutkenhaus, 1999; Raskin and de Boer, 1999b). Similar to GFP-$MinD_{Ec}$, refined imaging of GFP-$MinC_{Ec}$ expressing *E. coli* showed it also localized as a membrane-associated coiled structure (Shih *et al.*, 2003). While the majority of GFP-$MinC_{Ec}$ was assembled into spirals in one cell half, a residual array remains at the opposite cell pole, as observed with GFP-$MinD_{Ec}$ (Shih *et al.*, 2003).

Interestingly, using an N-terminal truncation to $MinC_{Ec}$ that does not inhibit Z-ring assembly, it was demonstrated that $MinD_{Ec}$ is able to direct the GFP-$MinC_{Ec}$ mutant to septal rings (Johnson *et al.*, 2002). Presumably, this was not observed previously since functional GFP-$MinC_{Ec}$ would immediately disassemble Z-rings and concurrently eliminate evidence of GFP-$MinC_{Ec}$ localization to these regions as well (Johnson *et al.*, 2002). Hence, the $MinCD_{Ec}$ complex not only accumulates within a coil along one half of the cell, but likely also actively targets impending division septa.

Although initially reported to localize as a ring at midcell (Raskin and de Boer, 1997), further studies with $MinE_{Ec}$-GFP revealed that this protein also displayed $MinD_{Ec}$-dependent intracellular oscillatory movement (Fu *et al.*, 2001; Hale *et al.*, 2001). In live cells, the majority of $MinE_{Ec}$-GFP signal was assembled in a ring-like structure near midcell; however, a significant amount of fluorescent signal was also seen along the membrane on one just side of the $MinE_{Ec}$-ring and was

termed the peripheral extra-annular (PEA) signal (Fu *et al.*, 2001; Hale *et al.*, 2001). Hence, $MinE_{Ec}$-GFP was proposed to localize as a tube-like structure with a defined 'rim' composed of the $MinE_{Ec}$-ring (Hale *et al.*, 2001).

Time-lapse imaging has revealed that the centrally located MinE-ring moved towards the cell pole containing the PEA signal such that the latter would decrease in size. Once the MinE-ring signal reached the cell pole, it would dissolve and reform at or near the middle of the cell. At the same time, a new PEA signal would form at the other cell half and the MinE-ring would subsequently move towards this other cell pole (Hale *et al.*, 2001; Fu *et al.*, 2001). The average time required for a complete cycle of MinE-ring movement, dissolution, and reformation at midcell was very similar to that required for a cycle of MinD oscillation (Hale *et al.*, 2001).

Recent studies by Shih *et al.* (2003) now suggest that $MinE_{Ec}$ actually localizes in a $MinD_{Ec}$-dependent coiled array within the cell. The MinE-ring did not appear to be closed, and seemed to be composed of 1-2 tight loops of the coil. These midcell $MinE_{Ec}$-GFP coils also appeared to be continuous with those that extended into the polar zone. Again, while the fluorescent intensity of the $MinE_{Ec}$-GFP coil was greater at midcell and along one half of the cell, a faint MinE array could still be observed in the other cell half (Shih *et al.*, 2003).

1.3.8. Min proteins and the bacterial membrane

Studies with GFP fusions to each Min_{Ec} protein have shown that the recruitment of both $MinC_{Ec}$ and $MinE_{Ec}$ to the inner cell membrane, and their characteristic intracellular oscillations, are dependent upon $MinD_{Ec}$. In addition, the oscillation of $MinD_{Ec}$ is dependent upon $MinE_{Ec}$ (Raskin and de Boer, 1999a: Raskin and de Boer, 1999b; Hu and Lutkenhaus, 1999; Shih *et al.*, 2003). What are the molecular mechanism(s) that drive this behaviour?

Recently, Hu *et al.* (2002) demonstrated that, in the presence of ATP, MinD could bind to phospholipid vesicles *in vitro*, forming an ordered helical array than converts round vesicles into extended tubes. The binding of phospholipid vesicles by MinD is also cooperative, such that

increasing the concentration of protein stimulates an increased fraction of MinD to become membrane-associated (Lackner *et al.*, 2003). In contrast, incubation of MinD with ADP, or the use of a MinD mutant bearing a K16Q substitution in its Walker A ATP-binding motif, did not result in protein binding to phospholipid vesicles (Hu and Lutkenhaus, 2002). Another group has also shown that, in the absence of phospholipid vesicles, MinD can rapidly assemble into filaments in an ATP-dependent manner (Suefuji *et al.*, 2002). The addition of *E. coli* phospholipid vesicles promoted lengthening and bundling of these MinD filaments (Suefuji *et al.*, 2002).

Interestingly, it was shown that the ATPase activity of $MinD_{Ec}$ could be stimulated almost 10-fold in the presence of $MinE_{Ec}$ and phospholipid vesicles (Hu and Lutkenhaus, 2001). Significantly, this stimulation of $MinD_{Ec}$ ATPase activity was accompanied by the release of MinD from the vesicles (Hu *et al.* 2002). Hence, it was proposed that ATP-binding may induce conformational change(s) in MinD that give it higher affinity for phospholipids, and that subsequent hydrolysis of ATP, induced by MinE, will result in the dissociation of MinD from the membrane (Hu *et al.*, 2002). *In vivo,* $MinE_{Ec}$ proteins containing mutations within their N-terminal anti-MinCD domain were less able to stimulate MinD ATPase activity. This was correlated with a loss of, or an increased oscillation period of, GFP-$MinD_{Ec}$ (Hu and Lutkenhaus, 2001).

Surprisingly, while wild-type $MinE_{Ec}$ could promote the disassembly of $MinD_{Ec}$ filaments (Hu *et al.*, 2002; Suefuji *et al.*, 2002), it could also induce additional bundling of $MinD_{Ec}$ polymers in the presence of lipid vesicles when both proteins were at equimolar amounts (Suefuji *et al.*, 2002). This dual role of $MinE_{Ec}$ may reflect the requirement of this protein for both $MinD_{Ec}$ oscillation and $MinD_{Ec}$ assembly into higher order structures (Suefuji *et al.*, 2002).

$MinD_{Ec}$-ATP was also able to recruit $MinC_{Ec}$ onto phospholipid vesicles (Hu *et al.*, 2003; Lackner *et al.*, 2003), in support of *in vivo* studies where the association of GFP-$MinC_{Ec}$ with the *E. coli* cell poles was dependent upon $MinD_{Ec}$ (Hu and Lutkenhaus, 1999; Raskin and de Boer, 1999a). Purified $MinD_{Ec}$ and a MalE-$MinC_{Ec}$ fusion have been shown to interact using size-exclusion chromatography in an ATP-dependent manner (Hu *et al.*, 2003). Yeast two-hybrid studies have

indicated that residues within the α-7 helix of $MinD_{Ec}$ (E146 and D152) may be involved in binding to $MinC_{Ec}$ (α-7 helix of *A. fulgidus* MinD is indicated in Figure 1.3 B, green arrow). Recent studies have also indicated that residues within the switch I and II sites of $MinD_{Ec}$ are involved in interaction with $MinC_{Ec}$. While these mutations (including G42A, R44G, and I125E) did not affect MinD membrane association, they impaired $MinC_{Ec}$ binding, as assessed by yeast two-hybrid methods (Zhou and Lutkenhaus, 2004).

In vitro, both $MinC_{Ec}$ and $MinD_{Ec}$ proteins can be removed from lipid vesicles by the addition of $MinE_{Ec}$ (Lackner *et al.*, 2003; Hu *et al.*, 2003). It has been suggested that a $MinE_{Ec}$-induced conformational change in membrane-bound $MinD_{Ec}$ may be responsible for displacing $MinC_{Ec}$ (Lackner *et al.*, 2003; Hu *et al.*, 2003). However, $MinE_{Ec}$-induced dissociation of $MinC_{Ec}$ and $MinD_{Ec}$ are likely distinct events, since $MinE_{Ec}$ could displace $MinC_{Ec}$ from vesicles even in the absence of ATP hydrolysis by $MinD_{Ec}$ (Lackner *et al.*, 2003; Hu *et al.*, 2003). $MinC_{Ec}$ and $MinE_{Ec}$ also do not seem to compete for the same $MinD_{Ec}$ binding site, since the former could not displace $MinD_{Ec}$-$MinE_{Ec}$ complexes from vesicles, nor interfere with $MinE_{Ec}$ stimulation of $MinD_{Ec}$ (Hu *et al.*, 2003). However, it is also possible that both $MinC_{Ec}$ and $MinE_{Ec}$ share similar or overlapping binding sites on $MinD_{Ec}$, and that $MinE_{Ec}$ has a greater affinity for this $MinD_{Ec}$ region than $MinC_{Ec}$ does (Dr. Glenn King, University of Connecticut Health Center).

A short C-terminal membrane targeting sequence (MTS) in MinD has been identified as the region responsible for membrane localization (Szeto *et al.*, 2002; Hu and Lutkenhaus, 2003). This extreme C-terminal region likely consists of a highly conserved 8-12 residue amphipathic helix (aa 261-268; KGFLKRLF in *E. coli* MinD as an example). In general, one face of the helix is polar (lysine and arginine residues in $MinD_{Ec}$), while the other face contains hydrophobic residues (leucine, phenylalanine, and methionine in $MinD_{Ec}$) (Szeto *et al.*, 2002). Removal of this predicted amphipathic helix from both *E. coli* MinD and *B. subtilis* MinD resulted in GFP-MinD fusions that were unable to localize to the membrane in *E. coli*, remaining in the cytosol instead (Szeto *et al.*,

2002; Hu and Lutkenhaus; 2003). Despite retaining interaction with $MinC_{Ec}$, these $MinD_{Ec}$ deletion variants were unable to activate MinC-dependent cell divison arrest (Hu and Lutkenhaus, 2003). Mutations that disrupted either the helicity or amphipathicity of the $MinD_{Ec}$ MTS also abrogated membrane localization of the protein (Szeto *et al.*, 2002).

Interestingly, the short MinD MTS can be fused to other proteins that are normally cytosolic and target them to the inner membrane of *E. coli*. However, while a single *B. subtilis* MinD MTS fused to proteins such as GFP or MinC could recruit them to the *E. coli* inner membrane, a bivalent arrangement of *E. coli* MinD MTSs was required to do the same. In *B. subtilis*, $MinD_{Bs}$ does not undergo the dynamic oscillation observed with $MinD_{Ec}$; therefore, it was suggested that the higher membrane affinity of the $MinD_{Bs}$ MTS may be responsible for this lack of intracellular mobility (Szeto *et al.*, 2003).

How does the C-terminus of MinD associate with the cell membrane? Although there are several MinD crystal structures available from Archaeal organisms, the proteins either do not naturally contain MTS regions or the corresponding region is structurally disordered (Cordell and Löwe, 2001; Hayashi *et al.*, 2001; Sakai *et al.*, 2001). Using far-UV circular dichroism, it was shown that the *E. coli* and *B. subtilis* MTSs do not exhibit any stable secondary structure in the absence of lipids. However, in the presence artificial phospholipid vesicles, these MTS peptides experienced a random coil-to-helix transition and adopted an α-helical conformation (Szeto *et al.*, 2003). The resulting amphipathic helix is predicted to generate a positively charged polar face; hence, it was predicted that the MinD MTS preferentially interacts with negatively-charged (anionic) phospholipids (Szeto *et al.*, 2003). In fact, MinD MTSs do display a preference for anionic phospholipids (Mileykovskaya *et al.*, 2003). While the $MinD_{Bs}$ MTS has distinct preference for phosphatidylglycerol (PG) over cardiolipin (CL), the $MinD_{Ec}$ MTS associates equally well with both of these anionic phospholipids (Szeto *et al.*, 2003). Hence, it is proposed that each MinD MTS is adapted to interact with specific phospholipids present in the inner membrane of their respective organisms (Szeto *et al.*, 2003).

The orientation of the MinD MTS helix is predicted to be parallel to the membrane surface, such that the hydrophobic residues on one face of the amphipathic helix are buried and interact with lipid acyl chains, while the cationic residues on the opposite face interact with the headgroups of anionic phospholipids (Szeto *et al.*, 2002; Mileykovskaya *et al.*, 2003). Experimental support for this was obtained by Zhou and Lutkenhaus (2003), who substituted the MTS hydrophobic residues with the hydrophobic residue tryptophan, and used fluorescence spectroscopy to reveal that tryptophan did insert into the hydrophobic interior of a lipid bilayer, likely reflecting what might occur with the wild-type MinD MTS (Zhou and Lutkenhaus, 2003).

Since dimerization and membrane association of $MinD_{Ec}$ are ATP-dependent (Hu *et al.*, 2003), a 'dimer trigger' model has been proposed in which $MinD_{Ec}$ dimerizes upon binding ATP, leading to conformational changes that activate, or expose, the $MinD_{Ec}$ MTS sequence for membrane binding (Hu and Lutkenhaus, 2003). This dimerization would also ensure that two MTSs are available to increase the membrane affinity of the $MinD_{Ec}$-ATP complex for the *E. coli* membrane (Hu and Lutkenhaus, 2003). It has also been recently proposed that the MTS itself may mask the MinD dimerization interface, and that the presence of ATP and phospholipid may promote MinD self-interaction by shifting its MTS to expose the dimeric interface (Zhou *et al.*, 2004).

A second model has also been proposed to explain how MinD may associate with membranes. In the 'zipper' model, ATP-binding will promote the cooperative assembly of a MinD polymer on the membrane (Szeto *et al.*, 2003). This model does not necessarily require MinD-ATP dimers, only the recruitment of MinD-ATP subunits that continually increase the valency of MTSs that result in enhanced membrane affinity (Szeto *et al.*, 2003). The growing MinD-ATP polymer(s) can thus be compared to a zipper that gains stability on the membrane as more subunits, and hence more MTSs, are recruited.

1.3.9. Model for Min system function in rod-shaped *E. coli*

The accumulation of data obtained from studying the three Min_{Ec} proteins has led to a gradual development of a model for Min-dependent cell division site selection in *E. coli* (Figure 1.5) (Hu and Lutkenhaus, 2003; Hu *et al.*, 2003; Lackner *et al.*, 2003; Shih *et al.*, 2003). In the cytosol, monomeric MinD is proposed to bind ATP, resulting in a MinD dimer with activated MTSs that confer membrane affinity. Alternatively, individual MinD-ATP subunits may be recruited in a cooperativemanner to the cell membrane as proposed by the 'zipper' model (Szeto *et al.*, 2003). Regardless, the majority of MinD-ATP becomes preferentially accumulated at the membrane and/or polymerized lattice (collectively referred to as a $MinD_{Ec}$ 'zone') at one half of the cell (Figure 1.5 A, B). This directed accumulation may be the result of a local self-enhancing reaction (Meinhardt and de Boer, 2001), and is supported by the cooperative nature of MinD binding to membranes *in vitro* (Lackner *et al.*, 2003). Based on the recent observation of MinC, MinD, and MinE spiral arrays *in E. coli* (Shih *et al.*, 2003), this lattice may actually consist of a permanent coiled array of Min proteins that extends across the entire cell length to be used as a template, or nucleation point, for the incorporation of more Min proteins to either cell half (Shih *et al.*, 2003) (Figures 1.4 B and 1.5).

$MinD_{Ec}$ is able to recruit the cell division inhibitor $MinC_{Ec}$ to the inner membrane/Min helical array at one end of the cell as well. Whether MinD interacts with MinC prior to associating with the membrane is presently unclear. On one hand, size-exclusion chromatography suggests a weak, ATP-dependent, interaction between the two purified proteins in solution; however, the recruitment of MinC by MinD is more easily observed using a sedimentation assay once phospholipids vesicles are also included (Hu *et al.*, 2003). Recent evidence also showed $MinD_{Ec}$ mutants that fail to bind membranes can still interact with $MinC_{Ec}$ (Zhou and Lutkenhaus, 2004), suggesting a cytosolic interaction between the two proteins may exist. As $MinD_{Ec}$ has been demonstrated to recruit GFP-$MinC_{Ec}$ to septal targets (Johnson *et al.*, 2002), any $FtsZ_{Ec}$ ring assembly, and cell division, would be transiently inhibited along one half of the cell where $MinC_{Ec}$-$MinD_{Ec}$ have accumulated (Figure 1.5 B).

Figure 1.5. Model for Min_{Ec}-dependent cell division regulation in cylindrical *E. coli*. This model is adapted from Shih *et al.* (2003) and incorporates culmulative data obtained from studying the three Min_{Ec} proteins. (A) In the cytosol, $MinD_{Ec}$ (open circles) is proposed to bind ATP ($MinD_{Ec}$-ATP; green circles), dimerize, and gain affinity for the membrane and/or a permanent $MinCDE_{Ec}$ scaffold base (coils). Alternatively, individual $MinD_{Ec}$-ATP subunits may be recruited in a cooperative manner according to the 'zipper model' (Szeto *et al.*, 2003). $MinD_{Ec}$ also recruits the division inhibitor $MinC_{Ec}$ (squares). $MinD_{Ec}$-ATP and $MinC_{Ec}$ preferentially accumulate at one half of the cell ($MinD_{Ec}$ 'zone'). (B) $MinE_{Ec}$, (triangles) attracted by $MinD_{Ec}$-ATP, localizes near the cell center as 1-2 loops of the coiled structure. $MinE_{Ec}$ induces the release of $MinC_{Ec}$ and stimulates the ATPase activity of $MinD_{Ec}$-ATP at the edge of the accumulated $MinD_{Ec}$ zone. $MinD_{Ec}$-ADP dissociates from the membrane/$MinCDE_{Ec}$ coil. $MinE_{Ec}$ travels along the Min helical array towards one cell pole and gradually induces the disassembly of the $MinD_{Ec}$ zone. (C) Cytoplasmic $MinD_{Ec}$ can diffuse towards the other cell pole, during which it binds ATP again, and associates with the membrane/Min lattice at the opposite cell pole. (D) The continuous $MinE_{Ec}$-dependent movement of $MinD_{Ec}$, and associated $MinC_{Ec}$, between each cell half will result in the inhibition of Z-ring assembly in these regions. Furthermore, this oscillation pattern keeps the time-averaged concentration of $MinC_{Ec}$ lowest at midcell, permitting stable FtsZ assembly at that point (thunderbolts).

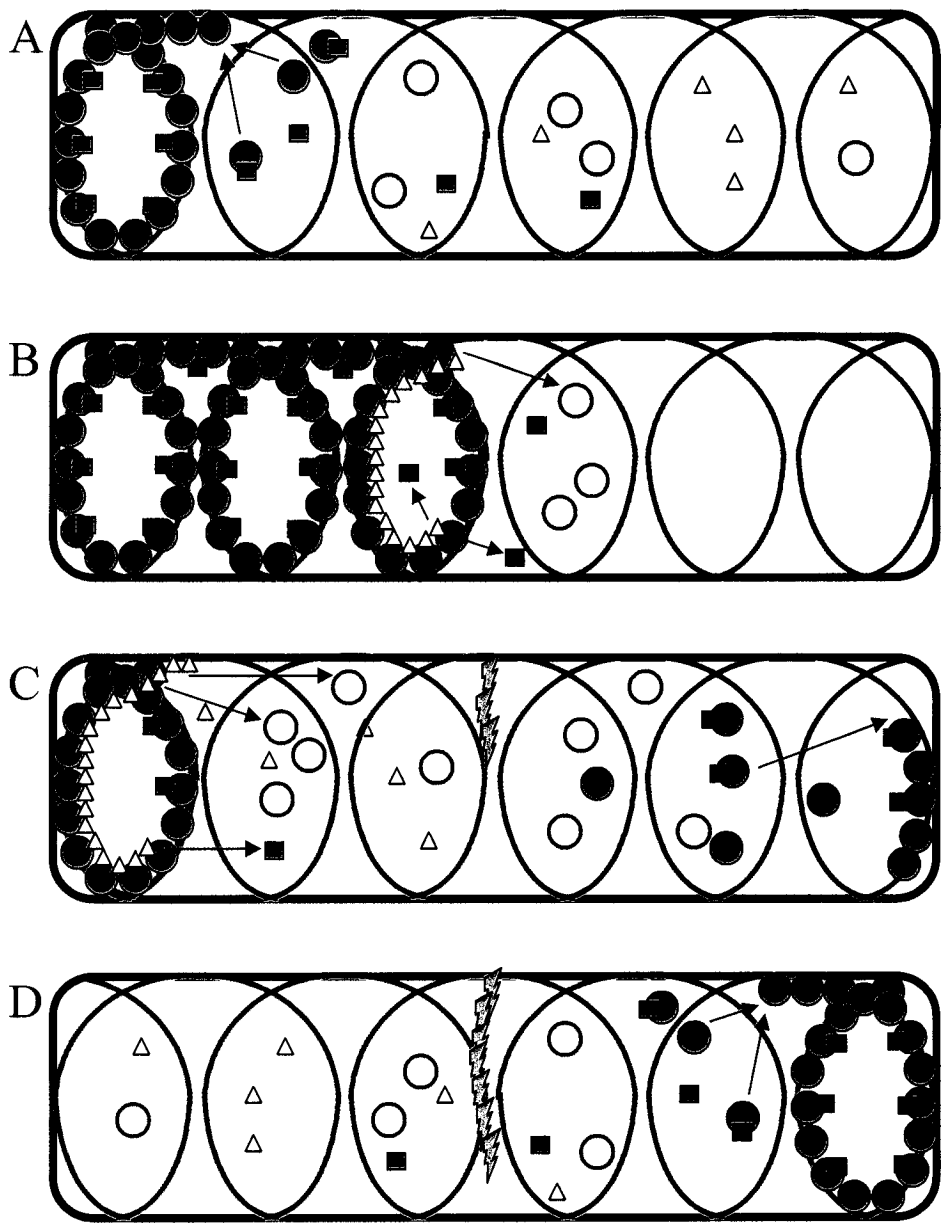
A
B
C
D
MinD$_{Ec}$-ATP
MinD$_{Ec}$-ADP and/or MinD$_{Ec}$ alone
MinC$_{Ec}$
MinE$_{Ec}$
Residual MinCDE$_{Ec}$ coiled array
FtsZ

$MinE_{Ec}$, attracted by $MinD_{Ec}$-ATP, forms a 'ring-like' structure near the cell center which actually consists of 1-2 loops of a coiled structure (Figure 1.5 B). (Shih *et al.*, 2003). The interaction of $MinE_{Ec}$ 'ring' molecules with $MinD_{Ec}$-ATP found at the edge of the accumulated $MinD_{Ec}$-ATP zone at one cell half would induce the release of $MinC_{Ec}$ from the membrane. Furthermore, $MinE_{Ec}$ will stimulate the ATPase activity of $MinD_{Ec}$ and cause the latter protein to dissociate from the membrane and into the cytoplasm (Figure 1.5 C). A constant 'wave' of MinE travelling along the Min helical array would gradually induce the disassembly of $MinD_{Ec}$ from the cell half in which it resides (or from its coiled array) (Margolin, 2001b) (Figure 1.5 C). Presumably, nucleoid occlusion will also prevent untimely cell division at the midcell (Figure 1.2).

The $MinE_{Ec}$-ring has also been proposed to act as a 'stop-growth' mechanism that prevents the MinC-MinD division complex from extending beyond the midcell division site. Studies have shown that a $MinE_{Ec}$ mutant that fails to form a MinE-ring (when tagged to GFP) will permit the extension of the $MinD_{Ec}$ polar zone well past the midcell (Shih *et al.*, 2002).

Cytoplasmic $MinD_{Ec}$ can subsequently diffuse to the other cell pole, during which it binds ATP again, and associates with the membrane/Min lattice at the opposite cell pole (Figure 1.5 C, D). It is proposed that any nascent cytosolic $MinD_{Ec}$-ATP will have diffused away sufficiently, such that it avoids being reincorporated into any remaining $MinD_{Ec}$ lattice at the original cell pole (Lackner *et al.*, 2003). In addition, a new $MinD_{Ec}$ zone can assemble at the opposite end of the cell, since the majority of $MinE_{Ec}$ is still involved in disassembling $MinD_{Ec}$ at the original cell half. Once the $MinE_{Ec}$-ring has completely disassembled the original MinD zone, it dissolves and reforms at midcell to act on $MinD_{Ec}$ in the other cell half (Lackner *et al.*, 2003).

The continuous movement of $MinD_{Ec}$, and associated $MinC_{Ec}$, between each cell half will result in the inhibition of Z-ring assembly in these regions (Raskin and de Boer, 1999a; Lackner *et al.*, 2003). This oscillation pattern will keep the time-averaged concentration of $MinC_{Ec}$ lowest at midcell, permitting stable FtsZ assembly at that point (Raskin and de Boer, 1999b) (Figure 1.5 D). The observed oscillations of each Min protein is proposed to be a result of the continuous

redistribution of $MinC_{Ec}$, $MinD_{Ec}$, and $MinE_{Ec}$ subunits across a permanent Min scaffold (Shih *et al.*, 2003); however, whether this scaffold requires another underlying cytoskeletal frame is not known.

Interestingly, several groups have used computer simulation models to show that Min protein oscillations can occur in a closed system, and that no other additional components other than MinD and MinE are required (Howard *et al.*, 2001, Meinhardt and de Boer, 2001; Kruse, 2002). However, since the discovery that Min proteins assemble as intracellular coils (Shih *et al.*, 2003), it is unclear whether these *in silico* models remain applicable.

1.3.10. Min proteins in the Gram-positive rod *Bacillus subtilis*

The only other organism in which Min proteins have been studied in significance is the Gram-positive rod *B. subtilis* (Bs). *B. subtilis* is the most widely studied model for Gram-positive cell division and clearly contains *minC* and *minD* homologues, while lacking *minE* (Levin *et al.*, 1992; Varley and Stewart, 1992).

Overexpression of both $MinC_{Bs}$ and $MinD_{Bs}$ will inhibit *B. subtilis* cell division and cause filamentation (Marston and Errington, 1999b), while inactivation of either gene results in a minicell-like phenotype (Varley and Stewart, 1992). Localization studies have shown that $MinD_{Bs}$ is found at both cell poles (forming an arc that follows the curvature of the cell membrane) and at the midcell between separated sister nucleoids. This suggests that the protein has affinity for impending and former division sites (Marston *et al.*, 1998). Presently it is not known whether $MinD_{Bs}$ can localize as higher ordered structures, such as coils. $MinD_{Bs}$ also interacts with $MinC_{Bs}$, as determined by yeast two-hybrid studies (Marston and Errington, 1999b), and $MinC_{Bs}$ has been shown to target both cell poles and the impending midcell division site in a $MinD_{Bs}$-dependent manner (Marston and Errington, 1999b).

Unlike *E. coli* MinC and MinD, the *B. subtilis* proteins do not display any periodic intracellular oscillations. In place of MinE, an unrelated protein termed DivIVA (~19 kDa) is involved in the topological regulation of the *B. subtilis* MinCD division inhibition complex (Cha and

Stewart, 1997; Edwards and Errington, 1997). Similar to $MinD_{Bs}$, studies using DivIVA-GFP show that the protein localizes as discrete foci at the cell poles (old division sites) and as bands near the cell center (new division sites) just prior to the completion of septation (Edwards and Errington, 1997; Marston *et al.*, 1998). In the absence of DivIVA, long *B. subtilis* filaments are formed (Edwards and Errington, 1997) and $MinD_{Bs}$ localizes throughout the cell in diffuse patches along the membrane; hence, proper $MinD_{Bs}$ localization is dependent upon DivIVA (Marston *et al.*, 1998).

How might DivIVA regulate the topological specificity of the $MinCD_{Bs}$ cell division inhibitor complex in *B. subtilis*? In the 'polar piloting' model, a cell would have DivIVA localized at both poles, sequestering $MinCD_{Bs}$ to these regions as well (Figure 1.6 A) (Marston *et al.*, 1998). Once DNA replication nears completion, Z-ring assembly and recruitment of other cell division proteins is free to occur at a midcell location. Recent evidence using germinating *B. subtilis* spores has indicated that DivIVA and $MinD_{Bs}$ (and presumably $MinC_{Bs}$) can assemble at midcell division sites before Z-ring constriction begins (Figure 1.6 B) (Harry and Lewis, 2003). Presumably, the Z-ring has assembled to a point where it will be resistant to the effects of $MinCD_{Bs}$. Upon completion of cell division, each daughter cell has an old cell pole and a new one formed by the act of division. Since the DivIVA-$MinCD_{Bs}$ complex remains associated with nascent and old cell poles in each daughter cell, both progeny will have $MinCD_{Bs}$ retained at each of their cell ends to control future cytokinetic events (Figure 1.6 C) (Marston *et al.*, 1998).

B. subtilis is a spore-forming bacterium. Sporulation involves the use of septation sites at cell pole regions, as opposed to midcell division sites, in order to divide the cell into mother and prespore compartments (Errington, 2001). Whether Min proteins have a role in this event is unclear, since *min* mutants are still able to sporulate quite efficiently (Lee and Price, 1993). However, one study showed that $MinC_{Bs}$ and $MinD_{Bs}$ may be involved in regulating the proper transfer of DNA from the mother cell into the forespore during sporulation (Sharp and Pogliano, 2002b). This function is fulfilled by the DNA translocase SpoIIIE (homologous to *E. coli* FtsK) and is normally found in both mother cell and forespore; however, SpoIIIE in the mother cell localizes specifically to the septum that separates

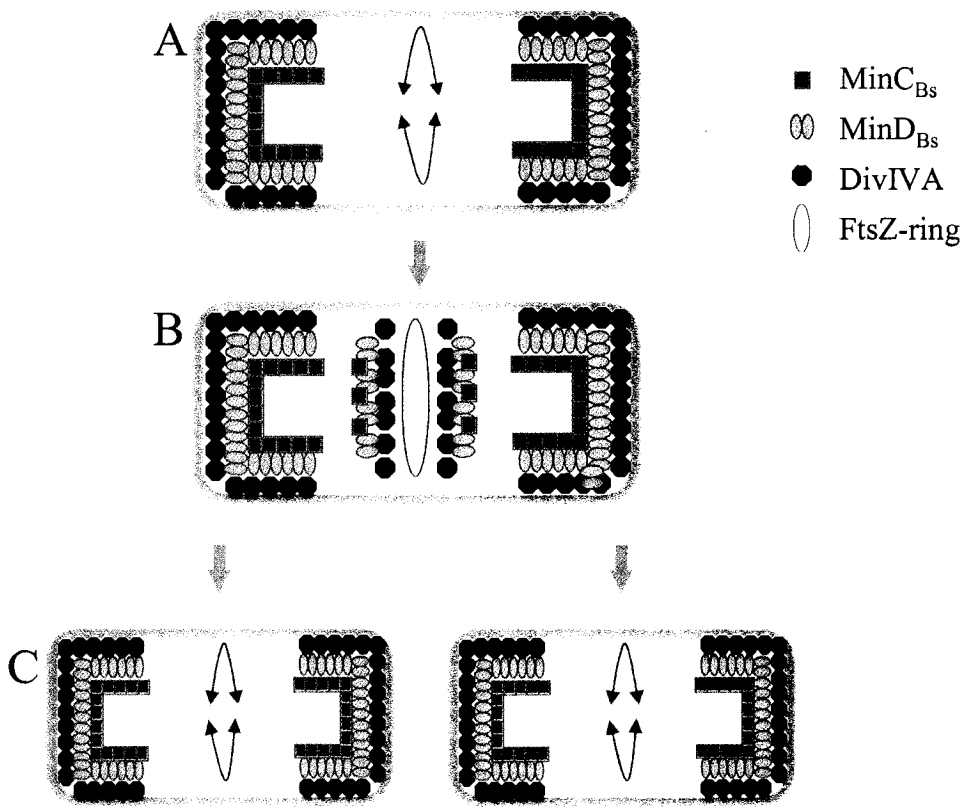

Figure 1.6. Model for MinCD$_{Bs}$-DivIVA dependent cell division regulation in *B. subtilis* (adapted from Marston *et al.*, 1998). (A) In the 'polar piloting' model, *B. subtilis* cells have DivIVA localized at both poles, which sequesters MinCD$_{Bs}$ to these regions as well, leading to division inhibition at the cell ends. (B) Once DNA replication nears completion, Z-ring assembly and recruitment of other cell division proteins is free to occur at a midcell location. DivIVA, MinD$_{Bs}$, and MinC$_{Bs}$ can assemble at midcell division sites before Z-ring constriction begins. Presumably, the Z-ring has assembled to a point where it will be resistant to the effects of MinCD$_{Bs}$. (C) Upon completion of cell division, the DivIVA-MinCD$_{Bs}$ complex remains associated with nascent and old cell poles in each daughter cell; thus, both cells have MinCD$_{Bs}$ retained at either ends to control future cytokinetic events.

the two compartments to ensure that the direction of DNA translocation proceeds towards the future spore (Sharp and Pogliano, 2002a). Interestingly, removal of $MinCD_{Bs}$ resulted in the assembly of *forespore*-expressed SpoIIIE to the septum, resulting in a reversal of DNA translocation. Therefore, $MinCD_{Bs}$ may play a role in inhibiting SpoIIIE assembly/activity within the forespore to ensure proper DNA translocation in sporulating *B. subtilis* (Sharp and Pogliano, 2002b). $MinD_{Bs}$ may also play a role in chromosome partitioning in *B. subtilis*. Interestingly, Soj internucleoid 'jumping' (reviewed above) has been shown to be dependent upon $MinD_{Bs}$ (Autret and Errington, 2003). In the absence of MinD, Soj patches were observed further away from cell poles, suggesting that MinD may be a target for Soj (Autret and Errington, 2003).

Hence, while having MinC and MinD in common, Gram-negative *E. coli* and Gram-positive *B. subtilis* rods appear to have significantly different mechanisms to control their subcellular localization and action. Interestingly, other bacilli such as *Caulobacter crescentus* and *Haemophilus influenzae* do not encode any Min proteins (Margolin, 2001a). In general, Gram-positive organisms lack *minE*, with the exception of *Clostridia* bacilli, which seem to encode MinC, MinD, MinE, *and* DivIVA in their genomes (Errington *et al.*, 2003). Interestingly, Gram-positive cocci, including *Staphylococcus aureus*, *Streptococcus pneumoniae*, and *Enterococcus faecalis*, do not have any Min proteins, despite retaining *divIVA* homologues (Margolin, 2001a; Massidda *et al.*, 1998; Ramirez-Arcos *et al.*, manuscript in preparation). Therefore, it is likely that several other mechanisms for regulating cell division site selection exist in different groups of bacteria.

In contrast to Gram-positive cocci, the Dillon laboratory has identified homologues to all three *min* genes in the Gram-negative coccus *Neisseria gonorrhoeae* (Ramirez-Arcos *et al.*, 2001a). The presence of these genes in a round bacterium was intriguing, particularly since Min protein functions have been well documented in rod-shaped bacteria, which have obvious cell poles and midcells. In addition, gonococcal cells divide along two perpendicular dimensions, in stark contrast to

the single division plane inherent to bacilli. Hence, *N. gonorrhoeae* was selected as a model organism to study the role of Min proteins in coccal sytems.

1.4. Current state of knowledge of cell division in the coccus *Neisseria gonorrhoeae*

1.4.1. The Gram-negative organism *N.gonorrhoeae*

Neisseria gonorrhoeae (Ng) is a Gram-negative coccus that is the causative agent of the sexually transmitted disease gonorrhea, perhaps the most reported communicable disease worldwide. The World Health Organization (1995) estimated that there are approximately 62 million reported cases of gonorrhea annually worldwide, although the actual number of infections is likely much higher due to asymptomatic infections. *N. gonorrhoeae* is an obligate human pathogen. The primary site of infection in males is the urethra, characterized by a painful urethral discharge. Gram-staining of this discharge invariably reveals the presence of Gram-negative diplococci found within polymorphonuclear neutrophils (Howard, 1994). Women typically experience endocervical infections; however, asymptomatic carriage of the disease is more common in females, making infection seem less obvious. If left untreated, the disease can ascend into the uterus and fallopian tubes and cause pelvic inflammatory disease (Howard, 1994). Persistent pain in the abdomen results and damage to the fallopian tubes may lead to ectopic pregnancy and infertility. Newborns can also acquire gonorrhea in their eyes as they pass through an infected birth canal. Rare cases of systemic infection have also been reported, leading to arthritis, endocarditis, and meningitis (Howard, 1994). Gonococcal infection, as well as infection with other bacterial sexually transmitted diseases (e.g. chlamydia), has also been linked to an increase in HIV transmission (Wasserheit, 1992). It is believed that genitial inflammation and lesions caused by STDs may accommodate HIV transmission from person to person (Holmes, 1994; Sparling *et al.*, 1994).

N. gonorrhoeae infects by adhering to and invading mucosal epithelial surfaces (Merz and So, 2000). The binding of gonococcal type IV pili and other adhesins can affect host cell signalling and stimulate bacterial ingestion. This is followed by transcytosis of bacteria to the basolateral surface, where they are released to the underlying tissue (Dehio *et al.*, 2000; Merz and So, 2000). To avoid the host immune system, the surface antigens of *N. gonorrhoeae*, including pilin subunits, opacity (Opa) proteins, and lipooligosaccharide (LOS) are extremely variable (Merz and So, 2000).

Such antigenic variation can be achieved through several mechanisms, including genetic recombination between multiple gene copies and slipped-strand mispairing (Kline *et al.*, 2003). To date, gonococcal surface variability has confounded the development of any successful vaccine.

1.4.2. Morphological analyses of dividing *N. gonorrhoeae*

The coccus *N. gonorrhoeae* exhibits cell division along two planes, resulting in the formation of a tetrad of daughter cells (Westling-Häggström *et al.*, 1977) (see also Figure 1.7 A, D). This differs from rod-shaped *E. coli* where cell division occurs along a single plane, resulting in two progeny cells (Nanninga, 1998). Analysis of gonococcal cell cultures invariably reveals the presence of single cocci, diplococci, and cells arranged in tetrads (Figure 1.7 A). By observing gonococci on agar slides, others have found that they grew in at least two dimensions, first expanding perpendicular to the initial division plane followed by growth along a second dimension that is parallel to the existing septum (Westling-Häggström *et al.*, 1977).

Using transmission electron microscopy, the earliest visible event of gonococcal cell division appeared to be a constriction that is more pronounced on one side of the coccus than the other (Fitz-James, 1964) (see also Figure 1.7 B). At the tip, or apex, of this constriction, extension of the inner membrane could be visualized forming ahead of the growing cell wall septum (Fitz-James, 1964; Westling-Häggström *et al.*, 1977); hence, the initial constriction serves as a marker for the plane of impending division (Fitz-James, 1964). Furthermore, as division proceeds, the growing constrictions did not appear to have any close association with chromosomal material (Fitz-James, 1964).

Although inner membrane constriction results in two separated gonococcal cell compartments, the completion of cell wall synthesis is delayed; hence, daughter cells remained attached to one another, resulting in a high proportion of diplococci (Fitz-James, 1964). Cell division along a second, perpendicular plane follows and is also characterized by an ingrowth of cytoplasmic membrane enclosing a peptidoglycan fold. This invagination occurs at the diplococcal cell junction

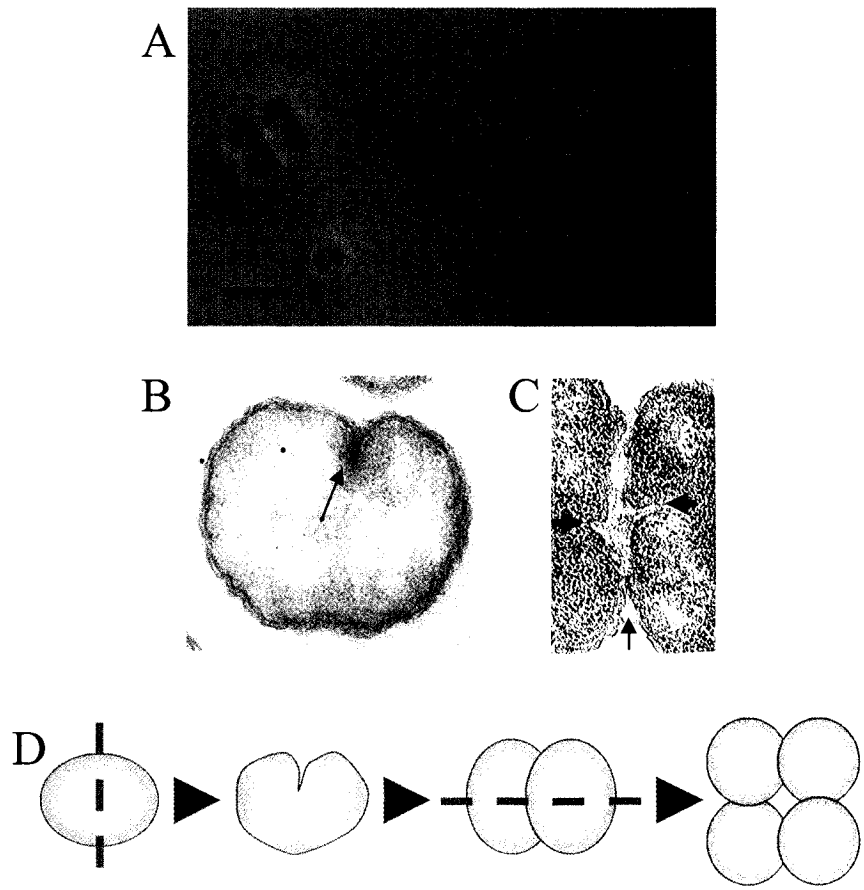

Figure 1.7. Cell division patterns in wild-type *N. gonorrhoeae*. (A) Differential interference contrast (DIC) image of wild-type *N. gonorrhoeae* CH811 cells showing single, diplococcal, and tetrad arrangements of cells. Bar indicates 2 μm length. (B) Transmission electron micrograph of *N. gonorrhoeae* CH811 cell at the start of cell division, showing initial invagination at one side of the coccus. (C) Transmission electron micrograph of secondary division planes (green arrows) initiating perpendicular to the original plane (black arrow) (figure obtained from Westling-Häggström *et al.*, 1977). Note the new constrictions occur at the diplococcal junction. (D) Schematic showing the perpendicularly alternating division pattern characteristic of *N. gonorrhoeae.*

(Figure 1.7 C, green arrows) and at a right angle to the first septum (Figure 1.7 C, black arrow; Westling-Häggström *et al.*, 1977), such that four cells result in a two-by-two (tetrad) arrangement (Figure 1.7 A, D).

The physical separation of gonococcal cells from each other may be partly mediated by the product of the *tpc* (tetrapac) gene (Fussenegger *et al.*, 1996). Disruption of *tpc* results in >95% of cells exhibiting a tetrad arrangement, instead of the usual diplococcal and single cell morphologies. Electron microscopic analysis of these mutants revealed that they shared continuous outer membrane, with the two diplococci interconnected by a double murein layer; hence, it is believed that *tpc* encodes a murein hydrolase that acts after septation to facilitate cell separation (Fussenegger *et al.*, 1996).

1.4.3. Identification and characterization of the *dcw* cluster of *N. gonorrhoeae*

Using raw data from the *N. gonorrhoeae* strain FA1090 genome project (Roe *et al.*, 2001), the *dcw* cluster of *N. gonorrhoeae* was identifed and assembled (Francis *et al.*, 2000). This gene cluster contained 17 genes in the following 5' to 3' order: *mraZ, mraW, ftsI (penA), murE, hyp1, murF, mraY, hyp2, murD, ftsW, murG, murC, ddl, ftsQ,, ftsA, ftsZ,* and *hyp3* (Francis *et al.*, 2000). Overall, the organization of the gonococcal *dcw* genes was similar to that found in the *E. coli dcw* cluster.

In *E. coli*, *ftsL* is located between *mraW* and *ftsI*; however, the putative protein encoded in this same region in *N. gonorrhoeae* had low similarity (22% at the amino acid level) to *E. coli* FtsL, hence *ftsL* was not included in this analysis of the gonococcal *dcw* cluster (Francis *et al.*, 2000). A subsequent Neisserial *dcw* cluster analysis by another group did include *ftsL* as part of this gene cluster (Snyder *et al.*, 2001). Three hypothetical genes, *hyp1, hyp2,* and *hyp3* were also identified between *murE-murF, mraY-murD,* and following *ftsZ,* respectively (Francis *et al.*, 2000). The *hyp1* gene, also named *dca* (division cluster associated), likely encodes an inner membrane protein that is

essential for DNA uptake by *N. gonorrhoeae* (Snyder *et al.*, 2001); however, the functions of the remaining *hyp* genes are currently unknown (Francis *et al.*, 2000).

Co-transcription of all the gonococcal *dcw* genes does not occur, since four transcriptional terminators were identified in the gene cluster and shown to be functional by RT-PCR strategies (Francis *et al.*, 2000). Three of these terminators consisted of inverted repeats of the gonococcal uptake sequence (5'-GCCGTCTGAA-3'), previously shown to be required for gonococcal DNA transformation and to act as transcriptional terminator sequences (Goodman and Scocca, 1988; Francis *et al.*, 2000). These uptake sequence repeats were located at the junctions between *mraY-hyp2*, *murD-ftsW*, and *murG-murC* genes. A novel transciptional terminator consisting of a Correia element, a repetitive sequence commonly found in *Neisseria* species, was also found to act as a transcriptional terminator between *murF* and *mraY* (Francis *et al.*, 2000). However, there is conflicting evidence for the role of this Correia element, as others studying the *dcw* clusters of *N. gonorrhoeae*, and the closely related *N. meningitidis*, have shown that the Correia element does not act to terminate transcription within the *dcw* cluster (Snyder *et al.*, 2003).

1.4.4. Gonococcal FtsZ

The gonococcal *ftsZ* gene was previously identified using raw data from the *N. gonorrhoeae* FA1090 genome project (Salimnia *et al.*, 2000). Gonococcal FtsZ ($FtsZ_{Ng}$, 392 aa long, 41.5 kDa) shares high identity (95-98%) with FtsZ from *N. meningitidis*. The protein also has 67% and 65% similarity with FtsZ from *E. coli* and *B. subtilis*, respectively. All attempts to generate a *N. gonorrhoeae ftsZ* knockout were unsuccessful, indicating that FtsZ was likely essential for gonococcal survival (Salimnia *et al.*, 2000). $FtsZ_{Ng}$ is active across species and could inhibit cell division when overexpressed in wild-type *E. coli*. Furthermore, a GFP-$FtsZ_{Ng}$ fusion could localize to the midcell in *E. coli*, similar to *E. coli* FtsZ (Salimnia *et al.*, 2000). Overexpression of GFP-$FtsZ_{Ng}$ in *N. gonorrhoeae* from a shuttle vector resulted in the formation of aberrant cells that had multiple and atypically positioned division sites that separated the cell into small compartments. However, most of

the GFP fusion protein was insoluble and subcellular localization of FtsZ within the gonococcus was not possible (Salimnia *et al.*, 2000).

There are at least six promoters that may control the expression of $ftsZ_{Ng}$ (Francis *et al.*, 2000). Under conditions of anaerobiosis, the $ftsZ_{Ng}$ promoter region had a significantly higher expression level than under aerobic conditions. In particular, of the three promoters that are directly upstream of $ftsZ_{Ng}$, the most proximal, P_Z1, seems to be the most active under anaerobic conditions (Francis *et al.*, 2000; Ramirez-Arcos *et al.*, 2001b). In addition, the presence of urea led to a decrease in $ftsZ_{Ng}$ promoter region activity (Ramirez-Arcos *et al.*, 2001b). Hence, it is possible that *ftsZ* expression (as well as other gonococcal cell division genes) is regulated, in part, by environmental conditions that mimic the host genitourinary tract (Ramirez-Arcos *et al.*, 2001b).

1.4.5. Identification of *min* genes in *N. gonorrhoeae.*

The Dillon laboratory is the first group to identify and to investigate Min proteins from a naturally occuring coccus. Analysis of the raw data from the *N. gonorrhoeae* strain FA1090 genome project (Roe *et al.*, 2001), revealed the presence of *minC*, *minD*, and *minE* homologues (Ramirez-Arcos *et al.*, 2001a). The three gonococcal *min* genes ($minC_{Ng}$, $minD_{Ng}$, and $minE_{Ng}$) are part of a large 17 kilobase (kb) gene cluster (Figure 1.8) (GenBank accession number AF345908; Ramirez-Arcos *et al.*, 2001a). In contrast, the three *min* genes in *E. coli* are within a 1.7 kb gene cluster (Figure 1.8), while *minC* and *minD* of *B. subtilis* are contained in a 5 kb gene cluster (Figure 1.8). Included in the *N. gonorrhoeae min* cluster are genes for *rpoA* (α subunit of RNA polymerase), *secY* (secretion protien Y), IF1 (initiation factor 1) and 20 structural ribosomal genes upstream of *minCDE*, with *oxyR* (oxidative stress transcriptional regulator) situated downstream (Figure 1.8). All genes are transcribed in the same direction and are flanked by Neisserial uptake sequences (Figure 1.8) (Ramirez-Arcos *et al.*, 2001a). In addition, the closely related *N. meningitidis* also contains a *minCDE* cluster, with the *min* cluster from *N. meningitidis* Z2491/serotype A sharing 97% identity with that of the gonococcus (Ramirez-Arcos *et al.*, 2001a).

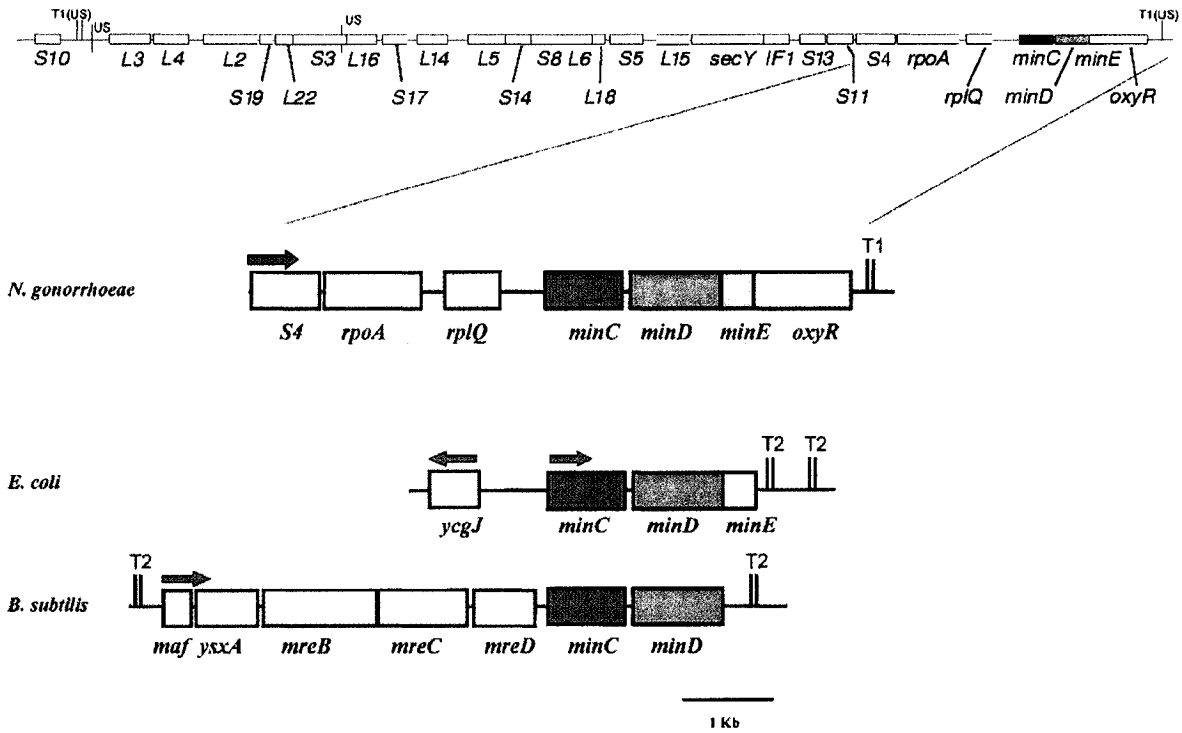

Figure 1.8. Comparison of *min* gene clusters from *N. gonorrhoeae*, *E. coli*, and *B. subtilis*. Gonococcal *minC*, *minD*, and *minE* homologues are part of a 17 kb gene cluster flanked by two neisserial uptake sequences (US) that can act as transriptional terminators (T1). *E. coli min* genes are found in a smaller 1.7 kb cluster, with rho-independent transcription terminator sequences (T2). *B. subtilis* contains *minC* and *minD* genes, but no *minE*. Arrows indicate direction of transcription (Figure from Ramirez-Arcos *et al.* 2001).

Within the *N. gonorrhoeae minCDE* cluster, $minC_{Ng}$ and $minD_{Ng}$ are separated by 28 bp, while $minD_{Ng}$ and $minE_{Ng}$ have only a 3 bp intergenic region (based on the distance between the stop codon of an upstream gene and the start codon of its downstream gene) (Ramirez-Arcos *et al.*, 2001a). Promoter regions for $minC_{Ng}$, $minD_{Ng}$, and $minE_{Ng}$ were also identified between *rplQ* and $minC_{Ng}$, at the 3' end of $minC_{Ng}$, and within the 3' half of $minD_{Ng}$, respectively (Ramirez-Arcos *et al.*, 2001b). Similar to the $ftsZ_{Ng}$ promoter region, $minC_{Ng}$ and $minD_{Ng}$ promoter regions are significantly more active under anaerobic conditions (Ramirez-Arcos *et al.*, 2001b).

1.4.6. Gonococcal MinC

Gonococcal MinC ($MinC_{Ng}$) is 237 aa in length (26.3 kDa) and is 36% and 22% identical to MinC from *E. coli* and *B. subtilis*, respectively. Deletion of *minC* in *N. gonorrhoeae* led to severe aberrations in cell morphology and cell division. Mutant cells appeared to have several planes of division resulting in the formation of multi-lobed compartments. In addition, there was significant evidence of cell lysis and cells devoid of intracellular contents (Ramirez-Arcos *et al.*, 2001a). Furthermore, the gonococcal *minC* mutant had significantly decreased cell viability (Ramirez-Arcos *et al.*, 2001a). $MinC_{Ng}$ is also active across species and inhibited wild-type *E. coli* cell division when overexpressed, causing the formation of long filamentous cells. The protein could also complement an *E. coli minC* mutant by restoring its ability to divide at midcell, further evidence of its cross species functionality (Ramirez-Arcos *et al.*, 2001a).

Based on sequence alignment of MinC proteins from various species, four completely conserved C-terminal glycine residues were identified (Ramirez-Arcos *et al.*, in press). Mutation of each of these residues in $MinC_{Ng}$ and in $MinC_{Ec}$ resulted in inactive proteins which were unable to arrest cell division in *E. coli* backgrounds. From yeast two-hybrid analyses, it was determined that glycines corresponding to $MinC_{Ec}$ G135, G154, and G171 are involved in MinC-MinD interaction, and that G161 was implicated in MinC dimerization. Each mutation was subsequently mapped onto the triangular β-helix surfaces (A, B, C) that form the C-terminus of the solved *T. maritima* MinC

crystal structure. This revealed that glycines at, or near, the B/C surface junction of MinC are implicated in MinD binding, while the single glycine within the A surface is involved in MinC dimerization (Ramirez-Arcos *et al.*, in press). Using molecular modeling, it was proposed that the exposed conserved glycines within the B/C surfaces junction of MinC may interact with exposed residues of the α-7 helix in MinD (Ramirez-Arcos *et al.*, in press) (α-7 helix of *A. fulgidus* MinD is indicated in Figure 1.3 B, arrow).

In addition, N-terminal truncation studies with $MinC_{Ng}$ revealed that the thirteenth amino acid is required for the ability of the protein to inhibit cell division. While the extreme N-terminus of MinC is not conserved across species, there may be conserved structural motifs that are important for protein function (Greco, 2004).

1.4.7. Gonococcal MinE

Studies with *N. gonorrhoeae* MinE ($MinE_{Ng}$) have also been initiated. Expression studies in *E. coli* indicate that this protein can disrupt cell division site, resulting in minicell formation (Eng and Dillon, unpublished results), similar to overexpression of *E. coli* MinE (de Boer *et al.*, 1989). Analytical ultracentrifugation of $MinE_{Ng}$ showed the protein could self-associate, existing in a monomer-dimer-tetramer equilibrium (Dillon laboratory, unpublished results), similar to *E. coli* MinE (Zhang *et al.*, 1998). Yeast two-hybrid assays also detected a $MinD_{Ng}$-$MinE_{Ng}$ interaction (see Chapter 5, this study); hence truncations to both the N- and C-termini of $MinE_{Ng}$ were constructed to delineate the minimum $MinD_{Ng}$-binding region of the protein (see Appendix, this study).

$MinE_{Ng}$ is currently being studied by another doctoral student in the Dillon laboratory. Sequence alignment of MinE proteins from various organisms revealed several highly conserved residues which were mutated to assess their functionality. These studies have indicated that residues within the N-terminus of $MinE_{Ng}$, specifically A18D and L22D, are required for interaction with $MinD_{Ng}$. As a result, these $MinE_{Ng}$ mutant proteins are unable to affect *E. coli* cell division (Eng and Dillon, unpublished results).

1.5. Rationale and Hypothesis of this study

Cytokinesis is a crucial event common to all lifeforms, including bacteria. From detailed studies in rod-shaped bacteria, it is evident that bacteria possess elaborate mechanisms to specify the localization of cell division sites. Bacteria exist in a number of morphologies, including rods, spirals, and round cells. While it is clearly established that Min proteins have a role in regulating proper septum placement in both Gram-negative and Gram-positive rod-shaped bacteria, comparatively little is known about how this is achieved in cells with other morphologies.

Since cell division is such a crucial event, components of the bacterial cell division machinery and their associated proteins can also provide promising targets for the development of new antimicrobials. This is especially important since bacteria are constantly acquiring resistance to our limited antibiotic arsenal. *N. gonorrhoeae* is a prime example of such developed resistance.

While gonorrhea is treatable with antibiotic therapy, *N. gonorrhoeae* has a well documented history of developing antibiotic resistance. The first treatment of gonorrhea used sulfonamide drugs to which gonococcal resistance developed quickly, prompting the use of penicillin as the primary therapy. By the 1970s and 1980s, resistance to penicillin developed through chromosomally-mediated mechanisms and the acquisition of penicillinase-producing plasmids which effectively terminated the use of this antibiotic to treat gonorrhea (Dillon and Yeung, 1989). High levels of resistance to tetracycline have also developed, mediated by the *tetM* determinant on a conjugative plasmid (Morse *et al.*, 1986; Roberts, 1988). Multidrug resistant strains of *N. gonorrhoeae* also contain the *mtr* (multiple transferable resistance) locus, which encodes components for an energy-dependent drug efflux pump (Hagman *et al.*, 1995) and confers resistance to a range of antimicrobials including erythromycin, tetracycline, chloramphenicol, rifampicin, and penicillin (Maness and Sparling, 1973; Hagman *et al.*, 1995; Shafer *et al.*, 1995; Veal *et al.*, 1998). Currently, gonococcal infections are treated with third generation cephalosporins (e.g. ceftriaxone) and fluoroquinolones (e.g. ciprofloxacin). Unfortunately, the adaptive nature of *N. gonorrhoeae* constantly challenges antibiotic therapy, such that resistance to current antimicrobials is now reported (Fox and Knapp, 1999).

The presence of these *minC*, *minD*, and *minE* genes in the gonococcus is intriguing, since these genes are already established to encode cell division site-determinants in rod-shaped bacteria. Since all three *min* genes are found in *N. gonorrhoeae,* it is possible that a functional Min system exists to direct septum placement in this round bacterium. Studies with $MinC_{Ng}$ have demonstrated that it is likely involved in determining proper cell division sites in *N. gonorrhoeae* (Ramirez-Arcos *et al.*, 2001). The high conservation of MinD across bacterial species also suggests that this protein is required to maintain the proper cell division pattern in a variety of bacteria, including round cells. **It is hypothesized that $MinD_{Ng}$ is involved in regulating the characteristic division pattern of the coccus *N. gonorrhoeae* and that the protein achieves this through interactions with the other Min proteins.**

These studies will help gain insight into the mechanisms that bacteria, other than rods, use to achieve proper cell division. In addition, due to the ever-increasing prevalence of antibiotic resistant bacteria, what can be learned from studying cell division processes in these organisms can ultimately be applied to the development of novel antimicrobials and therapies for treating bacterial infections.

1.6. Objectives

The present study will determine whether *N. gonorrhoeae* MinD is involved in cell division site selection in the gonococcus. In addition, functional regions of $MinD_{Ng}$ will be identified and characterized to better elucidate its role. Collectively, these studies will be used to generate a model for topological regulation of cell division site placement in *N. gonorrhoeae*. In order to achieve this, the following objectives are proposed:

a) To establish whether MinD is involved in maintaining the characteristic division pattern of the gonococcus by using gene disruption, mutation, and overexpression studies in *N. gonorrhoeae.*

b) To investigate the use of *E. coli* as an indicator system for $MinD_{Ng}$ functionality to further elucidate the role of this protein. This will be achieved by heterologous expression studies of $MinD_{Ng}$ in rod-shaped and round mutant *E. coli* strains, coupled with examination of cell morphology and protein localization studies using GFP-fusions.

c) To characterize functional regions within $MinD_{Ng}$ using various genetic and biochemical strategies, including yeast two-hybrid analyses, site-directed mutagenesis, gene truncations, and protein techniques.

d) To use the culmulative data from these studies to develop a model for Min function in coccal cell division, using *N. gonorrhoeae* as a model organism.

CHAPTER 2

GENERAL MATERIALS AND METHODS

The following protocols outline methods that were common to most, or all, of the studies in this project. In addition, Tables describing strains and DNA primers used in this project are also included in this chapter. More specific Materials and Methods, as well as plasmids for each particular study, are described in their respective chapters.

2.1. General protocols and methods

Strains and growth conditions. The strains used in this study are presented in Table 2.1. *E. coli* strains DH5α and XLI-Blue were used as hosts for DNA cloning. *N. gonorrhoeae* CH811 was used to generate gonococcal $minD_{Ng}$ mutant strains CJSD1 and SCD-1, and to provide chromosomal DNA template for PCR amplifications. *N. gonorrhoeae* F62 was used for min_{Ng} gene overexpression studies in the gonococcus. *N. gonorrhoeae* CH811 and F62 were grown on GC medium base (Difco) supplemented with Kellogg's defined supplement (GCMBK) for 18 to 24 hours at 35°C in a humid, 5% CO_2 environment (Kellogg *et al.,* 1963; Pagotto *et al.,* 2000). Liquid cultures of *N. gonorrhoeae* were grown in GCMBK containing 0.04% $NaHCO_3$, incubated at 35°C with 5% CO_2 and shaking at 200 rpm.

E. coli strains PB103, DR105 ($minC_{Ec}$), PB104 ($minD_{Ec}$), WM1032 ($\Delta minCDE_{Ec}$), PB114 ($\Delta minCDE_{Ec}$), and KJB24 (*rodA*) (Table 2.1) were used in $MinD_{Ng}$ expression and localization studies. *E. coli* PB103 was also used to provide chromosomal DNA for PCR amplification of *E. coli minD* ($minD_{Ec}$) and *minC* ($minC_{Ec}$). *E. coli* GM48 (*dam*) was used to provide unmethylated plasmid DNA necessary for construction of the *N. gonorrhoeae* $minD_{Ng}$ insertional mutant CJSD1 (Table 2.1). *E. coli* M15 and *E. coli* BL21 (DE3) were used as expression strains for the purification of N-terminal His-tagged $MinC_{Ng}$ (His-$MinC_{Ng}$) and His-$MinD_{Ng}$, respectively. *E. coli* C41 (DE3) (Table 2.1) was used to overexpress C-terminal His-tagged $MinD_{Ng}$ ($MinD_{Ng}$-His) proteins. *E. coli* C43 (DE3) (Table 2.1) was also used to overexpress N-terminal His-tagged $MinC_{Ng}$. *E. coli* strains WM1032 and PB114 were used for localization of GFP-$MinD_{Ng}$ fusions (Table 2.1). *E. coli* strains were grown at 37°C in

Table 2.1. Strains and plasmids used in this study

Strains	Relevant genotype	Source/Reference
E. coli DH5α	*supE44 ΔlacU169 (80lacZΔM15) hsdR17 endA1 gyrA96 thi-1 relA1*	Gibco
E. coli XLI-Blue	*recA1 endA1 gyrA96 thi-1 hsdR17 supE44 relA1 lac* [F' *proAB lacI*^{q} *ZΔM15* Tn*10* (Tet^r)]	Stratagene
N. gonorrhoeae CH811	Auxotype (A)/serotype (S)/plasmid content (P) class: nonrequiring/IB-2/plamid-free, Str^r	Picard and Dillon (1989)
N. gonorrhoeae CJSD1	*N. gonorrhoeae* CH811 Str^r *minD*::Cm^r	This study
N. gonorrhoeae SCD-1	*N. gonorrhoeae* CH811 Str^r Cm^r $minD_{K16Q}$	This study
N. gonorrhoeae F62	Auxotype (A)/serotype (S)/plasmid content (P) class: proline/IB/2.6	West and Clark (1989)
E. coli PB103	*dadR1 trpE61 trpA62 tna-5 purB*$^+$	de Boer *et al.* (1988)
E. coli DR105	*zcf-117*::Tn*10/dadR1 trpE61 trpA62 tna-5 minC3 tetR*	P. de Boer, Case Western Reserve University
E. coli PB104	*dadR1 trpE61 trpA62 tna-5 purB*$^+$ *λ*$^-$ *minD1*	de Boer *et al.* (1988)
E. coli WM1032	MG1655 *lacU169 ΔminCDE::kan*	Sun and Margolin (2001)
E. coli PB114	*dadR1 trpE61 trpA62 tna-5 purB*$^+$ λ$^-$ *ΔminCDE aph* (Kan^r)	de Boer *et al.* (1988)
E. coli KJB24	W3110 [*rodA* (*Am*)]	Begg and Donachie (1998)
E. coli GM48	*thr-1 ara-14 leuB6 fhuA31 lacY1 tsx-78 supE44 galT22 galK2 λ*$^-$ *dcm-1 dam-3 thi-1*	Marinus (1973)
E. coli M15	Nal^S Str^S Rif^S *lac*$^-$ *ara*$^-$ *gal*$^-$ *mtl*$^-$ *F*$^-$ *reca*$^+$ *uvr*$^+$ *lon*$^+$ pREP4	Qiagen
E. coli BL21(DE3)	*F*$^-$ *dcm ompT hsdS$_B$* (r^-_B m^-_B) *gal λ* (DE3)	Stratagene

E. coli C41(DE3)	*F⁻ ompT hsdSB* (r^-_B m^-_B) *gal dcmD(srl-recA)* 306::Tn10 (Tet^r) (DE3)	Miroux and Walker (1996)
E. coli C43 (DE3)	*F⁻ ompT hsdSB* (r^-_B m^-_B) *gal dcmD(srl-recA)* 306::Tn10 (Tet^r) (DE3)	Miroux and Walker (1996)
S. cerevisiae SFY526	*trp 1-901 leu2-3 112 can^r gal4-542 gal80-538 URA3::GaL1$_{UAS}$-GAL1$_{TATA}$-lacZ*	Clontech
Plasmids		
pET30a	P_{T7}:: 6XHis (Kan^R)	Novagen
pJSHD2	pET30a; P_{T7}:: 6XHis-*minD*$_{Ng}$ (Kan^R)	This study
pQE30	P_{T5} ::6XHis (Amp^R)	Qiagen
pJSHC	pQE30; P_{T5} ::6XHis-*minC*$_{Ng}$ (Amp^R)	This study
pEC1	pET30a; P_{T7}:: *minE*$_{Ng}$-6XHis (Kan^R)	This study

Luria-Bertani (LB) medium (Difco), except for *E. coli* strains WM1032 and PB114, which were grown at 30°C. Frozen stocks of all bacterial strains were stored at -70°C in brain heart infusion broth (Difco) supplemented with 20% glycerol.

When required, antibiotics were added to media in the following concentrations: 100 μg ampicillin (Amp)/ml, 25 μg chloramphenicol (Cm)/ml, and 100 μg kanamycin (Kan)/ml for *E. coli*; and 1 mg streptomycin (Str)/ml, 5 μg Cm/ml, and 75 μg (Kan)/ml for *N. gonorrhoeae*.

Saccharomyces cerevisiae SFY526 (Table 2.1) was used in yeast two-hybrid assays to study protein-protein interactions. Yeast were grown at 30°C on YPAD media, or on the appropriate synthetic dropout (SD) media, as described by the Clontech Yeast Two-Hybrid Protocols Manual (Clontech). Frozen stocks of yeast were stored at -70°C in YPAD media (Clontech Yeast Protocols Handbook) supplemented with 20% glycerol.

Oligonucleotide primers and PCR. Oligonucleotide primers used for PCR amplification (Table 2.2) were designed using Primer Designer Software (Scientific and Education Software). All primers were synthesized at the Core DNA Sequencing and Synthesis Facility, University of Ottawa. Whole cell suspensions of *N. gonorrhoeae* CH811 or *E. coli* PB103 (Table 2.1) were used to provide chromosomal DNA template for PCR by diluting cells in deionized distilled water (ddH_2O). Cell concentrations were adjusted to 0.5 McFarland Equivalence Turbidity Standard (Remel). Where required, plasmid DNA to be used as PCR template was adjusted to 0.01 μg/ml.

PCR reactions were carried out in a Perkin Elmer Gene Amp PCR System 9600 Thermocycler (Perkin Elmer Corp.) as follows: 3 minutes at 94°C; 30 cycles of 15 s at 94°C, annealing for 15 s at temperatures dependent upon the primer pair used, extension at 72°C for times dependent on expected product size, and a final 5 minutes extension at 72°C. Reactions were carried out in a final volume of 100 μl containing: 1X PCR buffer with 1.5 mM $MgCl_2$, 0.2 mM dNTPs, 0.2

Table 2.2. Primers used in this study

Primers are listed in alphabetical order

Primer	Sequence (5'-3')	Encoded mutation or truncation (in bold)	Restriction site (underlined)
A1	GCGCGAATTCATGGAACAGCAGTAAAGAT		*Eco*RI
A2[1]	GCGCGGATCCTCAATCCACCGCTTCAATC		*Bam*HI
CJ1	GCGCAAGCTT*GCCGTCTGAA*CTTTCTCATAGCTCACGCTG[2]		*Hind*III
CJ3	GCGCGAATTCTAATGGCAATCGCAAATTA		*Eco*RI
DJ1	GCTTCCCAGACTCGCGAT**GCC**GACGCTTTGACAC	$MinD_{Ng\text{-}K94A}$	*Nru*I
DJ2	GCATCGCAAACA**TTATTAATC**GATGCCCTCACCC	$MinD_{Ec\text{-}loop}$ (R92L, D93L, K94I)	*Vsp*I
DJ3[1]	CGGCAGAATATAGAGATTTTC		---
DJ26[1]	GCGCCTGCAGGGTACCATGGAATTCATATG*GCCGTCTG AA*ATTCTTAGAAAAACTCATCG[2]		*Pst*I, *Kpn*I, *Nco*I, *Eco*RI, *Nde*I
EcMinC-up	GCGCGAATTCATGTCAAACACGG		*Eco*RI
EcMinC-down[1]	GCGCGGATCCTCAATTTAACGGTTGAACGGG		*Bam*HI
EcMinD-up	GCGCGAATTCATGGCACGCATTATTGTTGT		*Eco*RI
EcMinD-down[1]	GCGCGGATCCTTATCCTCCGAACAAGCGTT[b]		*Bam*HI
ESminE1	GCGCCATATGTCATTGATCGAACTT		*Nde*I
ESminE2[1]	GCGCCTCGAGTACCTTTTTCTGTTC		*Xho*I
HLC1	CGTTAACCGAGTCTCATTCTTCGAACGCG		*Hind*III
Hmcat1	TGCTCACTTTGTGCTGGTGTCCCTGTTGATA		---
Hmcat2[1]	TCGTCACTTTGTGTTCTGCCATTCATCC		---
JSC1	GCGCGGATCCGGTTATATAATGAATGCCT		*Bam*HI
JSC2[1]	GCGCCTGCAGCAAACAATTACTCTGAG		*Pst*I
JSD2[1]	GCGCCTGCAGACCTTATCCTCCGAACAGA		*Pst*I
JSDATP1	GGT**CAG**ACGACTACCAGTGCAAGT	$MinD_{Ng\text{-}K16Q}$	*Hpy*188IX
JSDATP5[1]	GACACCGCCCTTGCCTGAAGTTAC		---
JSE2[1]	GCGCCTGCAGCATGTCCTATACCTTTTTC		*Pst*I

JSminE7	GCGCGAATTCCTTTTATTCGGTAGAAAGC		*Eco*RI
JSminE8	GCGCGAATTCCAGAAAACGGCAACCGTTG		*Eco*RI
JSminE9[1]	GCGCGGATCCTTCCGGCAAAGTAATGTTC		*Bam*HI
JSminE10[1]	GCGCGGATCCCATACCATCCTGCTTTTCT		*Bam*HI
min10	GCGCCTGCAGATGATGGTTTATATAAT		*Pst*I
min11[1]	ATGTGGTACCCTGATTGACGGCAAAGA		*Kpn*I
min12	GCGCGCGAATTCATGATGGTTTATATAAT		*Eco*RI
min15[1]	GCGCGGATCCATGATGGTTTATATAATGA		*Bam*HI
min21	CCTCTAGTCGACCCGTCAGTAGCTGAACA		---
min22[1]	ATGCCTGTCGACCATTTGAGAAGCACACG		---
min29[1]	GCGCGGATCCCAAACAATTACTCTGAGCC		*Bam*HI
min40	ACCTTAACCGAATTGCGGT		---
min40rev[1]	CATGTCCTATACCTTTTTC		---
minD1	GCGCGAATTCGTGGCAAAAATTATTGTAG		*Eco*RI
minD2[1]	GCGCGGATCCACCTTATCCTCCGAACAGA		*Bam*HI
minD3[1]	GCGCGGATCCGTTTTATATCCGCGTAATG		*Bam*HI
minD4[1]	GCGCGGATCCCACGTTCGGGAGAATAACG		*Bam*HI
minD5	GCGCGAATTCACTGCGGTAATTGATTTTG		*Eco*RI
minD6	GCGCGAATTCCCCGAACGTGTGGCAAAAG		*Eco*RI
minD7	GCGCGAATTCATTGTAGTAACTTCAGGCA		*Eco*RI
minD7pet30	CATGCCATGGTGGTGGCAAAAATTATTGTAG		*Nco*I
minD8	GCGCGAATTCAGTGCAAGTATTGCAACAG		*Eco*RI
minD9[1]	GCGCGGATCCCTCGCCCAAAAGACGGGCA		*Bam*HI
minD9B[1]	GCGCGGATCC**TTA**CTCGCCCAAAAGACGGGC	$MinD_{Ng\text{-}21aaCT}$[3] (stop codon in bold)	*Bam*HI
minD10[1]	GCGCGGATCCGCTGTCCTGATGGATGACC		*Bam*HI
minD10B[1]	GCGCGGATCC**TTA**GCTGTCCTGATGGATGAC	$MinD_{Ng\text{-}38aaCT}$ (stop codon in bold)	*Bam*HI
minD11B	GCGCGAATTC**GTG**ATTGTAGTAACTTCAGGC	$MinD_{Ng\text{-}4aaNT}$[4] (start codon in bold)	*Eco*RI
minD12B	GCGCGAATTC**GTG**AGTGCAAGTATTGCAACAG	$MinD_{Ng\text{-}19aaNT}$ (start codon in bold)	*Eco*RI

MinD-N2	GCGCGAATTC**GTG**AAAATTATTGTAGTAAC	$MinD_{Ng\text{-}2aaNT}$ (start codon in bold)	*Eco*RI
MinD-N3	GCGCGAATTC**GTG**ATTATTGTAGTAACTTC	$MinD_{Ng\text{-}3aaNT}$ (start codon in bold)	*Eco*RI
minE1	GCGCGAATTCATGTCATTGATCGAACTTT		*Eco*RI
minE2[1]	GCGCGGATCCCATGTCCTATACCTTTTTC		*Bam*HI
minE3[1]	GCGCGGATCCCTTGGGCAATGATGATTTG		*Bam*HI
minE4[1]	GCGCGGATCCGAAACATTCACATATTTGG		*Bam*HI
minE5	GCGCGAATTCGAGCGCGCCCAAGAAGGTC		*Eco*RI
minE6	GCGCGAATTCGTTTCATTAGACAATATCC		*Eco*RI
minE11	GCGCGAATTCGCAACCGTTGCCCGCGACC		*Eco*RI
minE12	GCGCGAATTCGCCCGCGACCGCCTTCAAA		*Eco*RI
minE13[1]	GCGCGGATCCCTGCTTTTCTTGGGAAATA		*Bam*HI
minE14[1]	GCGCGGATCCTTCGGAAATACGGATATTG		*Bam*HI
penA1	GCGCGAATTCATGTTGATTAAAAGCGAAT		*Eco*RI
penA2[1]	GCGCGGATCCGATTAAGACGGTGTTTTGA		*Bam*HI
SA2[1]	GCGTGTCAAAGCGTCTTTATCCCG		---
SA3	GAGGGCGTG**ATC**AAAGTGATGCAGGAG	$MinD_{Ng\text{-}E103I}$	*Bcl*I
SA5	GCGCGAATTCGTGGCA**GAG**ATATTGTAG	$MinD_{Ng\text{-}K3E}$	*Eco*RI
SA6	GCGCGAATTCGTGGCA**ATT**ATTATGTAG	$MinD_{Ng\text{-}K3I}$	*Eco*RI
SA7	GCGCGAATTCGTGGCA**GCA**ATTATTGTAG	$MinD_{Ng\text{-}K3A}$	*Eco*RI
SA8	GCGCGAATTCGTGGCAAAA**CAG**ATTGTAG	$MinD_{Ng\text{-}I4Q}$	*Eco*RI
SA10	GCGCGAATTCGTGGCAAAAATT**GAG**GTAGTAACTTC	$MinD_{Ng\text{-}I5E}$	*Eco*RI
SA11	GCGCGAATTCGTGGCAAAAATT**GCC**GTAGTAACTTC	$MinD_{Ng\text{-}I5A}$	*Eco*RI
SA12	GCGCGAATTCGTGGCAAAA**GAGGAG**GTAGTAACTTC	$MinD_{Ng\text{-}K3F}$	*Eco*RI
SA13	GCGCGAATTCGTGGCA**TTT**ATTATTGTAG	$MinD_{Ng\text{-}E103I}$	*Eco*RI
SA17	CATATGGCAAAAATT**GAG**GTAGTAACTTC	$MinD_{Ng\text{-}I5E}$	
SA18	CAT**ATG**ATTATTGTAGTAACTTC	$MinD_{Ng\text{-}3aaNT}$ (start codon in bold)	

SA19[1]	TATATCTCCTTCTTAAAG		
SJ1	GCTTCCCAGACT**TTATTAATC**GACGCTTTGACAC	$MinD_{Ng\text{-}loop}$ (R92L, D93L, K94I)	*Vsp*I
SJ2[1]	CGGCAAAATAAACAGGTTTTC		---
SJ3	GCGCCATATGGCAAAAATTATTGTAG		*Nde*I
SJ4[1]	GCGCCTCGAGTCCTCCGAACAGACG		*Xho*I
Y1	GCGCGAATTCATGTTCAGCTTCTTCCGTC		*Eco*RI
Y2[1]	GCGCGGATCCTCAATCCAGCAGTGCGTCC		*Bam*HI
Z1	GCGCGAATTCATGGAATTGTTTACGACG		*Eco*RI
Z2[1]	GCGCGGATCCTTATTGTCTGAATTGTGT		*Bam*HI

[1] Denotes primer annealing to complementary strand.
[2] Gonococcal uptake sequence indicated in italics.
[3] 'CT' denotes truncation from the C-terminus.
[4] 'NT' denotes deletion of the designated number of amino acids (or codons) from the N-terminus, which are replaced with a start codon.

μg of each primer and 2.5 U *Taq* DNA polymerase (Boehringer Mannheim or Fermentas). In PCR reactions where *Vent* or *Pfu* DNA polymerase was used, the reactions conditions were modified as follows: 0.2 U *Vent* (New England BioLabs) or 2.5 U *Pfu* (Fermentas) polymerase and 1X PCR buffer (*Vent* or *Pfu*-specific buffer provided by manufacturers) in 100 μl final reaction volumes. When required to screen for $minD_{Ng}$ mutations encoded on plasmids carried by *E. coli*, colony PCR was carried out as follows: individual *E. coli* colonies were selected with a sterile toothpick and resuspended in 25 μl ddH_2O. 1.25 μl of this suspension was used to provide plasmid DNA template for a 25 μl final volume PCR reaction, with volumes of other reagents adjusted accordingly.

Agarose gel electrophoresis, plasmid isolation, and PCR amplicon purification. DNA was separated on 1-2 % agarose gels using Tris-acetate EDTA (TAE) buffer (40 mM Tris-acetate, 1 mM EDTA) run at 6 volts/cm. The gels were stained in 1 mg/L ethidium bromide solution and the DNA visualized under a UV illuminator and digital imaging system (Alpha Innotech). Plasmids were isolated from *E. coli* and *N. gonorrhoeae* using the Qiagen Miniprep Kit according to the manufacturer's instructions. PCR amplicons to be used in restriction digestion and cloning were purified using the Qiagen PCR Purification kit in order to remove residual salts and nucleotides.

***E. coli* transformation** Plasmids were transformed into *E. coli* according to standard $CaCl_2$ methods outlined in Sambrook *et al.* (1989).

Protein sequence alignment of MinD homologues. The *minD* gene sequences from various bacteria were obtained at the WIT web site (formerly http://wit.mcs.anl.gov/WIT2 and now http://www.genomesonline.org). BLAST searches for *minD* homologues in other organisms were carried out in their respective sequence databases provided by The Institute for Genomic Research (TIGR) website (http://www.tigr.org). Protein sequences of MinD homologues were also obtained

from completed genome projects available from TIGR. When required, translation of *minD* gene sequences was done using PCGene Software (Intelligenetics Inc.). Protein alignments were performed using ClustalW Version 1.8 software (http://dot.imgen.bcm.tmc.edu:9331/multi-align/multi-align.html) and alignments were visualized using BOXSHADE Version 3.21 (http://www.ch.embnet.org/software/BOX _form.html).

Construction and purification of His-MinD$_{Ng}$ and production of polyclonal anti-MinD$_{Ng}$ antisera. To purify MinD$_{Ng}$, the coding region of *minD*$_{Ng}$ was cloned in frame with an N-terminal 6XHis tag encoded in pET30a (Table 2.1) using primers minD7pet30 and minD2 that included *Nco*I and *Bam*HI sites, respectively (Table 2.2). The resulting fusion protein (His-MinD$_{Ng}$) would possess an N-terminal tag consisting of six histidine residues followed by a linker region (SSGLVPRGSGMKETAAAKFERQHMDSPDLGTDDDDKA) fused to the N-terminus of MinD$_{Ng}$. The plasmid was named pJSHD2 and was transformed into *E. coli* BL21 (DE3) for overexpression (Table 2.1).

A 250 ml log-phase culture of *E. coli* BL21 (DE3) carrying pJSHD2 was induced with 1 mM IPTG for 4 hours at 37°C and shaking at 250 rpm. Cells were harvested by centrifugation (5,000 X g for 10 minutes) (Sorvall RC 50) and stored at –20°C. Cells were resuspended in 12 ml binding buffer (prepared according to Novagen His-Bind protocols) containing 5 mM imidazole. Cells were redistributed to three tubes and each sample was sonicated eight times, for 30 seconds each time, with 1 minute intervals on ice (Fisher Scientific 60 Sonic Dismembrator). Lysed cells were then centrifuged at 100,000 X g for 30 minutes at 4 °C (Beckman L8-55M ultracentrifuge). Soluble protein extract was applied to a column with 3 ml of His-Bind resin (Novagen) and protein purification was carried out as described by the manufacturer using the following solutions (with the indicated changes in imidazole concentration): 30 ml of binding buffer (5 mM imidazole), 21 ml wash buffer 1 (20 mM imidazole), 18 ml wash buffer 2 (30 mM imidazole), 9 ml wash buffer 3 (60 mM imidazole), and 12 ml elution buffer (250 mM imidazole). Eluted protein was dialyzed overnight at 4°C against Buffer A

(20 mM Tris-HCl pH 7.5, 2 mM EDTA, 200 mM NaCl, 10% glycerol; final pH adjusted to pH 7.2). Protein identity was confirmed by Dr. P. Thibault, Institute of Biological Sciences, National Research Council of Canada, using MALDI-TOF mass spectrometry.

To prepare His-$MinD_{Ng}$ for rabbit immunization, the protein was eluted from SDS-PAGE gel fragments using the Model 422 Electroeluter (Bio-RAD) and concentrated using Centricon YM-10 (10,000 molecular weight cutoff) centrifuge devices. This protein was used to immunize female New Zealand white rabbits. Each immunization consisted of 80 μg of His-$MinD_{Ng}$ mixed with Gerbu adjuvant according to the manufacturer's instructions (GERBU Biotechnik). Two additional boosters were administered over three week intervals. Whole serum was obtained from rabbit blood as outlined in established protocols (Sambrook *et al.*, 1989). $MinD_{Ng}$ specific antisera was affinity-purified using immobilized His-$MinD_{Ng}$ on nitrocellulose membranes, as outlined previously (Koelle, 1998).

Construction and purification of His-$MinC_{Ng}$, and production of polyclonal anti-$MinC_{Ng}$ antisera. Using the primer pair JSC1/JSC2 (Table 2.2), incorporating *Bam*HI and *Pst*I restriction sites, respectively, *min*C_{Ng} was PCR amplified and cloned into pQE30 to produce pJSHC (Table 2.1), encoding a 6XHis tag fusion to the N-terminus of $MinC_{Ng}$ (His-$MinC_{Ng}$).

Plasmid pJSHC was transformed into *E. coli* M15 (Table 2.1) for expression of His-$MinC_{Ng}$. One litre of LB broth supplemented with 100 μg/ml Amp and 25 μg/ml Kan was inoculated with 20 ml of overnight culture of *E. coli* M15 (pJSHC). Cells were grown at 250 rpm for 1 hour at 37°C prior to the addition of IPTG to 1 mM concentration, followed by an additional 3 hours of growth. 750 ml of culture was pelleted and resuspended in 15 ml of 8 M urea lysis buffer (pH 8.0), as outlined in the QIAexpressionist Protocols booklet for protein purification (Qiagen), in preparation for purifying His-$MinC_{Ng}$ from inclusion bodies. After incubation for 20 minutes at room temperature, cells were centrifuged at 10,000 X g for 25 minutes (Sorvall RC 50) and the supernatant was mixed gently with

1 ml of Ni-NTA resin (Qiagen) for 1 hour at room temperature. Resin and supernatant were then loaded into a 5 ml Qiagen polypropylene column. The resin bed was washed with 8 ml pH 6.3 buffer, 1 ml pH 5.9 buffer, 1.5 ml pH 5.0 buffer, and denatured His-$MinC_{Ng}$ was eluted with 1.5 ml of pH 4.5 buffer according to the manufacturer's instructions (Qiagen). Purified protein was used to immunize female New Zealand white rabbits for the production of polyclonal anti-$MinC_{Ng}$ sera. Each immunization consisted of 20 μg of His-$MinC_{Ng}$ mixed with Gerbu adjuvant according to the manufacturer's instructions (GERBU Biotechnik). Three additional boosters, similar to the initial immunization, were administered over three week intervals. Antisera were fractionated with 70% NH_4SO_4 and concentrated 10 times to obtain antiserum rich in IgG (Hebert *et al.*, 1973). The antiserum was subsequently affinity purified by binding to immobilized His-$MinC_{Ng}$ on nitrocellulose membranes, as outlined previously (Koelle, 1998).

Construction and purification of $MinE_{Ng}$-His, and production of polyclonal anti-$MinE_{Ng}$ antisera. To obtain purified $MinE_{Ng}$, *minE*$_{Ng}$ was PCR amplified from gonococcal cell suspensions using primers ESminE1 and ESminE2 (Table 2.2), and cloned into the *Nde*I and *Xho*I restriction sites of pET30a above to form plasmid pEC1 (Table 2.1). *E. coli* C41 (DE3) was transformed with pEC1 and 0.4 mM IPTG was used to induce a 350 ml log phase culture for 2-3 hours at 250 rpm and 37°C. Cells were harvested and resuspended in four 8 ml volumes of 5 mM imidazole binding buffer, prepared according to Novagen His-Bind resin protein purification protocols. Resuspended cells were lysed by sonication (45 second bursts, repeated four times on ice) (Fisher Scientific 60 Sonic Dismembrator). Soluble cell supernatant was applied to a 3 ml His-Bind resin column which was washed with buffers containing increasing concentrations of imidazole (5 mM to 100 mM; Novagen protocols), and $MinE_{Ng}$-His was eluted with 250 mM imidazole buffer. Purified protein was dialyzed in Buffer B (50 mM Tris, 20 mM NaCl, 1 mM EDTA, pH 7.4). $MinE_{Ng}$-His was concentrated using Biomax-5 centrifugal filter columns with a 5000 Dalton molecular weight cutoff (Millipore). Purified $MinE_{Ng}$ protein was provided to Dr. John Webb, Department of Biochemistry, Microbiology, and

Immunology, University of Ottawa, to immunize mice for raising polyclonal anti-$MinE_{Ng}$ antisera according to his established protocols.

Protein analysis and Western blots. In general, whole cell extracts from *N. gonorrhoeae* and *E. coli* were prepared by resuspending cells in appropriate volumes of PBS (pH 7.4) (depending on the size of initial harvested pellets), followed by the addition of 5X SDS-PAGE loading buffer (15% ß-mercaptoethanol, 15% SDS, 1.5% bromophenol blue, 50% glycerol). Cell suspensions were boiled for 10 minutes and then centrifuged for 10 minutes at 10,000 X g (Sorvall MC 12V Microfuge). The supernatant fractions were recovered and separated by SDS-PAGE using 12% polyacylamide gels (15% polyacrylamide gels when studying $MinE_{Ng}$) prepared as outlined in Sambrook *et al.* (1989). SDS-PAGE was carried out using the Mini-PROTEAN II electrophoresis system (Bio-Rad). Prior to Western blotting, protein concentrations were standardized for each sample using densitometric analysis of resolved cell extracts. In general, after Coomassie blue staining of resolved cell extracts (Sambrook *et al.*, 1989), the intensities of several common protein bands in each sample were compared using densitometric analysis available on Alpha imager 1220 v5.04 software (AlphaEase™ version 5.00, Alpha Innotech Corp.). These comparisons were then used to adjust, and equalize, the amount of each protein sample that was to be resolved in a subsequent polyacrylamide gel to be used in Western blotting. The Mini Trans-Blot Electrophoretic Transfer Cell (Bio-Rad) was used for Western transfer onto Immobilon-P membranes (Millipore Corporation). Immobilon-P^{SQ} membranes were used when $MinE_{Ng}$ was to be detected by Western blotting. After protein transfer, membranes were blocked with 3% skim milk for one hour at room temperature.

Blots were probed for one hour at room temperature (anti-$MinD_{Ng}$ sera) or overnight at 4°C (anti-$MinC_{Ng}$, anti-$MinD_{Ng}$, or anti-$MinE_{Ng}$ sera). Anti-gonococcal MinD antisera was diluted 1:800, while anti-$MinC_{Ng}$ and anti-$MinE_{Ng}$ antisera were used at 1:100 in TTBS (50 mM Tris, 1.25 M NaCl, 0.05% Tween-20, pH 7.5). Blots were then washed 3 X 10 minutes in TTBS, followed by incubation

with goat anti-rabbit secondary antibody conjugated to alkaline phosphatase (Bio-Rad, 1:3000 dilution) when anti-$MinC_{Ng}$ or anti-$MinD_{Ng}$ was used as a primary antibody. Biotinylated goat anti-mouse antisera was used as a secondary (1:40,000; 2 hours room temperature; Sigma) for blots probed with anti-$MinE_{Ng}$ sera, followed by 2 hour incubation with Extravidin (1:150,000; Sigma). All blots were then washed with TTBS (3 X 10 minutes) and developed using the AttoPhos Plus kit (JBL Scientific INC). Where required, densitometric analysis was performed using the Alpha imager 1220 v5.04 (AlphaEase™ version 5.00, Alpha Innotech Corp.) to compare signal intensity levels.

Phase contrast microscopy. *N. gonorrhoeae* and *E. coli* cells to be examined by phase contrast microscopy were fixed with 0.2% glutaraldehyde and 6% formaldehyde, prior to adhesion for 30 minutes onto coverslips precoated with 0.01% polylysine. Coverslips were then washed gently with PBS buffer (pH 7.4) and placed onto a slide containing a drop of 50% glycerol and sealed. Samples were analyzed by phase contrast microscopy using a Zeiss Axioskop microscope under a 100X oil immersion lens. Images were collected using Northern Eclipse (Version 5.0) software. When required, differential interference contrast (DIC) imaging was performed using Olympus BX60 or BX61 microscopes equipped with DIC prisms.

Yeast-two hybrid assays. Prior to testing for protein-protein protein interactions, each yeast plasmid was transformed singly using the lithium acetate method (Clontech Yeast Two-Hybrid Manual) into the yeast reporter strain *S. cerevisiae* SFY526 (Table 2.1) to ensure that the GAL4 fusions could not activate the β-galactosidase reporter gene by themselves. Transformants carrying pGBT9-derived vectors were plated on SD –Trp media, while those carying pGAD424-derived plasmids were grown on SD –Leu. When testing for interacting proteins, double transformants were plated on SD -Leu/-Trp plates. All media were prepared as described in the Clontech Yeast two-hybrid manual (Clontech). β-galactosidase activities were initially assessed using colony-lift assays and X-gal substrate, as

described by Clontech. The relative strength of each interaction was determined by β-galactosidase activity assays using o-nitrophenyl β-D-galactopyranoside (ONPG) as a substrate, as described by Clontech. These liquid assays were performed at least twice, in duplicate, for each interaction.

CHAPTER 3

MinD and *Neisseria gonorrhoeae* cell division

Portions of this chapter were published in:

[**Szeto, J.**, Ramirez-Arcos, S., Raymond, C., Hicks, L. D., Kay, C. M., and Dillon J. R. (2001a). Gonococcal MinD affects cell division in *Neisseria gonorrhoeae* and *Escherichia coli* and exhibits a novel self-interaction. J. Bacteriol. *183*, 6253-6264.]

3.1 PURPOSE OF THIS STUDY

Virtually all of our present knowledge of bacterial cell division has been obtained from studies with rod-shaped organisms, such as *E. coli* and *B. subtilis* (Errington *et al.*, 2003). Normally, cytokinesis in these bacteria occurs at a midcell site that results in two equally sized daughter cells. In both rods, the Min proteins have been shown to be involved in determining the proper placement of the cell division site (de Boer *et al.*, 1989, Levin *et al.*, 1992, Errington *et al.*, 2003).

Homologues to *minC*, *minD*, and *minE* have been identified in the coccus *N. gonorrhoeae* (Ramirez-Arcos *et al.*, 2001a). Unlike rod-shaped bacteria, *N. gonorrhoeae* divides along two dimensions (Fitz-James, 1964; Westling-Häggström *et al.*, 1977). We have previously shown that deletion of *minC* will disrupt normal cell division in *N. gonorrhoeae* (Ramirez-Arcos *et al.*, 2001a). Studies in this chapter were performed to determine whether $MinD_{Ng}$ is also involved in maintaining the characteristic cell division pattern in the gonococcus. Here, it is shown that $minD_{Ng}$ disruption or mutation in *N. gonorrhoeae* leads to aberrant cell division and morphology, and reduces cell viability. Furthermore, overexpression of $MinD_{Ng}$ and $MinC_{Ng}$ together from a *N. gonorrhoeae-E. coli* shuttle vector, modified from a previous vector constructed in our laboratory (Pagotto *et al.*, 2000), could induce cell division arrest in *N. gonorrhoeae*. $MinD_{Ng}$ was found to reside in both cytosolic and membrane fractions of the gonococcus. The localization of the essential cell division protein FtsZ in *N. gonorrhoeae* was also carried out using immunoelectron microscopy. Overall, these studies demonstrate that $MinD_{Ng}$ is required to maintain proper cell division site placement in the coccus *N. gonorrhoeae*.

3.2. MATERIALS AND METHODS

Identification of the gonococcal *min* gene cluster. Our laboratory previously identified and cloned the *N. gonorrhoeae minCDE* cluster (Ramirez-Arcos *et al.*, 2001a) after analysis of the raw DNA sequence data from the *N. gonorrhoeae* FA1090 genome project (Roe *et al.*, 2001). The $minC_{Ng}$, $minD_{Ng}$, and $minE_{Ng}$ genes from *N. gonorrhoeae* strain CH811 (Table 2.1) were PCR amplified, cloned into plasmid pSR1 (Table 3.1), and sequenced (GenBank accession number AF345908) (Ramirez-Arcos *et al.*, 2001a).

Insertional knockout of chromosomal $minD_{Ng}$ in *N. gonorrhoeae* CH811. A chloramphenicol acetyltransferase (*cat*) cassette was inserted into the chromosomal $minD_{Ng}$ gene of *N. gonorrhoeae* strain CH811 by allelic exchange in order to disrupt $minD_{Ng}$ expression. Plasmid pSR1 (Table 3.1) was transformed into *E. coli* GM48 (*dam*) in order to obtain unmethylated plasmid DNA. This plasmid was digested at its unique *Bcl*I site near the 5' end of $minD_{Ng}$, 179 bp downstream from the translational start site of $minD_{Ng}$. The *cat* cassette from pACYC184 (Table 3.1) was PCR amplified using primers HMcat1 and HMcat2 (Table 2.2). Both the *cat* cassette and *Bcl*I-digested pSR1 were blunt-ended with T4 DNA polymerase (New England Biolabs) and ligated to form pJSDcat (Table 3.1). The presence and orientation of the *cat* insert in $minD_{Ng}$ was confirmed by PCR analysis and by DNA sequencing at the Core DNA Sequencing and Synthesis Facility, University of Ottawa. *N. gonorrhoeae* CH811 cells (Table 2.1) were transformed with pJSDcat to allow for insertional inactivation of $minD_{Ng}$ by homologous recombination as described previously (Janik *et al.*, 1976). The insertion of *cat* into *N. gonorrhoeae* CH811 chromosomal $minD_{Ng}$ was confirmed by PCR analysis. The resulting gonococcal $minD_{Ng}$ knockout was named *N. gonorrhoeae* strain CJSD1 (Table 2.1).

Growth studies. The effect of $minD_{Ng}$ disruption in the gonococcus was monitored by growth and viability studies. To ensure that equivalent numbers of *N. gonorrhoeae* CH811 and CJSD1 cells

Table 3.1 Plasmids used in this study

Plasmids	Relevant genotype	Source or reference
Plasmids for generating *N. gonorrhoeae minD*$_{Ng}$ mutant strains		
pSR1	P_{lac}:: *minC*$_{Ng}$, *minD*$_{Ng}$, *minE*$_{Ng,}$, *oxyR* (Amp^R)	Ramirez-Arcos *et al.* (2001a)
pACYC184	Cm^R *cat*	New England Biolabs
pJSDcat	pSR1; P_{lac}:: *minC*$_{Ng}$, *minD*$_{Ng}$::*cat*, *minE*$_{Ng,}$, *oxyR* (Amp^{R}Cm^R)	This study
pJATP1	pSR1; P_{lac}:: *minC*$_{Ng}$, *minD*$_{Ng\text{-}K16Q}$, *minE*$_{Ng,}$, *oxyR* (Amp^R)	This study
pJATP1CAT	pSR1; P_{lac}:: *minC*$_{Ng}$, *minD*$_{Ng\text{-}K16Q}$, *minE*$_{Ng,}$, *cat*, *oxyR* (Amp^{R}Cm^R)	This study
***N. gonorrhoeae* shuttle vectors**		
pFP10	Gonococcal shuttle vector containing *ori* from β-lactamase producing plasmid pJD5 (Cm^R)	Pagotto *et al.* (2000)
pFP20	pFP10 with *cat* removed, replaced with *aph(3')* (Kan^r gene from pET30a)	This study
pFP21	pFP20 + *minC*$_{Ng}$, *minD*$_{Ng}$, *minE*$_{Ng}$ (Kan^R)	This study
pFP22	pFP20 + *minC*$_{Ng}$ (Kan^R)	This study
pFP23	pFP20 + *minD*$_{Ng}$ (Kan^R)	This study
pFP24	pFP20 + *minE*$_{Ng}$ (Kan^R)	This study
pFP25	pFP20 + *minC*$_{Ng,}$, *minD*$_{Ng}$ (Kan^R)	This study

would be used in growth studies, the inocula were standardized as follows. First, to determine the number of colony-forming units (cfu)/ml of wild-type and mutant bacteria in overnight cultures, each strain was diluted 25-fold from overnight liquid GCMBK cultures to obtain an OD_{550} of 0.05. Ten-fold serial dilutions were performed to determine the numbers of cfu/ml that were present in each culture.

For growth studies, equivalent numbers of cells (1×10^6 cfu) from overnight cultures of *N. gonorrhoeae* CH811 and CJSD1 were used to inoculate 25 ml of liquid GCMBK, and cells were grown as outlined in Chapter 2 for a 13 hour time period. 1 ml of culture was removed at fixed times to measure absorbance at OD_{550} and was serially diluted in liquid GCMBK. 100 µl from selected dilutions were plated on GCMBK agar media supplemented with Str for *N. gonorrhoeae* CH811, or with Str and Cm for *N. gonorrhoeae* CJSD1. The plates were incubated for 24 hours prior to enumerating colonies, or for an additional 24 hours if the colonies were too small to be effectively counted. Growth studies were performed twice for each strain.

Creation of a chromosomal *minD*$_{Ng}$ (K16Q) point mutation in *N. gonorrhoeae*. Allelic exchange was used to replace the wild-type chromosomal *minD*$_{Ng}$ gene of *N. gonorrhoeae* with a *minD*$_{Ng}$ gene encoding a K16Q mutation in the Walker A ATP-binding motif of the protein. The *minD*$_{Ng}$ gene in plasmid pSR1 (Table 3.1) was mutated using an inverse PCR (IPCR) strategy. Primers JSDATP1, encoding a K16Q mutation and a *Hpy*188IX restriction site, and JSDATP5 (Table 2.2) were designed to anneal adjacent to each other and amplify in opposite directions using *Pfu* DNA polymerase (Fermentas). The resulting blunt-ended amplicon was phosphorylated using T4 polynucleotide kinase (New England BioLabs), re-circularized with T4 DNA ligase (Gibco), and transformed into *E. coli* DH5α. Colony PCR was used to amplify plasmid-encoded *minD*$_{Ng}$ genes that could be screened for the K16Q mutation by virtue of their ability to be cleaved by *Hpy*188IX. The resulting plasmid (containing *minC*$_{Ng}$, *minD*$_{Ng\text{-}K16Q}$, *minE*$_{Ng}$, and *oxyR*) was named pJATP1 (Table 3.1).

A *cat* cassette was inserted between $minE_{Ng}$ and *oxyR* in pJATP1 prior to transformation into *N. gonorrhoeae* CH811 (Table 2.1). This site for *cat* insertion was selected to avoid disrupting the *min* cluster, and would allow for selection of successful chromosomal recombinants. To do this, IPCR was carried out using primers min40 and min40rev (Table 2.2), annealing adjacent to each other at the intergenic region between $minE_{Ng}$ and *oxyR,* and amplifying in opposite directions. The resulting amplicon was blunt-ended using T4 DNA polymerase (New England BioLabs) and T4 polynucleotide kinase (PNK) (New England BioLabs). A *cat* cassette, PCR amplified from pACYC184 (Table 3.1) using primers min21 and min22 (Table 2.2), was also blunt-ended as above and ligated into the min40/min40rev amplicon, to produce plasmid pJATP1CAT (Table 3.1). PCR methods were used to determine that the orientation of the *cat* cassette was in the same direction as *minCDE* transcription.

Plasmid pJATP1CAT was transformed into *N. gonorrhoeae* CH811 as outlined previously (Janik *et al.*, 1976). PCR using various combinations of primer pairs that annealed both outside and inside of the recombination region was performed on selected recombinants to confirm that a double crossover had occurred. DNA sequencing confirmed the presence of the chromosomal mutation. The resulting gonococcal strain, containing chromosomal $minD_{Ng\text{-}K16Q}$ was named *N. gonorrhoeae* SCD-1 (Table 2.1).

Overexpression studies of min_{Ng} genes in *N. gonorrhoeae.* The Dillon laboratory has previously constructed a cloning vector, pFP10 (Table 3.1), capable of replicating within several hosts, including *N. gonorrhoeae* and *E. coli* (Pagotto *et al.*, 2000). This *N. gonorrhoeae-E. coli* shuttle vector was modified by replacing its resident *cat* cassette with a kanamycin resistance cassette and by the incorporation of additional restriction sites as follows. The kanamycin resistance cassette from pET30a (Table 3.1) was PCR amplified using the 5' primer CJ1 and the 3' primer DJ26 (Table 2.2). Each primer also contained a gonococcal uptake sequence (US) (Goodman and Scocca, 1988) to better facilitate the transformation of *N. gonorrhoeae* cells. CJ1 also incorporated a *Hin*dIII site, while DJ26 contained restriction sites for *Pst*I, *Kpn*I, *Nco*I, *Eco*RI, and *Nde*I (Table 2.2). The amplicon was

digested with *Pst*I and *Hind*III prior to ligation. pFP10 was also digested with *Pst*I and *Hind*III to eliminate the *cat* cassette, and the desired vector fragment was isolated from 1% agarose gels using the QIAquik gel extraction kit (Qiagen). The resulting pFP10 vector fragment and kanamycin resistance cassette were subsequently ligated to generate pFP20 (Table 3.1).

Gonococcal *min* genes and their upstream regions shown previously to have promoter activity (Ramirez-Arcos *et al.*, 2001b) were PCR amplified from *N. gonorrhoeae* cell suspensions and cloned separately, or in combination, into pFP20. Gonococcal *minC* and its 503 bp upstream region shown to possess promoter activity (Ramirez-Arcos *et al.*, 2001b) were PCR amplified using the primer pair CJ3/JSC2 (Table 2.2) which incorporated *Eco*RI and *Pst*I sites, respectively. The resulting amplicon was digested with *Eco*RI and *Pst*I and ligated into similarly digested pFP20, forming plasmid pFP22 (Table 3.1). The other min_{Ng} genes were also amplified with their respective upstream regions as follows. Gonococcal $minD_{Ng}$ was PCR amplified with primers min12 and JSD2 (Table 2.2). This amplicon included $minD_{Ng}$ and an upstream region consisting of the coding region of $minC_{Ng}$, shown to have promoter activity (Ramirez-Arcos *et al.*, 2001b). The $minE_{Ng}$ gene and a 720 base pair upstream sequence, also shown to possess promoter activity (Ramirez-Arcos et al. 2001b), was amplified with primers minD5 and JSE2 (Table 2.2). Both $minC_{Ng}$ and $minD_{Ng}$ were amplified together using primers CJ3 and JSD2 (Table 2.2). The entire $minCDE_{Ng}$ cluster was also amplified with primers CJ3 and JSE2. All amplicons were digested with *Eco*RI and *Pst*I and individually ligated into pFP20 as above to form pFP21 ($minC_{Ng}$, $minD_{Ng}$, $minE_{Ng}$), pFP23 ($minD_{Ng}$), pFP24 ($minE_{Ng}$), and pFP25 ($minC_{Ng}$, $minD_{Ng}$).

Each plasmid was transformed into *N. gonorrhoeae* F62 using a protocol modified from Seifert and So (1991). Frozen stocks of *N. gonorrhoeae* F62 were restreaked onto GCMBK agar, grown for 18 hours, and examined for T2 colonies (Juni and Heym, 1977). T2 colonies were resuspended to a 0.5 MacFarland Standard, in GCMBK broth supplemented with 10 mM $MgSO_4$. 20 µl of the bacterial suspension was diluted in 200 µl of the same broth and 0.5-1.0 µg of plasmid DNA was added. The cells were mixed gently and incubated at 35°C and 5% CO_2 for 30 minutes without

shaking, then transferred to a 15 ml Falcon tube containing 2 ml of GCMBK supplemented with 10 mM $MgSO_4$. Cells were incubated for an additional 5-6 hours with shaking (150 rpm) at 35°C and 5% CO_2. Afterwards, 100 µl of cells were plated onto kanamycin selective GCMBK agar (100 µg Kan/ml) and incubated at 35°C and 5% CO_2. The stability of each plasmid within the transformants was verified by plasmid isolation and DNA gel electrophoresis.

Transmission electron microscopy and immunogold localization studies. Transmission electron microscopy was performed on *N. gonorrhoeae* strains CH811 and CJSD1 (Table 2.1) in collaboration with Dr. T. Beveridge, University of Guelph, using general protocols as previously described (Beveridge *et al.*, 1994). *N. gonorrhoeae* F62 (Table 2.1) transformed with pFP20 (negative control vector) and pFP25 (*minC*$_{Ng}$, *minD*$_{Ng}$) (Table 3.1), and *N. gonorrhoeae* SCD-1 (Table 2.1) were fixed in 1.6% glutaraldehyde, sectioned, and examined by transmission electron microscopy according to protocols established at the Laboratory Pathology facilities, Ottawa Hospital, Civic Campus, Ottawa Hospital, Ottawa, ON.

The diameters of forty *N. gonorrhoeae* F62 cells transformed with pFP20 or pFP25 (Table 3.1) were measured from electron micrographs taken at the same magnification and average diameters at their widest points were calculated for both samples. Statistical analysis using the unpaired Student's *t*-test was applied to the averages, and differences were considered significant for *p* values <0.001.

Immunogold labelling of *N. gonorrhoeae* CH811 to localize $MinD_{Ng}$ or $FtsZ_{Ng}$ protein was also carried out according to protocols established at the Laboratory Pathology facilities, Ottawa Hospital, using affinity purified anti-$MinD_{Ng}$ antisera (this study) or affinity purified anti-$FtsZ_{Ng}$ antisera prepared previously in our laboratory (Salimnia *et al.*, 2000).

Separation of soluble and insoluble gonococcal cell fractions. *N. gonorrhoeae* CH811 cells were collected from solid GCMBK media and resuspended in 2 ml of PBS (pH 7.4). Cells were lysed by

sonication (Fisher Scientific 60 Sonic Dismembrator) using 3 cycles of four 5 second bursts, with a 1 minute time interval on ice between cycles. The cell extract was centrifuged at 100,000 x g for 1 hour at 4°C (Beckman TL-100 ultracentrifuge) and the soluble supernatant was retained. The insoluble pellet was washed twice with 2 ml PBS and resuspended in 2 ml PBS. Protein concentrations for both soluble and insoluble fractions were determined using the Bio-Rad Protein assay kit and similar amounts of protein from each fraction were resolved by SDS-PAGE and used for Western blotting to detect $MinD_{Ng}$.

3.3. RESULTS

MinD proteins are highly conserved. The *minD* gene is the most ubiquitously distributed of the three *min* genes, with homologues being found in Gram-negative and Gram-postive bacteria, in chloroplasts, and in Archaea (Margolin, 2001). MinD from *N. gonorrhoeae* ($MinD_{Ng}$; 271 aa) is 73% identical and 85% similar to *E. coli* MinD ($MinD_{Ec}$), and is 42% identical and 66% similar to *B. subtilis* MinD ($MinD_{Bs}$).

Alignment of *N. gonorrhoeae* MinD from strain FA1090, used in the genome project (Roe *et al.*, 2001), with the deduced amino acid sequences of 23 other MinD homologues from various organisms shows regions of extensive conservation distributed throughout the protein, particularly the N-terminal half of the protein (corresponding to amino acids 1-166 of $MinD_{Ng}$) (Figure 3.1). All MinD proteins analyzed also have a conserved Walker A ATP-binding motif, corresponding to residues 10-17 of $MinD_{Ng}$ (GKGGVGKT) (Figure 3.1; residues underneath red line). The overall consensus sequence of this motif is G**K**GG[T/V]GK[T/S]. The MinD Walker A motif can be classified as a part of the 'deviant' subgroup of such motifs by virtue of the signature lysine (shown in bold) found at the N-terminus of the sequence (Koonin, 1993). Both *N. gonorrhoeae* and *N. meningitidis* MinD also contain a sequence at their extreme C-termini (KSFFKRLF) (Figure 3.1, residues underneath green line), which is nearly identical to the membrane targeting sequence (MTS) identified in *E. coli* MinD (KGFFKRLF) (Szeto *et al.*, 2002; Hu and Lutkenhaus, 2003). In addition, bacterial MinD proteins contain switch I and switch II sites, implicated in nucleotide-induced conformational changes (Vale, 1996), which have also been identified in Archaeal MinD structures (Cordell and Löwe, 2001; Sakai *et al.*, 2001) (Figure 3.1, residues underneath black lines).

There are only two nucleotide differences between *minD* from *N. gonorrhoeae* strain FA1090 (used in the genome project), and from strain CH811 (used in this study). In strain CH811, base number 479 is a cytosine, while in strain FA1090 the nucleotide is an adenine. In either case, the respective GGC and GGA codons still encode glycine at amino acid residue 160. Strain CH811 $minD_{Ng}$ also has a guanine nucleotide at base number 702, resulting in a

Figure 3.1. Sequence alignment of MinD proteins from various species. Abbreviations used: *Methanococcus janaaschii* (Mj), *Archaeoglobus fulgidus* (Af), *Pyrococcus furiosus* (Pf), *P. horikoshii* (Ph), *Neisseria gonorrhoeae* (Ng) strain FA1090, *N. meningitidis* (Nm), *Escherichia coli* (Ec), *Salmonella enterica* serovar Typhimurium (St), *Yersinia pestis* (Yp), *Vibrio cholerae* (Vc), *Pseudomonas aeruginosa* (Pa), *Brucella melitensis* (Bm), *B. suis* (Bsui), *Agrobacterium tumefaciens* (At), *Helicobacter pylori* (Hp), *Aquifex aeolicus* (Aa), *Thermotoga maritima* (Tm), *Bacillus subtilis* (Bs), *Listeria monocytogenes* (Lm), *Clostridium perfringens* (Cp), *Synechocystis sp.* (Sy), *Guillardia theta* (Gt), *Deinococcus radiodurans* (Dr), and *Chlamydia trachomatis* (Ct). Black boxes indicate amino acid residues that are identical to the consensus. Gray boxes indicate amino acids that are similar to the consensus. Single red bar indicates position of the deviant Walker A ATP-binding motif. Black bars indicate positions of switch I and II sites. Single green bar indicates MinD membrane targeting sequence (MTS) (Szeto *et al.*, 2002; Hu and Lutkenhaus, 2003). Short coloured bars adjacent to organism names indicate their general classification: green = Archaea, red = Gram-negatives, orange = Thermophilic bacteria, blue = Gram-positives, black = cyanobacteria, violet = chloroplast, grey = Chlamydiae. (*) indicates residue 235 (threonine) of *N. gonorrhoeae* MinD FA1090, which is appears as an alanine residue in *N. gonorrhoeae* CH811 MinD.

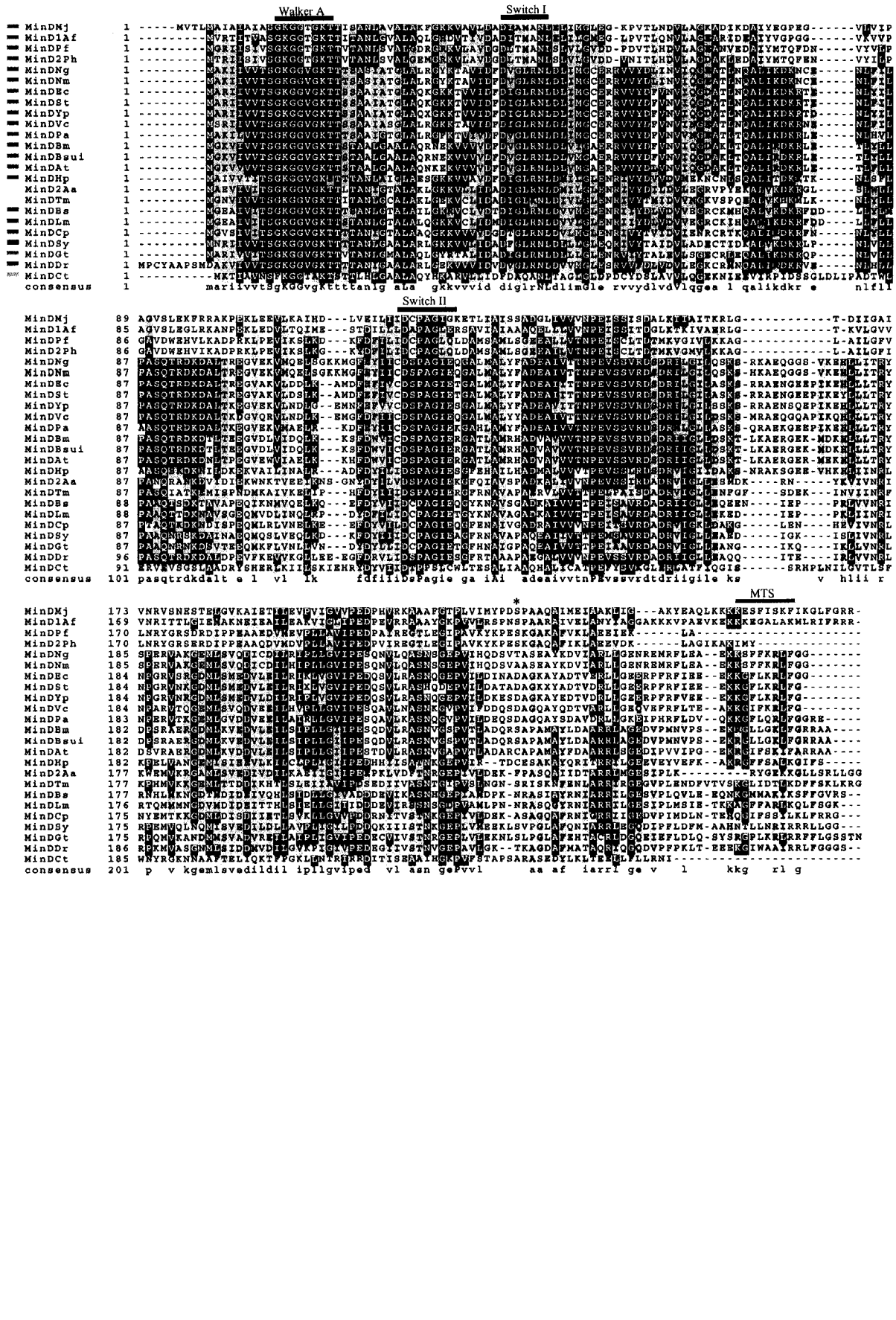
Walker A
Switch I
Switch II
MTS
MinDMj
MinD1Af
MinDPf
MinD2Ph
MinDNg
MinDNm
MinDEc
MinDSt
MinDYp
MinDVc
MinDPa
MinDBm
MinDBsui
MinDAt
MinDHp
MinD2Aa
MinDTm
MinDBs
MinDLm
MinDCp
MinDSy
MinDGt
MinDDr
MinDCt
consensus

GCG codon encoding alanine at residue 235 of its $MinD_{Ng}$. In this unconserved gene region, strain FA1090 contains an ACG codon encoding threonine at residue 235 (Figure 3.1, asterisk), instead of an alanine.

Disruption of *minD*$_{Ng}$ results in aberrant gonococcal cell division and morphology and decreases cell viability. To determine whether *minD*$_{Ng}$ is involved in maintaining proper cell division patterns in the gonococcus, the gene was disrupted using a homologous recombination strategy to insert a *cat* cassette near the 5' end of chromosomal *minD*$_{Ng}$ in *N. gonorrhoeae* CH811 (Table 2.1). PCR analysis and DNA sequencing showed that the *cat* insert was in the opposite orientation of transcription of *minD*$_{Ng}$. Using affinity purified anti-$MinD_{Ng}$ polyclonal antisera, Western blot analysis of cell extracts from wild-type *N. gonorrhoeae* CH811 (Figure 3.2 F, lane 1) and the *minD* knockout strain, CJSD1, (lane 2) showed no $MinD_{Ng}$ expression in the latter strain.

Under phase-contrast microscopy, *N. gonorrhoeae* CJSD1 exhibited cells of varying sizes which were often clustered together and showed signs of lysis (Figure 3.2 B), while wild-type *N. gonorrhoeae* CH811 cells displayed uniform size and shape (Figure 3.2 A). Closer inspection of *N. gonorrhoeae* CJSD1 by electron microscopy revealed grossly abnormal cell morphologies, characterized by irregularly shaped cells and the presence of lysed cells devoid of intracellular contents (Figure 3.2 D, E). Furthermore, septum formation resulted in unequally sized cells. These observations contrast the typical, uniform diplococcal morphology of wild-type *N. gonorrhoeae* CH811 (Figure 3.2 C).

The growth of *N. gonorrhoeae* CJSD1 was also compared to its parental wild-type strain in liquid cultures. The number of colony forming units (cfu)/ml of *N. gonorrhoeae* CJSD1 was higher than that of wild-type *N. gonorrhoeae* CH811 for approximately the first 6 hours, but subsequently became significantly less than that of wild-type for the following 7 hours (Figure 3.3 A). In addition, the mutant strain appeared to reach stationary phase after approximately 6 hours, which was 4-5 hours sooner than wild-type, as assessed by viable counts (Figure 3.3 A). Wild-type colonies were easily

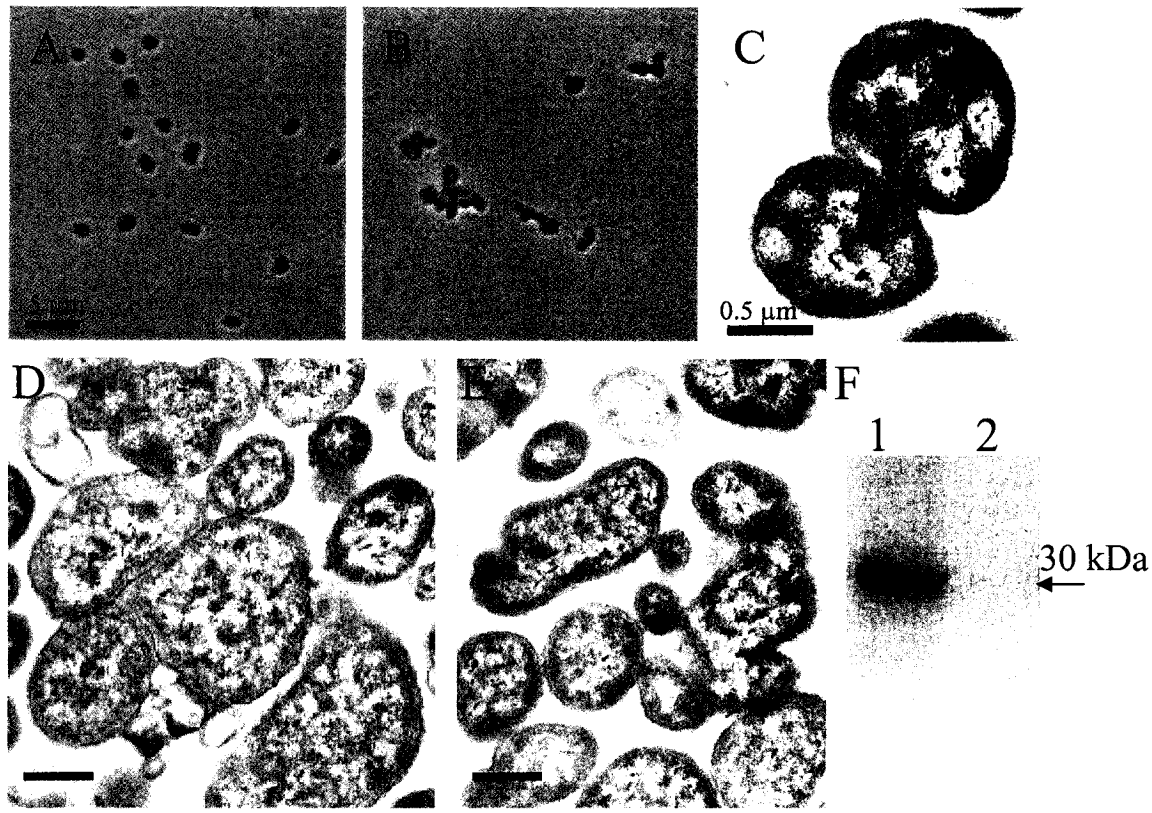

Figure 3.2. Effects of insertional inactivation of *minD* on the cell morphology of *N. gonorrhoeae* CH811. Phase contrast micrographs of wild-type *N. gonorrhoeae* CH811 (A) and *N. gonorrhoeae minD* knockout mutant, CJSD1 (B). Both (A) and (B) are at the same magnification and the scale bar in (A) represents 5 μm. (C) Transmission electron microscopy shows the typical diplococcal morphology of *N. gonorrhoeae* CH811. (D and E) Electron micrographs of *N. gonorrhoeae* CJSD1 showing aberrant cell morphologies, including cells of varying sizes and cells devoid of intracellular contents. Scale bars in (C, D and, E) represent 0.5 μm. (F) Western blot analysis of cell extracts using affinity-purified anti-$MinD_{Ng}$ antisera show the expression of $MinD_{Ng}$ in *N. gonorrhoeae* CH811 (lane 1), but not in *N. gonorrhoeae* CJSD1 (lane 2).

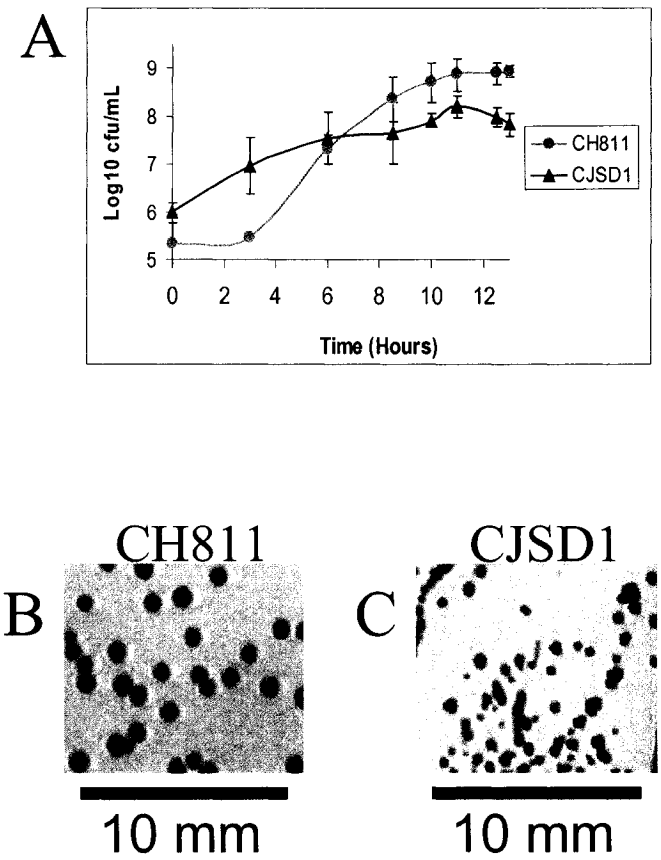

Figure 3.3. Cell viability of wild-type *N. gonorrhoeae* strain CH811 and $minD_{Ng}$ knockout strain CJSD1. (A) Comparison of the viability of wild-type *N. gonorrhoeae* CH811 (circles) and *minD* knockout CJSD1 (triangles) based on colony forming units (cfu)/ml counts of each strain grown in GCMBK broth over 13 hours. (B) Wild-type *N. gonorrhoeae* CH811 colonies appeared 18-24 hours after plating from broth to solid media and displayed uniform size, while CJSD1 colonies (C) were not readily visible until 42-48 hours, and appeared smaller. Both (B) and (C) display colonies at the same magnification.

visualized and counted after the normal incubation time of 18-24 hours; however, *N. gonorrhoeae* CJSD1 colonies did not appear until after 42-48 hours. Furthermore, once these colonies became visible, they were always variable in size, especially with the appearance of many tiny colonies (Figure 3.3 C). In contrast, *N. gonorrhoeae* CH811 colonies were much larger after only a single day of incubation, and were of uniform size (Figure 3.3B).

In addition to the insertional $minD_{Ng}$ knockout mutant, a second gonococcal mutant was generated to express $MinD_{Ng}$ bearing a glutamine substitution at the extremely conserved lysine-16 residue of the Walker A-ATP binding motif. The same mutation in *E. coli* MinD was shown to render the protein unable to induce cell division arrest in those cells (de Boer *et al.*, 1991). *N. gonorrhoeae* SCD-1, encoding $minD_{Ng\text{-}K16Q}$ in place of wild-type $minD_{Ng}$ (Table 2.1), showed aberrant morphology similar to strain CJSD1, including cells that possessed multiple invaginations (Figure 3.4 B, arrows), suggestive of multiple cell division events, as well as cells that had varying shapes and sizes (Figure 3.4 C, D). These morphologies were in contrast to the round diplococci typically seen in wild-type *N. gonorrhoeae* (Figure 3.4 A). Western blotting verified the expression of wild-type $MinD_{Ng}$ in *N. gonorrhoeae* CH811 (Figure 3.4 E, lane 1) and $MinD_{Ng\text{-}K16Q}$ in *N. gonorrhoeae* SCD-1 (Figure 3.4 E, lane 2).

Hence, the effects of abrogating $MinD_{Ng}$ expression, or replacing wild-type $minD_{Ng}$ with a gene containing a mutated Walker A ATP-binding motif, suggests that the protein is involved in maintaining proper cell division, cell morphology, and viability of the gonococcus.

Overexpression of $MinD_{Ng}$ and $MinC_{Ng}$ together in *N. gonorrhoeae* causes cell enlargement. Our laboratory has previously constructed a unique shuttle vector capable of replicating in *N. gonorrhoeae*, *E. coli*, and *Haemophilus* species (Pagotto *et al.*, 2000). To determine the effects of overexpressing gonococcal Min proteins in their native background, the shuttle vector pFP10 (Table 3.1) (Pagotto *et al.*, 2000) was first modified to include more restriction sites for cloning purposes, additional gonococcal uptake sequences to aid transformation, and a kanamycin resistance cassette.

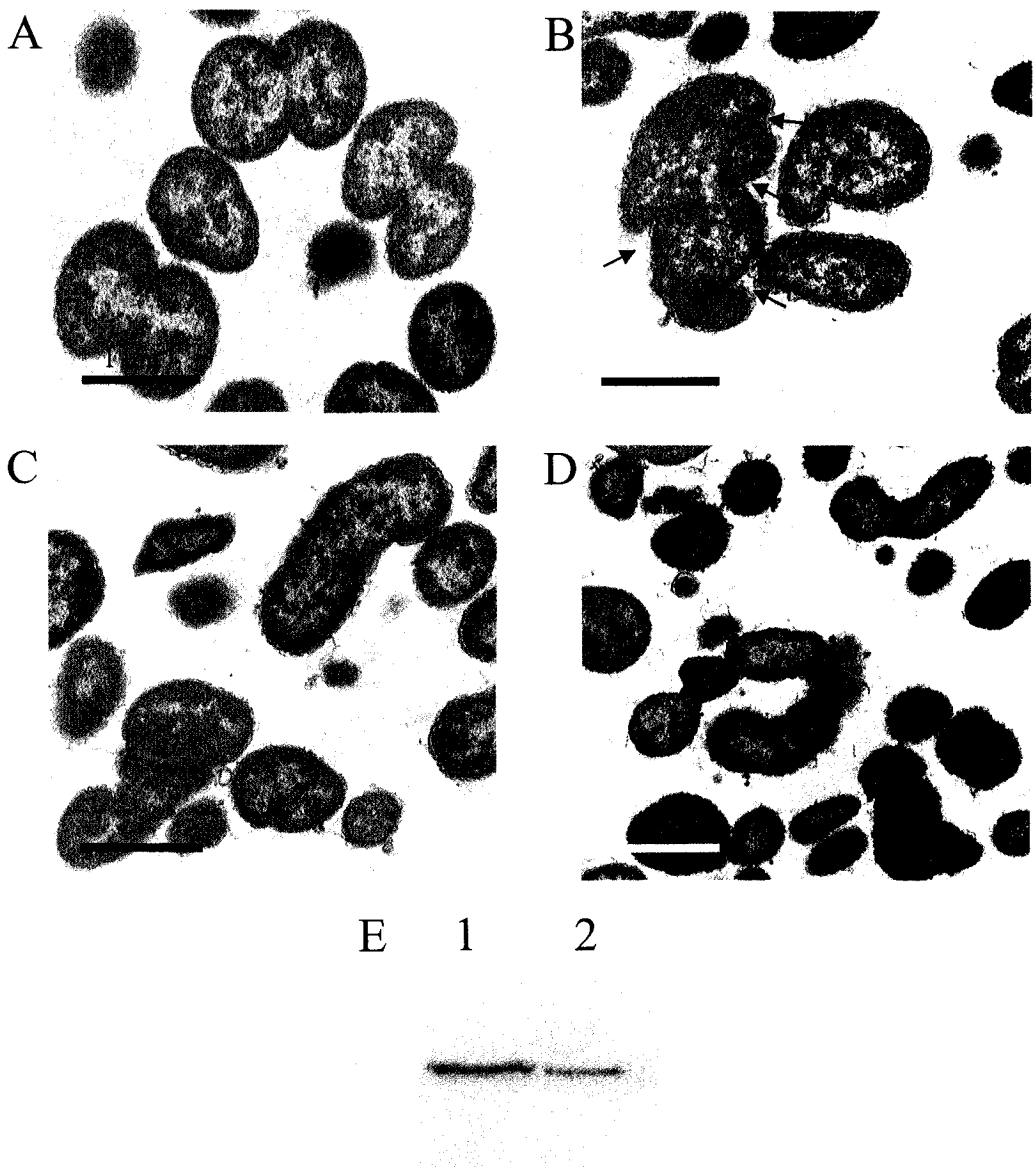

Figure 3.4. Transmission electron micrographs of wild-type *N. gonorrhoeae* CH811 and mutant SCD-1 encoding $MinD_{Ng\text{-}K16Q}$. (A) *N. gonorrhoeae* CH811 shows typical, round gonococcal morphology. (B, C, and D) Aberrant morphology is displayed by strain SCD-1, including multiple invaginations (arrows). Scale bar represents 1 μm in all figures. (E) Wild-type (lane 1) and mutant (lane 2) $MinD_{Ng}$ protein expression is confirmed in both strains by Western blotting with anti-$MinD_{Ng}$ antisera.

Each min_{Ng} gene was cloned individually, or in combination with the other min_{Ng} genes, into the new shuttle vector, pFP20 (Table 3.1).

Attempts to transform the shuttle expression vectors into the plasmid-free strain *N. gonorrhoeae* CH811 (Table 2.1) were unsuccessful. Interestingly, *N. gonorrhoeae* F62 (Table 2.1), which naturally carries a 4.2 kb cryptic plasmid found in many gonococcal strains (Roberts *et al.*, 1979), could be transformed with each of the shuttle vectors including pFP20 (negative control vector), pFP21 ($minC_{Ng}$, $minD_{Ng}$, $minE_{Ng}$), pFP22 ($minC_{Ng}$), pFP23 ($minD_{Ng}$), pFP24 ($minE_{Ng}$), and pFP25 ($minC_{Ng}$, $minD_{Ng}$) (Table 3.1). The cell morphologies of each transformant were examined by phase contrast microscopy. Gonococci transformed with the unmodified pFP20 vector exhibited a typical, uniform, round shape and cell diameters of ~1 μm or less (Figure 3.5 A). Cells transformed with pFP21, pFP22, pFP23, and pFP24 did not exhibit any noticeable morphological changes from the control, as assessed by phase contrast microscopy (Figure 3.5 B-E). However, transformants carrying pFP25, encoding both $minC_{Ng}$ and $minD_{Ng}$, exhibited obvious cell enlargement, with some cells having over twice the diameter of control cells (Figure 3.5 F-G, arrows).

Western blotting using affinity purified anti-$MinC_{Ng}$ antisera showed that gonococcal cells transformed with pFP21 ($minC_{Ng}$, $minD_{Ng}$, $minE_{Ng}$), pFP22 ($minC_{Ng}$), and pFP25 ($minC_{Ng}$, $minD_{Ng}$) had 4, 2, and 2 times, respectively, the level of $MinC_{Ng}$ (Figure 3.5 I; lanes 2, 3 and 6) found in negative control cells transformed with pFP20 (lane 1). $MinC_{Ng}$ levels in pFP23 ($minD_{Ng}$) and pFP24 ($minE_{Ng}$) transformants (lanes 4 and 5) resembled that in the control (lane 1).

When cell extracts were probed with affinity purified anti-$MinD_{Ng}$ antisera, cells transformed with pFP21 ($minC_{Ng}$, $minD_{Ng}$, $minE_{Ng}$) (Figure 3.5 J, lane 2) had approximately twice the amount of $MinD_{Ng}$ detected in negative control cells (lane 1). *N. gonorrhoeae* transformed with pFP25 ($minC_{Ng}$, $minD_{Ng}$) also had increased $MinD_{Ng}$ levels to ~1.2 times the control (Figure 3.5 J, lane 6). All other transformants did not have increased levels of $MinD_{Ng}$ (Figure 3.5 J, lanes 3, 4, and 5).

The ability of *N. gonorrhoeae* F62 to maintain the shuttle vectors was confirmed by plasmid isolation followed by gel electrophoresis of the isolated DNA. In addition to the cryptic plasmid (4.2

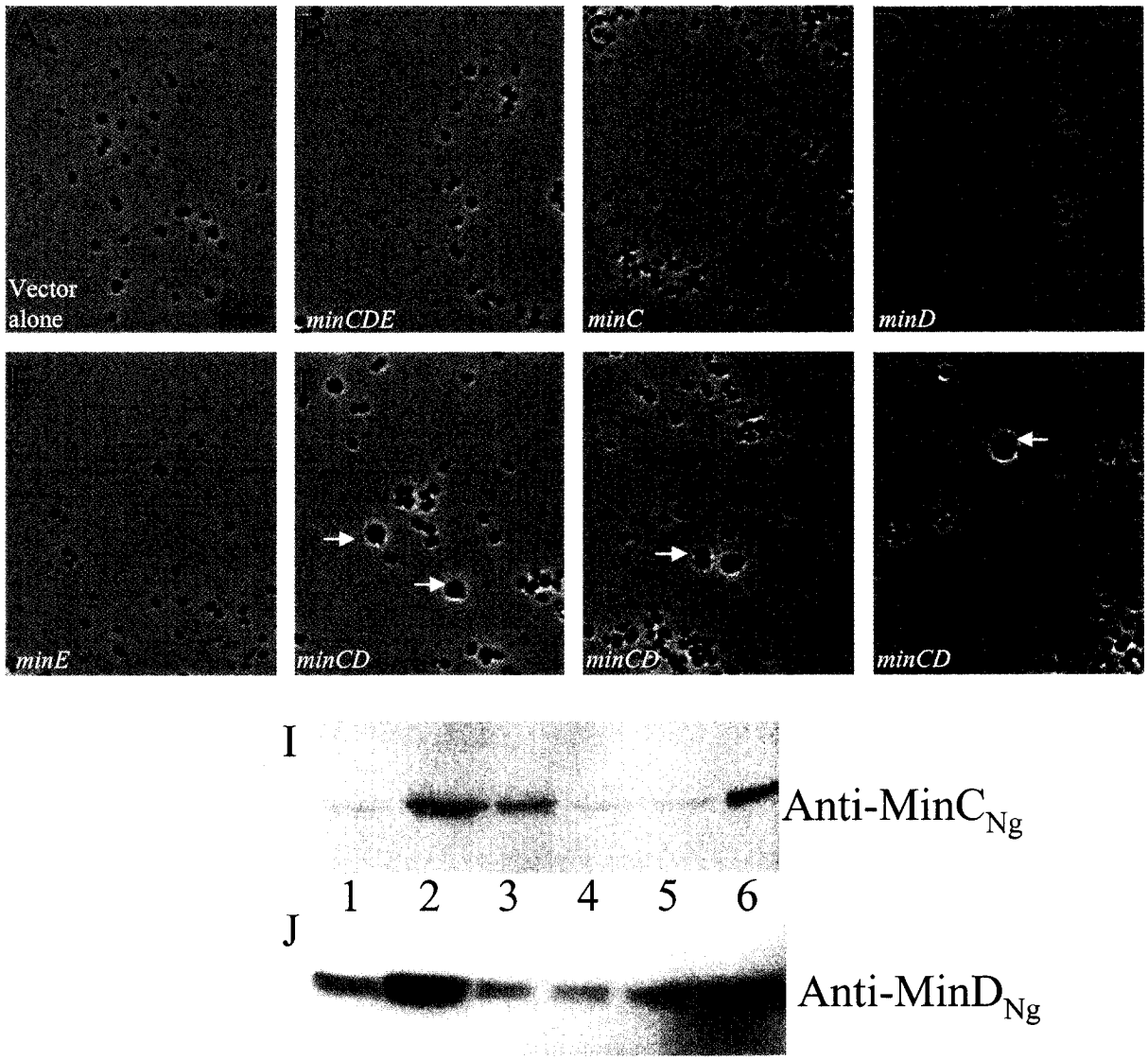

Figure 3.5. Phase contrast micrographs to determine the effects of transforming *N. gonorrhoeae* F62 with shuttle vector pFP20 encoding individual, and combinations of, *min* genes. (A) *N. gonorrhoeae* F62 transformed with control shuttle vector pFP20 exhibit characteristic uniform coccal morphology (diameter <1μm). *N. gonorrhoeae* F62 transformed with (B) pFP21 (*minC*$_{Ng}$, *minD*$_{Ng}$, *minE*$_{Ng}$), (C) pFP22 (*minC*$_{Ng}$), (D) pFP23 (*minD*$_{Ng}$), and (E) pFP24 (*minE*$_{Ng}$), do not show obvious altered morphologies by phase-contrast microscopy. (F-H) *N. gonorrhoeae* F62 transformed with pFP25 (*minC*$_{Ng}$, *minD*$_{Ng}$) exhibit noticeable cell enlargement, including cells up to twice the normal diameter. Panels A-H are all at the same magnification, and the scale bar in (A) represents 5 μm. Western blots to determine MinC$_{Ng}$ (I) and MinD$_{Ng}$ (J) expression levels in *N. gonorrhoeae* F62 transformants was carried out. Cell extracts of *N. gonorrhoeae* F62 transformed with: Lane 1, control pFP20; lane 2, pFP21 (*minC*$_{Ng}$, *minD*$_{Ng}$, *minE*$_{Ng}$); lane 3, pFP22 (*minC*$_{Ng}$); lane 4, pFP23 (*minD*$_{Ng}$); lane 5, pFP24 (*minE*$_{Ng}$); and lane 6, pFP25 (*minC*$_{Ng}$, *minD*$_{Ng}$) were probed with affinity-purified anti-MinC$_{Ng}$ (I) or anti-MinD$_{Ng}$ (J) antisera.

kb) of *N. gonorrhoeae* F62, transformants also maintained their respective shuttle vectors [Figure 3.6: lane 2, pFP20 (5.2 kb); lane 3, pFP21 (7.5 kb); lane 4, pFP22 (6.4 kb); lane 5, pFP23 (6.8 kb); lane 6, pFP24 (6.2 kb); and lane 7, pFP25 (7.2 kb)].

Electron microscopy was used to further examine the morphology of the enlarged *N. gonorrhoeae* F62 carrying pFP25 (*minC*$_{Ng}$, *minD*$_{Ng}$) (Figure 3.7 C-F). These cells were larger than those transformed with the negative control vector pFP20 (Figure 3.7 A, B), and still retained diplococcal morphology. Even individual cocci of enlarged pFP25 transformants were often as large as diplococci of control cells. Out of 40 randomly measured cells containing pFP25 (*minC*$_{Ng}$, *minD*$_{Ng}$), 38 had diameters ranging from ~0.95 μm to 1.50 μm, which were greater than the average diameter of the control transformants (~0.90 μm). The average diameter of pFP25 transformants was calculated to be ~28% greater than that of pFP20 transformants and statistical analysis confirmed that this difference was significant ($p<0.001$). Hence, gonococcal cell enlargement correlated with increased expression of both MinC$_{Ng}$ and MinD$_{Ng}$ together. Overall, these results indicated that MinD$_{Ng}$ acts in conjunction with MinC$_{Ng}$ to inhibit cell division in gonococcal cells.

MinD is located in cytosolic and membrane fractions of gonococcal cell extracts. Soluble and insoluble wild-type *N. gonorrhoeae* CH811 cell fractions were separated by high speed centrifugation and probed with affinity purified anti-MinD$_{Ng}$ antisera. Densitometric analysis revealed that approximately 40% of total MinD$_{Ng}$ was associated with the insoluble membrane fraction (Figure 3.8 A, lane 1), while 60% of the protein was detected in the cytosol (Figure 3.8 A, lane 2). Immunogold labeling of fixed *N. gonorrhoeae* CH811 cells to localize MinD$_{Ng}$ also showed that the protein could be found in the cytoplasm (Figure 3.8 B, D; black arrows) and along the inner cell membrane (Figure 3.8 B-D, red arrows). However, there was insufficient labeling in the cell sections to accurately determine any MinD$_{Ng}$ localization pattern in these samples.

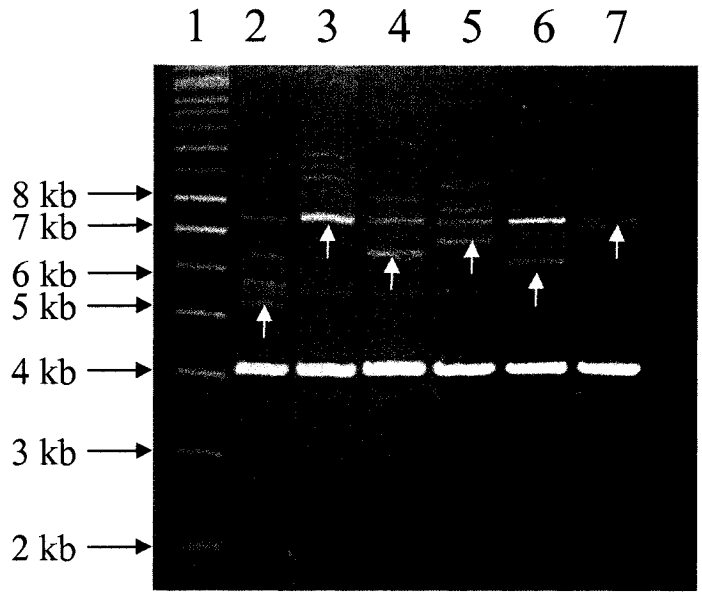

Figure 3.6. *N. gonorrhoeae* F62 are able to maintain shuttle vectors carrying gonococcal *min* genes. Plasmids isolated from gonococci transformed with pFP20 (negative control vector), pFP21 ($minC_N$g, $minD_{Ng}$, $minE_{Ng}$), pFP22 ($minC_{Ng}$), pFP23 ($minD_{Ng}$), pFP24 ($minE_{Ng}$), and pFP25 ($minC_{Ng}$, $minD_{Ng}$) were resolved by agarose gel electrophoresis to verify their presence and general integrity. Black arrows indicate supercoiled DNA ladder bands that were used to estimate plasmid size (lane 1). White arrows indicate resolved gonococcal plasmid bands used to estimate shuttle vector sizes. Lane 2 = pFP20 (5.2 kb); lane 3 = pFP21 (7.5 kb); lane 4 = pFP22 (6.4 kb); lane 5 = pFP23 (6.8 kb); lane 6 = pFP24 (6.2 kb); and lane 7 = pFP25 (7.2 kb). Plasmid band at ~4.2 kb represents gonococcal cryptic plasmid inherent to *N. gonorrhoeae* F62.

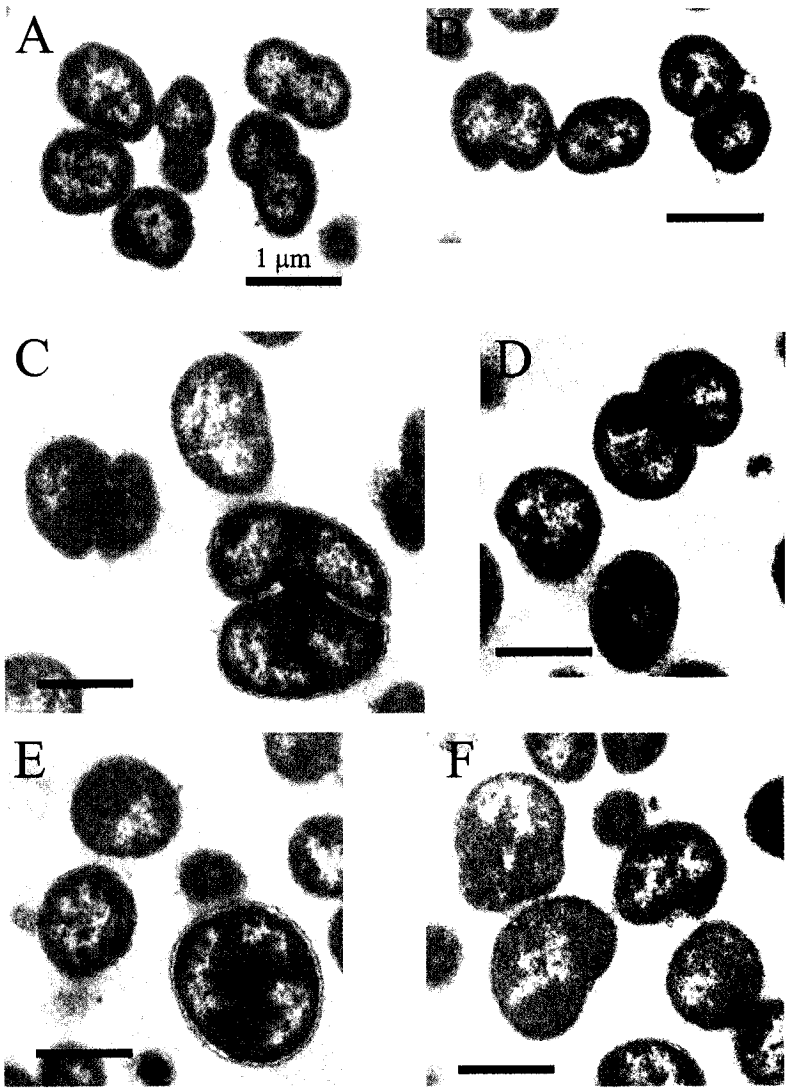

Figure 3.7. Electron micrographs of *N. gonorrhoeae* F62 transformed with pFP20 control shuttle vector and pFP25 encoding *min*C_{Ng} and *min*D_{Ng}. (A and B) Control transformants display normal gonococcal morphology. (C-F) *N. gonorrhoeae* F62 transformed with pFP25 (*min*C_{Ng}, *min*D_{Ng}) are noticeably enlarged. All panels are at the same magnification, and scale bars represent 1 μm.

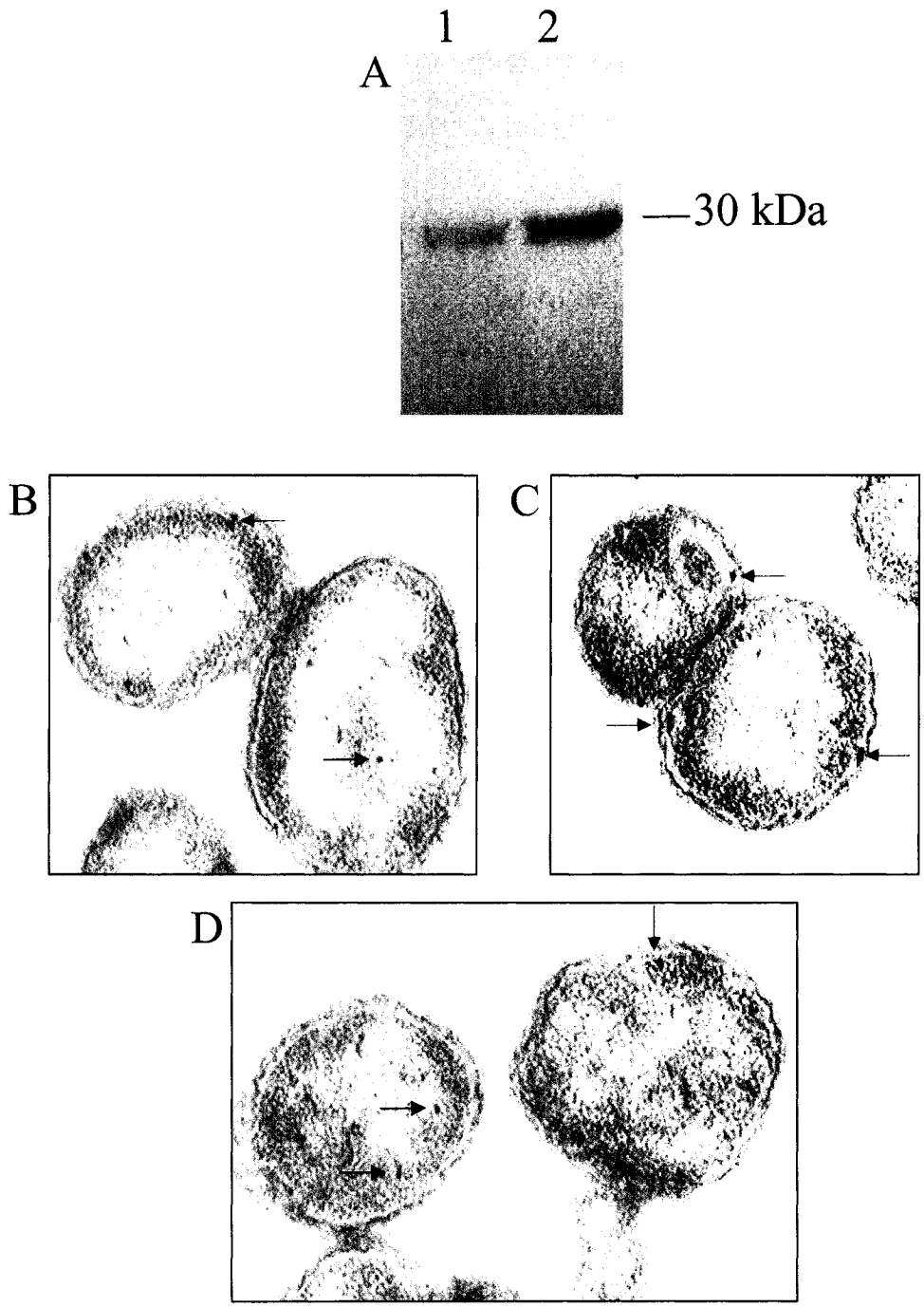

Figure 3.8. Detection of $MinD_{Ng}$ in gonococcal cell fractions. (A) Western blot using anti-$MinD_{Ng}$ antisera was used to probe insoluble membrane fraction (lane 1) and soluble cytosolic fraction (lane 2) of *N. gonorrhoeae* CH811 cell extracts. (B-D) Immunogold labeling and transmission electron microscopy was used to localize $MinD_{Ng}$ in *N. gonorrhoeae* CH811. Black arrows indicate cytosolic $MinD_{Ng}$ and red arrows show inner membrane associated $MinD_{Ng}$.

Localization of FtsZ in dividing *N. gonorrhoeae* cells. Gonococci characteristically divide along two alternating, perpendicular planes (Fitz-James, 1964; Westling-Häggström *et al.*, 1977). As part of the effort to generate a refined model of cell division in *N. gonorrhoeae*, localization of FtsZ in dividing gonococcal cells was conducted using immunoelectron microscopy. Previous studies in our laboratory have shown that *N. gonorrhoeae* possesses *ftsZ* (*ftsZ*$_{Ng}$) within the division cell wall (*dcw*) cluster of genes (Salimnia *et al.*, 2000).

Immunogold labeling using anti-FtsZ$_{Ng}$ antisera (Salimnia *et al.*, 2000) was performed on sections of fixed *N. gonorrhoeae*. In single cocci, transmission electron micrographs revealed a distinct accumulation of FtsZ along one side of the cell, within a single invagination point that presumably indicated the initiation of a cell division event along one plane (Figure 3.9 A, B; arrows). Further along in the division process, a constrictive septum was observed along a midline of the cell, with FtsZ$_{Ng}$ signal found predominantly at the two leading edges of the constriction (Figure 3.9 C, arrows). As division proceeded, a single band of FtsZ$_{Ng}$ signal is observed between two daughter cells (Figure 3.9 D), prior to the formation of a diplococcus.

In order to produce the typical 2 x 2 tetrad formation of daughter cells, the next FtsZ$_{Ng}$ assembly point must be repositioned perpendicularly to its initial point prior to cell division along the second plane. This was supported by observing FtsZ$_{Ng}$ signal distinctly localizing at single invagination points at the junction between each cell of a diplococcus (Figure 3.9 E, arrows), such that septum formation along this second, perpendicular plane should result in a tetrad of daughter cells.

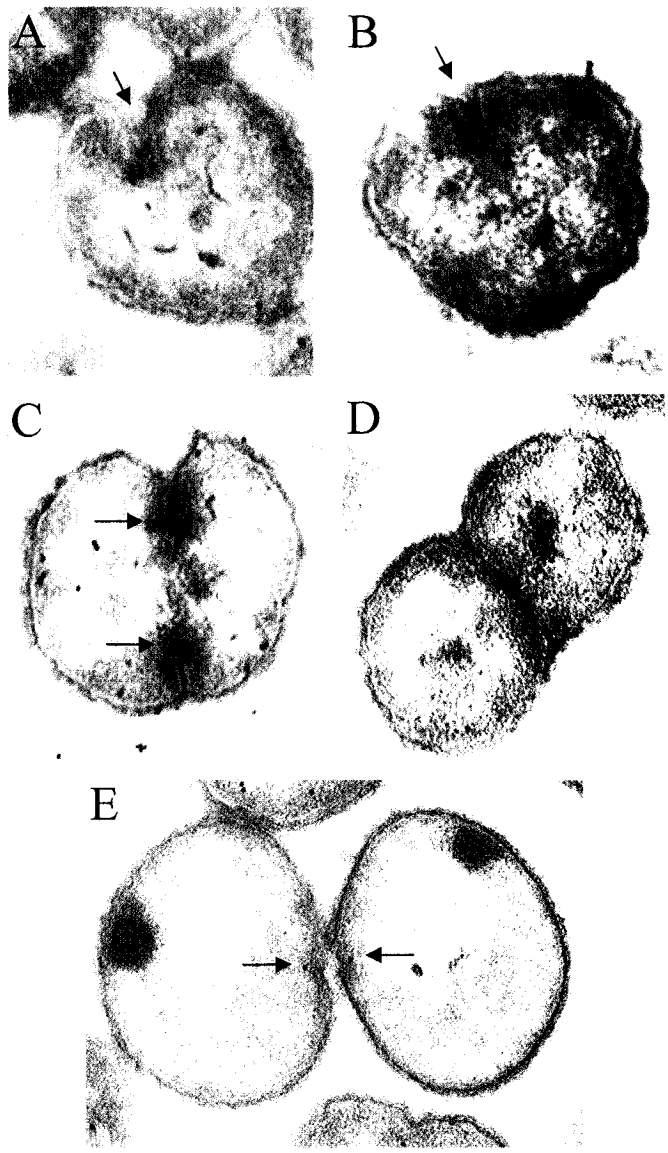

Figure 3.9. Immunogold localization of *N. gonorrhoeae* FtsZ ($FtsZ_{Ng}$) in cross sections of dividing gonococcal cells. (A and B) In individual cocci, cell division is initiated at a single invagination point (arrows), where distinct accumulation of $FtsZ_{Ng}$ is observed (black dots). (C) Further along in the division process, a constrictive septum is observed along a midline of the cell, with $FtsZ_{Ng}$ signal found predominantly at the two leading edges of the constriction (arrows). (D) As division proceeds, a single band of $FtsZ_{Ng}$ signal is observed between two daughter cells, prior to the formation of a diplococcus. (E) Septum formation along a second, perpendicular plane is initiated by $FtsZ_{Ng}$ localizing at single invagination points at the junction *between* each cell of a diplococcus (arrows).

3.4. DISCUSSION

Most of our present knowledge of bacterial cell division has arisen from extensive studies of cell division in rod-shaped bacteria. Since cocci lack obvious cell poles, it has been suggested that they would not contain any *min* genes (Weaver, 2000). Our laboratory has pioneered the study of cell division proteins from round bacteria, and we have shown that the Gram-negative coccus *N. gonorrhoeae* contains a *min* operon with *minC*, *minD*, and *minE* genes (Ramirez-Arcos *et al.*, 2001a). This is the first study to characterize MinD from a naturally occuring coccus.

MinD homologues are found in a variety of organisms, ranging from Gram-negative and Gram-positive bacteria to Archaea and chloroplasts (Margolin, 2001a). Alignment of MinD proteins showed that they are well conserved, particularly at the N-terminus, corresponding to the first 166 amino acids of $MinD_{Ng}$. From the crystal structure of *P. furiosus* MinD, the residues directly involved in binding ATP are mostly found distributed throughout the N-terminal half of the protein, in support of the overall conserved nature of this region (Hayashi *et al.*, 2001).

Their wide distribution across genera and species suggests MinD proteins have an important role for cellular function(s). It is noted that the presence of MinD in an organism does not necessarily indicate that MinC and/or MinE are present as well. For example, Archaeal organisms possess MinD homologues (Cordell and Löwe, 2001; Hayashi *et al.*, 2001; Sakai *et al.*, 2001), yet analysis of Archaeal genome projects show they lack MinC and MinE. In addition, no *min* genes have been identified in any Gram-positive cocci to date, with the exception of a *minD* homologue in *Deinococcus radiodurans*. However, like Archaea, the *D. radiodurans* genome project does not identify any *minC* or *minE* genes. Hence, MinD may serve another function in Archaea and in *D. radiodurans*, other than regulating cell division.

Since *N. gonorrhoeae* and *N. meningitidis* contain all three *min* genes, they provide exceptional cases for investigating the possible role of a Min system regulating the placement of cytokinetic machinery in naturally occurring cocci. Although these organisms do not have obvious cell poles, the disruption of cell division site machinery should elicit some morphological changes.

This was demonstrated by the *N. gonorrhoeae minD* knockout strain, CJSD1, and by strain SCD-1, bearing a $minD_{Ng\text{-}K16Q}$ chromosomal mutation. These strains exhibited grossly aberrant morphology characterized by daughter cells of differing sizes and shapes, and had multiple, improperly placed division planes initiated. A similar phenotype has also been observed in a *N. gonorrhoeae minC* insertional mutant, constructed in our laboratory, which displayed atypical division as well (Ramirez-Arcos *et al.*, 2001a). Hence, these studies indicate that $MinD_{Ng}$ is involved in maintaining proper cell division and morphology in the gonococcus.

Mutation of the conserved K16 Walker A ATP-binding motif of *E. coli* MinD has been shown to render the protein incapable of regulating proper cell division arrest and unable to associate with phospholipids (de Boer *et al.*, 1991; Hu *et al.*, 2002). It is proposed that the K16Q substitution may prevent $MinD_{Ec}$ from undergoing necessary conformational changes that permit membrane association (Hu *et al.*, 2002). Hence, the inability of $MinD_{Ng\text{-}K16Q}$ to properly bind to the inner membrane in *N. gonorrhoeae* SCD-1 would conceivably allow improper initiation of FtsZ constriction events. Similarly, the loss of $MinD_{Ng}$ in *N. gonorrhoeae* CJSD1 would presumably result in an inability for the division inhibitor $MinC_{Ng}$ to properly localize to the inner membrane and exert its effects.

To date, *N. gonorrhoeae* SCD-1 is the only described gonococcal strain, and perhaps natural coccus, that contains a constructed point mutation in one of its *min* genes. In *E. coli*, removal of MinD or MinC produces a minicell phenotype characterized by small anucleate minicells and rods of varying lengths (de Boer *et al.*, 1989); therefore, it is tempting to speculate the phenotypes observed with *N. gonorrhoeae* CJSD1 and SCD-1 represent the equivalent of a 'minicell' phenotype in cocci.

Although Western blotting confirmed that $MinD_{Ng\text{-}K16Q}$ was still expressed, it was present at a lower level compared to wild-type $MinD_{Ng}$ in control cells. It could be argued that $MinD_{Ng\text{-}K16Q}$ remains active, and that the aberrant phenotype of *N. gonorrhoeae* strain SCD-1 was due to lowered levels of $MinD_{Ng\text{-}K16Q}$, and not specifically to the K16Q mutation itself. However, further work with $MinD_{Ng\text{-}K16Q}$ in this study provides more evidence for its impaired activity (see following chapters). In

addition, the fact that the depletion of $MinD_{Ng\text{-}K16Q}$ itself (whether still functional or not) results in aberrant cell division is significant evidence in itself that MinD protein is required for proper gonococcal cell division.

Disruption of $minD_{Ng}$ may have affected gonococcal cell wall integrity as well. Evidence of cell lysis in *N. gonorrhoeae* CJSD1 was observed by phase contrast and electron microscopy, and a similar marked increase in lysis was observed in a *N. gonorrhoeae minC* insertional mutant constructed in our laboratory (Ramirez-Arcos *et al.*, 2001a). It is possible that the enlarged cells, produced as a result of asymmetric cell division in *N. gonorrhoeae* CJSD1 are more sensitive to lysis. From the surface stress theory of Koch (1985), where T=Pr/2 in cocci (T, surface tension; P, hydrostatic pressure; and r, radius), an increase in cell size (r) results in an increase in cell wall tension. Significant increases in cell size can result in sufficient tension on peptidoglycan bonds that make them more susceptible to breaking. Alternatively, peptidoglycan bonds may be more susceptible to hydrolysis since the activity of autolytic enzymes increases under stress conditions (Koch, 1985).

Since cocci need only half the hydrostatic pressure required in rods to increase their surface tension by similar amounts (Koch, 1985), gonococci are likely more sensitive to the effects brought by changes in cell size, including those caused by disrupting *minD*. It is also possible that lysis resulted from a compromise in cell wall integrity due to cell wall components/precursors being diverted to multiple division sites forming in the gonococcal *minD* mutant.

The lack of $MinD_{Ng}$ also led to decreased cell viability of *N. gonorrhoeae* CJSD1 during the latter half of the growth curve. In rod-shaped bacteria, polar divisions due to *min* mutations produce non-viable, anucleate minicells (de Boer *et al.*, 1988; de Boer *et al.*, 1989). It is possible that improper cell division in strain CJSD1 would also result in 'daughter' cells with decreased and/or lost viability, which was observed. Increased cell lysis likely further contributed to the lower viability of the gonococcal *minD* mutant. The production of non-viable cells and/or lysed cells during each

successive division event would also account for the delayed appearance and smaller size of *N. gonorrhoeae* CJSD1 colonies on solid media.

Curiously, this mutant displayed a higher viability compared to wild-type cells early in the growth experiments (<6 hours). It is possible that mutant cells may have become multinucleated at the onset of growth, resulting in a higher number of viable nucleated cells than the control. As more undesirable cell division events occur, a corresponding increase in anucleate and non-viable mutant cells may account for the decreased viability of strain CJSD1 at later growth stages. Unlike *E. coli*, all attempts by our laboratory to generate a *N. gonorrhoeae* mutant lacking all three *min* genes have been unsuccessful, suggesting that the gonococcus may be inherently more sensitive to the effects of *min* gene abrogation than *E. coli.* Hence, differences in the ability of Min proteins to affect cell division in rods and cocci may reflect differences in the sensitivity of each model system to these proteins.

In *E. coli*, MinD appears to dynamically shuttle between the cytoplasm and membrane target sites as it recruits MinC from pole-to-pole (Hu and Lutkenhaus, 1999; Raskin and de Boer, 1999a; Rowland *et al.*, 2000; Hu *et al.*, 2003). The detection of $MinD_{Ng}$ in both soluble and insoluble gonococcal fractions also suggests that the protein may exhibit such dynamic movement in *N. gonorrhoeae*. Furthermore, immunoelectron microscopy showed evidence that $MinD_{Ng}$ was found in both the cytosol and along the inner membrane. In support of this, examination of the $MinD_{Ng}$ sequence shows it contains a C-terminal motif that closely resembles the *E. coli* MinD membrane targeting sequence identified by others (Szeto *et al.*, 2002, Hu and Lutkenhuas, 2003). Experiments to attempt localization of GFP-$MinD_{Ng}$ fusions in live *N. gonorrhoeae* should prove interesting. Due to the small size and fastidious nature of this organism, such studies should prove challenging.

Cloning the gonococcal *min* genes into the modified shuttle vector pFP20 allowed the first study to examine the effects of Min protein overexpression in natural cocci. Such studies in *N. gonorrhoeae* would have previously been more difficult, if not impossible, due to a lack of suitable genetic tools for this organism. Overexpression studies provided further evidence that $MinD_{Ng}$ is involved in gonococcal cell division regulation. *N. gonorrhoeae* F62 cells became noticeably

enlarged when both $MinC_{Ng}$ and $MinD_{Ng}$ were overexpressed from pFP25 (*minC*$_{Ng}$, *minD*$_{Ng}$), indicative of a relationship between the two proteins to inhibit cytokinesis. Similarly, the *E. coli* and *B. subtilis* MinC-MinD complexes act together to inhibit cell division, with MinD recruiting MinC to the cell membrane (Huang *et al.*, 1996; Hu and Lutkenhaus, 1999; Marston and Errington, 1999b; Hu *et al.*, 2003; Lackner *et al.*, 2003). Other studies have shown that inhibiting cell division in cocci results in enlarged cells. For example, penicillin G induces cell enlargement in *N. gonorrhoeae* (Westling-Häggström *et al.*, 1977), and round *rodA* mutants of *Salmonella typhimurium* grown under conditions that prevent cell division become significantly larger in size (Costa and Antòn, 1999).

Gonococci transformed with pFP21 (encoding *minC*$_{Ng}$, *minD*$_{Ng}$, and *minE*$_{Ng}$) also had increased levels of $MinC_{Ng}$ and $MinD_{Ng}$; however, there was no obvious cell enlargement. It has been shown that *E. coli* transformed with a plasmid containing all three *E. coli min* genes exhibit a minicell phenotype, similar to overexpressing *minE*$_{Ec}$ alone. This suggests an increase in $MinE_{Ec}$ can overcome any cell division arrest that may arise from a concurrent increase in $MinC_{Ec}$-$MinD_{Ec}$ levels (de Boer *et al.*, 1989). Therefore, it is possible that, despite increased $MinC_{Ng}$ and $MinD_{Ng}$ levels in gonococcal pFP21 transformants, there may have been sufficient $MinE_{Ng}$ expression from this vector to maintain a proper stoichiometric ratio between the three Min_{Ng} proteins that countered any effects on cell morphology. Unfortunately, any increase in $MinE_{Ng}$ levels could not be ascertained in gonococcal transformants since our current polyclonal anti-$MinE_{Ng}$ antisera only has sufficient sensitivity to detect $MinE_{Ng}$ expressed from *high* copy number vectors in *E. coli* backgrounds.

Although $MinC_{Ng}$ levels were also increased in gonococci transformed with pFP22 (*minC*$_{Ng}$), there was no increase in $MinD_{Ng}$ levels in cells carrying pFP23 (*minD*$_{Ng}$). Studies in our laboratory indicated the region upstream of *minD*$_{Ng}$ (included in pFP23) possesses promoter activity (Ramirez-Arcos *et al.*, 2001b). However, it is possible that flanking chromosomal DNA sequences that normally influence *minD*$_{Ng}$ promoter activity are disrupted upon cloning *minD*$_{Ng}$ into the shuttle vector. Hence, whether the overexpression of $MinC_{Ng}$ and $MinD_{Ng}$ *together* is an absolute requirement for gonococcal cell enlargement is not known. In wild-type *E. coli*, the overexpression of

either $MinC_{Ec}$ or $MinD_{Ec}$ can inhibit cell division (de Boer *et al.*, 1989). Therefore, it is possible that overexpression of either $MinC_{Ng}$ or $MinD_{Ng}$ to levels *higher* than that achieved in the present study may affect normal cell division of *N. gonorrhoeae*. To further study the effects of overexpressing each min_{Ng} gene in the gonococcus, each gene could be introduced into the shuttle vector under the control of a more active, or inducible, promoter system, rather than their natural upstream promoter regions. While the consequences of overexpressing $MinD_{Ng}$ alone in *N. gonorrhoeae* could not be determined in the present study, it is predicted that sufficiently increased $MinD_{Ng}$ levels should lead to cell enlargement, similar to the elongation of wild-type *E. coli* cells that overexpress $MinD_{Ec}$ (de Boer *et al.*, 1989).

Interestingly, the plasmid-free *N. gonorrhoeae* strain CH811 used to generate the two gonococcal *minD* mutants in this study could not be transformed with the shuttle vector pFP20. In contrast, *N. gonorrhoeae* strain F62, which harbours a 4.2 kb cryptic plasmid (Roberts *et al.*, 1979), could successfully maintain pFP20 and its derivatives. It is noted that *N. gonorrhoeae* strain FA1090, which also carries the cryptic plasmid, can be transformed with the shuttle vector as well (data not shown). Although most *N. gonorrhoeae* clinical isolates bear the cryptic plasmid, it has, to date, no known function (Roberts *et al.*, 1979). Studies thus far have identified up to 10 open reading frames (ORFs) encoded by this plasmid (Korch *et al.*, 1985), including a possible Mob protein gene, which acts as a mobilization factor in other plasmid systems (Sarandopoulos and Davies, 1993). It is possible that the cryptic plasmid may encode other factors that permit the maintenance of other plasmids, including our shuttle vector. It is also possible that *N. gonorrhoeae* strain CH811 lacks certain chromosomally encoded determinants that are required for general plasmid upkeep.

Since Min proteins are implicated in the ultimate positioning of the Z-ring in bacteria (Margolin, 2001b; Errington *et al.*, 2003), FtsZ was localized in dividing *N. gonorrhoeae* in order to provide spatial information that will be used to generate a model for gonococcal cell division. Using immunoelectron microscopy, FtsZ was localized at the leading edge of constrictions, which defined cell division along one dimension. This is consistent with previous observations that gonococcal cell

division is initated by a single invagination point along one side of the cell (Fitz-James, 1964). In addition, the localization of FtsZ at invaginations between two daughter cells is consistent with observations that a second cytokinetic event occurs along a plane perpendicular to the first, which is initiated at the junction between two cells (Fitz-James, 1964; Westling-Häggström *et al.*, 1977).

These are the first studies of MinD function in coccal bacteria. By disrupting $minD_{Ng}$, it was demonstrated that $MinD_{Ng}$ is involved in maintaining the proper cell division pattern, morphology, and cell viability of the coccus *N. gonorrhoeae*. Using a stable shuttle vector, it was also demonstrated that $MinD_{Ng}$ likely acts with $MinC_{Ng}$ to inhibit cell division in the gonococcus. This, and other studies in our laboratory (Ramirez-Arcos *et al.*, 2001a), offer further evidence that a functional Min protein system exists in *N. gonorrhoeae* to regulate proper cytokinesis.

CHAPTER 4

Functionality of *Neisseria gonorrhoeae* MinD in *E. coli* backgrounds

Portions of this chapter were published in:

[**Szeto, J.**, Ramirez-Arcos, S., Raymond, C., Hicks, L. D., Kay, C. M., and Dillon J. R. (2001a). Gonococcal MinD affects cell division in *Neisseria gonorrhoeae* and *Escherichia coli* and exhibits a novel self-interaction. J. Bacteriol. *183*, 6253-6264.]

and

[Ramirez-Arcos, S., **Szeto, J.**, Dillon, J. R., and Margolin, W. (2002). Conservation of dynamic localization among MinD and MinE orthologues: oscillation of *Neisseria gonorrhoeae* proteins in *Escherichia coli*. Mol. Microbiol. *46*, 493-504.]

4.1. PURPOSE OF THIS STUDY

N. gonorrhoeae is a fastidious organism, with only a few genetic tools, such as the gonococcal shuttle vectors prepared in our laboratory, available for studying molecular mechanisms in this bacterium (Pagotto *et al.*, 2000; this study). In contrast, *E. coli* is much easier to culture and to genetically manipulate. Furthermore, there are many expression vectors that are suitable for protein studies in *E. coli*. Since both *N. gonorrhoeae* and *E. coli* are Gram-negative organisms that contain all three *min* genes, the present study was conducted to determine whether gonococcal MinD is functional in *E. coli* backgrounds.

The overexpression of *E. coli* MinD will induce $MinC_{Ec}$-dependent cell division arrest in wild-type cells (de Boer *et al.*, 1989). GFP-$MinD_{Ec}$ also oscillates *in vivo* in the presence of $MinE_{Ec}$ (Raskin and de Boer, 1999a; Rowland *et al.*, 2000), and does so by dynamically localizing within intracellular coiled arrays (Shih *et al.*, 2003). Hence, the ability of gonococcal MinD to perform the above activities was assessed to determine its functionality in *E. coli*. I show that $MinD_{Ng}$ can be expressed heterologously in *E. coli*, and can induce cell division arrest in these cells provided that resident *E. coli* MinC is available. In addition, $MinD_{Ng}$ is able to partially complement an *E. coli* *minD* mutant. Furthermore, GFP-$MinD_{Ng}$ exhibits dynamic intracellular movement in *E. coli* where it localizes, in a $MinE_{Ng}$-dependent manner, within coiled arrays, similar to studies with GFP-fusions to *E. coli* MinD (Raskin and de Boer, 1999a; Rowland *et al.*, 2000; Shih *et al.*, 2003). Hence, intracellular dynamism is not exclusive to *E. coli* MinD. These studies demonstrate that *E. coli* can be used as an effective indicator organism for $MinD_{Ng}$ functionality.

4.2. MATERIALS AND METHODS

Cloning *minD*$_{Ng}$ for expression studies in *E. coli*. Wild-type *minD*$_{Ng}$ was PCR amplified from gonococcal cell suspensions using the primers minD1 and minD2 (Table 2.2), incorporating *Eco*RI and *Bam*HI restriction sites to the 5' and 3' ends of the gene. The amplicon was ligated into *Eco*RI/*Bam*HI digested pUC18 (Amersham) to form pSR3 (Table 4.1). Plasmid pSR3 was transformed into *E. coli* strains PB103 (wild-type), DR105 (*minC*$_{Ec}$ mutant), PB104 (*minD*$_{Ec}$ mutant), PB114 (Δ*minCDE*$_{Ec}$), and KJB24 (*rodA* mutant) (Table 2.1) to assess the effects of MinD$_{Ng}$ expression in *E. coli* backgrounds using phase contrast microscopy. As a negative control, *minD*$_{Ng\text{-}K16Q}$ was PCR amplified from pJATP1 (Chapter 3, Table 3.1) using primers minD1 and minD2 (Table 2.2), and cloned into the *Eco*RI and *Bam*HI sites of pUC18 to form pMJ3 (Table 2.1).

Construction of GFP fusions to wild-type MinD$_{Ng}$. A fusion of green-fluorescent protein (GFP) to the N-terminus of wild-type MinD$_{Ng}$ was constructed for localization experiments in *E. coli* backgrounds. Primers minD1 and minE2 (Table 2.2) were used to PCR amplify both *minD*$_{Ng}$ and *minE*$_{Ng}$ from *N. gonorrhoeae* chromosomal DNA and the resulting amplicon was digested with *Eco*RI and *Bam*HI and ligated into similarly digested pDSW209 (encoding GFP) (Weiss *et al.*, 1999), forming plasmid pSR15 (Table 4.1). This plasmid encoded GFP fused to the N-terminus of wild-type MinD$_{Ng}$ and encoded MinE$_{Ng}$ immediately downstream.

A vector encoding GFP-MinD$_{Ng}$ alone (without MinE$_{Ng}$), was also constructed by amplifying *minD*$_{Ng}$ from *N. gonorrhoeae* CH811 chromosomal DNA using primers minD1 and minD2 (Table 2.2), digesting the amplicon with *Eco*RI and *Bam*HI, and ligating into pDSW209 as above. This plasmid was named pJS10 (Table 4.1). As a negative control, primers minD1 and minE2 were also used to amplify *minD*$_{Ng\text{-}K16Q}$ and *minE*$_{Ng}$ from plasmid pJATP1 (Chapter 3, Table 3.1) for ligation into pDSW209 as above to create plasmid pJDE1 (*gfp-minD*$_{Ng\text{-}K16Q}$, *minE*$_{Ng}$) (Table 4.1).

Table 4.1 Plasmids used in this study

Plasmids	Relevant genotype	Source or reference
Plasmids for expression studies		
pUC18	P_{lac} (Amp^R)	Amersham
pSR3	pUC18; P_{lac}::*minD*$_{Ng}$ (Amp^R)	This study
pJATP1	Amp^R P_{lac}:: *minC*$_{Ng}$, *minD*$_{Ng\text{-}K16Q}$, *minE*$_{Ng,}$, *oxyR*	Chapter 3
pMJ3	pUC18; P_{lac}::*minD*$_{Ng\text{-}K16Q}$ (Amp^R)	This study
GFP-fusion plasmids		
pDSW209	P_{trc}::*gfp* (Amp^R)	Weiss *et al.* (1999)
pSR15	pDSW209; P_{trc}::*gfp-minD*$_{Ng}$, *minE*$_{Ng}$ (Amp^R)	This study
pJS10	pDSW206; P_{trc}::*gfp-minD*$_{Ng}$ (Amp^R)	This study
pJDE1	pDSW209; P_{trc}::*gfp-minD*$_{Ng\text{-}K16Q}$, *minE*$_{Ng}$ (Amp^R)	This study
pWM1255	pDSW209; P_{trc}::*gfp-minD*$_{Ec}$, *minE*$_{Ec}$ (Amp^R)	Corbin *et al.* (2002)

Plasmid pWM1255 encoded a GFP-fusion to *E. coli* MinD (GFP-$MinD_{Ec}$), as well as $MinE_{Ec}$ downstream (Table 4.1) (Corbin *et al.*, 2002), and was used to compare oscillation cycles with GFP-$MinD_{Ng}$.

GFP-$MinD_{Ng}$ localization studies in *E. coli*. Protein localization studies were performed using two seperate fluorescent microscope systems. Initial studies were done in collaboration with Dr. William Margolin, University of Texas Medical School, using an Olympus BX60 fluorescence microscope and a 100X oil immersion objective. Images were captured with a Photometric CoolSnap fx CCD camera and QED software. Approximately 3 µl of log-phase *E. coli* WM1032 (Δ*minCDE*) (Table 2.1) transformed with pSR15 (Table 4.1) were grown for 4-5 hours under 40 µM isopropyl-beta-D-thiogalactopyranside (IPTG) induction and 30°C incubation. 3 µl of cells were immobilized by mixing with 3 µl of 2% low-melting-point agarose in LB and immediately applied to a microscope slide. Localization of GFP-$MinD_{Ng}$ in round *E. coli* KJB24 (*rodA*) cells (Table 2.1) containing pSR15 was also examined. *E. coli* KJB24 were grown overnight at room temperature without any agitation or IPTG, and supplemented with 50 µg/ml thymine. Time-lapse fluorescence images were taken every 10-15 seconds, with exposure times ranging from 0.5-1.2 sec. Images were saved and compiled with Adobe Photoshop software.

Subsequent GFP-$MinD_{Ng}$ localization studies were conducted in our laboratory, after acquiring an Olympus BX61 fluorescence microscope system equipped with oil-immersion 60X and 100X objectives, a Photometrics CoolSnap ES camera, and Image Pro (Version 4.5.1) software. Time lapse images were taken every 6 seconds, with exposure times of 0.250-0.500 seconds. Localization studies GFP-$MinD_{Ng}$ in *E. coli* PB114 (Δ*minCDE*) transformed with pSR15, pJDE1, or pJS10 were conducted (Table 4.1). In addition, GFP-$MinD_{Ng}$ localization in round *E. coli* KJB24 cells (Table 2.1) transformed with pSR15 (Table 4.1) was also investigated. GFP-$MinD_{Ng}$ oscillation cycles were defined as the time required for fusion protein signal to travel from one cell pole to the other, and

back again. The unpaired Student's *t*-test was used to determine whether average oscillation cycles differed from one another, with $p < 0.001$ considered significantly different.

4.3. RESULTS

Expression of $MinD_{Ng}$ in *E. coli* backgrounds indicates cross-species functionality. Since gonococcal MinD is 73% identical and 85% similar to *E. coli* MinD, $MinD_{Ng}$ was expressed in *E. coli* backgrounds to determine whether it could affect cell division in another organism. Because *E. coli* is easier to genetically manipulate and is less fastidious than *N. gonorrhoeae*, these studies will determine the possibility of using *E. coli* as an indicator strain for $MinD_{Ng}$ functionality.

Rod-shaped wild-type *E. coli* PB103 cells (Table 2.1) were transformed with plasmid pSR3, encoding $minD_{Ng}$ (Table 4.1). While cells transformed with the negative control pUC18 vector exhibited normal short rod morphology (Figure 4.1 A), the same strain transformed with pSR3 exhibited a filamentous phenotype, indicative of cell division arrest (Figure 4.1 B). As another negative control, *E. coli* PB103 was also transformed with pMJ3, encoding $MinD_{Ng\text{-}K16Q}$ (Table 4.1). Cells expressing $MinD_{Ng\text{-}K16Q}$ could still divide normally and appeared as short rods (Figure 4.1 C), similar to pUC18 transformants. Western blot analysis confirmed that $MinD_{Ng}$ was overexpressed in *E. coli* cells transformed with pSR3 (Figure 4.1 D, lane2). The anti-$MinD_{Ng}$ antisera could also detect the resident $MinD_{Ec}$ found in wild-type *E. coli*, which appeared as a faint band in pUC18 transformed cell extracts (Figure 4.1 D, lane 1). Western blotting also confirmed that wild-type $MinD_{Ng}$ (Figure 4.1 E, lane 1) and $MinD_{Ng\text{-}K16Q}$ (Figure 4.1 E, lane 2) were expressed at similar levels in *E. coli*.

Plasmid pSR3 was also transformed into *E. coli* PB104 (Table 2.1) to determine whether $minD_{Ng}$ could complement the $minD_{Ec}$ mutation in this strain. *E. coli* PB104 encodes a $MinD_{Ec}$ protein with a G262A substitution that results in an inactive protein (de Boer *et al.*, 1988), likely due to an abrogated C-terminal membrane targeting sequence (Szeto *et al.*, 2002). As a result, these cells display a classic minicell phenotype characterized by rods of varying lengths (Figure 4.2 A, black arrows) and minicells (Figure 4.2 A, white arrows). However, when transformed with pSR3, the majority of *E. coli* PB104 cells exhibited a short rod morphology, with very few filaments and minicells (Figure 4.2 B). This indicated that a partial complementation of the $minD_{Ec}$ mutation was achieved. Western blot analysis shows the overexpression of gonococcal $MinD_{Ng}$ in the

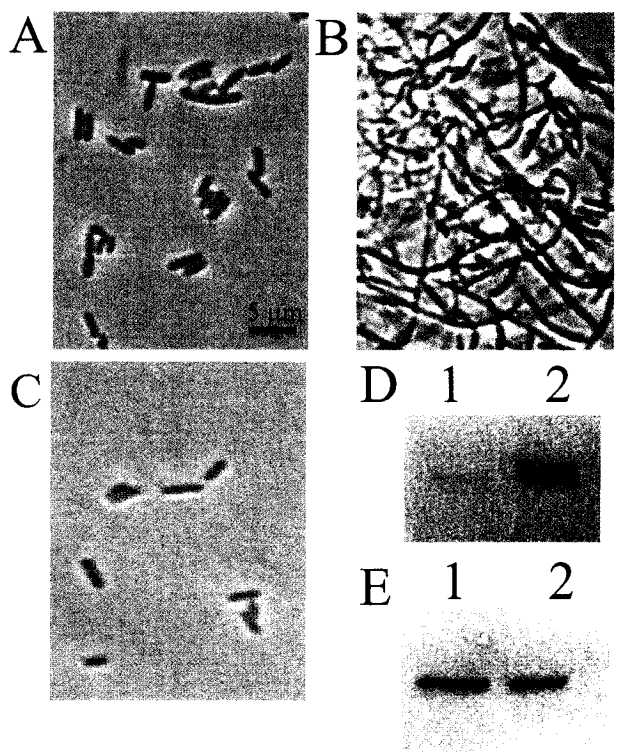

Figure 4.1. Effects of overxpressing $MinD_{Ng}$ in wild-type *E. coli* PB103. (A) *E. coli* PB103 transformed with pUC18 negative control vector have typical wild-type short rod morphology. (B) *E. coli* PB103 transformed with pSR3 ($minD_{Ng}$) exhibit a severe filamentous phenotype. Scale bar in (A) is 5 μm and all figures are at the same magnification. (C) *E. coli* PB103 transformed with pMJ3 ($minD_{Ng\text{-}K16Q}$) exhibit a short rod morphology. (D) Western blot using anti-$MinD_{Ng}$ antisera to probe cell extracts of *E. coli* PB103 pUC18 transformants (lane 1) and pSR3 ($minD_{Ng}$) transformants (lane 2). (E) Western blot using anti-$MinD_{Ng}$ antisera to probe cell extracts of *E. coli* PB103 pSR3 ($minD_{Ng}$) transformants (lane 1) and pMJ3 ($minD_{Ng\text{-}K16Q}$) transformants (lane 2). Note: (D) and (E) are separate blots. Protein concentrations for samples within each respective blot were equalized.

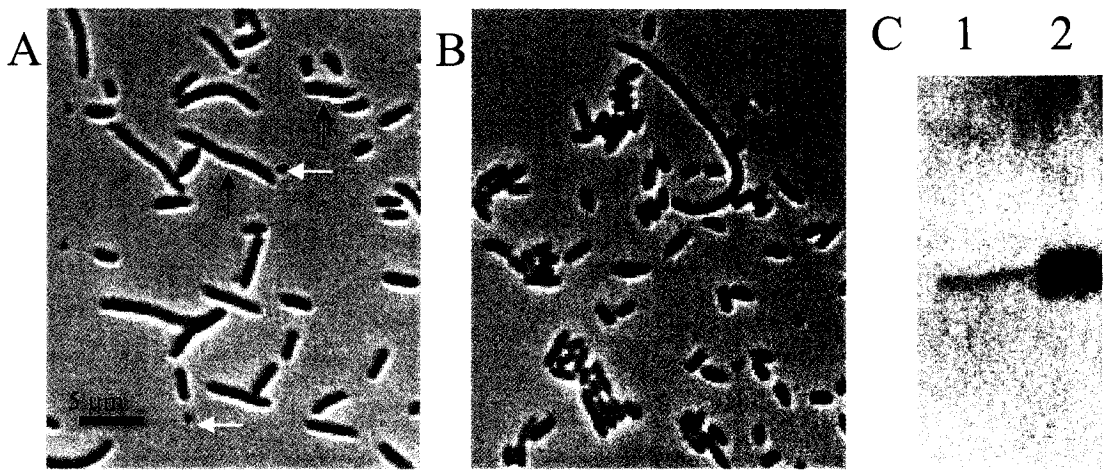

Figure 4.2. Complementation of *minD* mutation in *E. coli* PB104 expressing $MinD_{Ng}$. (A) *E. coli* PB104 transformed with pUC18 displays a typical minicell phenotype characterized by rods of varying lengths (black arrows), and minicells (white arrows) (B) The majority of *E. coli* PB104 transformed with pSR3 ($minD_{Ng}$) have restored short rod morphology, with few longer filaments and minicells. Scale bar in (A) is 5 μm and both figures are at the same magnification. (C) Western blot using anti-$MinD_{Ng}$ antisera to probe cell extracts of *E. coli* PB104 (pUC18) (lane 1) and *E. coli* PB104 (pSR3) (lane 2).

complemented cells (Figure 4.2 C, lane 2), compared to background expression of inactive $MinD_{Ec}$ (Figure 4.2 C, lane 1). Overall, these studies show that $MinD_{Ng}$ is active in *E. coli* and can influence cell division in these cylindrical cells.

To determine whether $MinD_{Ng}$ acted in a MinC-dependent manner in *E. coli*, $MinD_{Ng}$ expression studies were carried out in strains deficient in *minC* or all three *min* genes. When pSR3 ($minD_{Ng}$) was transformed into *E. coli* PB114 ($\Delta minCDE_{Ec}$) (Table 2.1), the cells retained their characteristic minicell phenotype (Figure 4.3 B), similar to the negative control pUC18 transformants (Figure 4.3 A), despite the overexpression of $MinD_{Ng}$ shown by Western blotting (Figure 4.3 C, lane 2). Furthermore, transformation of pSR3 into the *E. coli minC* mutant strain DR105 (Table 2.1) did not affect the minicell phenotype of this mutant (Figure 4.3 E), such that the cells were similar to pUC18 transformants (Figure 4.3 D). Western blotting confirmed the overexpression of $MinD_{Ng}$ in *E. coli* DR105 transformants (Figure 4.3 F, lane 2). Hence, these results indicate $MinD_{Ng}$ requires resident MinC to affect cell division in *E. coli* cells.

Round *E. coli* KJB24 cells (Table 2.1) were also transformed with pSR3 to determine the effects of $MinD_{Ng}$ overexpression in a coccal cell background. These cells lack the shape-determinant gene *rodA* and present a round cell morphology (Begg and Donachie, 1998). In addition, these cells divide along two planes, as *N. gonorrhoeae* does, to produce a tetrad of daughter cells (Begg and Donachie, 1998); hence, they may present a suitable model to study cell division in coccal Gram-negative organisms. *E. coli* cells KJB24 cells transformed with pUC18 appeared uniform in size and shape (Figure 4.4 A), while those transformed with pSR3 exhibited gross enlargement (Figure 4.4 B), with cell diameters up to 3-4 times that of control cells. Immunoblotting confirmed the overexpression of $MinD_{Ng}$ in the enlarged round cells (Figure 4.4 C, lane 2) compared to the background level of native *E. coli* MinD in negative control cells (Figure 4.4 C, lane 1).

Collectively, these heterologous expression studies indicate $MinD_{Ng}$ is able to induce cell division arrest in *E. coli* backgrounds, provided that functional *E. coli* MinC is present. In addition,

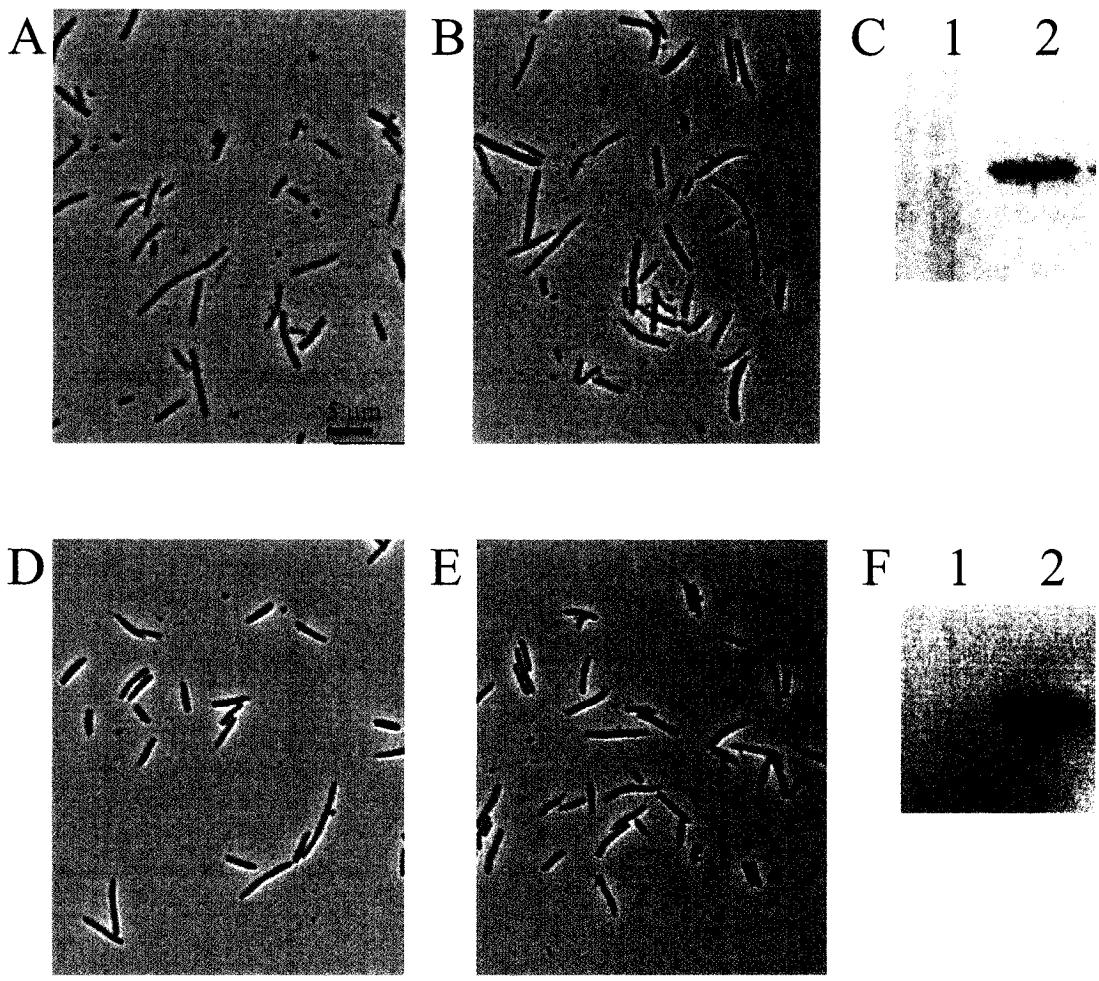

Figure 4.3. Expression of $MinD_{Ng}$ in *E. coli* PB114 (Δ*minCDE*) and *E. coli* DR105 (*minC* mutant). (A) *E. coli* PB114 (Δ$minCDE_{Ec}$) lacks all *min* genes and typically displays a minicell phenotype, as observed with pUC18 transformants. (B) *E. coli* PB114 transformed with pSR3 (*min*D_{Ng}) retain the minicell phenotype. (C) Western blotting confirmed the overexpression of $MinD_{Ng}$ in *E. coli* PB114 pSR3 transformants (lane 2) compared to pUC18 transformants (lane 1). (D) *E. coli* DR105, a *minC* mutant, also exhibits a minicell phenotype, as observed with pUC18 transformants. (E) Transformation of *E. coli* DR105 with pSR3 (*min*D_{Ng}) did not change its minicell phenotype. (F) Western blotting confirmed the overexpression of $MinD_{Ng}$ in *E. coli* DR105 pSR3 transformants (lane 2) compared to pUC18 transformants (lane 1). Scale bar in (A) is 5 μm and all figures are at the same magnification.

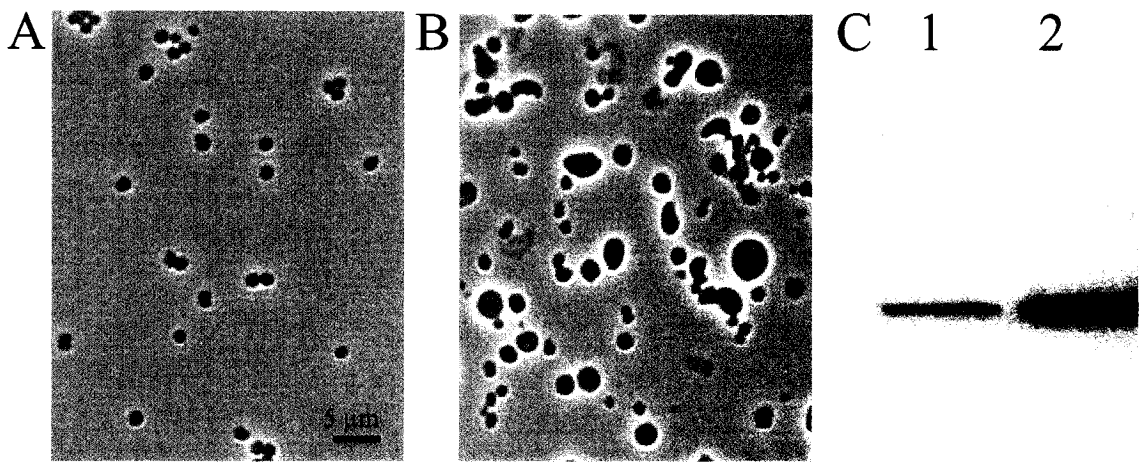

Figure 4.4. Overxpression of $MinD_{Ng}$ in round *E. coli* KJB24 (*rodA*) cells. (A) *E. coli* KJB24 transformed with pUC18 control display their characteristic coccal morphology, with all cells presenting a similar size. (B) Round *E. coli* transformed with pSR3 ($minD_{Ng}$) exhibit gross cell enlargement. The scale bar in (A) is 5 μm and both figures are at the same magnification. (C) Western blot using anti-$MinD_{Ng}$ antisera confirmed the overexpression of $MinD_{Ng}$ in cells transformed with pSR3 (lane 2), compared to pUC18 transformants (lane 1).

the functionality of $MinD_{Ng}$ in *E. coli* backgrounds showed that *E. coli* can be used as an effective reporter strain for gonococcal MinD function.

A GFP-$MinD_{Ng}$ fusion exhibits $MinE_{Ng}$-dependent intracellular movement in *E. coli* and localizes within coiled arrays. Since gonococcal MinD could affect *E. coli* cell division, a GFP-$MinD_{Ng}$ fusion was constructed to determine whether the protein would also oscillate intracellularly in *E. coli*. Since it is recognized that dynamic movement of *E. coli* GFP-MinD requires $MinE_{Ec}$ (Raskin and de Boer, 1999a; Rowland *et al.*, 2000), gonococcal *$minE_{Ng}$* was provided downstream of *gfp-$minD_{Ng}$* in pSR15 (Table 4.1). These initial localization studies were conducted in collaboration with Dr. W. Margolin, University of Texas Medical School. *E. coli* WM1032 (Table 2.1) was used in these studies since this strain lacks its own native *min* genes, thus eliminating any possible interference from endogeneous *E. coli* Min proteins.

Fluorescence microscopy of live cells revealed dynamic fusion protein behaviour characterized by intracellular shifting of fluorescent signals (Figure 4.5 A). Closer inspection of cells, particularly shorter rods (~3-4 μm in length), revealed GFP-$MinD_{Ng}$ moving from pole-to-pole (Figure 4.5 A), similar to reports for *E. coli* GFP-MinD (Raskin and de Boer, 1999a; Rowland *et al.*, 2000). Where pole-to-pole oscillation could be readily observed, the average oscillation cycle of GFP-$MinD_{Ng}$ (movement from one pole to the other, and back) in 14 cells examined took 70 ± 25 seconds. The average oscillation cycle of GFP-$MinD_{Ng}$ in *E. coli* WM1032 was significantly slower than GFP-$MinD_{Ec}$ (encoded on pWM1255; Table 4.1), which exhibited an average oscillatory cycle of 37 ± 12 seconds, measured in 10 cells ($p < 0.001$). Western blotting confirmed the expression of GFP-$MinD_{Ng}$ (Figure 4.5 B) and $MinE_{Ng}$ (Figure 4.5 C) in *E. coli* WM1032 cells containing pSR15. Hence, these preliminary studies showed that GFP-$MinD_{Ng}$ exhibits dynamic localization in an *E. coli* background. Furthermore, these studies indicated that intracellular oscillatory movement is not exclusive to *E. coli* MinD.

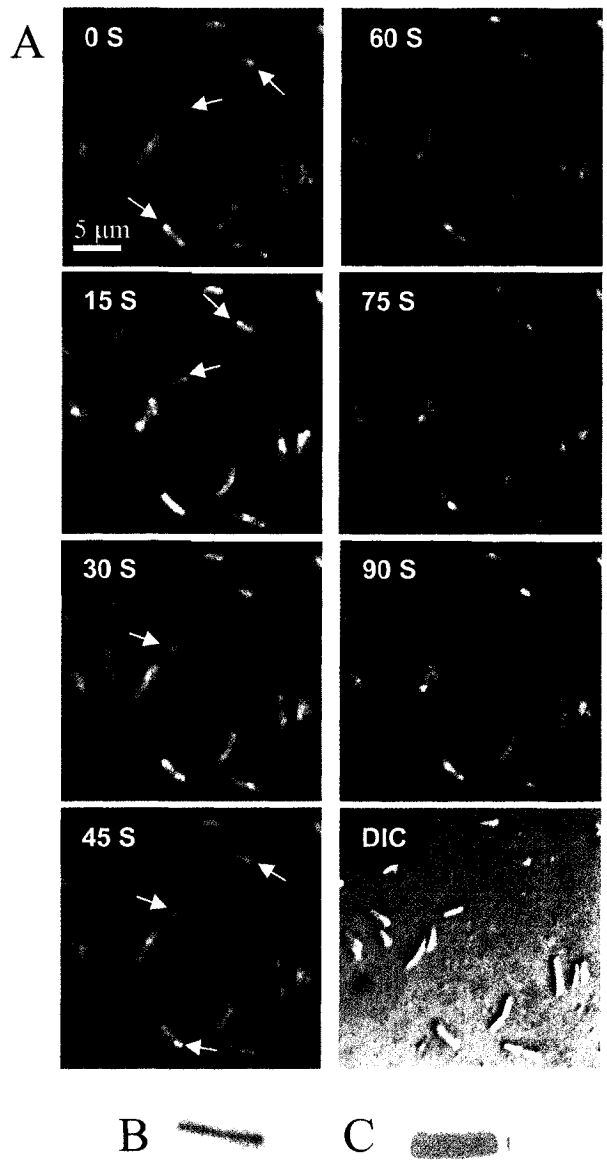

Figure 4.5. GFP-MinD$_{Ng}$ displays intracellular movement within rod-shaped *E. coli* WM1032 (Δ*minCDE*$_{Ec}$) cells. (A) Plasmid pSR15, encoding GFP-MinD$_{Ng}$ and untagged MinE$_{Ng}$ was transformed into *E. coli* WM1032 (Δ*minCDE*$_{Ec}$) and fusion protein localization was followed over time, as indicated in seconds. Arrows indicate pole-to-pole shifting of GFP-MinD$_{Ng}$ signal in three different cells. DIC = differential interference contrast image. Bar in first panel represents 5 µm. Western blotting using anti-MinD$_{Ng}$ antisera and anti-MinE$_{Ng}$ antisera detects GFP-MinD$_{Ng}$ (B), and MinE$_{Ng}$ (C) in cell extracts of *E. coli* WM1032 transformed with pSR15.

Upon acquiring a microscope system with improved magnification, resolution, and image analysis software, more refined GFP-$MinD_{Ng}$ localization studies were conducted. *E. coli* strain PB114 ($\Delta minCDE_{Ec}$) was used for these studies (Table 2.1). Similar to *E. coli* WM1032, wild-type GFP-$MinD_{Ng}$ expressed from pSR15 (Table 4.1) displayed oscillatory movement in *E. coli* PB114 (Figure 4.6). Since *E. coli* Δ*minCDE* strains exhibit a minicell phenotype that results in cells of varying lengths, pole-to-pole oscillatory cycles were monitored in rods of similar length (2.0-2.5 μm) to maintain consistency. In raw images, wild-type GFP-$MinD_{Ng}$ displayed periodic oscillations and moved from the membrane at one cell pole region to the other, forming a tube-shaped fluorescent signal that transiently lined each cell half (Figure 4.6 A, B). The average oscillation cycle (from one pole to the other and back) of GFP-$MinD_{Ng}$ measured in twenty short rods was 29.1 ± 7.3 seconds.

Studies with *E. coli* GFP-$MinD_{Ec}$ have shown that its dynamic localization is dependent upon $MinE_{Ec}$. To determine whether $MinE_{Ng}$ is responsible for the oscillatory movement of GFP-$MinD_{Ng}$, *E. coli* PB114 was transformed with pJS10 (Table 4.1), encoding GFP-$MinD_{Ng}$ but no $MinE_{Ng}$. In this case, the fusion protein appeared along the entire inner cell periphery, presenting a smooth and unbroken fluorescent signal without any evidence of pole-to-pole movement (Figure 4.6 C). Therefore, GFP-$MinD_{Ng}$ oscillates intracellularly in a $MinE_{Ng}$-dependent manner.

Since $MinD_{Ng\text{-}K16Q}$ could not induce cell division arrest in wild-type *E. coli*, it was fused to GFP as well to determine whether its inactivity was due to an inability to localize to the membrane, as reported with an *E. coli* $MinD_{K16Q}$ GFP-fusion (Hu *et al.*, 2002). As expected, expression of GFP-$MinD_{Ng\text{-}K16Q}$ from pJDE1 resulted in the fusion protein localizing throughout the cytoplasm in *E. coli*, despite the presence of $minE_{Ng}$ supplied on the same plasmid (Figure 4.6 D). Thus, due to its cytosolic localization, GFP-$MinD_{Ng\text{-}K16Q}$ can act as a suitable negative control for further *in vivo* membrane association studies.

Western blotting using affinity purified anti-$MinD_{Ng}$ antisera confirmed the expression of each GFP-$MinD_{Ng}$ protein in *E. coli* PB114 transformed with pSR15 (*gfp-*$minD_{Ng}$, $minE_{Ng}$) (Figure

Figure 4.6. GFP-MinD$_{Ng}$ localization in *E. coli* PB114 (Δ*minCDE*$_{Ec}$). (A and B) *E. coli* transformed with pSR15 (*gfp-minD*$_{Ng}$, *minE*$_{Ng}$) exhibit periodic GFP-MinD$_{Ng}$ movement from pole-to-pole. Time lapse between (A) and (B) is 18 seconds. Note the 'U'-shaped fluorescent pattern that transiently lines each cell pole. (C) In the absence of MinE$_{Ng}$, GFP-MinD$_{Ng}$ localizes along the inner cell periphery, presenting a smooth, unbroken signal. (D) GFP-MinD$_{Ng\text{-}K16Q}$ does not oscillate and remains distributed throughout the cytosol. (E and F) In longer *E. coli* cells (>5 μm) containing pSR15, a GFP-MinD$_{Ng}$ banding pattern is observed. These bands display dynamic localization, and shift positions rapidly (compare arrows in E and F; 12 seconds between each image). (G) Image enhancement of (E) shows fluorescent bands are composed of GFP-MinD$_{Ng}$ signal accumulating within segments of a coiled array. White arrows indicate regions of high GFP-MinD$_{Ng}$ accumulation. Red arrows show weaker GFP-MinD$_{Ng}$ signal indicating extension of the coiled array throughout the cell. Bar in (A) indicates 1 μm and (A-G) are all at the same magnification. (H) Magnified segment of *E. coli* cell showing GFP-MinD$_{Ng}$ coiled array. Note the different diagonal orientations of the GFP-MinD$_{Ng}$-containing coiled segments (white arrow compared to green arrow). (I) Western blotting using anti-MinD$_{Ng}$ antisera detects expression of GFP-MinD$_{Ng}$ (lanes 1, 4) and GFP-MinD$_{Ng\text{-}K16Q}$ (lane 2), in *E. coli* transformed with pSR15 (*gfp-minD*$_{Ng}$, *minE*$_{Ng}$), pJDE1 (*gfp-minD*$_{Ng\text{-}K16Q}$, *minE*$_{Ng}$), and pJS10 (*gfp-minD*$_{Ng}$ alone), respectively, compared to untransformed *E. coli* cell extract (lane 3). (J) Western blotting using anti-MinE$_{Ng}$ antisera detects expression of MinE$_{Ng}$ in cells transformed with pSR15 (lane 1) and pJDE1 (lane 3), but not in untransformed *E. coli* cell extract (lane 2).

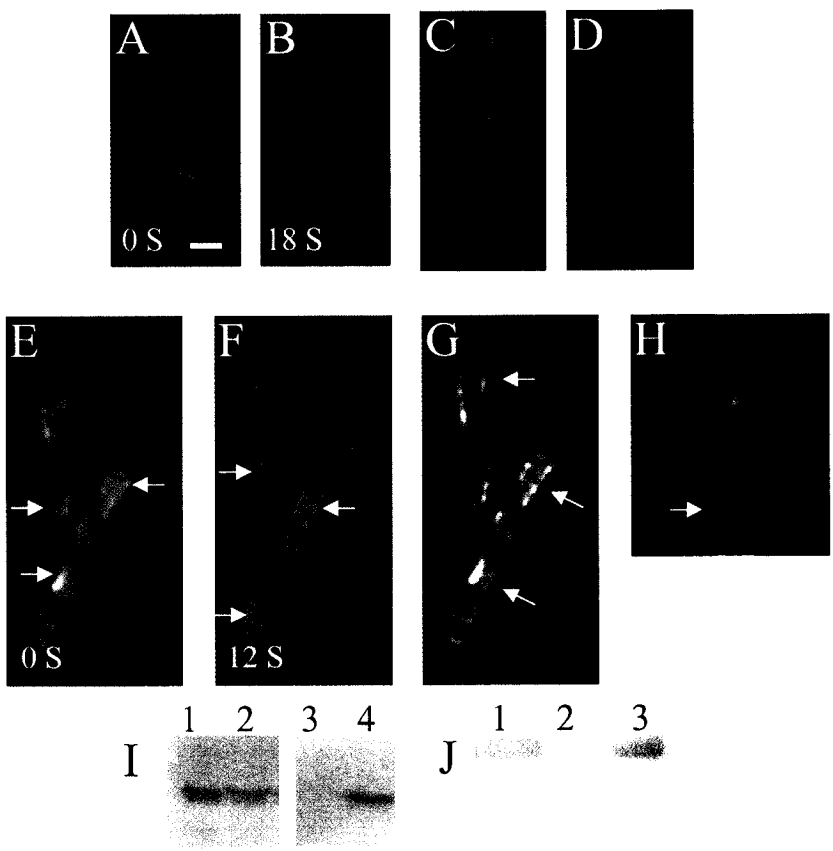
A
B
C
D
0 S
18 S
E
F
G
H
0 S
12 S
1 2 3 4
I
1 2 3
J

4.6 I, lane 1), pJDE1 (*gfp-minD*$_{Ng\text{-}K16Q}$, *minE*$_{Ng}$) (lane 2), and pJS10 (*gfp-minD*$_{Ng}$ alone) (lane 4), in comparison to untransformed negative control cells (lane 3). Western blotting also showed the expression of MinE$_{Ng}$ in *E. coli* PB114 transformed with pSR15 (Figure 4.6 J, lane 1) and pJDE1 (lane 3). No MinE$_{Ng}$ was detected in untransformed *E. coli* PB114 cell extracts (Figure 4.6 J, lane 2).

Raw fluorescent images also provided evidence that GFP-MinD$_{Ng}$ likely formed coil-like structures that wound around the inner cell periphery of *E. coli* (Figure 4.6 E, F). These coiled structures were more readily visible in longer cells, since fluorescent signal concentration at the poles of shorter cells tended to obscure details of the helical array. In elongated cells, GFP-MinD$_{Ng}$ signal appeared as regularly spaced bands that shifted position along the cell length over a matter of seconds (Figure 4.6 E, F; arrows indicate shifted fluorescent signals), similar to previous reports with GFP-MinD$_{Ec}$ (Raskin and de Boer, 1999a). This suggested that GFP-MinD$_{Ng}$ subunits move by undergoing dynamic assembly/disassembly along a helical array. Image enhancement revealed that these dynamic bands were actually composed of accumulated GFP-MinD$_{Ng}$ signal within at least two turns of a coil (Figure 4.6 G, white arrows). Weaker coil signals were also seen in areas with less fusion protein accumulation, suggesting the array extended the length of the cell (Figure 4.6 G, red arrows), as similarly reported with GFP-MinD$_{Ec}$ by Shih *et al.* (2003). In addition, some images showed fluorescent coil strands along different diagonal orientations (Figure 4.6 H, magnified section of filamentous cell transformed with pSR15; compare diagonal coil segment indicated by green arrow with diagonal coil segment indicated by white arrow). This suggested that the GFP-MinD$_{Ng}$ coiled array may consist of at least two coils, possibly arranged in a double-helix conformation (Figure 4.6 H), as noted with GFP-MinD$_{Ec}$ (Shih *et al.*, 2003).

Overall, these results show that wild-type GFP-MinD$_{Ng}$ exhibits MinE$_{Ng}$-dependent intracellular movement and localization within a coiled array in rod-shaped *E. coli*. Furthermore, these results indicate dynamic localization along a coiled array is not exclusive to *E. coli* Min proteins.

GFP-MinD$_{Ng}$ oscillates in round *E. coli* cells. In an effort to elucidate the intracellular localization of GFP-MinD$_{Ng}$ in cocci, *E. coli* KJB24 (*rodA*) (Table 2.1) was selected as a model organism, since it presents a round morphology, and divides in alternating perpendicular planes as *N. gonorrhoeae* does (Begg and Donachie, 1998; Westling-Häggström, 1977).

Upon expressing GFP-MinD$_{Ng}$ from pSR15 (Table 4.1), two cell populations of *E. coli* KJB24 were observed. Approximately 20% were normal-sized cells (~1 μm diameter), while the majority were enlarged cells (> 1 μm). In larger cells, the direction of GFP-MinD$_{Ng}$ movement appeared to be random, with fluorescent signals moving from one point to another without any obvious pattern (Figure 4.7 A). However, in smaller cells, the oscillation of GFP-MinD$_{Ng}$ presented a discernible pattern. In diplococci with apparently completed septa, fusion protein movement was characterized by a back and forth motion in parallel to the septum, with 15 second time lapses from one end of the cell to the other (Figure 4.7 B; arrows indicate fusion protein movement in right cell, arrowheads indicate fusion protein movement in left cell). Hence, GFP-MinD$_{Ng}$ is also able to move within coccal shaped *E. coli* along a direction that is parallel to nascent septa, provided that the cells are not grossly enlarged.

Using an improved microscopy system, round *E. coli* cells containing pSR15 also showed evidence of a GFP-MinD$_{Ng}$-containing coiled array as well. Due to their small size, these coils were much more difficult to visualize in round *E. coli* than in rod-shaped cells. *E. coli* KJB24 cells are not perfectly spherical and the coils appeared to wind around the inner cell membrane in a direction that was parallel to the longest available cell axis (Figure 4.7 C). The longitudinal axis also seemed to dictate the direction of GFP-MinD$_{Ng}$ oscillation, which moved along the same axis. The coiled array was most visible near the center of round cells, where cell diameter was greatest and where fluorescence would not be too concentrated to visualize the array (Figure 4.7 C, middle panel; red arrows indicate two segments of a possible coiled array). As GFP-MinD$_{Ng}$ moved, fluorescent coil signal would diminish at the cell center, and fluorescence lining one cell half would appear (Figure

Figure 4.7. GFP-MinD$_{Ng}$ localization in round *E. coli* cells. Time-lapse fluorescent images of round *E. coli* KJB24 (*rodA*) cells transformed with pSR15, encoding GFP-MinD$_{Ng}$ and untagged MinE$_{Ng}$. (A) GFP-MinD$_{Ng}$ movement in enlarged cells shows apparently uncoordinated movement (arrows indicate GFP-MinD$_{Ng}$ movement in the bottom cell, arrowheads indicate GFP-MinD$_{Ng}$ movement in top cell). (B) GFP-MinD$_{Ng}$ movement in normal sized cells shows an oscillation pattern parallel to the septum that separates two cells. Arrows indicate GFP-MinD$_{Ng}$ movement in rightmost cell, arrowheads indicate GFP-MinD$_{Ng}$ movement in leftmost cell. Times are indicated in seconds. Bar in (A, B) represents 1 μm. DIC = differential interference contrast image. (C) GFP-MinD$_{Ng}$ oscillates in the same direction as the longest available axis in round *E. coli* cells. White arrows in left and right panels indicate GFP-MinD$_{Ng}$ movement along this axis. Center panel shows evidence of GFP-MinD$_{Ng}$ localizing within a coiled array (coil segments indicated with red arrows). Bar represents 1 μm.

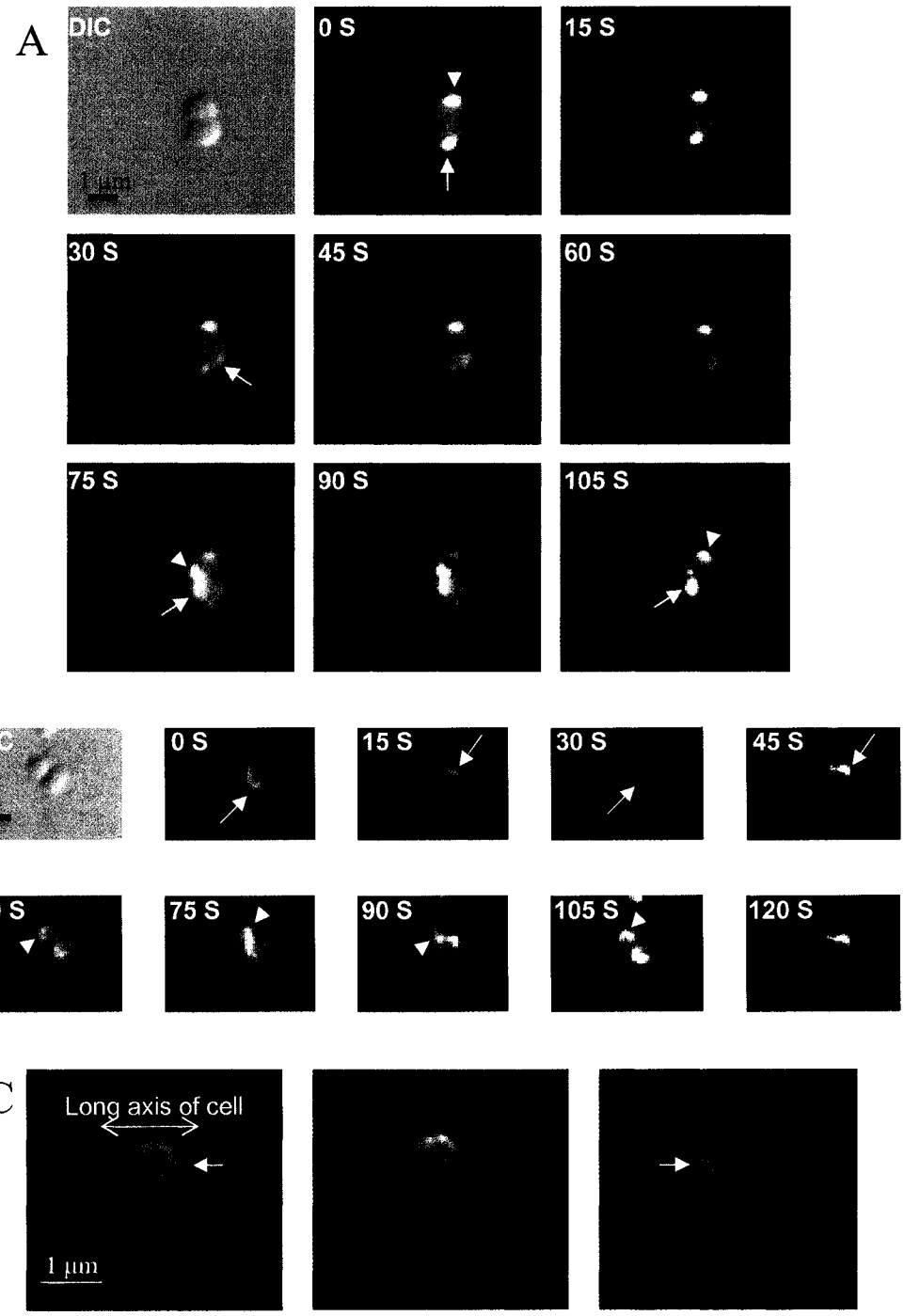
A
DIC
1 μm
0 S
15 S
30 S
45 S
60 S
75 S
90 S
105 S
B
DIC
0 S
15 S
30 S
45 S
60 S
75 S
90 S
105 S
120 S
C
Long axis of cell
1 μm

4.7 C, left and right panels). This suggested that the movement of fluorescent signal was due to GFP-$MinD_{Ng}$ subunits undergoing dynamic assembly/disassembly within a helical array, similar to GFP-$MinD_{Ng}$ movement in rod-shaped *E. coli* PB114. Overall, these results show that GFP-$MinD_{Ng}$ exhibits dynamic localization in round *E. coli* cells and can assemble into an intracellular helical array coiled in the same direction as the longest cell axis, which corresponds to the the axis of GFP-$MinD_{Ng}$ oscillation.

4.4. DISCUSSION

This study showed that $MinD_{Ng}$ is active across species of differing morphologies and can function with non-gonococcal Min systems. The high identity (73%) between MinD from *N. gonorrhoeae* and *E. coli* likely permitted the functionality of the protein in *E. coli* backgrounds.

The overexpression of $MinD_{Ng}$ in wild-type *E. coli* PB103 led to a filamentous phenotype, indicative of cell division arrest at all potential division sites along the length of the rod, similar to the effects of overexpressing *E. coli* MinD (de Boer *et al.*, 1989). This ability to arrest *E. coli* cell division indicates $MinD_{Ng}$ is able to recruit the resident *E. coli* MinC cell division inhibitor to inner cell membrane targets. This is consistent with the ability of both $MinD_{Ng}$ and $MinC_{Ng}$ to inhibit gonococcal cell division when overexpressed together (Chapter 3).

In the absence of $MinC_{Ec}$, the overexpression of $MinD_{Ng}$ did not alter the phenotype of *E. coli* strains DR105 (*minC*$_{Ec}$ mutant) and PB114 (Δ*minCDE*$_{Ec}$), further evidence that $MinD_{Ng}$ requires MinC protein, either from *N. gonorrhoeae* (Chapter 3) or from *E. coli*, to influence cell division. While unable to overexpress $MinD_{Ng}$ by itself from a shuttle vector in a *N. gonorrhoeae* background (Chapter 3), the overexpression of plasmid-encoded $MinD_{Ng}$ in a round *E. coli rodA* mutant provides evidence that increased levels of $MinD_{Ng}$ alone can induce cell division arrest in coccal backgrounds and lead to gross cell enlargement.

Expression of gonococcal MinD in *E. coli* PB104 (*minD*$_{Ec}$ mutant) could also partially correct the minicell phenotype of this strain. Since interactions between $MinC_{Ec}$, $MinD_{Ec}$, and $MinE_{Ec}$ are required for proper *E. coli* cell division site selection (Huang *et al.*, 1996; Raskin and de Boer, 1999a; Hu and Lutkenhaus, 1999; Hu and Lutkenhaus, 2000; Hale *et al.*, 2001; Lackner *et al.*, 2003; Hu *et al.*, 2003), $MinD_{Ng}$ likely interacted with $MinE_{Ec}$ in *E. coli* as well. In support of this, our laboratory has demonstrated the ability of *E. coli* MinE to induce GFP-$MinD_{Ng}$ oscillation in *E. coli* (Ramirez-Arcos *et al.*, 2002). Excessive production of gonococcal MinD may have prevented the full complementation of *E. coli* PB104. An increased MinD/MinE ratio is proposed to extend the oscillation cycle of MinD in *E. coli*, which would permit FtsZ ring formation at cell pole regions,

leading to some to minicell formation (Raskin and de Boer, 1999a), which was observed in the partially complemented *E. coli* PB104 cells of the present study.

Further evidence of $MinD_{Ng}$ cross species functionality was provided by dynamic localization patterns of GFP-$MinD_{Ng}$ expressed in *E. coli* backgrounds. These studies demonstrate, for the first time, that intracellular movement is not exclusive to *E. coli* MinD. In addition, these results indicate that $MinD_{Ng}$ can oscillate in *E. coli* independently of its native gonococcal environment. The fusion protein was able to move, in a $MinE_{Ng}$-dependent manner, from the membrane at one cell pole to the other in rod-shaped *E. coli*, similar to previous reports with GFP-$MinD_{Ec}$ (Raskin and de Boer, 1999a; Rowland *et al.*, 2000). In *E. coli*, $MinE_{Ec}$ is proposed to induce the ATPase activity of $MinD_{Ec}$, which stimulates dynamic $MinD_{Ec}$ movement *in vivo* (Hu *et al.*, 2002; Lackner *et al.*, 2003). Hence, it is highly likely that $MinE_{Ng}$ can interact with $MinD_{Ng}$ to stimulate the enzymatic activity, and subsequent movement, of the latter as well. In accordance with this, when expressed without any $MinE_{Ng}$, GFP-$MinD_{Ng}$ was localized all along the inner cell periphery of *E. coli* and did not show any evidence of movement. Similar peripheral localization has been observed with GFP-$MinD_{Ec}$ when $MinE_{Ec}$ is not present (Raskin and de Boer, 1999a, Shih *et al.*, 2003).

In contrast to wild-type GFP-$MinD_{Ng}$, GFP-$MinD_{Ng\text{-}K16Q}$ did not localize to the membrane, but remained distributed in the cytosol. A similar observation has been made with *E. coli* $MinD_{K16Q}$ fused to GFP, and it is proposed that such mutants may not respond to the effects of ATP, despite retaining the ability to bind this nucleotide (Hu *et al.*, 2002). The cytosolic distribution of GFP-$MinD_{Ng\text{-}K16Q}$ supports the aberrant phenotype of the *N. gonorrhoeae* $minD_{Ng\text{-}K16Q}$ encoding strain, SCD-1 (Chapter 3). By remaining in the cytoplasm, $MinD_{Ng\text{-}K16Q}$ would not be able to recruit $MinC_{Ng}$ to the inner membrane in order to regulate proper cell division in *N. gonorrhoeae* SCD-1.

The present study also shows the ability to assemble into higher ordered structures is not restricted to *E. coli* MinD. Moreover, GFP-$MinD_{Ng}$ required $MinE_{Ng}$ to localize within a helical array in *E. coli* backgrounds, suggesting the two proteins participated in the formation of this coiled structure. This is in support of observations by Shih *et al.* (2003), who also demonstrated a $MinE_{Ec}$-

dependent ability of GFP-$MinD_{Ec}$ to localize as a coiled array. Interestingly, it has recently been demonstrated that $MinE_{Ec}$ can promote the bundling of $MinD_{Ec}$ filaments, in addition to inducing filament disassembly; therefore, these two apparently opposing roles may explain the requirement for MinE in both MinD coil assembly and MinD oscillation (Suefuji *et al.*, 2002).

GFP-$MinD_{Ng}$ movement was also observed in round *E. coli* cells. Interestingly, these cells display an alternating division plane pattern similar to *N. gonorrhoeae* (Begg and Donachie, 1998). In stark contrast to its oscillation in rod-shaped *E. coli*, GFP-$MinD_{Ng}$ moved *parallel* to the nascent septum between two cells, consistent with restricting a subsequent division event to a plane that is perpendicular to the first. A similar localization pattern has been observed in round *E. coli* cells expressing GFP-$MinD_{Ec}$ (Corbin *et al.*, 2002).

Bacterial geometry may play a role in determining the direction of Min protein oscillation (Corbin *et al.*, 2002). While coccal in shape, *E. coli rodA* cells are not necessarily perfectly round, and a GFP-$MinD_{Ec}$ fusion has been shown to almost invariably oscillate parallel to the slight long axis that is characteristic of these cells (Corbin *et al.*, 2002). After one cell division event, a diplococcus is formed and the long axis of each newly formed round *E. coli* is parallel to the nascent septum. GFP-$MinD_{Ec}$ oscillates along this new plane (Corbin *et al.*, 2002), similar to GFP-$MinD_{Ng}$ observed in this study.

This distinct movement of MinD proteins in round *E. coli* cells suggested that a Min protein coiled array should exist in cocci as well, and would be arranged parallel to the longest available axis. Indeed, this was supported with evidence of GFP-$MinD_{Ng}$ decorated coils wound along the longest axis of round *E. coli* cells. This is the first observation of such helical structures in round bacteria. Hence, the ability of $MinD_{Ng}$ to localize within helical arrays in both rod-shaped and round bacteria suggests that this may represent the standard assembled conformation of the protein *in vivo*. Furthermore, it appears that the direction Min protein array coiling specifies the direction of GFP-$MinD_{Ng}$ movement. Whether the ability to localize as an extended intracellular coil is limited to MinD proteins from Gram-negative organisms is currently unknown. In the Gram-positive rod *B. subtilis*,

GFP-$MinD_{Bs}$ localizes distinctly at the cell poles (Marston *et al.*, 1998); however, the conformation of any higher ordered structures at the poles, if they exist, is unclear. Furthmore, it would be interesting to determine whether $MinD_{Bs}$ can be induced to oscillate by MinE in a Gram-negative background.

Although difficult to observe GFP-$MinD_{Ng}$ helical arrays in round cells, many enlarged coccal *E. coli* cells did display curiously uncoordinated movement of GFP-$MinD_{Ng}$, similar to a report with GFP-$MinD_{Ec}$ (Corbin *et al.*, 2002). Cells likely became enlarged due to functional GFP-$MinD_{Ng}$ acting with resident $MinC_{Ec}$ to inhibit cell division. It has been proposed that such enlarged cells are more 'round' and may not have obvious long axes, resulting in apparently disordered MinD protein movement (Corbin *et al.*, 2002). It is also possible that cell enlargement, combined with a dosage effect due to endogenous $MinD_{Ec}$, might disrupt the proper coiling specification of the Min protein array upon overexpression of GFP-$MinD_{Ng}$ in round *E. coli*. This could conceivably lead to the apparent uncoordinated movement of GFP-$MinD_{Ng}$ within enlarged cocci. Such disruption of intracellular cytoskeletal structures upon overexpression of their subunits has been observed with FtsZ protein. FtsZ-GFP normally localizes as a ring at the *E. coli* midcell (Ma *et al.*, 1996); however, severe overexpression of FtsZ-GFP fusion protein can lead to the formation of tubules that localize improperly and extend throughout the length of the cell (Ma *et al.*, 1996; Salimnia *et al.*, 2000).

The average oscillation cycle of GFP-$MinD_{Ng}$ was slower than that of GFP-$MinD_{Ec}$ in *E. coli* WM1032 cells. This may be due to differences in the membrane/phospholipid targets that each MinD protein normally associates with. Although $MinD_{Ng}$ and $MinD_{Ec}$ share nearly identical membrane targeting sequences (MTSs), it is possible that the single amino acid difference between each MTS (S263 in $MinD_{Ng}$ and G262 in $MinD_{Ec}$) represents species specific adaptations that optimize *in vivo* interactions with phospholipids in their respective inner membranes.

The orientation of the MinD MTS is predicted to be parallel to the membrane surface (Mileykovskaya *et al.*, 2003). This would permit the hydrophobic residues on one face of the amphipathic helix to be buried within lipid acyl chains, and allow the charged residues on the opposite face to interact with phospholipids headgroups, preferably those with anionic charge (Szeto

et al., 2002; Szeto *et al.*, 2003; Mileykovskaya *et al.*, 2003). In comparison to the helicity of the *E. coli* MinD MTS (Szeto *et al.*, 2002), the S263 residue of the $MinD_{Ng}$ MTS is predicted to lie on the polar face of the helix. Hence, it is possible that this residue plays a role in modulating protein-membrane association. Similarly, apparent *in vitro* differences in membrane affinity between the MTSs of *E. coli* and *B. subtilis* may be due to inherent amino acid differences (Szeto *et al.*, 2003).

The main constituents of the *E. coli* cell membrane are phosphatidylethanolamine (PE; ~75%), phosphatidylglycerol (PG; ~20%) and cardiolipin (CL; ~5%) (Raetz, 1978). Several groups have also characterized the phospholipids in *N. gonorrheoae* membranes and have shown that the major classes include PE (65-77%) and PG (14-24%); however, there are conflicting results for the proportion of CL, with reports ranging from trace levels up to ~20% of total phospholipids (Senff *et al.*, 1976; Sud and Feingold, 1975; Rahman *et al.*, 2000). Since it is likely that $MinD_{Ng}$ and $MinD_{Ec}$ would each be adapted to optimally bind membranes from their own respective organisms, it is possible that the difference in the oscillation frequency of each protein in *E. coli* is a reflection of this evolution. Differences in oscillation periods could also account for the inability of $MinD_{Ng}$ to fully complement the *E. coli minD* mutant.

In addition, it is currently unknown whether MinD helical arrays associate with another, as yet unidentified, cytoskeletal scaffold (Shih *et al.*, 2003). Should this be the case, then differences in interaction with this latter scaffold may also account for the differences in the oscillation period of heterologously expressed $MinD_{Ng}$ in *E. coli.*

It is noted that the average oscillation cycle of GFP-$MinD_{Ng}$ was significantly faster in *E. coli* PB114 cells than in *E. coli* WM1032 cells. It is possible that interstrain differences in inner membrane phospholipid composition may be responsible for this observation. GFP-$MinD_{Ng}$ localization studies in *E. coli* WM1032 were also carried in a collaborating laboratory using a less advanced microscope system, which did not provide the accurate, automated time-lapse capabilities of the microscope system used to study GFP-$MinD_{Ng}$ movement in *E. coli* PB114. Furthermore, strict

cell length limitations were used in GFP-$MinD_{Ng}$ localization studies in *E. coli* PB114, which may have also contributed to the difference in fusion protein oscillation cycles in *E. coli* WM1032.

Due to their small size (less than or equal to 1 μm) and fastidious nature, it would be difficult to localize Min proteins in live gonococci; hence, round *E. coli rodA* cells were used to gain insight on how $MinD_{Ng}$ might behave in a coccus. However, from the studies in various *E. coli* backgrounds, it is highly likely that $MinD_{Ng}$, as well as the other gonococcal Min proteins, undergo dynamic localization and assembly into higher ordered structures in their native organism, *N. gonorrhoeae*. Indirect evidence of dynamic behaviour is provided by the detection of $MinD_{Ng}$ in both soluble and insoluble fractions of gonococcal cell extracts, suggesting an exchange of protein between the cytosol and membrane (Chapter 3). Furthermore, there is evidence from immunogold localization that $MinD_{Ng}$ is found in the cytoplasm and along the inner cell membrane (Chapter 3). In addition, electron micrographs show that gonococci exhibit growth along one dimension before dividing, and can therefore possess a slight long axis, which is parallel to the nascent septum in diplococci (Westling-Häggström *et al.*, 1977). Hence, it is likely that a Min protein array forms along this axis in *N. gonorrhoeae* as well, similar to the observation with GFP-$MinD_{Ng}$ in round *E. coli* cells used in this study. Future considerations should be directed towards localizing $MinD_{Ng}$ in live *N. gonorrhoeae* to ultimately verify dynamic $MinD_{Ng}$ protein localization in this organism.

Overall, these studies show that $MinD_{Ng}$ is fully active in *E. coli* backgrounds. The gonococcal protein is able to induce cell division arrest in the presence of $MinC_{Ec}$ and can complement an *E. coli minD* mutant. Furthermore, GFP-$MinD_{Ng}$ can oscillate intracellularly and localize within helical arrays *independent* of its native gonococcal environment. These studies also indicate that dynamic behaviour and coiled array formation is not exclusive to *E. coli* MinD. Therefore, it is demonstrated that *E. coli* can act as a suitable indicator strain for gonococcal MinD function.

CHAPTER 5

Identification of $MinD_{Ng}$ protein-protein interactions

Portions of this chapter were published in:

[**Szeto, J.**, Ramirez-Arcos, S., Raymond, C., Hicks, L. D., Kay, C. M., and Dillon J. R. (2001a). Gonococcal MinD affects cell division in *Neisseria gonorrhoeae* and *Escherichia coli* and exhibits a novel self-interaction. J. Bacteriol. *183*, 6253-6264.]

and

[Ramirez-Arcos, S., **Szeto, J.**, Dillon, J. R., and Margolin, W. (2002). Conservation of dynamic localization among MinD and MinE orthologues: oscillation of *Neisseria gonorrhoeae* proteins in *Escherichia coli*. Mol. Microbiol. *46*, 493-504.]

5.1. PURPOSE OF THIS STUDY

In *E. coli*, the three Min proteins are dependent upon each other to properly regulate cell division site placement (Hu and Lutkenhaus, 1999; Raskin and de Boer, 1999a; Rowland *et al.*, 2000; Fu *et al.*, 2001; Hu *et al.*, 2003; Lackner *et al.*, 2003). $MinD_{Ec}$ recruits $MinC_{Ec}$ to the membrane where it can act to inhibit cell division (Hu and Lutkenhaus, 1999; Hu *et al.*, 2003). $MinE_{Ec}$ acts with $MinD_{Ec}$ to localize within intracellular helical arrays and can stimulate the ATPase activity of $MinD_{Ec}$ to induce its dynamic protein movement (Hu and Lutkenhaus, 2001; Shih *et al.*, 2003). Having demonstrated that gonococcal MinD requires the presence of MinC to induce cell division arrest (Chapters 3 and 4) and can localize dynamically, in a MinE-dependent manner, within coiled arrays in *E. coli* (Chapter 4), yeast two-hybrid assays were used to determine what protein interactions $MinD_{Ng}$ may participate in.

Using this system, I was the first to demonstrate that MinD proteins can self-associate. $MinD_{Ng}$, as well as $MinD_{Ec}$, displayed self-interaction. Purified $MinD_{Ng}$ was also shown to exist as a dimer using size-exclusion chromatography and sedimentation equilibrium analysis. In addition, an interaction between $MinD_{Ng}$ and $MinE_{Ng}$ was detected using the yeast two-hybrid system. Although yeast two-hybrid assays did not detect $MinD_{Ng}$-$MinC_{Ng}$ binding, likely due to $MinC_{Ng}$ instability in the yeast reporter strain, a strong interaction between $MinD_{Ng}$ and *E. coli* MinC was observed, in support of $MinD_{Ng}$ functionality in *E. coli* backgrounds. The ability of each gonococcal Min protein to interact with other cell division proteins, including FtsZ, FtsA, PenA (FtsI), and FtsY, was also investigated.

These studies indicate that interactions do exist between $MinD_{Ng}$ and other Min proteins. The self-interaction of MinD proteins from cocci and rods was the first evidence that this property of MinD may be important for controlling cell division site selection across species, even those with morphological differences.

5.2. MATERIALS AND METHODS

Cloning *min* genes into yeast two-hybrid vectors. The yeast two-hybrid system was used to determine interactions between the gonococcal Min proteins. The genes $minC_{Ng}$, $minD_{Ng}$, and $minE_{Ng}$ were individually PCR amplified from gonococcal chromosomal DNA using the primer pairs min12/min29, minD1/minD2, and minE1/minE2, respectively (Table 2.2). Each amplicon was digested at their ends with *Eco*RI and *Bam*HI and ligated in frame to both the GAL4-activation domain (AD) of pGAD424 and the GAL4 DNA-binding domain (BD) of pGBT9 (Clontech; Table 5.1). The plasmids obtained were pGADminC (GAL4-AD-$MinC_{Ng}$), pGBT9minC (GAL4-DNA-BD-$MinC_{Ng}$), pGADminD (GAL4-AD-$MinD_{Ng}$), pGBT9minD (GAL4-DNA-BD-$MinD_{Ng}$), pGADminE (GAL4-AD-$MinE_{Ng}$), and pGBT9minE (GAL4-DNA-BD-$MinE_{Ng}$) (Table 5.1). *E. coli minC* and *minD* were also amplified using the primer pairs EcMinC-up/EcMinC-down and EcMinD-up/EcMinD-down (Table 2.2) and were ligated into the *Eco*RI/*Bam*HI sites of pGAD424 and pGBT9 as above, generating plasmids pSRAD-C (GAL4-AD-$MinC_{Ec}$), pSRBD-C (GAL4-DNA-BD-$MinC_{Ec}$), pSRAD-D (GAL4-AD-$MinD_{Ec}$) and pSRBD-D (GAL4-DNA-BD-$MinD_{Ec}$) (Table 5.1).

Cloning *ftsZ, ftsA, ftsY*, and *penA* into yeast two-hybrid vectors. Similar to each min_{Ng} gene, gonococcal *ftsZ*, *ftsA*, *penA (ftsI)*, and *ftsY* were PCR amplified from gonococcal chromosomal DNA using primer pairs Z1/Z2, A1/A2, penA1/penA2, and Y1/Y2, respectively (Table 2.2). Each gene was cloned into pGBT9 and pGAD424 as above. Plasmids encoding FtsZ, FtsA, PenA(FtsI), and FtsY fused to the GAL4-DNA-AD were: pGADftsZ, pGADftsA, pGADpenA, and pGADftsY (Table 5.1). Plasmids encoding FtsZ, FtsA, PenA(FtsI), and FtsY fused to the GAL4-AD were: pGBT9ftsZ, pGBT9ftsA, pGBT9penA, and pGBT9ftsY (Table 5.1).

Yeast-two hybrid assays. Yeast two-hybrid plasmids were transformed into yeast as outlined in Chapter 2. None of the GAL4-fusions could activate the reporter gene when expressed by themselves,

Table 5.1. Plasmids used in this study

Plasmids	Relevant genotype	Source or reference
Yeast two-hybrid plasmids		
pGAD424	P_{ADH1}[a]::*gal4*(AD)[1] (Amp^R)	Clontech
pGBT9	P_{ADH1}::*gal4*(BD)[2] (Amp^R)	Clontech
pGADminC	pGAD424; P_{ADH1}::*gal4*(AD)-*minC*$_{Ng}$ (Amp^R)	This study
pGBT9minC	pGBT9; P_{ADH1}::*gal4*(BD)-*minC*$_{Ng}$ (Amp^R)	This study
pGADminD	pGAD424; P_{ADH1}::*gal4*(AD)-*minD*$_{Ng}$ (Amp^R)	This study
pGBT9minD	pGBT9; P_{ADH1}::*gal4*(BD)-*minD*$_{Ng}$ (Amp^R)	This study
pGADminE	pGAD424; P_{ADH1}::*gal4*(AD)-*minE*$_{Ng}$ (Amp^R)	This study
pGBT9minE	pGBT9; P_{ADH1}::*gal4*(BD)-*minE*$_{Ng}$ (Amp^R)	This study
pSRAD-C	pGAD424; P_{ADH1}::*gal4*(AD)-*minC*$_{Ec}$ (Amp^R)	This study
pSRBD-C	pGBT9; P_{ADH1}::*gal4*(BD)-*minC*$_{Ec}$ (Amp^R)	This study
pSRAD-D	pGAD424; P_{ADH1}::*gal4*(AD)-*minD*$_{Ec}$ (Amp^R)	This study
pSRBD-D	pGBT9; P_{ADH1}::*gal4*(BD)-*minD*$_{Ec}$ (Amp^R)	This study
pGADftsZ	pGAD424; P_{ADH1}::*gal4*(AD)-*ftsZ*$_{Ng}$ (Amp^R)	This study
pGADftsA	pGAD424; P_{ADH1}::*gal4*(AD)-*ftsA*$_{Ng}$ (Amp^R)	This study
pGADpenA	pGAD424; P_{ADH1}::*gal4*(AD)-*penA*$_{Ng}$ (Amp^R)	This study
pGADftsY	pGAD424; P_{ADH1}::*gal4*(AD)-*ftsY*$_{Ng}$ (Amp^R)	This study
pGBT9ftsZ	pGBT9; P_{ADH1}::*gal4*(BD)-*ftsZ*$_{Ng}$ (Amp^R)	This study
pGBT9ftsA	pGBT9; P_{ADH1}::*gal4*(BD)-*ftsA*$_{Ng}$ (Amp^R)	This study
pGBT9penA	pGBT9; P_{ADH1}::*gal4*(BD)-*penA*$_{Ng}$ (Amp^R)	This study
pGBT9ftsY	pGBT9; P_{ADH1}::*gal4*(BD)-*ftsY*$_{Ng}$ (Amp^R)	This study
Plasmids for protein purification		
pET30a	Kan^R P_{T7}:: 6XHis	Novagen
pJSHD2	pET30a; P_{T7}:: 6XHis-*minD*$_{Ng}$ (Kan^R)	Chapter 3, this study
pMJ1	pUC18; P_{lac}:: 6XHis-*minD*$_{Ng}$ (Amp^R)	This study
pHLCN	Kan^R P_{T7}:: 6XHis-*minC*$_{Ng}$	This study

[1] GAL4-activation domain
[2] GAL4-DNA binding domain

with the exception of GAL4-BD-FtsZ (encoded on pGBT9ftsZ; Table 5.1). β-galactosidase activities were assessed by colony-lift and liquid assays using X-gal and ONPG substrates, as outlined in Chapter 2.

Purification of His-MinD$_{Ng}$. N-terminal His-tagged MinD$_{Ng}$ (His-MinD$_{Ng}$) was purified from *E. coli* BL21 (DE3) transformed with pJSHD2 (Tables 2.1) as detailed in Chapter 2. The His-*minD*$_{Ng}$ gene was also excised from pJSHD2 using *Xba*I and *Sal*I and cloned into similarly digest pUC18 (Table 2.1) to produce plasmid pMJ1 (Table 5.1) for use in *E. coli* morphology studies.

Gel-filtration chromatography of His-MinD$_{Ng}$. His-MinD$_{Ng}$ protein was dialyzed overnight at 4°C against PBS (pH 7.4) with 0.2% Tween-20. The protein was applied to a 25 ml Sephadex 200 column (Amersham Pharmacia Biotech) equilibrated with PBS (pH 7.4) and a flow rate of 0.5 ml/min for size-exclusion chromatography. Protein from the column was monitored by UV absorbance at 280 nm and 0.5 ml fractions were collected and analyzed by SDS-PAGE. The elution pattern of His-MinD$_{Ng}$ was compared to that of standard proteins provided in the Bio-Rad Gel-Filtration Standard.

Sedimentation equilibrium analysis. Sedimentation equilibrium analyses on purified His-MinD$_{Ng}$ was done in collaboration with Dr. Cyril Kay and Leslie Hicks, University of Alberta. Prior to analytical ultracentrifugation analysis, purified His-MinD$_{Ng}$ was dialyzed overnight at 4°C against Buffer A (50 mM Tris, 20 mM NaCl, 3 mM β-mercaptoethanol, 1 mM EDTA; pH 7.5). Sedimentation equilibrium experiments were carried out at 20°C in a Beckman XLI analytical ultracentrifuge using absorbance optics following the procedures previously described (Laue and Stafford, 1999). 110 µl aliquots of sample solution were loaded into 6-sector CFE sample cells, allowing 3 concentrations of sample to be run simultaneously. Runs were performed at a minimum of

2 different speeds and each speed was maintained until there was no significant difference in $r^2/2$ versus absorbance scans taken 2 hours apart to ensure that equilibrium was achieved.

The sedimentation equilibrium data was evaluated using the NONLIN program, which incorporates a nonlinear least-squares curve-fitting algorithm (Johnson *et al.*, 1981). This program allows the analysis of both single and multiple data files. Data can be fit to either a single ideal species model or models containing up to four associating species, depending on which parameters are permitted to vary during the fitting routine. The partial specific volume of the protein and the buffer solution density were estimated using the SEDNTERP program, which incorporates calculations detailed previously (Laue *et al.*, 1991).

Purification of soluble $MinC_{Ng}$. To obtain soluble $MinC_{Ng}$, gonococcal *minC* was PCR amplified using primers min15 and HLC1 (Table 2.2), which incorporated *Bam*HI and *Hind*III sites, respectively. *Bam*HI/*Hind*III-digested amplicon was digested and ligated into similarly treated pET30a to give plasmid pHLCN, encoding His-$MinC_{Ng}$ (Table 5.1). This plasmid was transformed into the expression strain *E. coli* C43 (Table 2.1). A one litre log-phase culture of these cells was induced with 1 mM IPTG for 4 hours at 37°C and shaking at 250 rpm. Cells were harvested by centrifugation (5,000 X g for 10 minutes) (Sorvall RC 5C) and soluble protein purification using 3 ml His-Bind resin (Novagen) was carried out as described by the manufacturer using the following solutions (with the indicated changes in imidazole concentration): 30 ml of binding buffer (5mM imidazole), 18 ml wash buffer 1 (20 mM imidazole), 18 ml wash buffer 2 (30 mM imidazole), 18 ml wash buffer 3 (60 mM imidazole), and 18 ml elution buffer (250 mM imidazole). Construction of pHLCN and purification of His-$MinC_{Ng}$ was carried out by Hui Li, University of Ottawa.

Dot blot assay to detect His-$MinC_{Ng}$ and His-$MinD_{Ng}$ interaction. A dot blot assay was used to determine whether purified His-$MinC_{Ng}$ and His-$MinD_{Ng}$ could interact together. Immobilin-P membrane (Millipore) was washed in methanol for 15 seconds, in ddH_2O for 2 minutes, and in TBS

buffer (50 mM Tris, 1.25 M NaCl, pH 7.5) for 5 minutes. The membrane was then placed over 3 MM filter paper (Whatman) soaked in TBS. Membrane and filter were assembled into a Bio-Dot vacuum dot blot apparatus (Bio-Rad). Low vacuum pressure was applied to the assembled apparatus to draw out excess buffer.

Two-fold serial dilutions of His-$MinD_{Ng}$ were made in TBS buffer, such that 1.2 μg, 0.6 μg, 0.3 μg, 0.15 μg and 0.075 μg of protein in 20 μl volumes could be loaded into the dot blot chambers under light vacuum pressure. 10 μl of TBS was added to each well and vacuum was applied again. The membrane was then removed and blocked with 1% skim milk overnight at 4°C. Purified His-$MinC_{Ng}$ (final concentration of 1.5 μg protein/ml) diluted in TTBS (TTBS = TBS with 0.05% Tween) was subsequently used as a probe to detect His-$MinD_{Ng}$ on the dot blot membrane. After 2 hours exposure at room temperature to His-$MinC_{Ng}$, the membrane was washed 3 times in TTBS (10 minutes per wash) and probed with anti-$MinC_{Ng}$ sera (1:170 in TTBS) for 1.5 hours. Following three additional TTBS washes, the membrane was probed with goat anti-rabbit sera (Bio-Rad, 1:3000 in TTBS) for 1 hour, washed again, and developed using Attophos substrate (JBL Scientific INC.). As a negative control, serial dilutions of lysozyme protein (Sigma) were also prepared similarly, transferred onto Immobilin-P membrane, and probed with His-$MinC_{Ng}$ as above.

5.3. RESULTS

Interactions between Min proteins detected by yeast two-hybrid assays. To determine what interactions might exist between the gonococcal Min proteins, fusions of $MinC_{Ng}$, $MinD_{Ng}$, and $MinE_{Ng}$ were made to GAL4-DNA-binding (BD) and GAL4-activation (AD) domains for yeast two-hybrid protein-protein interaction assays.

Using this system, a novel gonococcal MinD self-interaction was detected (Table 5.2). Yeast colonies transformed with pGBT9minD and pGADminD (Table 5.1), encoding fusions of $MinD_{Ng}$ to GAL4-BD and GAL4-AD, respectively, appeared blue in colour. This was the first report of MinD self-association. Yeast transformed singly with either one of the plasmids appeared white, indicating that the fusion proteins themselves were incapable of activating the yeast *lacZ* reporter gene. Liquid β-galactosidase assays performed on the yeast transformants also verified the $MinD_{Ng}$-$MinD_{Ng}$ interaction, giving values of 12.3 ± 7.3 Miller units relative to the 27.2 ± 6.0 Miller units recorded for the positive control interaction of SV40 large T-antigen and p53 (Table 5.2). For the first time, the self-association of *E. coli* MinD was also detected, although the strength of interaction was not as strong as that observed for gonococcal MinD, based on β-galactosidase activity (Table 5.2). Interestingly, $MinD_{Ng}$ and $MinD_{Ec}$ could interact with each other in either orientation tested (Table 5.2). The self-association of $MinE_{Ng}$ or of $MinC_{Ng}$ was not observed (Table 5.2).

$MinD_{Ng}$ was also able to interact with $MinE_{Ng}$ and produced a β-galactosidase activity of 2.8 ± 0.4 Miller units (Table 5.2). This interaction was only detected when $MinE_{Ng}$ was fused to the GAL4-DNA-BD (Table 5.2). An interaction between $MinE_{Ng}$ and $MinC_{Ng}$ was not detected in this assay (Table 5.2).

Yeast two-hybrid assays have revealed strong interactions between MinC and MinD from *E. coli* (Huang *et al.*, 1996) and from *B. subtilis* (Marston and Errington, 1999b). However, interaction between gonococcal MinC and MinD was not detected using the yeast two-hybrid system in this

TABLE 5.2. Yeast two-hybrid assays of Min protein interactions

Fusion to GAL4-AD[1]	Fusion to GAL4-DNA-BD[2]	Intensity of blue colony colour[3]	β-galactosidase Activity (Miller Units)[4]
$MinD_{Ng}$[5]	$MinD_{Ng}$	++	12.3 ± 7.3
$MinD_{Ec}$[6]	$MinD_{Ec}$	++	4.4 ± 0.9
$MinD_{Ng}$	$MinD_{Ec}$	++	14.3 ± 0.6
$MinD_{Ec}$	$MinD_{Ng}$	++	28.8 ± 7.8
$MinE_{Ng}$	$MinE_{Ng}$	-	ND[7]
$MinC_{Ng}$	$MinC_{Ng}$	-	ND
$MinE_{Ng}$	$MinD_{Ng}$	-	ND
$MinD_{Ng}$	$MinE_{Ng}$	++	2.8 ± 0.4
$MinE_{Ng}$	$MinC_{Ng}$	-	ND
$MinC_{Ng}$	$MinE_{Ng}$	-	ND
$MinD_{Ng}$	$MinC_{Ng}$	-	ND
$MinC_{Ng}$	$MinD_{Ng}$	-	ND
$MinD_{Ng}$	$MinC_{Ec}$[8]	+++	131.5 ± 84.6
$MinC_{Ec}$	$MinD_{Ng}$	+	0.2 ± 0.1
$MinC_{Ec}$	$MinD_{Ec}$	+++	ND
SV40-Large T Antigen	p53	+++	27.2 ± 6.0

[1] GAL4-activation domain
[2] GAL4-DNA binding domain
[3] Yeast colony colour indicating strength of interaction: (+++) = dark blue; (++) = blue; (+) = faint blue; (-) = white colonies
[4] One unit equals the amount of β-galactosidase which hydrolyzes 1 μmol of ONPG per minute per cell
[5] *N. gonorrhoeae* MinD
[6] *E. coli* MinD
[7] 'ND' indicates β-galactosidase activity Not Determined
[8] *E. coli* MinC

study (Table 5.2). It is noted that gonococci become enlarged when $MinC_{Ng}$ and $MinD_{Ng}$ are overexpressed simultaneously (Chapter 3), suggesting an interaction between the two proteins. From heterologous expression studies of $MinD_{Ng}$ in *E. coli* backgrounds, it is clear that gonococcal MinD can act with *E. coli* MinC to inhibit cell division (Chapter 4). $MinC_{Ec}$ has 36% identity to *N. gonorrhoeae* MinC. Therefore, the ability of $MinC_{Ec}$ to interact with $MinD_{Ng}$ was assessed. Using the yeast two-hybrid system, $MinD_{Ng}$ and $MinC_{Ec}$ interaction was observed in both orientations tested, with the fusion of GAL4-AD-$MinD_{Ng}$ interacting particularly well with the GAL4-BD-$MinC_{Ec}$ fusion to produce a β-galactosidase activity of 131.5 ± 84.6 units (Table 5.2). In addition, the stong interaction between *E. coli* MinC and *E. coli* MinD (Huang *et al.*, 1996) was also confirmed (Table 5.2).

Overall, these studies demonstrate that interactions between the gonococcal Min proteins exist. Significantly, the detected self-associations of $MinD_{Ng}$ and of $MinD_{Ec}$ were novel findings. The self-association of MinD from species with differing morphologies suggests that this characteristic is important for MinD function in general. Furthermore, $MinD_{Ng}$ interacts with MinE and MinC, in support of previous yeast two-hybrid studies with *E. coli* Min proteins (Huang *et al.*, 1996).

Testing gonococcal Min protein interactions with cell division proteins. Each gonococcal Min protein was also assayed for interaction with other *N. gonorrhoeae* cell division and cell growth proteins, including FtsZ, FtsA, and PenA (FtsI) from the *dcw* cluster (Francis *et al.*, 2000; Salimnia *et al.*, 2000) (see Introduction for a review of these proteins). FtsZ and FtsA were selected since they are recruited early in the cell division process, when Min proteins appear to act (Hu *et al.*, 1999; Errington *et al.*, 2003; Johnson *et al.*, 2002). FtsI acts at a later stage in cell division to help form the cell wall between daughter cells (Bramhill, 1997). FtsY, an inner membrane protein, was also included since it was originally classified as a cell division protein (Gill and Salmond, 1987). This protein has since been characterized as a receptor for the signal recognition particle (SRP) involved in

targeting integral membrane proteins to the inner membrane (Luirink *et al.*, 1994). In *N. gonorrhoeae*, the FtsY homologue is also known as PilA (Arvidson *et al.*, 1999).

Using the yeast two-hybrid system, no interactions between any of the Min proteins and FtsZ, FtsA, FtsI or FtsY were detected (Table 5.3). In addition, no interactions between FtsZ, FtsA, PenA, and FtsY were detected. When fused to the GAL4-BD, gonococcal FtsZ was able to activate the yeast *lacZ* reporter gene by itself, similar to a report of *E. coli* FtsZ (Huang *et al.*, 1996); therefore, only FtsZ-GAL4-AD was used in these experiments (Table 5.3).

His-MinD$_{Ng}$ exhibits self-association. To confirm that MinD$_{Ng}$ can self-associate, N-terminal His-tagged MinD$_{Ng}$ (His-MinD$_{Ng}$) was purified for gel-filtration and sedimentation equilibrium analyses. *E. coli* BL21(DE3) expressing the fusion protein were filamentous, indicating cell division arrest (Figure 5.1 B). This was in contrast to the short rod morphology of *E. coli* BL21 (DE3) cells transformed with the control pET30a vector (Figure 5.1 A). SDS-PAGE analysis of IPTG induced cell extracts from pET30a (Figure 5.1C, lane 2) and pJSHD2 (lane 3) transformants show high overexpression of His-MinD$_{Ng}$ in the latter cells (lane 3, arrow).

The functionality of the fusion protein was further verified by expressing His-MinD$_{Ng}$ from the pUC18-derived plasmid pMJ1 (Table 5.1) in *E. coli minC* and *minD* mutants, specifically strains DR105 and PB104, respectively (Table 2.1). *E. coli* DR105 expressing His-MinD$_{Ng}$ from pMJ1 retained its minicell phenotype (compare Figures 5.1 D, E), while *E. coli* PB104 became filamentous (compare Figures 5.1 G with F), indicative of cell division arrest. Overexpression of the fusion protein in both strains was verified by Western blotting [Figure 5.1 H; lane 1, *E. coli* DR105 (pMJ1); lane 2, *E. coli* PB104 (pMJ1)]. Together these observations show that His-MinD$_{Ng}$ is active and requires the presence of functional MinC, found in strain PB104, but not in DR105, to inhibit cell division.

His-MinD$_{Ng}$ was purified from the *E. coli* BL21 (DE3) expression strain (Figure 5.2) and subsequently applied to a 25 mL Superdex 200 size exclusion column (Figure 5.3 A, B). At the time

Table 5.3. Yeast two-hybrid assays to assess gonococcal Min protein interactions with selected cell division and cell growth proteins

	FUSION WITH GAL4 DNA BINDING DOMAIN						
	$MinC_{Ng}$	**$MinD_{Ng}$**	**$MinE_{Ng}$**	**$FtsZ_{Ng}$**[1]	**$FtsA_{Ng}$**	**$FtsY_{Ng}$**	**$PenA_{Ng}$**
$MinC_{Ng}$	No	No	No	-	No	No	No
$MinD_{Ng}$	No	***Yes***	***Yes***	-	No	No	No
$MinE_{Ng}$	No	No	No	-	No	No	No
$FtsZ_{Ng}$	No	No	No	-	No	No	No
$FtsA_{Ng}$	No	No	No	-	No	No	No
$FtsY_{Ng}$	No	No	No	-	No	No	No
$PenA_{Ng}$	No	No	No	-	No	No	No

[1] A fusion of the GAL4-DNA binding domain to $FtsZ_{Ng}$ could activate the β-galactosidase reporter gene in yeast; therefore, GAL4-DNA-BD-$FtsZ_{Ng}$ fusion was not tested for interaction with other proteins.

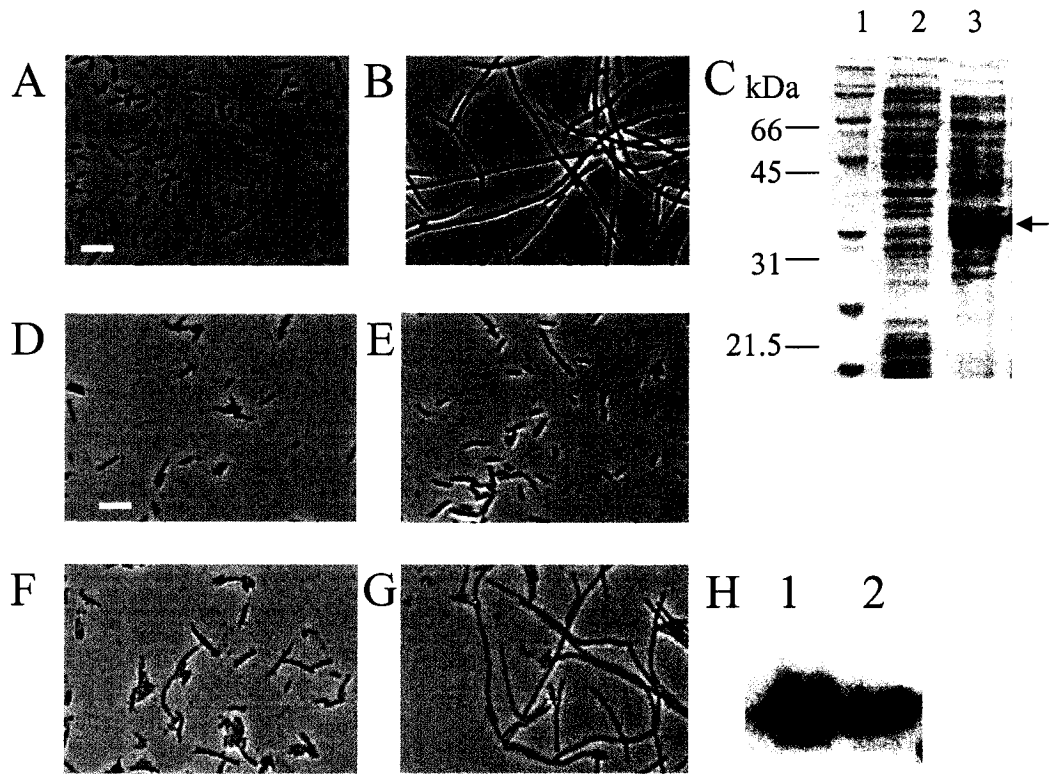

Figure 5.1. Functionality of N-terminal His-tagged $MinD_{Ng}$ (His-$MinD_{Ng}$). (A) *E. coli* BL21 (DE3) cells transformed with pET30a control vector display short rod morphology after induction with 1 mM IPTG, while (B) induced cells transformed with pJSHD2, encoding His-$MinD_{Ng}$, have a filamentous phenotype. (C) Induced cell extract from *E. coli* BL21 pET30a transformants was resolved by SDS-PAGE (lane 2) and compared to induced pJSHD2 transformant cell extracts (lane 3; arrow indicates overexpressed His-$MinD_{Ng}$). Lane 1 contains broad range protein marker. (D) *E. coli* DR105 (*minC* mutant) transformed with pUC18 display a typical minicell phenotype, which is also retained upon transformation with pMJ1 (E), a pUC18 derived plasmid encoding His-$MinD_{Ng}$. (F) *E. coli* PB104 (*minD* mutant) transformed with pUC18 also exhibits a minicell phenotype; however, cells transformed with pMJ1 (G) become very filamentous. Scale bar in (A) is 5 μm and all figures are at the same magnification. (H) Western blotting using affinity-purified anti-$MinD_{Ng}$ antisera detects His-$MinD_{Ng}$ expression in *E. coli* DR105 (pMJ1) and *E. coli* PB104 (pMJ1).

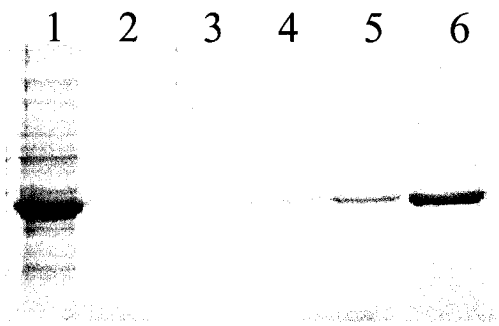

Figure 5.2. Purification of His-MinD$_{Ng}$ from *E. coli* BL21 (DE3). Nickel affinity chromatography was used to purify His-MinD$_{Ng}$ from induced *E. coli* BL21 (DE3) transformed with pJSHD2. Lane 1, induced whole cell extract; lane 2, 5 mM imidazole buffer wash; lane 3, 20 mM imidazole buffer wash; lane 4, 30 mM imidazole buffer wash; lane 5, 60 mM imidazole buffer wash; lane 6, 250 mM imidazole elution.

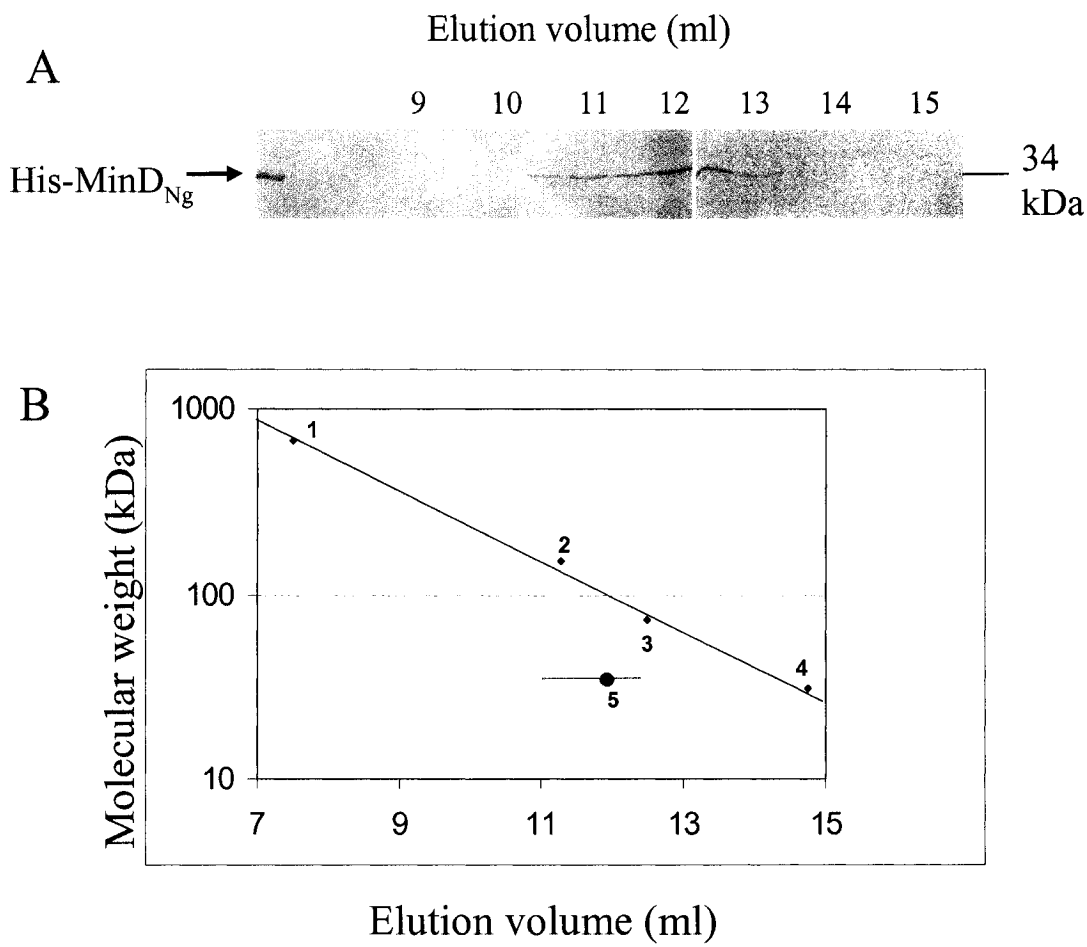

Figure 5.3. Size exclusion chromatography of purified His-MinD$_{Ng}$. Purified protein was applied to a Superdex 200 column equilibrated with PBS (pH 7.4) at a flow rate of 0.5 ml/min. (A) Eluted fractions were analyzed by SDS-PAGE. (B) Elution of His-MinD$_{Ng}$ relative to protein standards (1) thyroglobulin (~669 KDa), (2) goat anti-human IgG (~150 kDa), (3) bovine prothrombin (72 KDa), and (4) carbonic anhydrase (31 KDa). His-MinD$_{Ng}$ eluted between 11 and 12.5 ml (horizontal line), with the majority eluting at ~12 ml (red circle).

of these particular studies, the implications of ATP for MinD self-association were not considered; hence, experiments with His-$MinD_{Ng}$ in this chapter were conducted in the absence of ATP. In comparison to the elution of control proteins thyroglobulin (~669 kDa), goat IgG (~150 kDa), bovine prothrombin (~72 kDa), and carbonic anhydrase (31 kDa), the majority of His-$MinD_{Ng}$ eluted from the size exclusion column at an apparent molecular weight of at least twice its predicted monomeric molecular weight of 34 kDa (Figure 5.3 A, B). This indicated that the protein passed through the column at least as a dimer, in support of the yeast two-hybrid data. The elution of proteins from size-exclusion columns is dependent upon protein mass and shape. Since the crystal structure of several MinD proteins show it is a globular protein (Cordell and Löwe, 2001; Hayashi *et al.*, 2001; Sakai *et al.*, 2001), the elution profile of purified $MinD_{Ng}$ in this study likely correlates well with apparent state of protein association.

The self-interaction of His-$MinD_{Ng}$ was also confirmed by sedimentation equilibrium analysis. The data points from three different loading concentrations of His-$MinD_{Ng}$, depicting both the concentration and migration of the protein matched well with the theoretical fit lines of a dimer (Figure 5.4 A-C, lower panels). Further analysis showed that these data points had little deviation from their respective theoretical fit lines (Figure 5.4 A-C, upper panels). The protein was shown to have an average apparent molecular weight of 67,955, supporting a single species model of a dimer, which would have an expected molecular weight of 69,364. At a rotor speed of 16,000 rpm, there was also some evidence of decreasing apparent molecular weight with decreasing loading concentrations, suggesting that the protein could exist in a monomer-dimer equilibrium model (Table 5.4). Degradation and/or dissociation of the protein sample was observed over time when sedimentation analyses were run at rotor speeds greater than 16,000 rpm (Table 5.4).

Collectively, yeast two-hybrid, size-exclusion chromatography, and sedimentation equilibrium analyses show for the first time that bacterial MinD proteins are capable of dimer formation, suggesting that self-association may be important for MinD function across species.

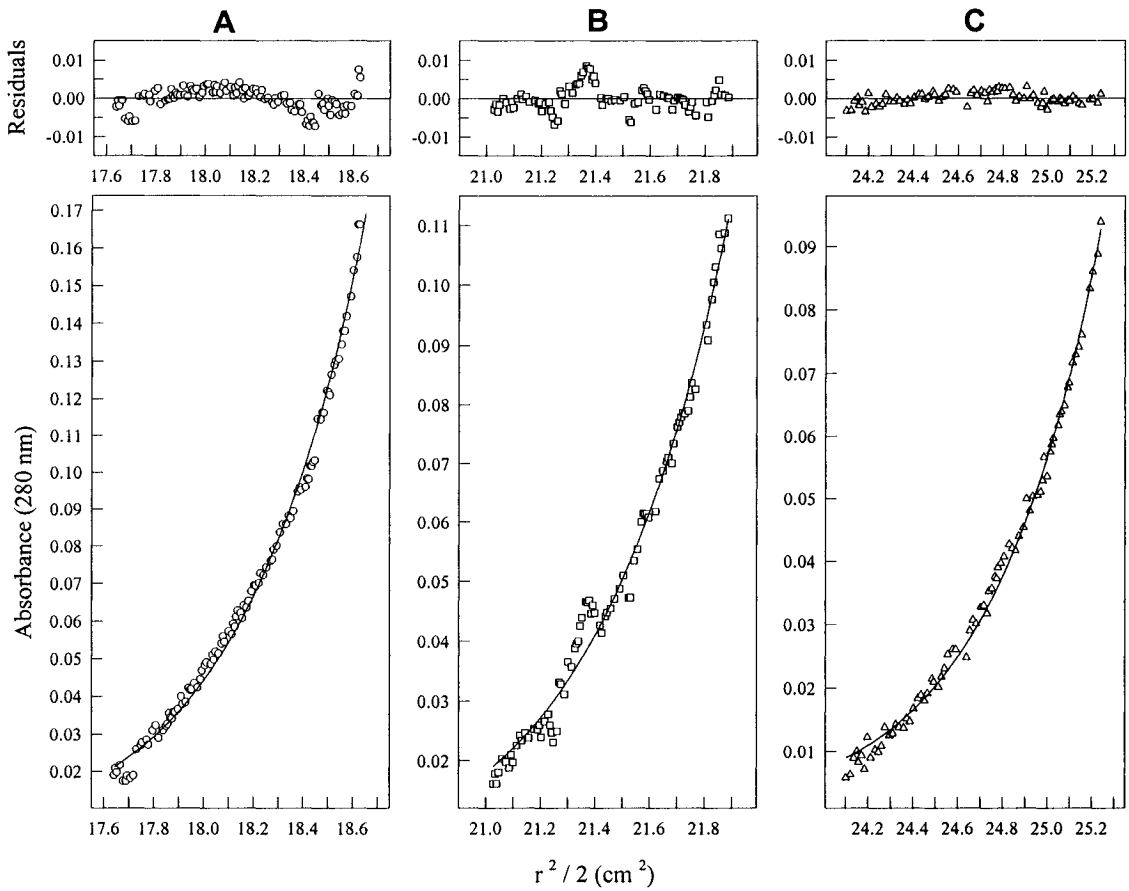

Figure 5.4. Analytical ultracentrifugation analyses of His-MinD$_{Ng}$. Plots illustrating sedimentation equilibrium data from 3 loading concentrations of His-MinD$_{Ng}$ fit globally to a single species model indicating a dimeric protein. A: 0.39 mg/ml. B: 0.27 mg/ml. C: 0.18 mg/ml. The run was performed at 20°C and 16,000 rpm. Lower panels display radial distance2/2 versus absorbance plots. Symbols represent measured data points and solid lines represent theoretical fit lines. Upper panels display the random deviation of the data points from the fit lines, indicating a good fit to the dimeric model.

Table 5.4. Sedimentation equilibrium data obtained for His-MinD$_{Ng}$

Protein concentration (mg/ml)	Ultracentrifugation speed (rpm)	Apparent molecular weight[1] (Daltons)	Probable state of protein
0.18	16,000	59,581	
0.27	16,000	61,123	Dimer
0.39	16,000	72,067	
0.18	22,000	27,927	
0.27	22,000	49,435	Monomer-dimer and/or degradation
0.39	22,000	32,270	
0.18	28,000	37,951	
0.27	28,000	29,588	Monomer or degradation
0.39	28,000	18,260	

[1] Predicted molecular weight of His-MinD dimer is 69,364 Daltons

$MinD_{Ng}$ interaction with $MinC_{Ng}$ detected using a dot blot assay. Since the yeast two-hybrid system did not detect $MinD_{Ng}$-$MinC_{Ng}$ interaction, a dot blot assay was developed to determine whether the two gonococcal proteins could bind to one another (Figure 5.5).

His-$MinC_{Ng}$ was incubated over an Immobilin-P membrane previously spotted with varying concentrations of His-$MinD_{Ng}$. His-$MinC_{Ng}$ could bind to the immobilized His-$MinD_{Ng}$, as detected by polyclonal anti-$MinC_{Ng}$ (Figure 5.5, rows 1-4). This ability to interact was also dependent upon the amount of His-$MinD_{Ng}$ present, as evidenced by the decreased His-$MinC_{Ng}$ signal as levels of His-$MinD_{Ng}$ dropped from 1.2 μg to 0.075 μg spotted per well (Figure 5.5, rows 1-4). As a negative control, lysozyme, an unrelated protein, was also spotted onto the membrane and probed for interaction with His-$MinC_{Ng}$. As expected, no significant binding of His-$MinC_{Ng}$ to lysozyme was detected (Figure 5.5, row 5). In addition, His-$MinC_{Ng}$ was not included as a probe in some experiments to determine whether the anti-$MinC_{Ng}$ sera itself would detect His-$MinD_{Ng}$ on the membrane and produce a false positive signal. It was found that the anti-$MinC_{Ng}$ antibodies presented only minimal detection of His-$MinD_{Ng}$ (Figure 5.5, rows 6-7). This minor cross-reaction of anti-$MinC_{Ng}$ antisera can likely be attributed to the common N-terminal peptide sequence found, in addition to the 6XHis tag, within both His-$MinC_{Ng}$ and His-$MinD_{Ng}$ (see description of pJSHD2 construction, Chapter 2).

Hence, a direct interaction was observed between purified $MinD_{Ng}$ and $MinC_{Ng}$ proteins, in support of overexpression studies in *N. gonorrhoeae* (Chapter 3), as well as yeast two-hybrid results using $MinD_{Ng}$ and *E. coli* MinC.

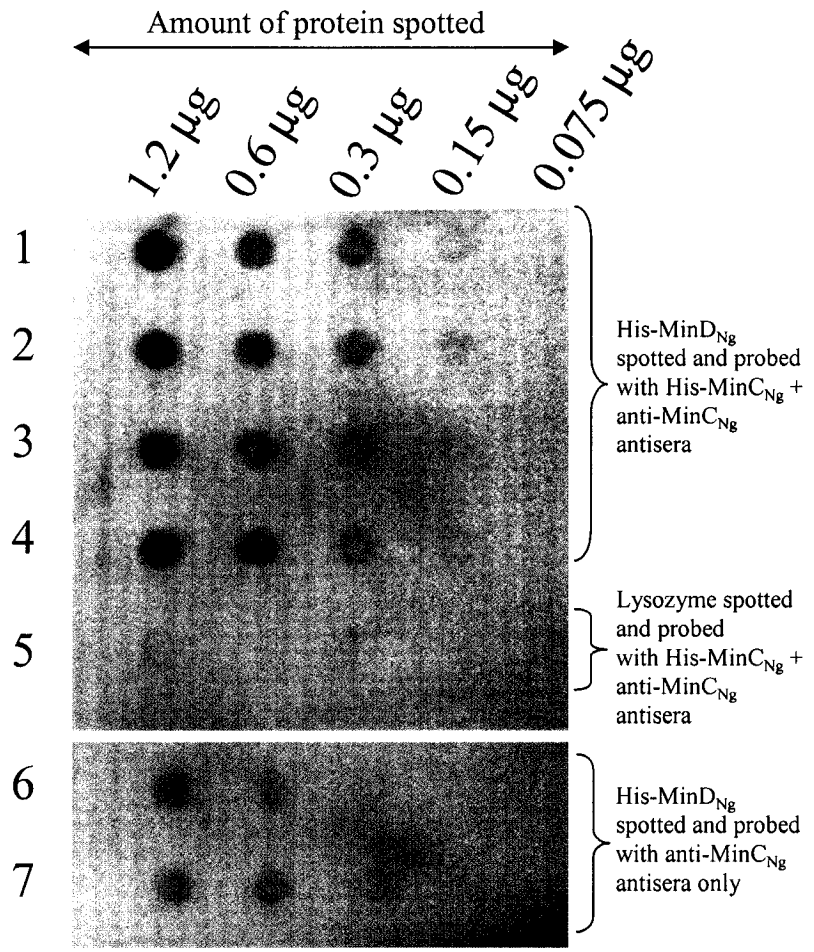

Figure 5.5. Dot blot assay to detect MinD$_{Ng}$ interaction with MinC$_{Ng}$. The ability of purified His-MinC$_{Ng}$ to bind membrane-immobilized His-MinD$_{Ng}$ was determined. Two-fold serial dilutions of purified His-MinD$_{Ng}$ were applied to an Immobilin-P membrane. (Rows 1-2 and 3-4): His-MinD$_{Ng}$ from two separate purification preparations. (Row 5): Lysozyme was used as a negative control and was applied to the same blot. Following blocking, the membrane was probed with purified His-MinC$_{Ng}$ and bound His-MinC$_{Ng}$ was detected by incubating the membrane with affinity-purified anti-MinC$_{Ng}$ antisera. (Rows 6-7): A parallel blot was also spotted with His-MinD$_{Ng}$ and probed with anti-MinC$_{Ng}$ antisera, without prior incubation with His-MinC$_{Ng}$ itself, to determine the degree of cross-reactivity with His-MinD$_{Ng}$.

5.4. DISCUSSION

This study is the first to identify the ability of bacterial MinD proteins to self-associate. Using the yeast two-hybrid system, both $MinD_{Ng}$ and $MinD_{Ec}$ displayed self-association, and could interact as heterodimers as well. These interaction studies offered the first physical evidence for the possibility that bacterial MinD might self-assemble. The self-association of MinD from either cocci or rods suggests that this interaction may be important for controlling cell division site selection in both cell types despite their morphological differences. In support of this, GFP-$MinD_{Ng}$ (Chapter 4) and GFP-$MinD_{Ec}$ (Shih *et al.*, 2003) are shown to assemble along higher ordered coil structures *in vivo*.

What is the role for *dimeric* MinD? $MinD_{Ec}$ has recently been shown to dimerize in the presence of ATP, which is proposed to activate its membrane targeting sequence to promote membrane affinity, as proposed by the 'dimer trigger' model (Hu and Lutkenhaus, 2003; Hu *et al.*, 2003). $MinD_{Ec}$ can also polymerize *in vitro,* and these polymers appear to consist of paired protofilaments with a combined diameter of ~ 6 nm, consistent with a pair of MinD monomers when measured across their narrowest profile (~3 nm) (Hayashi *et al.*, 2001; Suefuji *et al.*, 2002). Hence, dimeric MinD may be the basic building block, and perhaps nucleating seed, of MinD polymers (D. RayChaudhuri, Tufts University, personal communication). Dimerization may also be important for optimizing the ATPase activity of MinD proteins once at the membrane. Examination of a modeled MinD dimer suggested that the signature lysine (corresponding to K11 in $MinD_{Ng}$ and $MinD_{Ec}$) within the deviant Walker A motif of each MinD subunit may stabilize ATP that is bound by the opposite subunit, thus aiding nucleotide hydrolysis (Lutkenhaus and Sundaramoorthy, 2003).

Size-exclusion chromatography and sedimentation equilibrium analyses also indicated that purified N-terminal His-tagged $MinD_{Ng}$ was dimeric, in support of yeast two-hybrid studies. Although these *in vitro* studies were performed prior to indications that ATP may play a role in MinD dimerization (Hu *et al.*, 2003), purified His-$MinD_{Ng}$ was observed to be dimeric, despite the *absence*

of ATP. In the following chapter, evidence that *C-terminal* His-tagged $MinD_{Ng}$ can be induced to dimerize in the presence of ATP is presented (Chapter 6).

What might account for the ATP-independent dimerization of N-terminal His-tagged $MinD_{Ng}$? It is possible that ATP remained bound to His-$MinD_{Ng}$ during the purification process, causing it to remain dimeric during its gel-filtration and sedimentation equilibrium assays. The relatively long peptide sequence that is fused to the N-terminus of His-$MinD_{Ng}$, in addition to the His-tag, may have also affected the ability of the protein to hydrolyze ATP, thus maintaining its self-association. However, it is clear that this long N-terminal peptide did not abrogate the ability of His-$MinD_{Ng}$ to induce MinC-mediated cell division, as evidenced by the functional expression studies in various *E. coli* backgrounds. Interestingly, others have also observed that $MinD_{Ec}$ can exist as a dimer in the absence of ATP (D. RayChaudhuri, Tufts University, personal communication).

Furthermore, it is possible that MinD proteins can exist in ATP-independent monomer-dimer equilibria which, in the case of His-$MinD_{Ng}$, was shifted in favour of dimers under its assay conditions. It is noted that the concentrations of His-$MinD_{Ng}$ (0.18-0.39 mg/ml) used in sedimentation equilibrium analyses were higher than *in vivo* estimates in *E. coli* (~1-2 μM or 0.03-0.06 mg/ml) (Mileykovskaya *et al.*, 2003), and likely in *N. gonorrhoeae*. Thus, it is possible that these higher protein concentrations may have driven His-$MinD_{Ng}$ more favourably towards dimerization, even in the absence of ATP. Interestingly, sedimentation equilibrium analyses of His-$MinD_{Ng}$ provided some evidence of decreasing apparent molecular weight with decreasing loading concentrations, suggesting the protein might exist in a monomer-dimer equilibrium model (Leslie Hicks, University of Alberta, personal communication), however, further testing would need to be done to verify this. There are many examples of protein monomer-dimer equilbria being influenced by environmental factors. *E. coli* SecA and *P. furiosus* ferredoxin can both experience different monomer-dimer equilibrium reactions depending upon ionic strength and/or temperature (Hasan *et al.*, 2002; Woodbury *et al.*, 2002). In addition, the *B. subtilis* ATP-binding protein OpuAA also exhibits increased dimerization

upon increasing protein concentration, despite the absence of its nucleotide substrate (Horn *et al.*, 2003).

In *E. coli*, MinE interacts with MinD to promote the ATPase activity, oscillation, and coiled-array localization of MinD (Huang *et al.*, 1996; Raskin and de Boer, 1999a; Rowland *et al.*, 2000; Hu and Lutkenhaus, 2001; Hu *et al.*, 2002; Shih *et al.*, 2003). This study also detected an interaction between $MinD_{Ng}$ and $MinE_{Ng}$, further supporting the *in vivo* dynamism and helical assembly of GFP-$MinD_{Ng}$ in the presence of $MinE_{Ng}$ (Chapter 4). The association of $MinD_{Ng}$ with $MinE_{Ng}$ indicates that the latter likely stimulates the ATPase activity of $MinD_{Ng}$ to drive its intracellular movement, both in *E. coli* and, most probably, in *N. gonorrhoeae*.

Although evidence from overexpression studies suggests $MinC_{Ng}$ and $MinD_{Ng}$ are both required to inhibit gonococcal cell division (Chapter 3), a $MinC_{Ng}$-$MinD_{Ng}$ interaction was not detected using the yeast two-hybrid system. This is in contrast to reports for MinC and MinD homologues from *E. coli* or *B. subtilis*, which do interact (Huang *et al.*, 1996, Marston and Errington, 1999b). However, the yeast two-hybrid system did detect a strong interaction between gonococcal MinD and *E. coli* MinC, in support of its functionality in *E. coli* backgrounds (Chapter 4).

It is noted that different yeast two-hybrid systems may detect different Min protein interactions. For example, the dimerization of *E. coli* MinE was detected by one group using yeast two-hybrid methods (Pichoff *et al.*, 1995), but not by others using a different yeast two-hybrid system (Huang *et al.*, 1996; this study). These differences may be due to steric considerations, protein expression, and protein stability within various yeast systems. Hence, it is possible that the GAL4-$MinC_{Ng}$ fusions were unstable or poorly expressed in the yeast reporter strain, such that no interation between $MinC_{Ng}$ and $MinD_{Ng}$ was detected. Studies have indicated that the C-terminus of *E. coli* MinC is responsible for interaction with its MinD partner (Hu and Lutkenhaus, 2000). From this, our laboratory has constructed a chimeric protein consisting of the N-terminus of *E. coli* MinC and the C-terminus of *N. gonorrhoeae* MinC. Using the yeast two-hybrid system, we were able to observe a strong interaction between the chimeric MinC and $MinD_{Ng}$ (Ramirez-Arcos *et al.*, in press).

Therefore, this chimeric MinC protein is likely more stable in our yeast reporter strain than $MinC_{Ng}$, and can be used to study $MinC_{Ng}$ and $MinD_{Ng}$ interactions in future experiments.

No interactions between the three Min proteins and the cell division/cell development proteins FtsZ, FtsA, PenA (FtsI), and FtsY were detected. An interaction between $MinC_{Ng}$ and FtsZ would be expected, since purified *E. coli* MinC has been demonstrated to interact with FtsZ (Hu *et al.*, 1999). However, yeast two-hybrid assays also do not detect any association between *E. coli* MinC and FtsZ (Huang *et al.*, 1996; Hu *et al.*, 1999), suggesting this system may not be the optimal for studying this interaction.

Studies with *E. coli* proteins have shown that the ATP-bound form of $MinD_{Ec}$ is required to interact with $MinC_{Ec}$ *in vitro* (Hu *et al.*, 2003), suggesting dimeric MinD is the active MinC partner. However, in the present study, an interaction between purified His-$MinC_{Ng}$ and His-$MinD_{Ng}$ was detected in the *absence* of additional ATP. Hence, it is possible that His-$MinD_{Ng}$ could bind His-$MinC_{Ng}$ under these conditions since His-$MinD_{Ng}$ was already dimerized, as discussed above.

Could there be a biological function for ATP-free MinD dimers? In order to oscillate within the cell, membrane-associated MinD must be released into the cytoplasm upon hydrolysis of its bound ATP molecule (Hu *et al.*, 2002; Lackner *et al.*, 2003). It has been proposed that simple diffusion in the cytosol may be sufficient to ensure that ATP-free MinD proteins do not re-associate with existing MinD assemblies (Lackner *et al.*, 2003). However, it is possible that rapid ATP-binding may drive the protein back to its original membrane (or MinCDE array) location, and thus negate proper MinD movement. It is tempting to speculate that, *in vivo*, nucleotide-free MinD dimers may form from nascent ATP-free MinD monomers that are released from the membrane. This could conceivably delay ATP-binding and serve as an additional safeguard that prevents MinD from re-associating at the same membrane location.

This study demonstrates that interactions exist between $MinD_{Ng}$ and the other Min proteins. The $MinD_{Ng}$-$MinE_{Ng}$ interaction offers support for the ability of GFP-$MinD_{Ng}$ to undergo $MinE_{Ng}$-dependent movement and localization within a helical array in *E. coli* backgrounds. The $MinD_{Ng}$-

MinC interaction is consistent with the ability of $MinD_{Ng}$ to induce MinC-mediated cell division arrest in *N. gonorrhoeae* and *E. coli* backgrounds. Significantly, a novel self-association of bacterial MinD proteins was observed. Both $MinD_{Ng}$ and $MinD_{Ec}$ were able to interact with themselves, suggesting the self-interaction of MinD may be a conserved characteristic that is important for MinD function in different species of varying morphologies. This self-association also supports the ability of MinD proteins to localize as higher ordered structures *in vivo* (Chapter 4; Raskin and de Boer, 1999a; Rowland *et al.*, 2000; Shih *et al.*, 2003).

CHAPTER 6

Structural homology modeling strategy identifies a region in $MinD_{Ng}$ that sensitizes the protein to MinE stimulation

Portions of this chapter are found in the following submitted manuscript:

[**Szeto, J.**, Eng, N. F., Acharya, S., Rigden, M. D., and Dillon, J. R. (2004). A distinct region in the cell division site-determinant MinD is implicated in sensitizing the protein to MinE stimulation Submitted for publication to Research in Microbiology.]

6.1. PURPOSE OF THIS STUDY

Is is now established that bacterial MinD proteins dimerize (this study; Hu *et al.*, 2003). The self-association of MinD is proposed to be important for its ability to localize to the membrane and to hydrolyze ATP (Hu and Lutkenhaus, 2001; Hu *et al.*, 2003). The crystal structures of several MinD homologues from Archaeal organisms show that the protein is monomeric. These crystal structures observed were probably monomeric because the proteins were bound to ADP, AMPPCP, or to no nucleotide (Cordell and Löwe, 2001; Hayashi *et al.*, 2001; Sakai *et al.*, 2001). Interestingly, the Archaeal MinD proteins most closely resemble the monomeric subunits that form dimeric nitrogenase iron proteins (NIPs) (Cordell and Löwe, 2001; Hayashi *et al.*, 2001; Sakai *et al.*, 2001), such as NifH from *Azotobacter vinelandii* (Schindelin *et al.*, 1997).

In order to identify regions in $MinD_{Ng}$ that may be involved in homodimerization, a model of dimeric MinD was generated by superimposition of solved Archaeal MinD monomers onto NifH. Structural modeling and sequence alignment of 24 MinD proteins revealed a polar region in residues 92-94 of bacterial MinD. To assess the importance of this region in MinD functionality, mutant proteins were generated and subjected to several functional assays. These $MinD_{Ng}$ mutants inhibited *E. coli* cytokinesis and retained interaction with all Min proteins, including $MinE_{Ng}$. GFP-$MinD_{Ng}$ and GFP-$MinD_{Ec}$, both mutated at MinD residues 92-94, localized as coiled arrays in *E. coli*, similar to wild-type GFP-MinD. However, unlike wild-type fusions, mutant proteins were distributed uniformly throughout the array and presented no obvious oscillation patterns, despite the presence of MinE. Although the $MinD_{Ng}$ mutant dimerized in the presence of ATP, its ATPase activity was not stimulated by $MinE_{Ng}$, unlike wild-type $MinD_{Ng}$. Hence, despite localizing to the membrane as a helical array and interacting with $MinE_{Ng}$, the mutant MinD proteins in this study have lost the abililty to be efficiently stimulated by $MinE_{Ng}$, resulting in a loss of distinct pole-to-pole oscillation.

6.2. MATERIALS AND METHODS

Structural modeling of dimeric MinD. NifH from the nitrogenase complex of *Azotobacter vinelandii* (PDB# 1N2C; Schindelin *et al.*, 1997) is a structural homologue of MinD proteins (Cordell and Löwe, 2001; Hayashi *et al.*, 2001; Sakai *et al.*, 2001), and was used as a template to generate a model for dimeric MinD. Using SWISS-PDB Viewer (Version 3.7 b2), the solved structure for monomeric *P. furiosus* MinD bound to ADP (PDB# 1G3Q; Hayashi *et al.*, 2001) was superimposed manually onto each monomeric subunit of NifH that comprises the solved NifH dimer. Ribbon diagrams were generated with RasMol Molecular Graphics Visualization Tool, (Version 2.7.2.1) [http://www.bernstein-plus-sons.com/software/RasMol_ 2.7.2.1/doc/rasmol.html].

Construction of *minD*$_{Ng}$ genes encoding point mutations to amino acids 92-94. Plasmid pSR3 (Table 6.1 and Chapters 4) encoding wild-type *minD*$_{Ng}$ was used as a template to generate the simultaneous substitutions R92L, D93L, K94I (collectively referred to as 'loop' mutations) using IPCR and *Vent* DNA polymerase.

Primers SJ1 (encoding all three amino acid mutations) and SJ2 (Table 2.2) were designed to anneal within *minD*$_{Ng}$ at the region of interest and to initiate amplification in opposite directions. The resulting blunt-ended amplicon was phosphorylated using T4 polynucleotide kinase (New England BioLabs), recircularized with T4 DNA ligase (Gibco BRL), and transformed into *E. coli* DH5α. Plasmid-encoded mutant genes were screened by performing colony PCR on candidate clones to amplify an internal segment of *minD*$_{Ng}$ and digesting the amplicons with *Vsp*I, since this restriction site would have been incorporated by primer SJ1 (Table 2.2). The resulting plasmid encoding MinD$_{Ng\text{-}R92L,D93L,K94I}$, (referred to as MinD$_{Ng\text{-}loop}$), was named pJS7 (Table 6.1).

Similar IPCR strategies were employed to generate *minD*$_{Ng}$ genes encoding K94A and E103I mutations. K94A mutations were made using the mutant primer DJ1 (which also incorporated an *Nru*I restriction site for screening purposes) and primer SJ2 (Table 2.2) on pSR15 template to form plasmid pJS32, encoding GFP-MinD$_{Ng\text{-}K94A}$ (Table 6.1). The *minD*$_{Ng\text{-}K94A}$ gene was subsequently PCR

Table 6.1. Strains and plasmids used in this study

Strains/Plasmids	Relevant genotype	Source/reference
Strains		
E. coli DH5α	*supE44 ΔlacU169 (80lacZΔM15) hsdR17 endA1 gyrA96 thi-1 relA1*	Gibco
E. coli PB103	*dadR1 trpE61 trpA62 tna-5 purB*$^+$	de Boer *et al.*(1988)
E. coli PB114	*dadR1 trpE61 trpA62 tna-5 purB*$^+$ λ$^-$ Δ*minCDE aph* (Kan^R)	de Boer *et al.*(1988)
E. coli C41(DE3)	*F$^-$ ompT hsdSB* (r^-_B m^-_B) *gal dcmD (srl-recA)* 306::Tn10 (DE3)	Miroux and Walker (1996)
S. cerevisiae SFY526	*trp 1-901 leu2-3 112 can^r gal4-542 gal80-538 URA3::GAL1$_{UAS}$-GAL1$_{TATA}$-lacZ*	Clontech
Plasmids used for expression studies and/or template DNA		
pUC18	P_{lac} (Amp^R)	Amersham
pSR3	pUC18; P_{lac}::*minD*$_{Ng}$ (Amp^R)	Chapter 4, this study
pJS7	pUC18; P_{lac}::*minD*$_{Ng\text{-}loop}$ (R92L, D93L, K94I) (Amp^R)	This study
pSIA5	pUC18; P_{lac}::*minD*$_{Ng\text{-}E103I}$ (Amp^R)	This study
pJATP1	pSR1; P_{lac}:: *minC*$_{Ng}$, *minD*$_{Ng\text{-}K16Q}$, *minE*$_{Ng}$, *oxyR* (Amp^R)	Chapter 3, this study
pMJ3	pUC18; P_{lac}::*minD*$_{Ng\text{-}K16Q}$ (Amp^R)	Chapter 4, this study
pJS31	pUC18; P_{lac}::*minD*$_{Ng\text{-}K94A}$ (Amp^R)	This study
Plasmids used for GFP-fusion localization studies		
pDSW209	P_{trc}::*gfp* (Amp^R)	Weiss *et al.* (1999)
pSR15	pDSW209; P_{trc}::*gfp-minD*$_{Ng}$, *minE*$_{Ng}$ (Amp^R)	Chapter 4,this study

pJS9	pDSW209; P_{trc}::*gfp-minD*$_{Ng\text{-}loop}$, *minE*$_{Ng}$ (Amp^R)	This study
pJS17	pDSW209; P_{trc}::*gfp-minD*$_{Ng\text{-}E103I}$, *minE*$_{Ng}$ (Amp^R)	This study
pJDE1	pDSW209; P_{trc}::*gfp-minD*$_{Ng\text{-}K16Q}$, *minE*$_{Ng}$ (Amp^R)	Chapter 4, this study
pJS10	pDSW209; P_{trc}::*gfp-minD*$_{Ng}$ (Amp^R)	Chapter 4, this study
pJS32	pDSW209; P_{trc}::*gfp-minD*$_{Ng\text{-}K94A}$, *minE*$_{Ng}$(Amp^R)	This study
pDR122	Amp^R P_{lac}::*gfp-minD*$_{Ec}$, *minE*$_{Ec}$ (Amp^R)	Raskin and de Boer (1999a)
pJS35	pDR122; P_{lac}::*gfp-minD*$_{Ec\text{-}loop}$ (R92L, D93L, K94I), *minE*$_{Ec}$ (Amp^R)	This study
Yeast-two hybrid plasmids		
pGAD424	P_{ADH1}::*gal4*(AD)[a] (Amp^R)	Clontech
pGBT9	P_{ADH1}::*gal4*(BD)[b] (Amp^R)	Clontech
pGADminD	pGAD424; P_{ADH1}::*gal4*(AD)-*minD*$_{Ng}$ (Amp^R)	Chapter 5, this study
pGBT9minD	pGBT9; P_{ADH1}::*gal4*(BD)-*minD*$_{Ng}$ (Amp^R)	Chapter 5, this study
pGBT9minE	pGBT9; P_{ADH1}::*gal4*(BD)-*minE*$_{Ng}$ (Amp^R)	Chapter 5, this study
pSRBD-C	pGBT9; P_{ADH1}::*gal4*(BD)-*minC*$_{Ec}$ (Amp^R)	Ramirez-Arcos *et al.*, in press
pJminD18	pGAD424; P_{ADH1}::*gal4*(AD)-*minD*$_{Ng\text{-}loop}$ (Amp^R)	This study
pSIA8	pGAD424; P_{ADH1}::*gal4*(AD)-*minD*$_{Ng\text{-}E103I}$ (Amp^R)	This study
pJminD16	pGAD424; P_{ADH1}::*gal4*(AD)-*minD*$_{Ng\text{-}K16Q}$ (Amp^R)	This study
pJminD19	pGBT9; P_{ADH1}::*gal4*(BD)-*minD*$_{Ng\text{-}loop}$ (Amp^R)	This study
pSIA7	pGBT9;P_{ADH1}::*gal4*(BD)-*minD*$_{Ng\text{-}E103I}$ (Amp^R)	This study
pJminD17	pGBT9; P_{ADH1}::*gal4*(BD)-*minD*$_{Ng\text{-}K16Q}$ (Amp^R)	This study
pJminD19	pGBT9; P_{ADH1}::*gal4*(BD)-*minD*$_{Ng\text{-}loop}$ (Amp^R)	This study

Plasmids used for protein purification		
pET30a	P_{T7}:: 6XHis (Kan^R)	Novagen
pSC9	pET30a; P_{T7}:: $minD_{Ng}$-6XHis (Kan^R)	This study
pSC10	pET30a; P_{T7}:: $minD_{Ng\text{-}K16Q}$-6XHis (Kan^R)	This study
pJS8	pET30a; P_{T7}:: $minD_{Ng\text{-}loop}$-6XHis (Kan^R)	This study
pEC1	pET30a; P_{T7}:: $minE_{Ng}$-6XHis (Kan^R)	This study

[a] GAL4 activation domain

[b] GAL4 DNA binding domain

amplified from pJS32 using primers minD1/minD2 (Table 2.2) and ligated into pUC18 to give plasmid pJS31 (Table 6.1).

An E103I substitution in $MinD_{Ng}$ was made using primer SA2 and the mutant primer SA3 (Table 2.2) on pSR3 template (Table 6.1). Clones were screened by digestion of $minD_{Ng}$ colony PCR amplicons with *Bcl*I (incorporated by primer SA3), and the resulting plasmid encoding $MinD_{Ng\text{-}E103I}$ was named pSIA5 (Table 6.1). Gene integrity and the presence of the each mutation was verified by DNA sequencing performed at the Core DNA Sequencing and Synthesis Facility, University of Ottawa. Plasmids pSR3, pJS7, pJS31, and pSIA5 (Table 6.1) were transformed into *E. coli* PB103 (Table 2.1) for morphology studies.

IPCR methods using the relevant primers listed above were also used on pSR15 template (Chapter 4; encoding wild-type GFP-$MinD_{Ng}$ and $MinE_{Ng}$) (Table 6.1) to generate GFP-fusions to $MinD_{Ng\text{-}loop}$ (pJS9), $MinD_{Ng\text{-}K94A}$ (pJS32), and $MinD_{Ng\text{-}E103I}$ (pJS17) for localization studies. Plasmid pJS10, encoding GFP-$MinD_{Ng}$ alone (without downstream $minE_{Ng}$), as well as pJDE1, encoding GFP-$MinD_{Ng\text{-}K16Q}$, were constructed previously in Chapter 4. In addition, R92L, D93L, and K94I substitutions were also simultaneously introduced into *E. coli* MinD ($MinD_{Ec}$) by using IPCR on pDR122 ($gfp\text{-}minD_{Ec}$, $minE_{Ec}$) (Raskin and de Boer, 1999a) with primers DJ2 (mutant primer, incorporating *Vsp*I site as well for screening) and DJ3 (Table 2.2). The resulting plasmid, encoding GFP-$MinD_{Ec\text{-}R92L,D93L,K94I}$ (referred to as GFP-$MinD_{Ec\text{-}loop}$), was named pJS35 (Table 6.1). The integrity of all *min* genes was confirmed by DNA sequencing performed at the Core DNA Sequencing and Synthesis Facility, University of Ottawa.

Yeast two-hybrid plasmids. Fusions of $MinD_{Ng\text{-}loop}$, and $MinD_{Ng\text{-}E103I}$ to GAL4-DNA-BD and to GAL-4AD were constructed. Each gene was PCR amplified using primers minD1 and minD2 (Table 2.2) from pJS7 and pSIA5, respectively, digested with *Eco*RI and *Bam*HI, and cloned into pGBT9 and pGAD424. Fusions of $MinD_{Ng\text{-}loop}$, and $MinD_{Ng\text{-}E103I}$ to GAL4-DNA-BD were encoded on

plasmids pJminD19 and pSIA7 (Table 6.1). Fusions of $MinD_{Ng\text{-}loop}$, and $MinD_{Ng\text{-}E103I}$ to GAL4-AD were similarly constructed, and encoded on plasmids pJminD18 and pSIA8 (Table 6.1). Fusions of GAL4-AD (pJminD16) and GAL4-DNA-BD (pJminD17) to $MinD_{Ng\text{-}K16Q}$ were also constructed similarly (Table 6.1), using pJATP1 (Table 3.1) as a PCR template with primers minD1 and minD2 (Table 2.2). Yeast two-hybrid assays were conducted as outlined in Chapter 2.

GFP-MinD fusion localization. For protein localization studies, *E. coli* PB114 cells (Table 2.1) transformed with plasmids encoding various GFP-$MinD_{Ng}$ fusions were induced with 40 μM IPTG, grown, and immobilized on coverslips as previously described (Chapter 4). *E. coli* PB114 cells transformed with plasmids encoding GFP-$MinD_{Ec}$ were induced with 27 μM IPTG (Raskin and de Boer, 1999a) and also grown and immobilized, as described before (Chapter 4). Fluorescence microscopy was performed with an Olympus BX61 microscope equipped with a Photometrics CoolSnap ES camera and Image Pro (Version 4.5.1) software. To maintain consistency, the oscillation cycle (movement from one pole to the opposite, and back again) of each GFP-$MinD_{Ng}$ fusion was measured in 20 cells of near equivalent length (~2.0-2.5 μm). Time lapse images were taken every 10 seconds. In each cell observed, at least two complete oscillation cycles were used to verify oscillation periods. Statistical analyses using unpaired Student's *t*-tests were performed to determine whether differences in average oscillation times between GFP-$MinD_{Ng}$ fusions were significant, with ($p<0.001$) considered significant. When required, enhancement of raw images was done using standard options available on Image Pro software: Contrast enhancement was used to increase contrast and to decrease gamma. Gauss filtering using a 3 X 3 kernel size with 4 passes at strength 10 was also used to help visualize intracellular substructures.

Protein purification. PCR was carried out using primers SJ3 and SJ4 (Table 2.2) on four templates: pSR3, pJATP1, and pJS7 (Table 6.1) in order to amplify wild type $minD_{Ng}$, $minD_{Ng\text{-}K16Q}$, and $minD_{Ng\text{-}}$

$_{loop}$, respectively. Each amplicon was digested with *Nde*I and *Xho*I and ligated into similarly digested pET30a (Table 6.1) to generate plasmids encoding C-terminal His-tagged $MinD_{Ng}$ (pSC9), $MinD_{Ng\text{-}K16Q}$ (pSC10), and $MinD_{Ng\text{-}loop}$ (pJS8) (Table 6.1) for purification using nickel affinity chromatography.

Each plasmid was transformed into *E. coli* C41 (DE3) (Table 2.1) for overexpression. 50 ml log phase cultures of cells were induced with 1mM IPTG for 4 hours at 37°C and shaking at 250 rpm. Induced cells were pelleted for 10 minutes at 5000 X g resuspended in 2 ml binding buffer (5mM imidazole, 1M NaCl, 20mM Tris-HCl pH 7.9) and incubated on ice for 30 minutes. The cells were lysed by sonication (Fisher Scientific 60 Sonic Dismembrator) using 4 cycles, each consisting of two six-second bursts, with at least a 1 minute interval on ice between cycles. Cell extracts were centrifuged at 100,000 X g for 20 minutes at 4°C (L8-M Ultracentrifuge, Beckman) and the soluble supernatant fraction was retained.

Protein purification was performed with a 1ml bed volume of His-Bind resin (Novagen) for each protein using the following solutions, described by the manufacturer, for column washing: 10 ml binding buffer (5 mM imidazole), 5 ml wash solution (60 mM imidazole), and 1 ml of elution buffer (1 M imidazole). Eluted protein was dialyzed overnight at 4 °C against Buffer A (20 mM Tris-HCl pH 7.5, 2 mM EDTA, 200 mM NaCl, 10% glycerol; final pH adjusted to pH 7.2) in glassware previously washed with 7X detergent (ICN Biomedicals Inc.), distilled/deionized water (ddH_2O), 1 M HCl, and a final ddH_2O rinse to eliminate possible contaminating inorganic phosphates.

To obtain purified $MinE_{Ng}$, $minE_{Ng}$ was PCR amplified from gonococcal cell suspensions using primers ESminE1 and ESminE2 (Table 2.2), and cloned into pET30a as above to form plasmid pEC1 (Table 6.1). *E. coli* C41 (DE3) was transformed with pEC1 and 0.4 mM IPTG was used to induce a 350 ml log phase culture for 2-3 hours at 250 rpm and 37°C. Soluble cell supernatant was applied to 3 ml of His-Bind resin and the column was washed with buffer containing increasing concentrations of imidazole buffer (5 mM to 100 mM; Novagen) and $MinE_{Ng}$-His was eluted with 250 mM imidazole. Purified protein was dialyzed in Buffer B, consisting of 50 mM Tris, 20 mM

NaCl, 1 mM EDTA, pH 7.4. $MinE_{Ng}$-His was concentrated using Biomax-5 centrifugal filter columns with a 5000 Dalton molecular weight cutoff (Millipore).

Circular dichroism spectroscopy. Circular dichroism (CD) spectroscopy was performed on purified C-terminal His-tagged wild-type $MinD_{Ng}$, $MinD_{Ng\text{-}K16Q}$, and $MinD_{NgNg\text{-}loop}$ using an AVIV Model 62DS CD spectrometer (AVIV Instruments, Inc, Lakewood NJ), with a 1 mm path length quartz cell at 20°C. The temperature of the sample was computer controlled to within 0.2 °C. For the wild-type protein and the mutant, far-UV CD spectra were recorded at a protein concentration of ~0.1 mg/ml in Buffer B. All CD experiments were repeated three times to ensure reproducibility. Following the baseline subtraction, the CD data were normalized to the protein concentration measured by Bradford method.

$MinD_{Ng}$ ATPase stimulation assays. A rapid protocol for the formation of vesicles composed of the anionic phospholipid 1,2-dioleoyl-sn-glycero-3-[phospho-rac-(1-glycerol) (phosphatidyglycerol; PG) (Avanti Polar Lipids, Inc.) was developed. 0.1 ml of PG (10 mg/ml in chloroform) was dried under a stream of filtered air and resuspended with reaction buffer (25 mM Tris-Cl, 50 mM KCl, pH 7.5) to give a stock PG vesicle solution of 5 mg/ml. PG vesicles were visualized by phase contrast microscopy to verify structural integrity and stored at -20°C. PG vesicles appeared to remain stable for at least four months, as assessed by phase contrast microscopy.

Prior to each experiment, the concentrations of $MinD_{Ng}$ and $MinE_{Ng}$ proteins were determined using the Bio-Rad protein assay and adjusted as required by diluting in their respective dialysis buffers. In a typical 100 µl reaction, the following reagents were added (final concentrations in brackets): reaction buffer (volume added dependant on other reagents to be included), $MinD_{Ng}$ protein (0.012 mg/ml), ATP (1 mM), PG vesicles (0.5 mg/ml), and $MgCl_2$ (1 mM). Reactions were incubated at room temperature for five minutes and, if required, $MinE_{Ng}$-His (0.012 mg/ml) was added followed

by an additional five minutes incubation. Storage buffers for $MinD_{Ng}$ or $MinE_{Ng}$ were used to adjust reaction volumes to 100 µl when protein was not used.

At specified timepoints, 30 µl of the each reaction was removed, centrifuged at high speed for 1 minute, and 25 µl of supernatant was removed and added to 50 µl of malachite green solution in a microtitre dish, similar to the procedure described by Harder *et al.* (1994). Colour development was allowed to proceed for 20 minutes at room temperature and the absorbance of the reaction at 620 nm was determined using a TECAN Spectra Shell microplate reader (TECAN U.S. Inc.) and compared to a blank containing all the reagents in a standard reaction, except storage buffers were used in place of each protein.

All reactions were carried out in duplicate and colour development was compared to a blank containing ATP, PG, and $MgCl_2$, as described above, with the remaining volume consisting of Buffers A and B. The amount of inorganic phosphate released was determined by comparing absorbance readings with those obtained from inorganic phosphate standards prepared from dilutions of KH_2PO_4 in the blank buffer.

Size exclusion chromatography. Purified $MinD_{Ng}$, $MinD_{Ng\text{-}K16Q}$, and $MinD_{Ng\text{-}loop}$ (0.35-0.45 mg/ml) were preincubated with, or without, 1 mM ATP-γ-S and 1 mM $MgCl_2$ for 40 minutes at room temperature and 450 µl reaction volumes were each applied to a 100 ml column of Superdex 200 (Amersham Pharmacia) equilibrated with PBS (pH 7.4). Flow rate was set at 0.7 ml/min. Eluted protein from 0.5 ml fractions was collected and detected in a microtitre plate using the Bio-Rad protein assay. Protein elution profiles were compared to those of Amersham Gel-filtration Standards.

6.3. RESULTS

Generating a proposed model for dimeric MinD

To identify regions in MinD that may be implicated in homodimerization and/or function, structural homology alignment was used to generate a possible model for dimeric MinD (Figure 6.1 A). Structurally, the Archaeal MinD proteins are very similar to the monomeric subunits of dimeric nitrogenase iron proteins (Cordell and Löwe, 2001; Hayashi *et al.*, 2001; Sakai *et al.*, 2001), such as NifH from *Azotobacter vinelandii* (Schindelin *et al.*, 1997). Therefore, solved monomeric structures of a representative Archaeal MinD from *Pyrococcus furiosus* ($MinD_{Pf}$) (Hayashi *et al.*, 2001) were superimposed onto the structure of dimeric NifH (Schindelin *et al.*, 1997).

Structural alignment of the predicted $MinD_{Pf}$ dimer (Figure 6.1 B) and the solved *A. vinelandii* NifH dimer (Figure 6.1 A) revealed a common exposed region in both proteins. In each $MinD_{Pf}$ monomer, this region appears as a short α-helix containing residues 87-93 (Figure 6.1 B, green residues; Figure 6.2, residues of $MinD_{Pf}$ below the bar indicated '2'). In each NifH monomer, the corresponding region is in the form of a loop comprising residues 92-98 (Figure 6.1 A green residues; Figure 6.2, residues of NifH above the bar indicated '4') (Schindelin *et al.*, 1997; Schlessman *et al.*, 1998). Previous structural analyses of NifH indicated that amino acids within this region (particularly Glu92, Pro93, Val95, Ala98) are involved in mediating monomer-monomer contact through polar interactions, such as hydrogen bonding and salt-bridge formation (Schlessman *et al.*, 1998).

Sequence alignment of twenty-four MinD proteins showed the presence of several consecutive polar amino acids in a corresponding region in bacteria (Figure 6.2; as a reference, residues 86-97 of $MinD_{Ng}$ are aligned below the bar indicated '3'). These residues are highly conserved, particularly among Gram-negative organisms, which have a consensus sequence of L[P/A]ASQ[T/S][R/K]DK[D/N][A/T/N/I]L (polar amino acids are underlined). Since this region also comprises the NifH loop, it is reasoned that it may be implicated in protein interactions and/or function; hence, three conserved polar residues in $MinD_{Ng}$ were selected for simultaneous substitution

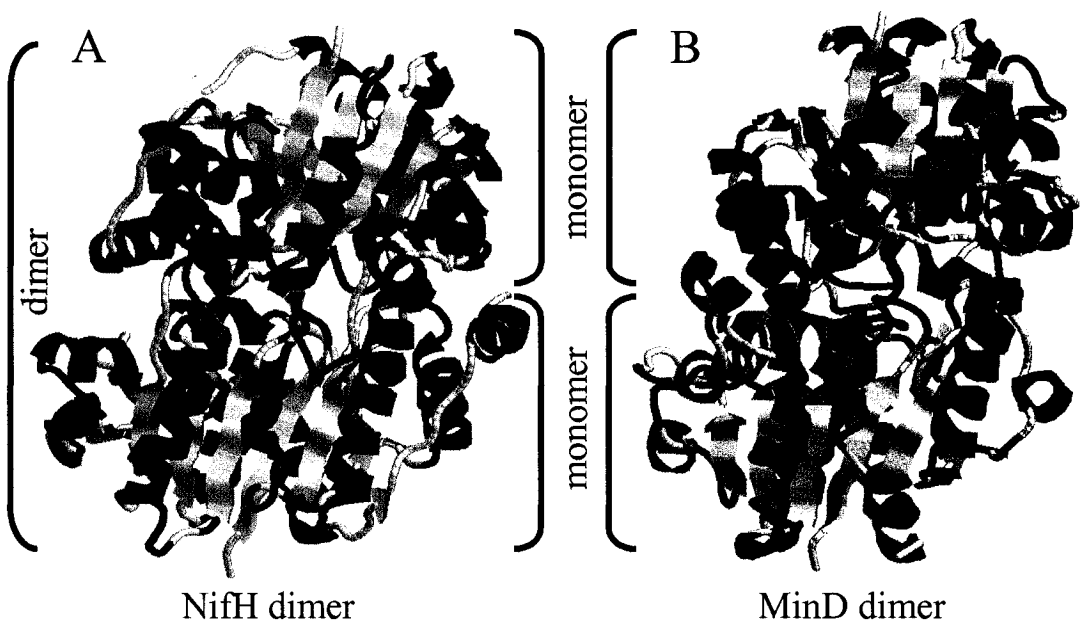

Figure 6.1. Model of dimerized MinD based on structural alignment with *Azotobacter vinelandii* NifH dimer. (A) The crystal structure of NifH from *A. vinelandii* shows a dimeric protein (Schindelin *et al.*, 1997). Position of each NifH monomer is indicated by brackets. Green residues correspond to a loop region (aa 92-98) in each monomer that is implicated in mediating monomer-monomer contact (Schlessman *et al.*, 1998). (B) Model of dimeric MinD generated by superimposition of *P. furiosus* MinD ($MinD_{Pf}$) (Hayashi *et al.*, 2001) monomers onto each subunit of the *A. vinelandii* NifH dimer. The green residues (aa 87-93) of $MinD_{Pf}$ represent a region that corresponds with the loop region in each NifH monomer [green residues in (A)]. Cyan residues indicate $MinD_{Pf}$ residues involved in binding ATP (Hayashi *et al.*, 2001).

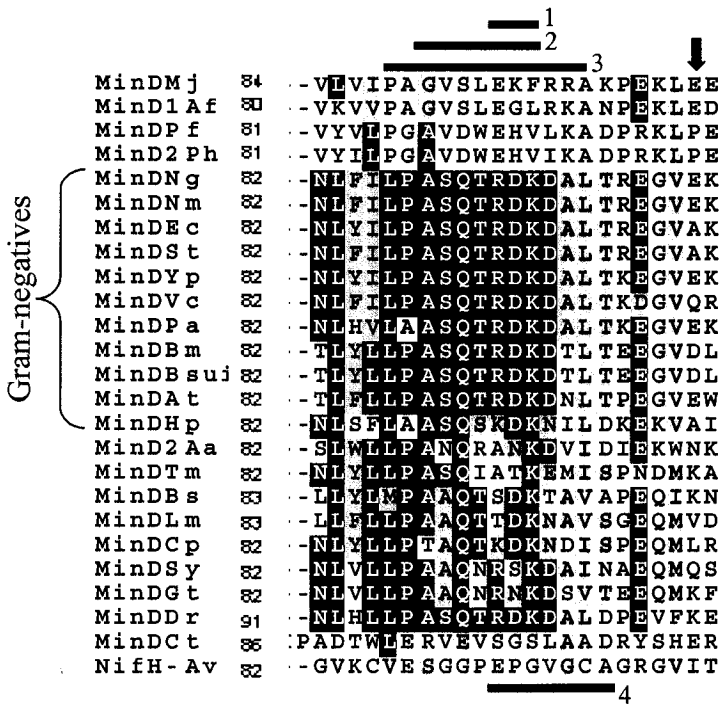

Figure 6.2. Alignment of MinD sequences corresponding to residues 82-104 of *A. vinelandii* NifH. Abbreviations used: *Methanococcus janaaschii* (Mj), *Archaeoglobus fulgidus* (Af), *Pyrococcus furiosus* (Pf), *P. horikoshii* (Ph), *Neisseria gonorrhoeae* (Ng), *N. meningitidis* (Nm), *Escherichia coli* (Ec), *Salmonella enterica* serovar Typhimurium (St), *Yersinia pestis* (Yp), *Vibrio cholerae* (Vc), *Pseudomonas aeruginosa* (Pa), *Brucella melitensis* (Bm), *B.suis* (Bsui), *Agrobacterium tumefaciens* (At), *Helicobacter pylori* (Hp), *Aquifex aeolicus* (Aa), *Thermotoga maritima* (Tm), *Bacillus subtilis* (Bs), *Listeria monocytogenes* (Lm), *Clostridium perfringens* (Cp), *Synechochistis sp.* (Sy), *Guillardia theta* (Gt), *Deinococcus radiodurans* (Dr), and *Chlamydia trachomatis* (Ct). Residues R92, D93, K94 of $MinD_{Ng}$ and $MinD_{Ec}$ are aligned below the bar designated '1'. $MinD_{Pf}$ residues 87-93 are aligned below the bar designated '2'. Residues 86-97 of $MinD_{Ng}$ are aligned aligned below the bar designated '3'. Residues in NifH aligned above the bar designated '4' are part of one region involved in NifH dimerization through polar interactions (Schlessman *et al.*, 1998). Arrow shows position of E103 in $MinD_{Ng}$

with hydrophobic residues (R92L, D93L, and K94I) (Figure 6.2, residues of $MinD_{Ng}$ below the bar indicated '1'). For convenience, the resulting mutant will be referred to as $MinD_{Ng\text{-}loop}$, although the exact structure of this region in bacterial MinD is currently not known.

Furthermore, an E103I mutant was also generated at this non-conserved residue position (Figure 6.2, arrow), in close proximity to $MinD_{Ng}$ residues 92-94. This mutation is predicted not to adversely affect $MinD_{Ng}$ function and was constructed to evaluate any functional significance of mutations in non-conserved residues in this region. In addition, $MinD_{Ng\text{-}K16Q}$ was selected as a negative control since it is unable to induce cell division arrest in *N. gonorrhoeae* (Chapter 3) and *E. coli* backgrounds (Chapter 4), and localizes to the cytosol *in vivo* (Chapter 4).

$MinD_{Ng}$ with mutations at residues 92-94 can still induce cell division arrest in *E. coli*

$MinD_{Ng}$ is active in *E. coli* and works with *E. coli* MinC to arrest cell division in this background. To initially assess the functionality of the various $MinD_{Ng}$ mutants, the ability of each protein to induce cell division arrest in wild-type *E. coli* was determined. Wild-type *E. coli* PB103 (Table 2.1) was transformed with plasmids encoding wild-type $MinD_{Ng}$, $MinD_{Ng\text{-}loop}$, $MinD_{Ng\text{-}E103I}$, and $MinD_{Ng\text{-}K16Q}$. Overexpression of wild-type $MinD_{Ng}$ or $MinD_{Ng\text{-}E103I}$ could induce cell division arrest in these cells, leading to cell filamentation (Figure 6.3 B, E). Similarly, *E. coli* cells overexpressing $MinD_{Ng\text{-}loop}$ displayed filamentation as well (Figure 6.3 C). Residue K94, the most conserved of the polar residues at positions 92-94 in $MinD_{Ng}$, was also substituted with an alanine (K94A) to determine the effects of mutating only a single residue in this region. *E. coli* overexpressing $MinD_{Ng\text{-}K94A}$ were also filamentous (Figure 6.3 D). As negative controls, *E. coli* cells were transformed with the pUC18 plasmid or with a derivative plasmid encoding $MinD_{Ng\text{-}K16Q}$. Both transformants presented normal short rod morphology (Figure 6.3 A, pUC18 transformed cells shown).

Western blotting confirmed the overexpression of wild-type (Figure 6.3 F, lane 5) and mutant $MinD_{Ng}$ ($MinD_{Ng\text{-}loop}$, lane 3; $MinD_{Ng\text{-}K94A}$, lane 2; $MinD_{Ng\text{-}E103I}$, lane 1) in *E. coli* PB103 relative to

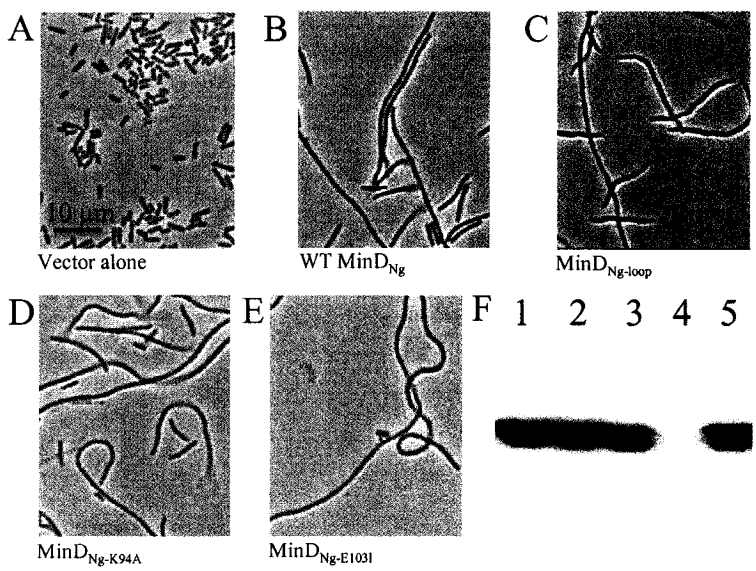

Figure 6.3. Effects of overexpressing MinD$_{Ng}$ proteins bearing mutations in the 'loop' region in wild-type *E. coli* PB103. (A) Cells transformed with pUC18 show normal short rod morphology. Cells transformed with (B) pSR3 (*minD*$_{Ng}$), (C) pJS7 (*minD*$_{Ng\text{-}loop}$), (D) pJS31 (*minD*$_{Ng\text{-}K94A}$), and (E) pSIA5 (*minD*$_{Ng\text{-}E103I}$) displayed filamentous phenotypes. Bar shown in (A) is 10 μm, and all images are at the same magnification. (F) Western blot analysis using anti-MinD$_{Ng}$ antisera shows the overexpression of each MinD$_{Ng}$ protein in *E. coli* PB103: Lane 1, MinD$_{Ng\text{-}E103I}$; lane 2, MinD$_{Ng\text{-}K94A}$; lane 3, MinD$_{Ng\text{-}loop}$; lane 4, pUC18 transformed *E. coli* cell extract; lane 5, wild-type MinD$_{Ng}$.

background *E. coli* MinD signal (lane 4). These results show that radical mutations to residues R92, D93 and K94 do not affect the ability of $MinD_{Ng}$ to induce cell division arrest in wild-type *E. coli.*

$MinD_{Ng\text{-}loop}$ retains self-association and interaction with all Min proteins

To determine whether the identified polar region in $MinD_{Ng}$ is involved in protein dimerization, as predicted by structural homology modeling with the NifH dimer, the yeast two-hybrid system was used to test protein-protein interactions. As expected, wild-type $MinD_{Ng}$ could self-associate, in addition to the $MinD_{Ng\text{-}E103I}$ mutant (Table 6.2). Interestingly, $MinD_{Ng\text{-}loop}$ retained the ability to self-associate as well. Both $MinD_{Ng\text{-}loop}$ and $MinD_{Ng\text{-}E103I}$ self-interactions were stronger than the wild-type $MinD_{Ng}$ control. In contrast, the negative control mutant $MinD_{Ng\text{-}K16Q}$ displayed a significantly decreased ability to dimerize (Table 6.2). $MinD_{Ng\text{-}loop}$ and $MinD_{Ng\text{-}E103I}$ also retained interactions with $MinE_{Ng}$ which were either stronger than, or comparable with, wild-type $MinD_{Ng}$, respectively. Conversely, $MinD_{Ng\text{-}K16Q}$ did not display interaction with $MinE_{Ng}$ (Table 6.2).

$MinD_{Ng\text{-}loop}$ also retained an ability to interact with $MinC_{Ec}$, as did $MinD_{Ng\text{-}E103I}$. Both interactions were weaker relative to the wild-type control, based on β–galactosidase activities (Table 6.2). *E. coli* MinC was used in these assays since $MinC_{Ng}$ is likely unstable in the yeast reporter strain (Chapter 5, Ramirez-Arcos *et al.*, in press). Despite diminished interactions observed by the yeast two-hybrid system, the abilities of $MinD_{Ng\text{-}loop}$ and $MinD_{Ng\text{-}E103I}$ to effectively inhibit cell division in wild-type *E. coli* (Figure 6.3 C, E) shows that sufficient functional interaction is retained between each mutant MinD and $MinC_{Ec}$ (Table 2). In contrast to the other $MinD_{Ng}$ proteins tested, $MinD_{Ng\text{-}K16Q}$ did not display interaction with $MinC_{Ec}$. Overall, these results show that mutations within, or in proximity to, the predicted 'loop' region of $MinD_{Ng}$ do not abrogate interactions with other Min proteins or $MinD_{Ng}$ homodimerization.

Table 6.2. Yeast two-hybrid analysis of the interactions of wild-type and mutant $MinD_{Ng}$ with the Min system

Fusion to GAL4-BD[a]	Fusion to GAL4-AD[b]	Intensity of colony[c]	β-galactosidase activity[d]
$MinD_{Ng}$[e]	$MinD_{Ng}$	+++	8.81 ± 0.20
$MinD_{Ng\text{-}loop}$[f]	$MinD_{Ng\text{-}loop}$	+++	21.79 ± 0.64
$MinD_{Ng\text{-}E103I}$	$MinD_{Ng\text{-}E103I}$	+++	15.18 ± 0.08
$MinD_{Ng\text{-}K16Q}$	$MinD_{Ng\text{-}K16Q}$	+	1.68 ± 0.09
$MinE_{Ng}$	$MinD_{Ng}$	+++	8.31 ± 0.40
$MinE_{Ng}$	$MinD_{Ng\text{-}loop}$	+++	31.24 ± 0.22
$MinE_{Ng}$	$MinD_{Ng\text{-}E103I}$	+++	7.60 ± 0.42
$MinE_{Ng}$	$MinD_{Ng\text{-}K16Q}$	-	0.08 ± 0.06
$MinC_{Ec}$[g]	$MinD_{Ng}$	+++	935.43 ± 19.90
$MinC_{Ec}$	$MinD_{Ng\text{-}loop}$	+++	75.76 ± 0.96
$MinC_{Ec}$	$MinD_{Ng\text{-}E103I}$	+++	149.71 ± 2.71
$MinC_{Ec}$	$MinD_{Ng\text{-}K16Q}$	-	Not determined

[a]GAL4-DNA binding domain

[b]GAL4-activation domain

[c]Colour intensity relative to the respective positive control interactions: (+++) dark blue; (++) blue; (+) faint blue; (-) white colonies

[d]Activity in Miller Units. One unit equals the amount of β-galactosidase which hydrolyzes 1 μmol of ONPG per minute per cell

[e]*N. gonorrhoeae* MinD

[f]$MinD_{Ng\text{-}loop}$ contains R92L, D93L, K94I substitutions

[g]*E. coli* MinC

$MinD_{Ng\text{-}loop}$ can still dimerize in the presence of ATP

It was recently shown that *E. coli* MinD dimerizes in the presence of ATP (Hu *et al.*, 2003). To confirm that $MinD_{Ng\text{-}loop}$ could still self-interact in an ATP-dependent manner, the dimerization potential of purified $MinD_{Ng\text{-}loop}$ in the presence or absence of nucleotide was compared to that of purified wild-type $MinD_{Ng}$ and $MinD_{Ng\text{-}K16Q}$ using size-exclusion chromatography. The short C-terminal His-tag of both $MinD_{Ng}$ and $MinD_{Ng\text{-}loop}$ did not affect the function of the proteins as they both caused a filamentous phenotype upon overexpression in *E. coli* C41 (DE3) (Figure 6.4 A), similar to the untagged proteins in wild-type *E. coli* PB103 (Figure 6.3 B, C). Overexpression of the negative control, His-tagged $MinD_{Ng\text{-}K16Q}$, in *E. coli* C41 (DE3) did not inhibit cell division (Figure 6.4 E), and cells appeared as short rods, similar to cells carrying the negative control vector pET30a (Figure 6.4 G). His-tagged $MinE_{Ng}$ was also active, causing a minicell phenotype in *E. coli* (Figure 6.4 H, arrows indicate minicells), similar to overexpression of untagged *E. coli* MinE (de Boer *et al.*, 1989).

Each MinD protein was readily purified using nickel-affinity chromatography (Figure 6.4 B-F). Far-UV circular dichroism analyses conducted on each $MinD_{Ng}$ protein confirmed they all had similar secondary structure; hence, the mutant proteins did not have significant structural perturbations compared to the wild-type (Figure 6.5 A, B).

Purified MinD has been shown to bind to the non-hydrolyzable ATP derivative, ATP-γ-S (Hu *et al.*, 2002; Lackner *et al.*, 2003). ATP-γ-S was used in these experiments to prevent any nucleotide hydrolysis that may occur during gel-filtration. In the absence of nucleotide, the majority of wild-type $MinD_{Ng}$ (Figure 6.6 A), $MinD_{Ng\text{-}K16Q}$ (Figure 6.6 C), and $MinD_{Ng\text{-}loop}$ (Figure 6.6 E) eluted from the column at an apparent molecular weight consistent with monomeric protein, as seen by a large single absorbance peak corresponding to elution volumes from 71-75 ml. In each case, a small fraction of protein was dimeric, as indicated by a minor absorbance peak that appeared in the 63-68 ml fractions.

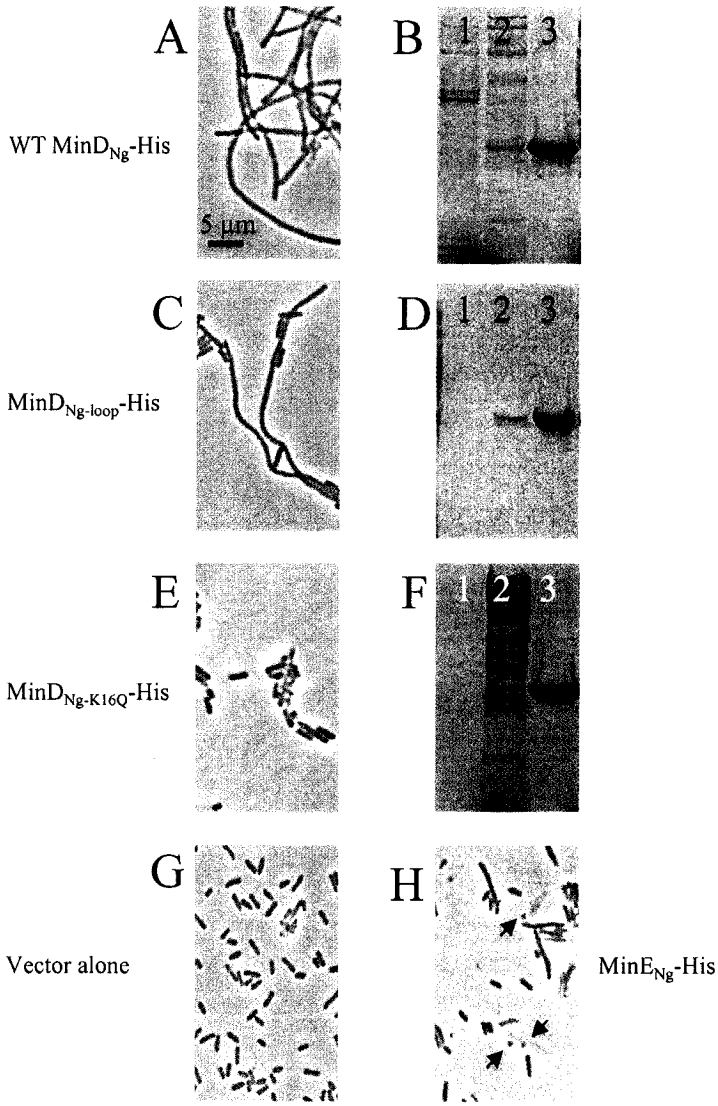

Figure 6.4. Expression and purification of C-terminal His-tagged MinD$_{Ng}$ proteins in *E. coli* C41 (DE3). A) Cells transformed with pSC9 (*minD*$_{Ng}$-His) display a filamentous phenotype. B) Purification of MinD$_{Ng}$-His from induced *E. coli* cultures. Lane 1, 5 mM imidazole wash buffer eluate; lane 2, 60 mM imidazole wash buffer eluate; lane 3, 1 M imidazole elution. (C) Cells transformed with pJS8 (*minD*$_{Ng\text{-}loop}$-His) display a filamentous phenotype. (D) Purification of MinD$_{Ng\text{-}loop}$-His from induced *E. coli* cultures. Lane 1, 5 mM imidazole wash buffer eluate; lane 2, 60 mM imidazole wash buffer eluate; lane 3, 1 M imidazole elution. E) Cells transformed with pSC10 (*minD*$_{Ng\text{-}K16Q}$-His) have a short rod morphology. (F) Purification of MinD$_{Ng\text{-}K16Q}$-His from induced *E. coli* cultures. Lane 1, 5 mM imidazole wash buffer eluate; lane 2, 60 mM imidazole wash buffer eluate; lane 3, 1 M imidazole elution. G) Cells transformed with the negative control vector pET30a have a short rod morphology. (H) Cells transformed with pEC1 (*minE*$_{Ng}$-His) have a minicell phenotype. Arrows indicate minicells. Scale bar in (A) represents 5 µm and all figures are at the same magnification.

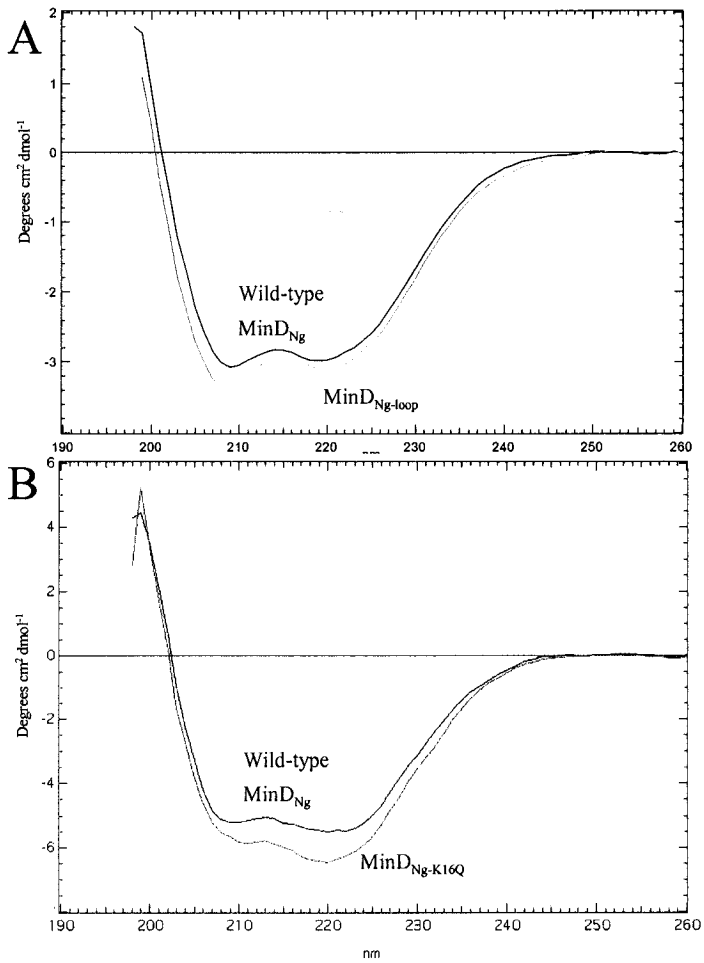

Figure 6.5. Circular dichroism spectroscopy analysis of purified C-terminal His-tagged MinD$_{Ng}$, MinD$_{Ng-K16Q}$, and MinD$_{Ng-loop}$. Far-UV Circular dichroism (CD) spectroscopy was performed at 20°C and at protein concentrations of ~0.1 mg/ml in Buffer A. All CD experiments were repeated three times to ensure reproducibility. *(A)* Far-UV spectra of wild-type (WT) MinD$_{Ng}$ and MinD$_{Ng-K16Q}$. *(B)* Far-UV spectra of wild-type MinD$_{Ng}$ and MinD$_{Ng-loop}$.

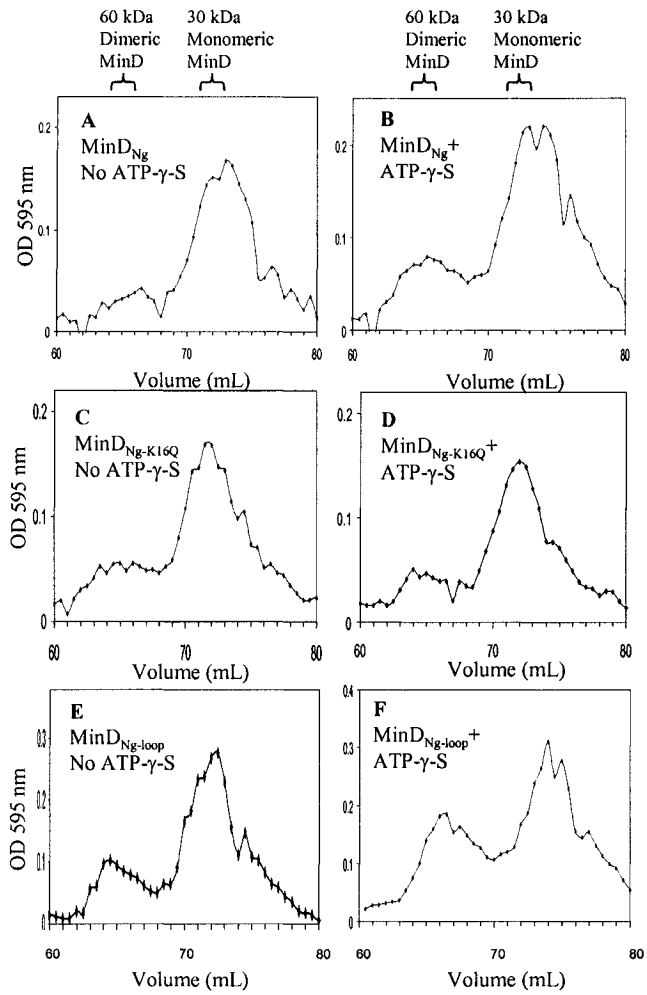

Figure 6.6. Gel-filtration of purified wild-type MinD$_{Ng}$, MinD$_{Ng-loop}$, and MinD$_{Ng-K16Q}$. (A, C, E) Elution profiles of (A) wild-type MinD$_{Ng}$, (C) MinD$_{Ng-K16Q}$, and (E) MinD$_{Ng-loop}$ applied individually to a Superdex 200 column equilibrated with PBS (pH 7.4). (B, D, F) Elution profiles of (B) wild-type MinD$_{Ng}$, (D) MinD$_{Ng-K16Q}$, and (F) MinD$_{Ng-loop}$ preincubated with 1 mM ATP-γ-S and 1 mM $MgCl_2$ and applied individually to the same column equilibrated with PBS (pH 7.4) supplemented with 0.5 mM ATP and 1 mM $MgCl_2$. Flow rate was set at 0.7 ml/min. 0.5 ml fractions were collected and analyzed for protein content in order to generate elution profiles. The association state of MinD$_{Ng}$ proteins, based on elution profiles of gel-filtration standards, is also shown above the elution profiles.

Upon addition of ATP-γ-S, the elution profile of wild-type protein changed, with more protein shifting in favour of a dimeric association (Figure 6.6 B). $MinD_{Ng\text{-}loop}$ also had an increase in eluted dimeric protein, with a greater proportion of dimers formed relative to monomers compared to wild-type (Figure 6.6 F). This result is consistent with the stronger self-interaction of $MinD_{Ng\text{-}loop}$ compared to wild-type $MinD_{Ng}$, observed using the yeast two-hybrid system. No significant increases in the absorbance peak corresponding to dimeric $MinD_{Ng\text{-}K16Q}$ was observed when this protein was preincubated with ATP-γ-S (Figure 6.6 D) compared to protein in the absence of nucleotide. Overall, these results confirm the self-association of $MinD_{Ng\text{-}loop}$ observed by the yeast two-hybrid system and shows the mutant protein dimerizes in an ATP-dependent manner.

ATPase activity of purified $MinD_{Ng\text{-}loop}$ is not stimulated by $MinE_{Ng}$ and phospholipids

Since $MinD_{Ng\text{-}loop}$ could still dimerize in the presence of ATP, the ATPase activity of this mutant was investigated to determine whether mutations to residues 92-94 affect MinD enzymatic activity. *E. coli* MinD has been shown to preferentially bind anionic phospholipids (Mileykovskaya, 2003; Szeto *et al.*, 2003); hence, artificial phosphatidylglycerol (PG) vesicles were made and used for $MinD_{Ng}$ ATPase stimulation assays with $MinE_{Ng}$. In the absence of $MinE_{Ng}$, wild-type $MinD_{Ng}$ exhibited a basal level of ATPase activity when combined with phospholipid vesicles (Figure 6.7). However, the addition of $MinE_{Ng}$ resulted in a significantly increased release of inorganic phosphate, up to threefold the basal level after 90 minutes (Figure 6.7).

Without $MinE_{Ng}$, the ATPase activities of $MinD_{Ng\text{-}loop}$ and $MinD_{Ng\text{-}K16Q}$ were low, similar to wild-type protein (Figure 6.7). Interestingly, the addition of $MinE_{Ng}$ did not significantly raise the levels of inorganic phosphate released from $MinD_{Ng\text{-}loop}$, similar to $MinD_{Ng\text{-}K16Q}$ (Figure 6.7). Therefore, despite retaining homodimerization and strong interaction with MinE, as shown by yeast two-hybrid assays, and the ability to form cell-spanning intracellular coils *in vivo*, the ATPase activity of $MinD_{Ng\text{-}loop}$ could not be stimulated in the presence of $MinE_{Ng}$ and lipid vesicles.

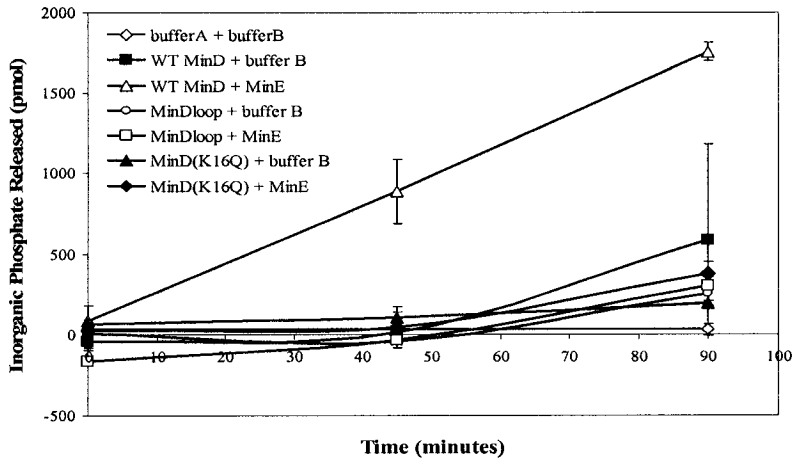

Figure 6.7. MinD ATPase stimulation assays using wild-type $MinD_{Ng}$, $MinD_{Ng\text{-}loop}$, and $MinD_{Ng\text{-}K16Q}$. Equal amounts of purified $MinD_{Ng}$, $MinD_{Ng\text{-}loop}$, and $MinD_{Ng\text{-}K16Q}$ were incubated with PG vesicles and 1 mM ATP. The ATPase activities of each were tested in the presence or absence of $MinE_{Ng}$ over a 90 minute period. Inorganic phosphate released due to ATP hydrolysis was monitored using a malachite green based method. Buffer A is $MinD_{Ng}$ storage buffer, Buffer B is $MinE_{Ng}$ storage buffer.

GFP-fusions to $MinD_{Ng}$ and $MinD_{Ec}$ proteins containing substitutions within residues 92-94 do not display distinct pole-to-pole oscillations in *E. coli*

While mutations at residues 92-94 did not disrupt the ability of $MinD_{Ng\text{-}loop}$ to inhibit cytokinesis in wild-type *E. coli*, the inability of $MinD_{Ng\text{-}loop}$ to be stimulated by $MinE_{Ng}$ suggested the dynamic localization of the mutant might be affected. GFP-$MinD_{Ng}$ exhibits distinct, $MinE_{Ng}$-dependent, pole-to-pole oscillation in *E. coli* rods (Chapter 4). Hence, plasmid-encoded GFP fusions to mutant $MinD_{Ng}$ were constructed for dynamic localization studies in *E. coli* PB114 (Δ*minCDE*) (Table 2.1). The *minE*$_{Ng}$ gene was included downstream of each fusion gene to provide the stimulation needed to induce $MinD_{Ng}$ oscillation. Since *E. coli* PB114 has a minicell phenotype consisting of small anucleate cells and rods of varying lengths, oscillatory movement was measured in cells of similar length (2.0-2.5 μm) to maintain consistency.

As expected, wild-type GFP-$MinD_{Ng}$ displayed periodic oscillations and clearly moved from the membrane at one polar region to the other (Figure 6.8 A, B). The average oscillation cycle of GFP-$MinD_{Ng}$ (from one pole to the other, and back again) measured in twenty cells was 29.1 ± 7.3 seconds. GFP-$MinD_{Ng\text{-}E103I}$ also displayed a similar pole-to-pole oscillation in *E. coli* PB114 rods as the wild-type fusion (Figure 6.8 E, F), with an average cycle, calculated from twenty cells, of 18.6 ± 2.0 seconds. In the absence of $MinE_{Ng}$, GFP-$MinD_{Ng}$ appeared along the entire inner cell periphery, presenting a smooth, unbroken fluorescent signal without evidence of oscillatory movement (Figure 6.8 K), similar to a report with GFP-$MinD_{Ec}$ (Raskin and de Boer, 1999a).

Despite the presence of $MinE_{Ng}$, raw images of GFP-$MinD_{Ng\text{-}loop}$ localization in *E. coli* PB114 showed that the fusion protein displayed no obvious pole-to-pole oscillations and was distributed along the entire inner periphery of the cell (Figure 6.8 H). This resulted in GFP-$MinD_{Ng\text{-}loop}$ localizing not only along cell pole regions, but across the membrane at midcell as well, similar to wild-type GFP-$MinD_{Ng}$ in the absence of $MinE_{Ng}$ (Figure 6.8 K). Western blotting confirmed similar expression

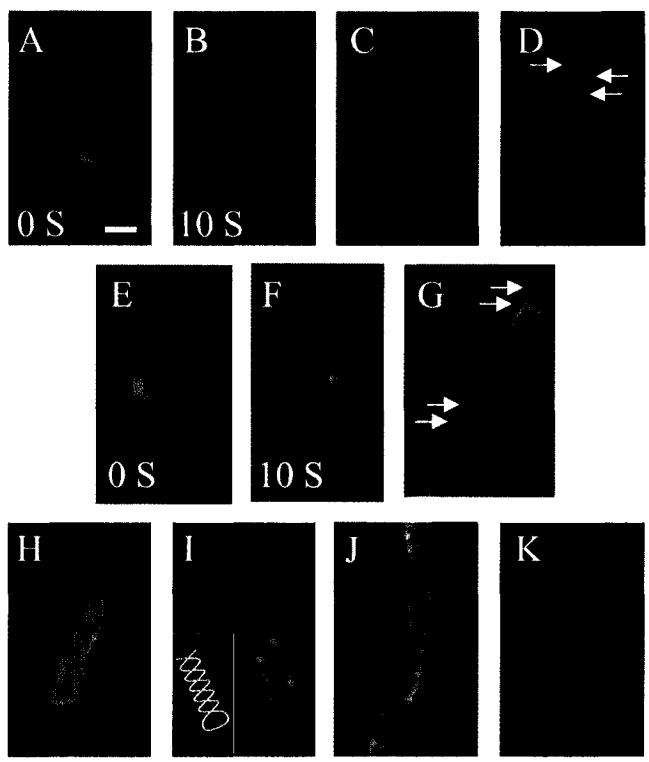
A
0 S
B
10 S
C
D
E
0 S
F
10 S
G
H
I
J
K

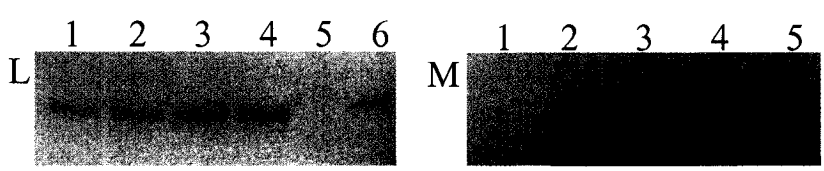
1 2 3 4 5 6
L
1 2 3 4 5
M

levels of all GFP-$MinD_{Ng}$ fusions (Figure 6.8 L) and the expression of $MinE_{Ng}$ (Figure 6.8 M) in each *E. coli* transformant used in localization studies.

Hence, these experiments indicate that mutations within amino acid residues 92-94 of $MinD_{Ng}$ and $MinD_{Ec}$ disrupt the topological specificity of MinD in *E. coli*, despite the presence of MinE. As a result, the mutant proteins no longer undergo the distinct pole-to-pole movement that normally sequesters the protein away from the midcell.

Uniform distribution of GFP-$MinD_{loop}$ proteins throughout an intracellular coiled array

Closer examination of GFP-$MinD_{Ng\text{-}loop}$ localization revealed that its membrane association appeared discontinuous, with punctate points of higher fluorescence along the membrane (Figure 6.8 H). Since this localization of GFP-$MinD_{Ng\text{-}loop}$ might represent contact sites between the membrane and an intracellular GFP-$MinD_{Ng\text{-}loop}$-containing array, image enhancement was used to determine whether such a higher ordered structure could be visualized *in vivo*.

As observed previously (Chapter 4), raw fluorescent images of wild-type GFP-$MinD_{Ng}$, provided evidence of the fusion dynamically localizing within coil-like structures extending along the long axis of cells that also encoded $MinE_{Ng}$ (Figure 6.8 C), similar to a recent report of wild-type GFP-$MinD_{Ec}$ (Shih *et al.*, 2003). Again, these coiled structures were readily visible in longer cells ($\geq$ 5 μm), since fluorescent signal concentration at the poles of shorter cells tended to obscure details of the helical array. Image enhancement revealed that these dynamic bands were composed of accumulated GFP-$MinD_{Ng}$ signal that localized in at least two adjacent turns of a coil (Figure 6.8 D, arrows).

It was also revealed that GFP-$MinD_{Ng\text{-}E103I}$ assembled dynamically within coiled structures similar to wild-type GFP-$MinD_{Ng}$, with brighter regions defined by accumulated fluorescent signal along at least two turns of the coil (Figure 6.8 G, arrows). Although localized along the entire inner cell membrane, there was no evidence of any GFP-$MinD_{Ng}$ decorated coils when the fusion was

expressed in the absence of $MinE_{Ng}$ (Figure 6.8 K). The negative control GFP-$MinD_{Ng\text{-}K16Q}$ appeared distributed in the cytoplasm, despite the presence of $MinE_{Ng}$ (see Figure 4.6 D).

Interestingly, enhancement of raw images revealed that GFP-$MinD_{Ng\text{-}loop}$ still localized as coiled structures along the length of the cell. However, unlike wild-type protein, coordinated fluorescent signal movement could not be distinguished at all. While there seemed to be some movement of protein, it appeared highly disordered along the coil, such that any distinct pole-to-pole motion or fusion protein banding was not observed. As a result, fluorescent signal was distributed throughout the entire helical array extending the length of the cell (Figure 6.8 I). Due to this uniform localization of GFP-$MinD_{Ng\text{-}loop}$, it was also possible to discern that MinD coiled arrays likely consisted of at least two coils arranged in a double-helix conformation (Figure 6.8 I), similar to observations with $MinD_{Ec}$ (Shih *et al.*, 2003). Hence, while still able to localize as a membrane-associated coil, GFP-$MinD_{Ng\text{-}loop}$ has lost its topological specificity, since the protein did not preferably localize to any particular region of the inner membrane or the coiled array. Similar uniform distribution of fluorescent signal along a coiled array was also observed with GFP-$MinD_{Ng\text{-}K94A}$ (Figure 6.8 J), again in stark contrast to the obviously distinct banding seen with wild-type GFP-$MinD_{Ng}$ (Figure 6.8 D).

To determine whether these attributes were characteristic of other MinD proteins bearing mutations within the 'loop' region, a GFP fusion to an *E. coli* MinD mutant containing R92L, D93L, and K94I substitutions (GFP-$MinD_{Ec\text{-}loop}$) was created. This mutant also did not display obvious oscillation patterns. Image enhancement revealed that the fusion protein still localized uniformly along a coiled array throughout the cell, including at the midcell (Figure 6.9 D), similar to its gonococcal counterpart. In contrast, wild-type GFP-$MinD_{Ec}$ exhibited pole-to-pole oscillation (Figure 6.9 A, B). Furthermore, unlike GFP-$MinD_{Ec\text{-}loop}$, evidence of wild-type GFP-$MinD_{Ec}$ localizing within a coiled array could only be clearly visualized in specific regions (e.g. the cell poles) at any particular time (Figure 6.9 C), consistent with the coordinated dynamic movement of GFP-$MinD_{Ec}$ subunits over the array.

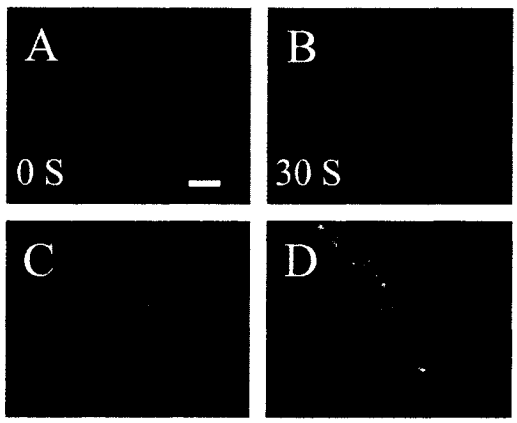

Figure 6.9. Localization of GFP-fusions to wild-type *E. coli* MinD ($MinD_{Ec}$) and a 'loop' region $MinD_{Ec}$ mutant in the presence of $minE_{Ec}$ within *E. coli* PB114. (A, B) Pole-to-pole oscillation of wild-type GFP-$MinD_{Ec}$. Time between images is 30 seconds. (C) Enhanced image showing localization of wild-type GFP-$MinD_{Ec}$ as a coil at one cell pole. (D) Enhanced image of GFP-$MinD_{Ec\text{-}loop}$ localizing throughout a coiled structure extending the length of the cell. Bar in (A) indicates 1 μm and all images are at the same magnification.

Hence, GFP-MinD mutants bearing hydrophobic substitutions in the polar region encompassing residues 92-94 of MinD can still localize as intracellular coils. However, they do not display obvious intracellular oscillation patterns. As a result, they appear to have lost normal topological specificity by accumulating at all potential division sites, including the midcell, by virtue of their uniform distribution along a membrane-associated helical array.

6.4 DISCUSSION

Using both structural and protein sequence alignments, coupled with a number of functional assays, a region in bacterial MinD has been identified to be implicated in rendering the protein responsive to MinE stimulation. Originally, this study was directed towards characterizing potential MinD homodimerization interfaces; however, unlike its structural counterpart NifH, the polar residues at positions 92-94 of $MinD_{Ng}$ are not required for $MinD_{Ng}$ dimerization. Furthermore, mutation of these residues did not disrupt the ability of $MinD_{Ng}$ to induce cell division arrest or to abrogate its interaction with MinC and MinE.

The relatively uniform distribution of GFP-MinD 'loop' mutants within coiled arrays was a striking contrast to wild-type GFP-MinD coiled arrays, which displayed clearly defined regions of dynamic protein accumulation. GFP-$MinD_{Ec}$ has been shown to localize within coils in a $MinE_{Ec}$-dependent manner (Shih *et al.*, 2003). It is likely that GFP-$MinD_{Ng\text{-}loop}$ was still able to form coiled arrays because $MinD_{Ng\text{-}loop}$ retained interaction with $MinE_{Ng}$, as shown by our yeast two-hybrid assays. Since GFP-fusions to either $MinD_{Ng\text{-}K94A}$ or $MinD_{Ec\text{-}loop}$ also localized as helical arrays *in vivo,* they likely interact with $MinE_{Ng}$ as well.

This study indicates that the inability of $MinE_{Ng}$ to effectively stimulate the ATPase activity of $MinD_{Ng\text{-}loop}$ might account for the absence of distinct, coordinated oscillations of GFP-$MinD_{Ng\text{-}loop}$ *in vivo*. It is also likely that $MinD_{Ng\text{-}K94A}$ and $MinD_{Ec\text{-}loop}$ are not responsive to MinE stimulation, leading to their near uniform distribution along intracellular coiled arrays. In support of this, *E. coli* MinE mutants that are deficient in stimulating the ATPase activity of wild-type GFP-$MinD_{Ec}$ cannot induce the intracellular oscillation of the latter, which remains distributed along the entire inner cell membrane (Hu and Lutkenhaus, 2001); however, whether GFP-$MinD_{Ec}$ can still localize within coiled arrays in this case is not known. Moreover, the diminished interaction of $MinD_{Ng\text{-}loop}$ with MinC could not possibly have contributed to the loss of coordinated $MinD_{Ng\text{-}loop}$ oscillation, since MinC was not present in the *E. coli* strain used in our localization studies. Furthermore, it is established that MinC is not required for MinD oscillation (Raskin and de Boer, 1999a).

The lack of distinct pole-to-pole movement in *N. gonorrhoeae* and *E. coli* GFP-MinD 'loop' mutants effectively led to their localization along coiled arrays across the midcell, in addition to the remainder of the cell. This indicated a loss of topological specificity normally defined by clear oscillations that direct MinD away from the midcell site (de Boer *et al.*, 1989; Raskin and de Boer, 1999a; Hu and Lutkenhaus, 2001). This disrupted topological specificity differed fundamentally from that of wild-type GFP-$MinD_{Ng}$ expressed in the absence of MinE. While the lack of $MinE_{Ng}$ resulted in a uniform distribution of GFP-$MinD_{Ng}$ along the inner cell membrane, the fusion protein did not localize within any coiled arrays, in stark contrast to our mutant GFP-MinD proteins. It is noted that GFP-MinD 'loop' mutants were not totally devoid of dynamism, and did exhibit what appeared to be random disordered shifting throughout their coiled structures. The residual basal ATPase activity remaining in these mutants may have been sufficient to allow this disorganized protein movement that clearly did not present any preference for specific coil and/or membrane regions. Hence, the $MinD_{Ng\text{-}loop}$ mutant, and likely $MinD_{Ng\text{-}K94A}$ and $MinD_{Ec\text{-}loop}$, of the present study represent the first MinD proteins characterized to be non-responsive to MinE-induced stimulation and topological specificity, despite the ability to interact with all other Min proteins and to localize within a membrane-associated coiled array.

$MinE_{Ec}$ has also been shown to promote the bundling of $MinD_{Ec}$ filaments under certain *in vitro* conditions, leading to the suggestion that MinE may have a secondary role of cross-linking polymerized MinD (Suefuji *et al.*, 2002). Since an increased interaction of $MinD_{Ng\text{-}loop}$ with $MinE_{Ng}$ was detected using the yeast two-hybrid system, it is tempting to speculate that, in addition to its inability to be stimulated by $MinE_{Ng}$, increased bundling of GFP-$MinD_{Ng\text{-}loop}$ by $MinE_{Ng}$ may have prevented the normal dissociation of GFP-$MinD_{Ng}$ subunits from the membrane-associated Min protein coil. It is possible that the residues within the defined 'loop' region of MinD are involved in providing optimal binding affinity to MinE to correctly regulate MinD bundling and/or ATPase activity. Proper protein bundling has also been shown to be important in FtsZ function, as it was recently shown that a mutant FtsZ with altered bundling properties could not initiate cell division,

despite its proper localization at midcell (Koppelman *et al.*, 2004). In addition, the increased affinity between $MinD_{Ng\text{-}loop}$ and $MinE_{Ng}$, as observed by yeast two-hybrid assays, may prevent proper conformational changes from occurring in each protein that are essential prerequisites for MinD ATPase induction.

Possibly the stronger self-association of $MinD_{Ng\text{-}loop}$ compared to wild-type $MinD_{Ng}$ (determined by the yeast two-hybrid system) may have contributed to the inefficient disassembly of $MinD_{Ng\text{-}loop}$ subunits from their intracellular helical array. However, yeast two-hybrid assays also detected a stronger self-association of $MinD_{Ng\text{-}E103I}$ in comparison to wild-type $MinD_{Ng}$. Since GFP-$MinD_{Ng\text{-}E103I}$ could still clearly oscillate *in vivo*, it argues against the idea that increased MinD self-association affinity would lead to a loss of pole-to-pole oscillation along the coiled-array.

The $MinD_{Ng\text{-}K16Q}$ mutant did not dimerize as efficiently as the other $MinD_{Ng}$ proteins, although there was slight shift of the $MinD_{Ng\text{-}K16Q}$ 'monomer' peak towards shorter retention times suggesting weak self-association. An *E. coli* $MinD_{K16Q}$ mutant was reported to bind ATP as strongly as wild-type protein (Hu and Lutkenhaus, 2001); hence, the diminished self-association of $MinD_{Ng\text{-}K16Q}$ in the present study suggests that such mutants in general may be deficient in a conformational change that normally allows efficient protein dimerization following nucleotide binding. As a result of disrupted homodimerization, this mutant protein would not bind membrane targets, in accordance with the 'dimer trigger' model of MinD membrane association (Hu and Lutkenhaus, 2003), and would not be stimulated by MinE. Since $MinD_{Ng\text{-}K16Q}$ lost interaction with MinC and MinE, it also raises the possibility that dimerization of MinD may have a role in its interaction with the other two Min proteins. The lack of interaction detected between $MinD_{Ng\text{-}K16Q}$ and $MinE_{Ng}$ would also likely render this MinD mutant unable to form any helical array, further contributing to its uniform cytoplasmic distribution. It is also noted that, given the high $MinD_{Ng}$ concentrations and excess ATP-γ-S used in the gel-filtration studies, the proportion of wild-type $MinD_{Ng}$ or $MinD_{Ng\text{-}loop}$ that dimerized was still quite low. This might signify a low dimerization constant for $MinD_{Ng}$ proteins in general.

Alternatively, it has been shown that MinD has less affinity for ATP-γ-S than ATP (Lackner *et al.*, 2003), which may have contributed to less dimerization than expected.

Whether the affinity of MinD 'loop' mutants for ATP is altered remains to be determined. The R92, D93, and K94 residues of $MinD_{Ng}$ and $MinD_{Ec}$ do not correspond to ATP-binding residues, based on Archaeal MinD structures (Figure 6.1B, cyan residues) (Hayashi *et al.*, 2001; Sakai *et al.*, 2001). However, should an increased affinity for ATP exist, it is conceivable that these MinD mutants may have increased propensities to remain on, or rapidly return to, their membrane-associated coiled array, such that normal dynamic oscillation is lost. The loss of topological specificity of MinD aa 92-94 mutants in this study was also not a result of mutating residues directly implicated in hydrolyzing ATP (e.g. D40 and A121, as indicated by the *P. furiosus* MinD structure) (Hayashi *et al.*, 2001) or those found in the switch I and switch II sites of MinD (Cordell *et al.*, 2001; Sakai *et al.*, 2001). Switch I and II sites in various ATPases normally undergo conformational changes during nucleotide hydrolysis (Vale, 1996). A recent report showed that $MinD_{Ec}$ switch I and II mutants lose interaction with $MinC_{Ec}$, but not their MinE-induced ATPase activity (Zhou and Lutkenhaus, 2004), in contrast to $MinD_{Ng\text{-}loop}$ in this study. Hence, the activity of the switch I and II sites in our $MinD_{Ng\text{-}loop}$ mutant was likely not affected.

What function might the polar MinD 'loop' region have in allowing the protein to be topologically regulated? Based on our model of dimeric MinD, the residues of interest correspond to a short α-helix in each *P. furiosus* MinD monomer (Figure 6.10 A, green residues) located directly opposite the C-terminal membrane targeting sequence (MTS). While the actual crystal structure of the MTS of Archaeal MinD has not been obtained due to structural disorder in this region (Cordell and Löwe, 2001; Hayashi *et al.*, 2001), it will be assumed that the MTS is in proximity to the C-terminus indicated in Figure 6.10 A (cyan residues). *In vitro* experiments have shown that MinD polymer bundles may possess polarity (Suefuji *et al.*, 2002), similar to other proteins such as tubulin; hence, a possible arrangement for MinD polymers at the membrane surface is shown in Figure 6.10 C'. Upon

Fig. 6.10. A proposed model for MinD 'loop' region function. (A) The predicted MinD dimer generated by superimposition of *P. furiosus* MinD ($MinD_{Pf}$) (Hayashi *et al.*, 2001) monomers onto each subunit of the *A. vinelandii* NifH dimer. The green residues (aa 87-93) of $MinD_{Pf}$ represent a region that corresponded with the loop region in each NifH monomer. Note: the structure and exact location of the C-terminal membrane targeting sequence (MTS) of MinD has not been determined yet. The cyan residues indicate the C-terminal residues in the solved structure that are likely in proximity to the MTS. Dotted line indicates proposed MinD dimerization interface. (B) A schematic representation of a MinD monomer. Here, the membrane targeting sequence (MTS), is deployed in this representative molecule, which has bound ATP (red circle) at the dimerization interface (partner MinD not shown). (B) Conserved polar residues R92, D93, and K94 of $MinD_{Ng}$ and $MinD_{Ec}$ are predicted to be in proximity to the MinD dimerization interface and exposed to the cytosol. The 'loop' region, containing R92, D93, and K94 residues is shown opposite of the MTS. (C) Dimeric, ATP-bound MinD associates with the inner cell membrane and/or Min protein coil through the activated MTS. The division inhibitor MinC (not shown) would also be recruited to the membrane by MinD. MinE (triangles) initiates binding to MinD-ATP. MinD will also polymerize along the membrane to form polymeric structures. (C') Possible arrangement of a MinD protofilament at the membrane. Note, the membrane is not shown to simplify the schematic. (+) and (-) symbols designate the possibility of polarity in the MinD filaments (Szeto *et al.*, 2003), as suggested by *in vitro* polymerization studies (Suefuji *et al.*, 2002). (D) Residues R92, D93, and K94 are not directly involved in MinE binding; however, the effects of MinE binding may be transmitted by these MinD residues (blue ovals) to other parts of the protein, particularly sites involved in ATPase activity at the MinD dimer interface. As a result, MinD ATPase activity is stimulated and ATP is hydrolyzed to form ADP (white circles). (E) ATP hydrolysis terminates MinD dimerization and its association at the membrane and with the remaining MinD polymer (not shown). Cytosolic MinD subunits are free to move to other membrane/Min coil segments.

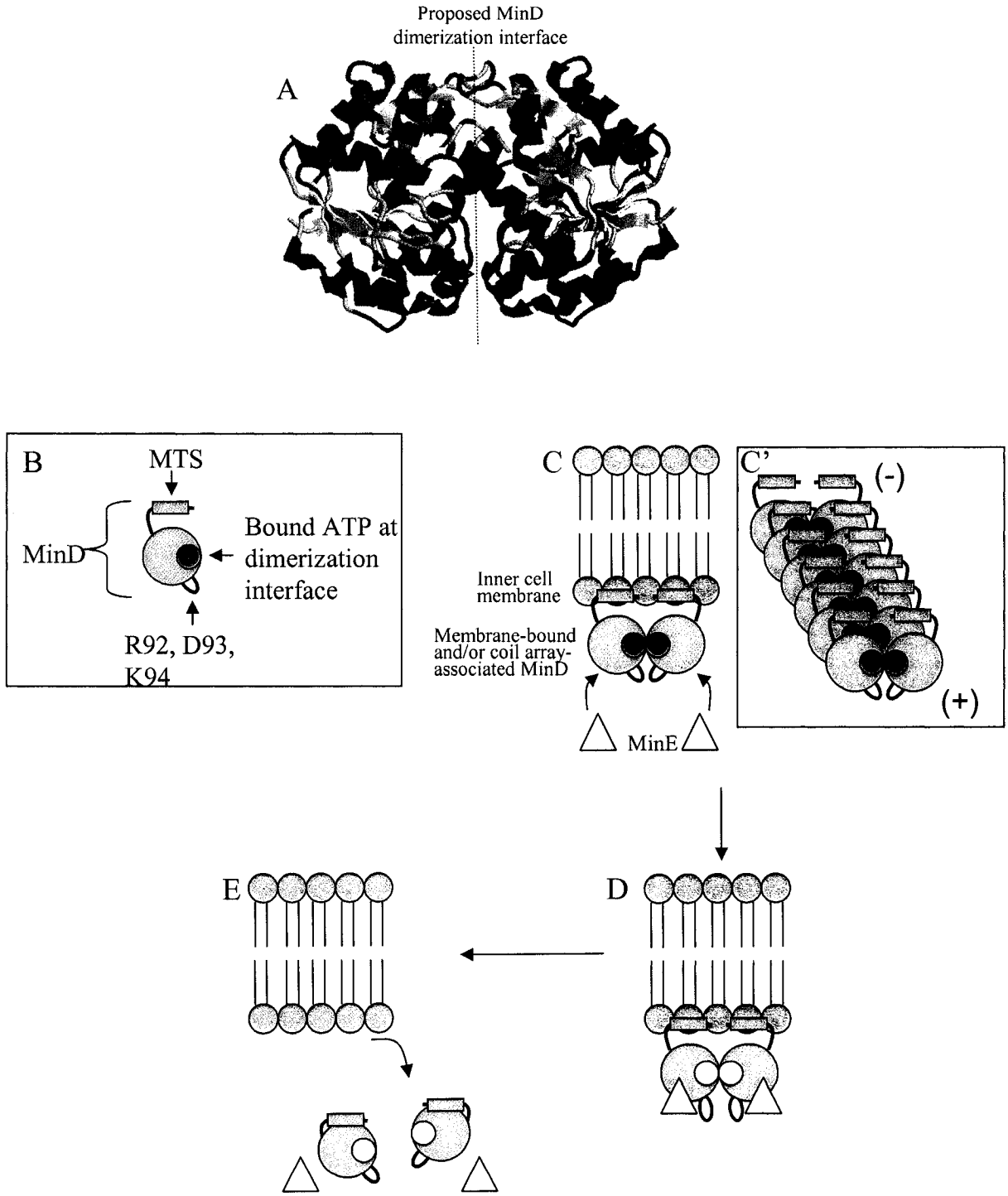
Proposed MinD
dimerization interface
A
B
MTS
MinD
Bound ATP at
dimerization
interface
R92, D93,
K94
C
Inner cell
membrane
Membrane-bound
and/or coil array-
associated MinD
MinE
C'
(-)
(+)
D
E

membrane association, it is possible that R92, D93, K94, and surrounding residues of bacterial MinD proteins, will remain exposed and oriented towards the cytoplasm, opposite the MTS (Figure 6.10 B, C). These residues would be situated in close proximity to, but not within, the MinD dimerization interface (Figure 6.10 A and B). This interface includes the ATP binding sites of each MinD monomer (Figure 6.1 B, cyan residues), based on structural similarities of MinD to NifH (Lutkenhaus and Sundaramoorthy, 2003; Cordell and Löwe, 2001; Sakai *et al.*, 2001; this study), such that the dimerized form of MinD is primed for ATP hydrolysis (Lutkenhaus and Sundaramoorthy, 2003).

Although not essential for interaction with MinE, the residues in the 'loop' region may serve to sensitize and/or transmit the effects of MinE binding to the MinD-MinD interface through conformational change, thus inducing ATPase activity and MinD oscillation (Figure 6.10 D, E). The B-factor profile of residues corresponding to the 'loop' region in at least one Archaeal MinD homologue (from *Archaeoglobus fulgidus*) (Cordell and Löwe, 2001) shows this region possesses some flexibility, which might also be found in bacterial MinD homologues to allow for conformational change. By mutating this region, the ability of MinD to properly respond to MinE binding would be disrupted and its ATPase activity and coordinated pole-to-pole oscillation would not be induced.

The $MinD_{Ng\text{-}loop}$ mutant, and likely $MinD_{Ng\text{-}K94A}$ and $MinD_{Ec\text{-}loop}$, constructed in the present study represent the first MinD proteins characterized to have retained interaction with all components of the Min protein system, and yet have truly lost topological specificity while at the membrane. Without an intact C-terminal membrane targeting sequence, mutants of *E. coli* MinD also do not oscillate (Szeto *et al.*, 2002; Hu and Lutkenhaus, 2003), and it could be argued that they have lost topological specificity. However, like $MinD_{K16Q}$ mutants, this 'loss' of topological specificity is simply due the inability of these C-terminal MinD mutants to localize to the membrane. Topological specificity mutants of *B. subtilis* MinD ($MinD_{Bs}$) have been described that localize peripherally along the membrane (El Karoui and Errington, 2001). However, unlike the MinD 'loop' mutants in the present study, the $MinD_{Bs}$ mutants no longer activated MinC cell division arrest, or had lost

interaction with their Gram-positive specific topological specificity determinant DivIVA (El Karoui and Errington, 2001). Interestingly, while residues 86-97 of the predicted 'loop' region of $MinD_{Ng}$ are extremely conserved in Gram-negative organisms, there is less conservation in the corresponding region of MinD from Gram-positive bacteria. It is possible that this amino acid degeneracy reflects the absence of MinE homologues in Gram-positive bacteria (Margolin, 2001a).

This study employed a homologous structure-based approach to identify a polar region in bacterial MinD that, when mutated, clearly disrupts MinD pole-to-pole oscillation, but not its ability to localize as intracellular coils. Hence, these mutations disrupted the ability of MinD to have topological specificity imparted upon it. It is proposed that amino acid residues 92-94, and possibly the spatially proximal residues as well, may play a role in transmitting the effects of MinE-binding to the ATPase regions of MinD dimers. Significantly, these studies show the ability of MinD to bind to MinE is not sufficient for the latter to stimulate MinD ATPase activity and to coordinate its dynamism. While MinD proteins bearing mutations in residues 92-94 can still interact with MinE, the latter protein cannot efficiently stimulate MinD ATPase activity and/or induce significant MinD movement along the Min protein membrane lattice. Clearly, structural studies should provide additional insight into the role that specific residues selected in this study may have in modulating effective MinD-MinE interaction.

CHAPTER 7

Mutational analysis of the N-terminus of $MinD_{Ng}$ indicates this region contains determinants that affect $MinD_{Ng}$ ATPase activity and dynamic localization

Portions of this chapter were published in:

[Ramirez-Arcos, S., **Szeto, J.**, Dillon, J. R., and Margolin, W. (2002). Conservation of dynamic localization among MinD and MinE orthologues: oscillation of *Neisseria gonorrhoeae* proteins in *Escherichia coli*. Mol. Microbiol. *46*, 493-504.]

and also included in the following submitted manuscipt:

[**Szeto, J.**, Acharya, S., Eng, N. F., and Dillon, J. R. (2004). The N-terminus of MinD contains determinants which affect its dynamic localization and enzymatic activity. Submitted for publication to the Journal of Bacteriology]

7.1. PURPOSE OF THIS STUDY

Sequence alignment of MinD proteins show they are highly conserved. In general, the N-terminus of MinD appears to have greater sequence conservation than the C-terminal half (See Figure 3.1). While there is increasing information regarding the membrane targeting role of the extreme C-terminus of MinD (Szeto *et al.*, 2002; Szeto *et al.*, 2003; Hu and Lutkenhaus, 2003; Zhou and Lutkenhaus, 2003), little is known about its N-terminus. Perhaps the most characterized N-terminal region of MinD is its Walker A ATP-binding motif [amino acids (aa) 10-17 in $MinD_{Ec}$ and $MinD_{Ng}$] (Figure 3.1). In particular, mutation of the conserved K16 residue disrupted $MinD_{Ng}$ ATPase activity, dimerization, and membrane localization (Chapters 5 and 6).

This study was conducted to determine whether the conserved residues at the extreme N-terminus of $MinD_{Ng}$ are involved in protein functionality. To characterize this region, sequential deletions or point mutations were generated to residues at the N-terminus of $MinD_{Ng}$ and mutant proteins were evaluated using several functional assays. These truncations or mutations disrupted $MinD_{Ng}$ interaction with other Min proteins, particularly with itself and MinE. The majority of GFP-$MinD_{Ng}$ mutants could still oscillate from pole-to-pole in *E. coli*. However, as truncations or mutations were successively generated from the N-terminus of $MinD_{Ng}$, GFP-$MinD_{Ng}$ oscillation cycles became significantly faster, accompanied by an increased tendency for GFP-$MinD_{Ng}$ fusions to remain distributed in the cytoplasm. Interestingly, *in vitro* ATPase assays indicated that $MinD_{Ng}$ proteins lacking the first three residues (replaced with a start codon), or having an I5E substitution, possessed hyper-ATPase activities that were independent of $MinE_{Ng}$. From these studies, it is proposed that determinants found within the extreme N-terminus of $MinD_{Ng}$ are involved in regulating the enzymatic activity of the protein, which in turn affects its dynamic localization.

7.2. MATERIALS AND METHODS

Generation of deletions derivatives and N-terminal mutants of *minD*$_{Ng}$ for *E. coli* expression studies. N-terminal truncated *minD*$_{Ng}$ genes were cloned into pUC18 (Table 7.1) for morphology studies in *E. coli* PB103 (Table 2.1). In order to preserve protein translation, the primers used to generate N-terminal deletions were designed to place the natural GTG start codon of *minD*$_{Ng}$ directly upstream of codons encoding residues 3, 4, 5, and 20, to generate N-terminal deletions to MinD$_{Ng}$. These primers included MinD-N2, MinD-N3, minD11B, and minD12B, and were used in conjunction with primer minD2 (Table 2.2) to PCR amplify truncated *minD*$_{Ng}$ from gonococcal DNA. As a result, *minD*$_{Ng}$ genes where generated where the first 2, 3, 4, and 19 codons (and hence, amino acids) were deleted and replaced with a start codon. The resulting amplicons were digested with *Eco*RI and *Bam*HI (incorporated by each mutant primer and minD2, respectively) and ligated into similarly digested pUC18 to produce plasmids pSIA10 (*minD*$_{Ng\text{-}2aaNT}$), pSIA11 (*minD*$_{Ng\text{-}3aaNT}$), pJS4B (*minD*$_{Ng\text{-}4aaNT}$), and pJS5B (*minD*$_{Ng\text{-}19aaNT}$), where 'NT' designates the number of N-terminal amino acids replaced with a start codon (Table 7.1).

To create mutant *minD*$_{Ng}$ genes containing specific N-terminal substitutions, site-directed mutagenesis was employed. Primers incorporating the specific mutation of interest were used with primer minD2 (Table 2.2) to amplify *minD*$_{Ng}$ from pSR3 (Table 7.1) or from gonococcal cell suspensions. Mutant primers included (with respective substitutions in parentheses): SA5 (K3E), SA6 (K3I), SA7 (K3A), SA13 (K3F), SA8 (I4Q), SA10 (I5E), and SA11 (I5A) (Table 2.2). Each amplicon was digested with *Eco*RI and *Bam*HI and ligated into similarly digested pUC18 to generate plasmids pSIA13, pSIA22, pSIA23, pJS16, pSIA24, pJS13 and pJS14 (Table 7.1), respectively.

Construction of yeast two-hybrid vectors encoding GAL4 fusions to N-terminal mutants of MinD$_{Ng}$. Amplicons used to generate the N-terminal deletion and mutant forms of *minD*$_{Ng}$ were also cloned into *Eco*RI and *Bam*HI digested yeast two-hybrid vectors pGAD424 and pGBT9 (Table 7.1).

Table 7.1. Plasmids used in this study

Plasmids	Relevant genotype	Source or reference
Plasmids for expression studies		
pUC18	Amp^R P_{lac}	Amersham
pSR3	pUC18; P_{lac}::*minD*$_{Ng}$ (Amp^R)	Chapter 4, this study
pSIA10	pUC18; P_{lac}::*minD*$_{Ng\text{-}2aaNT}$[a] (Amp^R)	This study
pSIA11	pUC18; P_{lac}::*minD*$_{Ng\text{-}3aaNT}$ (Amp^R)	This study
pJS4B	pUC18; P_{lac}::*minD*$_{Ng\text{-}4aaNT}$ (Amp^R)	This study
pJS5B	pUC18; P_{lac}::*minD*$_{Ng\text{-}19aaNT}$ (Amp^R)	This study
pSIA13	pUC18; P_{lac}::*minD*$_{Ng\text{-}K3E}$ (Amp^R)	This study
pSIA22	pUC18; P_{lac}::*minD*$_{Ng\text{-}K3I}$ (Amp^R)	This study
pSIA23	pUC18; P_{lac}::*minD*$_{Ng\text{-}K3A}$ (Amp^R)	This study
pJS16	pUC18; P_{lac}::*minD*$_{Ng\text{-}K3F}$ (Amp^R)	This study
pSIA24	pUC18; P_{lac}::*minD*$_{Ng\text{-}I4Q}$ (Amp^R)	This study
pJS13	pUC18; P_{lac}::*minD*$_{Ng\text{-}I5E}$ (Amp^R)	This study
pJS14	pUC18; P_{lac}::*minD*$_{Ng\text{-}I5A}$ (Amp^R)	This study
Yeast two-hybrid plasmids		
pGAD424	P_{ADH1}[a]::*gal4*(AD)[b] (Amp^R)	Clontech
pGBT9	P_{ADH1}::*gal4*(BD)[c] (Amp^R)	Clontech
pGADminD	pGAD424; P_{ADH1}::*gal4*(AD)-*minD*$_{Ng}$ (Amp^R)	Chapter 5, this study
pGBT9minD	pGBT9; P_{ADH1}::*gal4*(BD)-*minD*$_{Ng}$ (Amp^R)	Chapter 5, this study
pGBT9minE	pGBT9; P_{ADH1}::*gal4*(BD)-*minE*$_{Ng}$ (Amp^R)	Chapter 5, this study
pSRBD-C	pGBT9; P_{ADH1}::*gal4*(BD)-*minC*$_{Ec}$ (Amp^R)	Chapter 5, this study
pSIA1	pGBT9; P_{ADH1}::*gal4*(BD)-*minD*$_{Ng\text{-}2aaNT}$ (Amp^R)	This study
pSIA2	pGBT9; P_{ADH1}::*gal4*(BD)-*minD*$_{Ng\text{-}3aaNT}$ (Amp^R)	This study
pJminD8	pGBT9; P_{ADH1}::*gal4*(BD)-*minD*$_{Ng\text{-}4aaNT}$ (Amp^R)	This study
pJminD9	pGBT9; P_{ADH1}::*gal4*(BD)-*minD*$_{Ng\text{-}19aaNT}$ (Amp^R)	This study
pSIA15	pGBT9; P_{ADH1}::*gal4*(BD)-*minD*$_{Ng\text{-}K3E}$ (Amp^R)	This study
pJS26	pGBT9; P_{ADH1}::*gal4*(BD)-*minD*$_{Ng\text{-}K3I}$ (Amp^R)	This study
pSIA29	pGBT9; P_{ADH1}::*gal4*(BD)-*minD*$_{Ng\text{-}K3A}$ (Amp^R)	This study
pJS22	pGBT9; P_{ADH1}::*gal4*(BD)-*minD*$_{Ng\text{-}I4Q}$ (Amp^R)	This study
pJS24	pGBT9; P_{ADH1}::*gal4*(BD)-*minD*$_{Ng\text{-}I5E}$ (Amp^R)	This study

pJS21	pGBT9; P_{ADH1}::*gal4*(BD)-*minD*$_{Ng\text{-}I5A}$ (Amp^R)	This study
pSIA3	pGAD424; P_{ADH1}::*gal4*(AD)-*minD*$_{Ng\text{-}2aaNT}$ (Amp^R)	This study
pSIA4	pGAD424; P_{ADH1}::*gal4*(AD)-*minD*$_{Ng\text{-}3aaNT}$ (Amp^R)	This study
pJminD12	pGAD424; P_{ADH1}::*gal4*(AD)-*minD*$_{Ng\text{-}4aaNT}$ (Amp^R)	This study
pJminD13	pGAD424; P_{ADH1}::*gal4*(AD)-*minD*$_{Ng\text{-}19aaNT}$ (Amp^R)	This study
pJminD3	pGAD424; P_{ADH1}::*gal4*(AD)-*minD*$_{Ng\text{-}31aaNT}$ (Amp^R)	This study
pJminD4	pGAD424; P_{ADH1}::*gal4*(AD)-*minD*$_{Ng\text{-}183aaNT}$ (Amp^R)	This study
pSIA14	pGAD424; P_{ADH1}::*gal4*(AD)-*minD*$_{Ng\text{-}K3E}$ (Amp^R)	This study
pJS25	pGAD424; P_{ADH1}::*gal4*(AD)-*minD*$_{Ng\text{-}K3I}$ (Amp^R)	This study
pSIA27	pGAD424; P_{ADH1}::*gal4*(AD)-*minD*$_{Ng\text{-}K3A}$ (Amp^R)	This study
pSIA28	pGAD424; P_{ADH1}::*gal4*(AD)-*minD*$_{Ng\text{-}I4Q}$ (Amp^R)	This study
pJS11	pGAD424; P_{ADH1}::*gal4*(AD)-*minD*$_{Ng\text{-}I5E}$ (Amp^R)	This study
pJS20	pGAD424; P_{ADH1}::*gal4*(AD)-*minD*$_{Ng\text{-}I5A}$ (Amp^R)	This study
GFP-fusion plasmids		
pDSW209	pDSW209; P_{trc}::*gfp* (Amp^R)	Weiss *et al.*, 1999
pSR15	pDSW209; P_{trc}::*gfp-minD*$_{Ng}$, *minE*$_{Ng}$ (Amp^R)	Chapter 4, this study
pJDE1	pDSW209; P_{trc}::*gfp-minD*$_{Ng\text{-}K16Q}$, *minE*$_{Ng}$ (Amp^R)	Chapter 4, this study
pSIA16	pDSW209; P_{trc}::*gfp-minD*$_{Ng\text{-}2aaNT}$, *minE*$_{Ng}$ (Amp^R)	This study
pSIA17	pDSW209; P_{trc}::*gfp-minD*$_{Ng\text{-}3aaNT}$, *minE*$_{Ng}$ (Amp^R)	This study
pJDE2	pDSW209; P_{trc}^{d}::*gfp-minD*$_{Ng\text{-}4aaNT}$, *minE*$_{Ng}$ (Amp^R)	This study
pJDE3	pDSW209; P_{trc}^{d}::*gfp-minD*$_{Ng\text{-}19aaNT}$, *minE*$_{Ng}$ (Amp^R)	This study
pSIA18	pDSW209; P_{trc}::*gfp-minD*$_{Ng\text{-}K3E}$, *minE*$_{Ng}$ (Amp^R)	This study
pJS30	pDSW209; P_{trc}::*gfp-minD*$_{Ng\text{-}K3I}$, *minE*$_{Ng}$ (Amp^R)	This study
pJS18	pDSW209; P_{trc}::*gfp-minD*$_{Ng\text{-}I4Q}$, *minE*$_{Ng}$ (Amp^R)	This study
pJS29	pDSW209; P_{trc}::*gfp-minD*$_{Ng\text{-}I5E}$, *minE*$_{Ng}$ (Amp^R)	This study
pJS19	pDSW209; P_{trc}::*gfp-minD*$_{Ng\text{-}I5A}$, *minE*$_{Ng}$ (Amp^R)	This study
Plasmids for protein purification		
pET30a	P_{T7}:: 6XHis (Kan^R)	Novagen
pSC9	pET30a; P_{T7}:: *minD*$_{Ng}$-6XHis (Kan^R)	Chapter 6, this study
pJS33	pET30a; P_{T7}:: *minD*$_{Ng\text{-}I5E}$-6XHis (Kan^R)	This study
pJS34	pET30a; P_{T7}:: *minD*$_{Ng\text{-}3aaNT}$-6XHis (Kan^R)	This study

pSC10	pET30a; P_{T7}:: $minD_{Ng\text{-}K16Q}$-6XHis (Kan^R)	Chapter 6, this study

[a] NT denotes N-terminal truncation [e.g. 2aaNT = deletion of first 2 amino acids (codons) from N-terminus]. In place of the removed codons is a start codon.
[b] Encodes GAL4 activation domain (AD)
[c] Encodes GAL4 DNA-binding domain (BD)

GAL4-DNA-BD fusions to $MinD_{Ng\text{-}2aaNT}$, $MinD_{Ng\text{-}3aaNT}$, $MinD_{Ng\text{-}4aaNT}$, $MinD_{Ng\text{-}19aaNT}$ were encoded on pSIA1, pSIA2, pJminD8, and pJminD9, respectively (Table 7.1). GAL4-AD fusions to $MinD_{Ng\text{-}2aaNT}$, $MinD_{Ng\text{-}3aaNT}$, $MinD_{Ng\text{-}4aaNT}$, and $MinD_{Ng\text{-}19aaNT}$ were encoded pSIA3, pSIA4, pJminD12, and pJminD13, respectively (Table 7.1). Additional N-terminal deletions, $MinD_{Ng\text{-}31aaNT}$ and $MinD_{Ng\text{-}183aaNT}$, were also made using primers minD5 or minD6 paired with minD2 (Table 2.2), which were ligated in-frame with the GAL4-AD in pGAD424 to produce pJminD3 and pJminD4, respectively (Table 7.1). PCR amplicons encoding $minD_{Ng}$ with N-terminal substitutions K3E, K3I, K3A, I4Q, I5E, and I5A (see above) were also cloned into *Eco*RI/*Bam*HI digested yeast two-hybrid vectors. Plasmids encoding fusions to the GAL4-DNA-BD include, pSIA15 ($MinD_{Ng\text{-}K3E}$), pJS26 ($MinD_{Ng\text{-}K3I}$), pSIA29 ($MinD_{Ng\text{-}K3A}$), pJS22 ($MinD_{Ng\text{-}I4Q}$), pJS24 ($MinD_{Ng\text{-}I5E}$), and pJS21 ($MinD_{Ng\text{-}I5A}$) (Table 7.1). Vectors encoding fusions to the GAL-4-AD include pSIA14 ($MinD_{Ng\text{-}K3E}$), pJS25 ($MinD_{Ng\text{-}K3I}$), pSIA27 ($MinD_{Ng\text{-}K3A}$), pSIA28 ($MinD_{Ng\text{-}I4Q}$), pJS11 ($MinD_{Ng\text{-}I5E}$), and pJS20 ($MinD_{Ng\text{-}I5A}$) (Table 7.1). Plasmids encoding GAL4 fusions to wild-type $MinD_{Ng}$, $MinE_{Ng}$, and $MinC_{Ec}$ (Table 7.1) were constructed previously (Chapter 5). Yeast two-hybrid studies were carried out as described in Chapter 2.

Nucleoid localization in *E. coli* using DAPI staining. To determine the location of nucleoids in *E. coli*, DAPI stain (4' 6-diamidino-2-phenylindole-2HCl) (Molecular Probes) was employed. Cells were fixed and adhered to polylysine coated coverslips as outlined in Chapter 2. Five μl of DAPI (0.2 μg/ml stock) was placed on a small sheet of Parafilm and coverslips containing attached bacteria were gently pressed onto the DNA stain. After 2 minutes incubation, coverslips were removed and gently washed with 10 ml PBS (pH 7.4) dispensed dropwise from a pipette. Coverslips were then placed over a 5 μl drop of 50% glycerol on a coverslip and sealed. Fluorescence microscopy was performed

on an Olympus BX61 microscope equipped with a Photometrics CoolSnap ES camera and Image Pro Version 5.0 software.

Construction of GFP-fusions to $MinD_{Ng}$ mutants. For localization studies, GFP-fusions to mutant $MinD_{Ng}$ were constructed. Primer MinE2 was used in combination with primers MinD-N2, MinD-N3, minD7, minD8, SA5, SA6, SA8, SA10, or SA11 (Table 2.2) to amplify specific truncated/mutated $minD_{Ng}$ genes together with $minE_{Ng}$ from gonococcal chromosomal DNA. The PCR amplicons, as well as plasmid pDSW209, encoding GFP (Weiss *et al.*, 1999) (Table 7.1), were digested with *Eco*RI and *Bam*HI and ligated. The resulting plasmids encoded GFP-$MinD_{Ng\text{-}2aaNT}$ (pSIA16), GFP-$MinD_{Ng\text{-}3aaNT}$ (pSIA17), GFP-$MinD_{Ng\text{-}4aaNT}$ (pJDE2), GFP-$MinD_{Ng\text{-}19aaNT}$ (pJDE3), GFP-$MinD_{Ng\text{-}K3E}$ (pSIA18), GFP-$MinD_{Ng\text{-}K3I}$ (pJS30), GFP-$MinD_{Ng\text{-}I4Q}$ (pJS18), GFP-$MinD_{Ng\text{-}I5E}$ (pJS29), and GFP-$MinD_{Ng\text{-}I5A}$ (pJS19) (Table 7.1). Plasmids encoding wild-type GFP-$MinD_{Ng}$ (pSR15) and GFP-$MinD_{Ng\text{-}K16Q}$ (pJDE1) (Table 7.1) were constructed previously (Chapter 4). All plasmids also encoded $MinE_{Ng}$ downstream of each *gfp-*$minD_{Ng}$ variant.

Localization of GFP-$MinD_{Ng}$ fusions. *E. coli* WM1032 (Table 2.1) transformed with pSR15 (encoding wild-type GFP-$MinD_{Ng}$) pJDE1 (GFP-$MinD_{Ng\text{-}K16Q}$), pJDE2 (GFP-$MinD_{Ng\text{-}4aaNT}$), and pJDE3 (GFP-$MinD_{Ng\text{-}19aaNT}$) (Table 7.1) were examined using an Olympus BX60 fluorescence microscope, in collaboration with Dr. W. Margolin, University of Texas Medical School. Localization studies were carried out as essentially described in Chapter 4 Materials and Methods.

Subsequent studies involving wild-type GFP-$MinD_{Ng}$ (pSR15), GFP-$MinD_{Ng\text{-}K16Q}$ (pJDE1), GFP-$MinD_{Ng\text{-}2aaNT}$ (pSIA16), GFP-$MinD_{Ng\text{-}3aaNT}$ (pSIA17), GFP-$MinD_{Ng\text{-}K3E}$ (pSIA18), GFP-$MinD_{Ng\text{-}K3I}$ (pJS30), GFP-$MinD_{Ng\text{-}I4Q}$ (pJS18), GFP-$MinD_{Ng\text{-}I5E}$ (pJS29), and GFP-$MinD_{Ng\text{-}I5A}$ (pJS19) (Table 7.1) were conducted using an Olympus BX61 microscope system equipped with a Photometrics CoolSnap ES camera and Image Pro (Version 5.0) software. To measure oscillation cycle periods,

each GFP-$MinD_{Ng}$ fusion was observed in 30 cells of near equivalent length (~2.0-2.5 μm) and time-lapse images were taken every 5 seconds. In each cell observed, at least two complete oscillation cycles were used to verify oscillation periods. Statistical analyses using unpaired Student's *t*-tests were performed to determine whether differences in average oscillation periods between GFP-$MinD_{Ng}$ fusions were significant, with $p<0.001$ considered significant. When required, enhancement of raw images was done using standard options available on Image Pro software. Contrast enhancement was used to increase contrast and to decrease gamma. Gauss filtering using a 3 X 3 kernel size with 4 passes at strength 10 was performed to help visualize intracellular substructures.

Purification of $MinD_{Ng}$ N-terminal mutants and ATPase stimulation assays. Plasmids encoding C-terminal His-tagged $MinD_{Ng\text{-}I5A}$ and $MinD_{Ng\text{-}3aaNT}$ were obtained using an inverse PCR strategy with pSC9 (encoding C-terminal His-tagged wild-type $MinD_{Ng}$) (Chapter 6 and Table 7.1) as a template. Primer SA19 and a mutant primer (SA17 or SA18; incorporating I5E or 3aaNT mutations, respectively) (Table 2.2) were designed to anneal adjacent to each other and amplify in opposite directions using *Pfu* DNA polymerase (Fermentas). The resulting blunt-ended linear DNA product was subsequently religated to give pJS33 and pJS34 (Table 7.1). Plasmids pSC9 and pSC10, encoding C-terminal His-tagged wild-type $MinD_{Ng}$ and $MinD_{Ng\text{-}K16Q}$ (Chapter 6 and Table 7.1), served as a sources for positive and negative control proteins, respectively. Protein purification was carried out as described in Chapter 6. Following dialysis in Buffer A, purified $MinD_{Ng\text{-}I5A}$ and $MinD_{Ng\text{-}3aaNT}$ were concentrated using Microcon YM-3 centrifuge devices (3,000 molecular weight cutoff) (Amicon). $MinD_{Ng}$ ATPase stimulation assays with PG vesicles and $MinE_{Ng}$ were also conducted as outlined in Chapter 6 Materials and Methods.

7.3. RESULTS

Deletion and point mutation studies of the $MinD_{Ng}$ N-terminus indicate this region contains residues that are important for inducing cell division arrest. The high conservation of MinD makes it difficult to select any one particular amino acid for functional studies. Sequence alignment of MinD proteins revealed that the extreme N-terminus is well conserved (Figure 7.1), suggesting this region is important for protein function. In particular, Gram negative organisms feature a consensus sequence of M[A/G][K/R][I/V][I/V] for the first five residues, with the exception of *Vibrio cholerae* MinD, which contains a serine at position two; *Helicobacter pylori* MinD, which contains isoleucine at position three; and *Pseudomonas aeruginosa* MinD, containing a leucine at position five (Figure 7.1). Of particular note is that this region is identical in MinD from either *N. gonorrhoeae* or *E. coli*, except that $MinD_{Ec}$ contains an arginine residue instead of a lysine residue at position three. Thus, structure/function analyses of the gonococcal protein can serve as a paradigm for other MinD proteins, especially those from Gram negative organisms including *E. coli*, since it is evident that $MinD_{Ng}$ behaves in a similar manner as $MinD_{Ec}$ (Chapter 4).

To elucidate residues at the extreme N-terminus of $MinD_{Ng}$ that may be involved in protein function, deletion derivatives of $MinD_{Ng}$ were constructed that removed the first 2, 3, 4 or 19 amino acids of the protein. As a result, each gene contained the 3rd, 4th, 5th, and 20th codon of $minD_{Ng}$ immediately downstream of a start codon. The resulting truncated $MinD_{Ng}$ proteins will be referred to as $MinD_{Ng\text{-}2aaNT}$, $MinD_{Ng\text{-}3aaNT}$, $MinD_{Ng\text{-}4aaNT}$, and $MinD_{Ng\text{-}19aaNT}$ (NT indicating 'N-terminal deletion' of the specifed number of residues, which are replaced by a single start codon). While the first three mutant proteins are comprised of successive deletions, $MinD_{Ng\text{-}19aaNT}$ would contain a deletion of the entire Walker A ATP-binding motif (aa 10-17) (Figure 7.1, residues underneath black bar).

To determine whether these truncations affect the ability of $MinD_{Ng}$ to induce cell division arrest in wild-type *E. coli* PB103 (Table 2.1), plasmids encoding each truncated protein were transformed into the indicator strain. While cells transformed with pUC18 negative control vector exhibited normal short rod morphologies (Figure 7.2 A), transformant expressing wild-type $MinD_{Ng}$

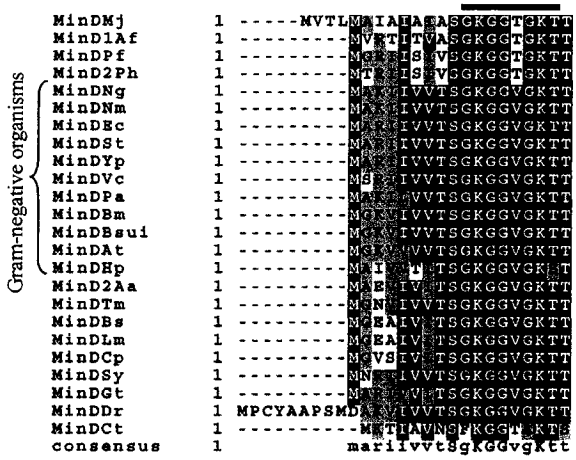

Figure 7.1. Sequence alignment of the N-terminus of MinD proteins. Abbreviations used: *Methanococcus janaaschii* (Mj), *Archaeoglobus fulgidus* (Af), *Pyrococcus furiosus* (Pf), *P. horikoshii* (Ph), *Neisseria gonorrhoeae* (Ng), *N. meningitidis* (Nm), *Escherichia coli* (Ec), *Salmonella enterica* serovar Typhimurium (St), *Yersinia pestis* (Yp), *Vibrio cholerae* (Vc), *Pseudomonas aeruginosa* (Pa), *Brucella melitensis* (Bm), *B. suis* (Bsui), *Agrobacterium tumefaciens* (At), *Helicobacter pylori* (Hp), *Aquifex aeolicus* (Aa), *Thermotoga maritima* (Tm), *Bacillus subtilis* (Bs), *Listeria monocytogenes* (Lm), *Clostridium perfringens* (Cp), *Synechocystis sp.* (Sy), *Guillardia theta* (Gt), *Deinococcus radiodurans* (Dr), and *Chlamydia trachomatis* (Ct). Residues of the Walker A ATP-binding motif are aligned below the black bar.

from pSR3 (Table 7.1) exhibited a filamentous phenotype, indicative of cell division arrest (Figure 7.2 B). *E. coli* expressing $MinD_{Ng\text{-}2aaNT}$ were filamentous as well (Figure 7.2 C). In contrast, cells expressing $MinD_{Ng\text{-}3aaNT}$ or $MinD_{Ng\text{-}4aaNT}$ presented a minicell phenotype, characterized by rods of varying lengths and round minicells (Figure 7.2 D, E; arrows indicate minicells). Cells transformed with pJS5B (*minD*$_{Ng\text{-}19aaNT}$) (Table 7.1) presented a short rod morphology (Figure 7.2 F), similar to the negative control cells containing pUC18 (Figure 7.2 A). Western blotting showed the overexpression of wild-type $MinD_{Ng}$ (Figure 7.2 G, lanes 2, 6), $MinD_{Ng\text{-}2aaNT}$ (lane 3), $MinD_{Ng\text{-}3aaNT}$ (lane 4), and $MinD_{Ng\text{-}4aaNT}$ (lane 7), in comparison to background levels of resident *E.coli* MinD (lanes 1 and 5). The expression of $MinD_{Ng\text{-}19aaNT}$ could not be detected in *E. coli*, and only background $MinD_{Ec}$ was observed by Western blotting (lane 8). Overall, these studies suggested that removal of only 3 amino acids from the N-terminus of $MinD_{Ng}$ will affect its ability to induce total cell division arrest.

Amino acid substitutions were also made to alter the charge and/or side chain bulkiness of selected N-terminal residues. These mutations included K3E, K3I, K3A, K3F, I4Q, I5A and I5E. Expression of most $MinD_{Ng}$ N-terminal point mutants, including $MinD_{Ng\text{-}K3E}$, $MinD_{Ng\text{-}K3I}$, $MinD_{Ng\text{-}K3A}$, $MinD_{Ng\text{-}K3F}$, and $MinD_{Ng\text{-}I4Q}$, also produced filamentous *E. coli* (Figure 7.3 C-G), similar to cells expressing wild-type $MinD_{Ng}$ (Figure 7.3 B). In contrast, expression of $MinD_{Ng\text{-}I5E}$ or $MinD_{Ng\text{-}I5A}$ did not lead to *E. coli* filamentation, but produced a minicell phenotype instead (Figure 7.3 H, I; arrows show minicells). The levels of each $MinD_{Ng}$ point mutant in *E. coli* PB103 were similar or slightly greater than wild-type $MinD_{Ng}$ (Fig. 2I), as determined by Western blotting. In addition, DAPI staining confirmed the absence of DNA in minicells of *E. coli* expressing $MinD_{Ng\text{-}3aaNT}$ (Figure 7.4 A), $MinD_{Ng\text{-}I5E}$ (Figure 7.4 B), and $MinD_{Ng\text{-}I5A}$ (Figure 7.4 C).

N-terminal deletions and point mutations to $MinD_{Ng}$ affect protein-protein interactions. Since interactions between the Min proteins are important for proper functioning of the Min system (Huang *et al.*, 1996; Hu and Lutkenhaus, 2003; Lackner *et al.*, 2003; Chapters 4, 5 and 6, this study), yeast

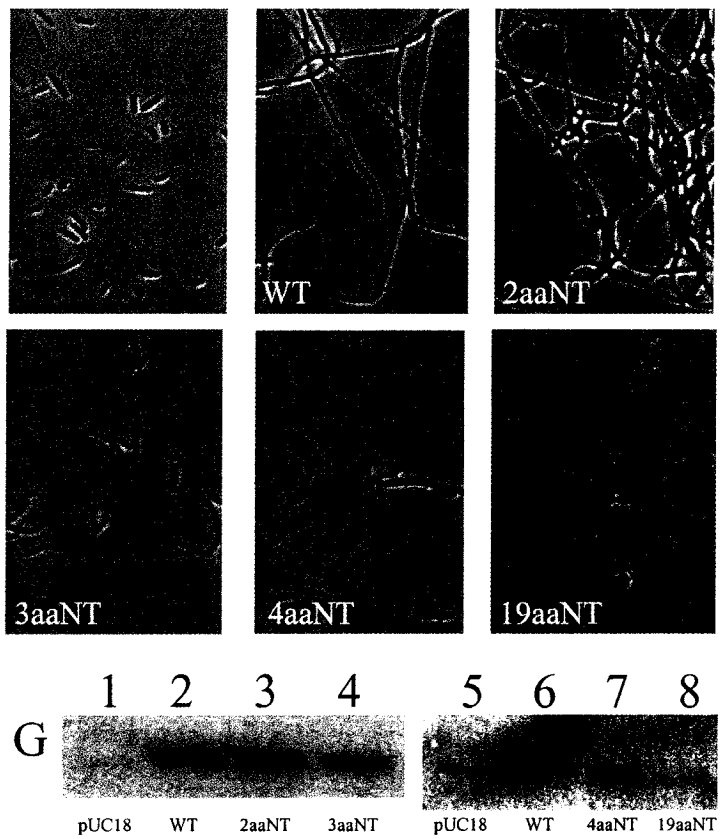

Figure 7.2. Expression of wild-type and N-terminal deletion derivatives of $MinD_{Ng}$ in wild-type *E. coli* PB103. (A) *E. coli* PB103 transformed with pUC18 exhibit a typical short rod morphology, while (B) cells transformed with pSR3 ($minD_{Ng}$) display a filamentous phenotype. (C) pSIA10 ($minD_{Ng\text{-}2aaNT}$) transformants also display filamentation. D) pSIA11 ($minD_{Ng\text{-}3aaNT}$) transformants exhibit a minicell morphology, as do (E) cells containing pJS4B ($minD_{Ng\text{-}4aaNT}$). (F) pJS5B ($minD_{Ng\text{-}19aaNT}$) transformants have a short rod morphologies. Scale bar in (A) represents 5 μm and all figures are at the same magnification. Arrows indicate minicells. (G) Western blotting using anti-$MinD_{Ng}$ antisera to probe *E. coli* cell extracts transformed with: lanes 1 and 5, pUC18; lanes 2 and 6, pSR3 ($minD_{Ng}$); lane 3, pSIA10 ($minD_{Ng\text{-}2aaNT}$); lane 4, pSIA11 ($minD_{Ng\text{-}3aaNT}$); lane 7 pJS4B ($minD_{Ng\text{-}4aaNT}$); and lane 8, pJS5B ($minD_{Ng\text{-}19aaNT}$). The antiserum also detects background expression of native *E. coli* MinD in strain PB103 (lane 1). Each panel in (G) was a separate Western blot experiment, with equalized loading concentrations in their respective wells.

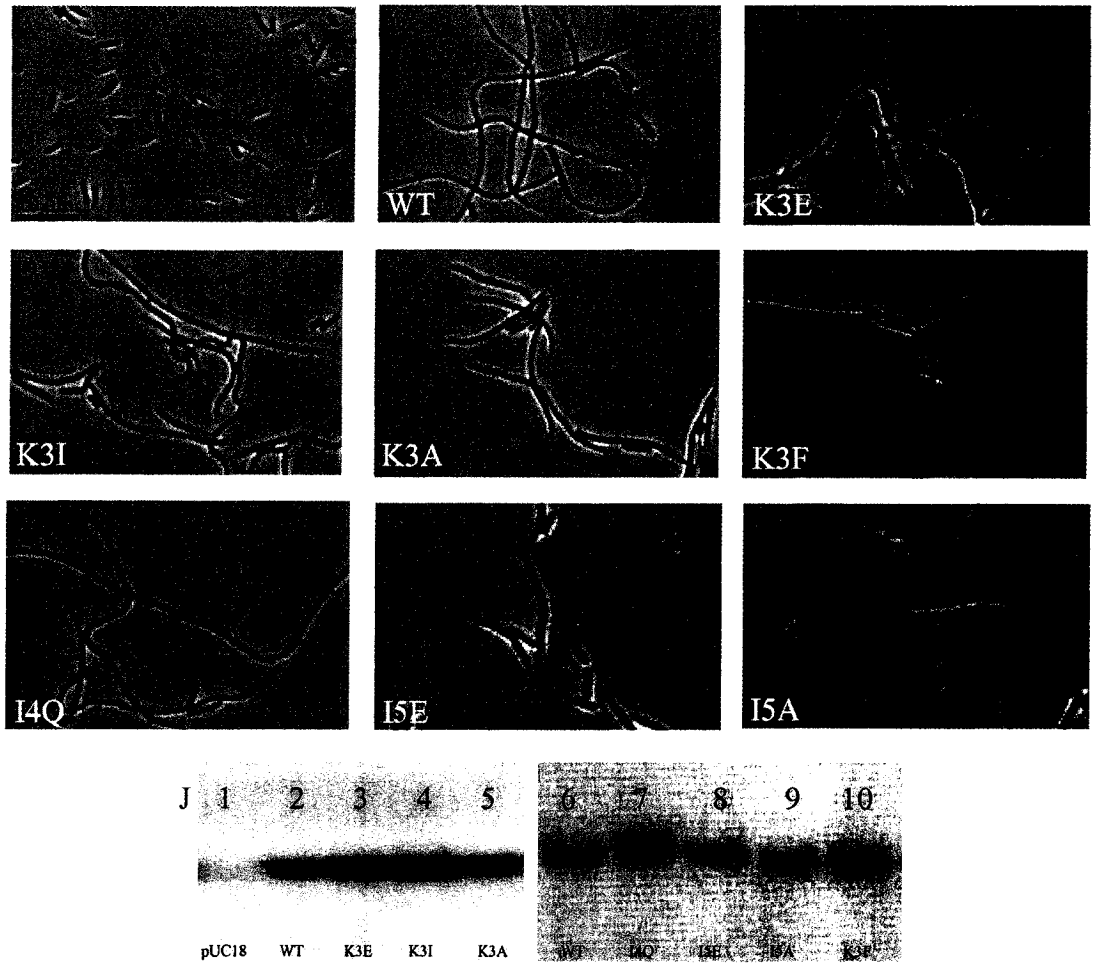

Figure 7.3. Expression of wild-type $MinD_{Ng}$ and N-terminal $MinD_{Ng}$ mutants in wild-type *E. coli* PB103. (A) Cells transformed with pUC18 negative control have a normal short rod morphology. (B) pSR3 ($minD_{Ng}$) transformants display a filamentous phenotype. Cells transformed with (C) pSIA13 ($minD_{Ng\text{-}K3E}$), (D) pSIA22 ($minD_{Ng\text{-}K3I}$), (E) pSIA23 ($minD_{Ng\text{-}K3A}$), (F) pJS16 ($minD_{Ng\text{-}K3F}$) or (G) pSIA24 ($minD_{Ng\text{-}I4Q}$) all exhibited filamentation. Cells transformed with (H) pJS13 ($minD_{Ng\text{-}I5E}$) or (I) pJS14 ($minD_{Ng\text{-}I5A}$) displayed minicell phenotypes. Scale bar in (A) represents 10 μm and all figures are at the same magnification. (J) Western blotting using anti-$MinD_{Ng}$ antisera confirms expression of each $MinD_{Ng}$ protein in *E. coli*: lane 1, negative control pUC18 transformants; lane 2, wild-type $MinD_{Ng}$; lane 3, $MinD_{Ng\text{-}K3E}$; lane 4, $MinD_{Ng\text{-}K3I}$; lane 5, $MinD_{Ng\text{-}K3A}$; lane 6, wild-type $MinD_{Ng}$; lane 7, $MinD_{Ng\text{-}I4Q}$; lane 8, $MinD_{Ng\text{-}I5E}$; lane 9, $MinD_{Ng\text{-}I5A}$; and lane 10, $MinD_{Ng\text{-}K3F}$. Each panel in (J) was a separate Western blot experiment.

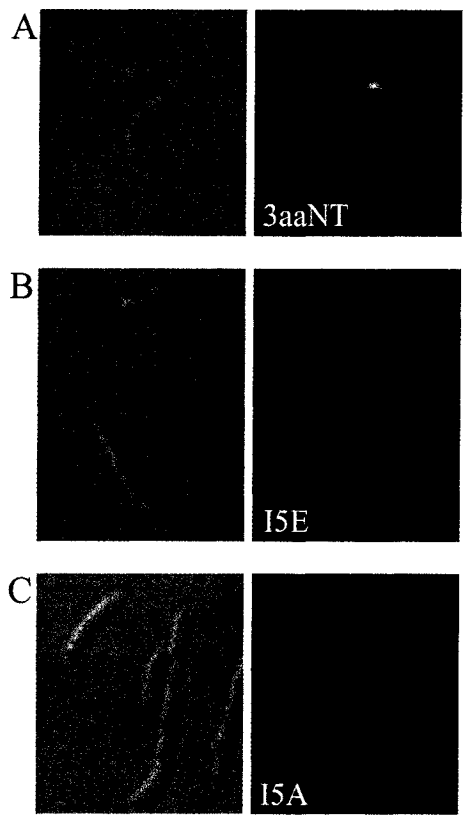

Figure 7.4. DAPI staining verifies absence of DNA in minicells resulting from expression of N-terminal $MinD_{Ng}$ truncation and mutation derivatives in wild-type *E. coli* PB103. In all cases, the left panel represents DIC image, while the right panel shows the corresponding DAPI fluorescence image. Black arrows indicate minicells. Note these minicells are devoid of DNA in all cases.(A) *E. coli* PB103 transformed with pSIA11 ($minD_{Ng\text{-}3aaNT}$). (B) *E. coli* transformed with pJS13 ($minD_{Ng\text{-}I5E}$). (C) *E. coli* transformed with pJS14 ($minD_{Ng\text{-}I5A}$).

two-hybrid assays were employed to determine how mutations to the N-terminus of $MinD_{Ng}$ may affect interactions with other Min proteins. Since interactions between wild-type $MinD_{Ng}$ and $MinE_{Ng}$ or $MinC_{Ec}$ are easily detected when the latter two proteins are fused to the GAL4-BD (Chapter 5), each N-terminal $MinD_{Ng}$ truncation was tested for interaction with other Min proteins fused to this particular GAL4 domain. As in Chapters 5 and 6, *E. coli* $MinC_{Ec}$ was used in these studies since it could interact well with wild-type $MinD_{Ng}$.

Removal of the first four residues of $MinD_{Ng}$ drastically reduced the strength of $MinD_{Ng\text{-}4aaNT}$ interaction with $MinC_{Ec}$, based on β-galactosidase activities (3.18 ± 0.16 Miller units for the mutant and 141.07 ± 4.43 units for wild-type (Table 7.2). $MinD_{Ng\text{-}4aaNT}$ lost interaction with itself and with $MinE_{Ng}$; however, it still maintained weak interaction with wild-type $MinD_{Ng}$ (Table 7.2). More drastic deletions from the N-terminus of $MinD_{Ng}$, including $MinD_{Ng\text{-}19aaNT}$, $MinD_{Ng\text{-}31aaNT}$ and $MinD_{Ng\text{-}183aaNT}$ derivatives, resulted in lost interaction with $MinC_{Ec}$, $MinE_{Ng}$, and $MinD_{Ng}$ (Table 7.2). Similar to wild-type $MinD_{Ng}$ (Szeto *et al.*, 2001), $MinD_{Ng\text{-}2aaNT}$ could interact with itself and with wild-type $MinD_{Ng}$ (Table 7.2). Furthermore, $MinD_{Ng\text{-}2aaNT}$ retained strong interaction with $MinE_{Ng}$, and $MinC_{Ec}$, relative to the respective wild-type control interactions (Table 7.2). In contrast, yeast two-hybrid assays showed that $MinD_{Ng\text{-}3aaNT}$ did not interact with itself, and had severely diminished interactions with wild-type $MinD_{Ng}$ and $MinE_{Ng}$ (Table 7.2). However, $MinD_{Ng\text{-}3aaNT}$ retained interaction with $MinC_{Ec}$ to produce dark blue yeast colonies, but this interaction was weaker (57.45 ± 9.64 Miller units) relative to wild-type control (141.07 ± 4.43 Miller units), based on β-galactosidase activity (Table 7.2). Since $MinD_{Ng\text{-}3aaNT}$ had disrupted interaction with itself and with $MinE_{Ng}$, but retained interaction with $MinC_{Ec}$, this suggests that the truncated protein is likely to be folded correctly, and can be stably expressed in the yeast reporter strain.

Hence, in support of its preserved functionality, $MinD_{Ng\text{-}2aaNT}$ interacted with all other Min proteins as did wild-type $MinD_{Ng}$. However, removal of only the first three residues of the $MinD_{Ng}$

Table 7.2. Yeast two-hybrid assays to determine Min protein interactions with N-terminal deletion derivatives of $MinD_{Ng}$

Fusion to GAL4- AD[1]	Fusion to GAL4-DNA-BD[2]	Intensity of blue colony colour[3]	β-galactosidase Activity (Miller Units)[4]
$MinD_{Ng}$[5]	$MinD_{Ng}$	+++	23.14 ± 7.33
$MinD_{Ng}$	$MinE_{Ng}$	++	8.70 ± 0.05
$MinD_{Ng}$	$MinC_{Ec}$[6]	++++	141.07 ± 4.43
$MinD_{Ng\text{-}2aaNT}$[7]	$MinD_{Ng\text{-}2aaNT}$	+++	11.93 ± 0.75
$MinD_{Ng\text{-}2aaNT}$	$MinD_{Ng}$	+++	16.59 ± 0.96
$MinD_{Ng\text{-}2aaNT}$	$MinE_{Ng}$	++	6.41 ± 0.52
$MinD_{Ng\text{-}2aaNT}$	$MinC_{Ec}$	++++	299.59 ± 22.92
$MinD_{Ng\text{-}3aaNT}$	$MinD_{Ng\text{-}3aaNT}$	-	0.02 ± 0.01
$MinD_{Ng\text{-}3aaNT}$	$MinD_{Ng}$	+	0.55 ± 0.14
$MinD_{Ng\text{-}3aaNT}$	$MinE_{Ng}$	+	0.16 ± 0.02
$MinD_{Ng\text{-}3aaNT}$	$MinC_{Ec}$	+++	57.45 ± 9.64
$MinD_{Ng\text{-}4aaNT}$	$MinD_{Ng\text{-}4aaNT}$	-	0.033 ± 0.002
$MinD_{Ng\text{-}4aaNT}$	$MinD_{Ng}$	+	1.93 ± 0.15
$MinD_{Ng\text{-}4aaNT}$	$MinE_{Ng}$	-	0.02 ± 0.01
$MinD_{Ng\text{-}4aaNT}$	$MinC_{Ec}$	+	3.18 ± 0.16
$MinD_{Ng\text{-}19aaNT}$	$MinD_{Ng\text{-}19aaNT}$	-	0.033 ± 0.002
$MinD_{Ng\text{-}19aaNT}$	$MinD_{Ng}$	-	0.04 ± 0.01
$MinD_{Ng\text{-}19aaNT}$	$MinE_{Ng}$	-	0.01 ± 0.01
$MinD_{Ng\text{-}19aaNT}$	$MinC_{Ec}$	-	0.03 ± 0.01
$MinD_{Ng\text{-}31aaNT}$	$MinD_{Ng}$	-	ND
$MinD_{Ng\text{-}31aaNT}$	$MinE_{Ng}$	-	ND
$MinD_{Ng\text{-}31aaNT}$	$MinC_{Ec}$	-	ND[8]
$MinD_{Ng\text{-}183aaNT}$	$MinD_{Ng}$	-	ND
$MinD_{Ng\text{-}183aaNT}$	$MinE_{Ng}$	-	ND
$MinD_{Ng\text{-}183aaNT}$	$MinC_{Ec}$	-	ND

[1] GAL4-activation domain

[2] GAL4-DNA binding domain

[3] Yeast colony colour intensity indicating strength of interaction, ranging from dark blue (++++) to faint blue (+); (-) = white colonies

[4] One unit equals the amount of β-galactosidase which hydrolyzes 1 μmol of ONPG per minute per cell

[5] *N. gonorrhoeae* MinD

[6] *E. coli* MinC

[7] NT denotes N-terminal truncation [e.g. 2aaNT = deletion of first 2 amino acids (codons) from N-terminus]. In place of the removed codons is a start codon.

was sufficient to disrupt or reduce interaction with all other Min proteins, particularly with itself and $MinE_{Ng}$.

$MinD_{Ng}$ bearing N-terminal point mutations were also examined for Min protein interactions. Each of the $MinD_{Ng}$ mutants, with the exception of $MinD_{Ng\text{-}I5E}$ and possibly $MinD_{Ng\text{-}K3A}$, retained the ability to self-associate as determined by the appearance of blue yeast colonies (Table 7.3). Overall, the strengths of mutant $MinD_{Ng}$ self-interaction, as assessed by β-galactosidase activities, were less than that of wild-type $MinD_{Ng}$ (8.75 ± 0.29 Miller units) (Table 7.3). In addition, all the proteins that retained self-interaction could interact with wild-type $MinD_{Ng}$ (Table 7.3).

Most of the $MinD_{Ng}$ point mutants had noticeably less interaction with $MinE_{Ng}$, as indicated by faint blue and/or white yeast colonies (Table 7.3). This was confirmed by β-galactosidase assays showing all mutants, with the exception of $MinD_{Ng\text{-}K3E}$ and $MiinD_{Ng\text{-}I4Q}$, had clearly diminished interaction with $MinE_{Ng}$ (Table 7.3).

In general, almost all $MinD_{Ng}$ mutants retained interaction with $MinC_{Ec}$, to produce dark blue colonies when assayed with the yeast two-hybrid system (Table 7.3). Only the $MinD_{Ng\text{-}I5E}$–$MinC_{Ec}$ interaction produced faint blue colonies (Table 7.3). β-galactosidase assays showed that, with the exception of $MinD_{Ng\text{-}K3E}$, the interaction between each N-terminal $MinD_{Ng}$ mutant and $MinC_{Ec}$ was markedly decreased compared to the wild-type $MinD_{Ng}$-$MinC_{Ec}$ interaction. However, it is noted that, although mutations at the third or fourth residues of $MinD_{Ng}$ diminished $MinD_{Ng}$-$MinC_{Ec}$ interactions, it is apparent that these mutant proteins (K3E, K3I, K3A, and I4Q mutants) could still recruit sufficient $MinC_{Ec}$ to the *E. coli* membrane to arrest cell division in wild-type *E. coli* (Figure 7.3 C, D, E, and G).

It is also noted that all but one ($MinD_{Ng\text{-}I5E}$) of the six $MinD_{Ng}$ N-terminal mutants retained interaction with at least one of $MinC_{Ec}$, wild-type $MinD_{Ng}$, $MinE_{Ng}$, or with itself. This indicates that these $MinD_{Ng}$ mutants were likely folded properly, without gross structural perturbations. $MinD_{Ng\text{-}I5E}$ did not have detectable interactions with most of the other Min proteins, Ideally, Western blotting

Table 7.3. Yeast two-hybrid assays of the interactions between Min proteins and N-terminal mutation derivatives of $MinD_{Ng}$

Fusion to GAL4-DNA-AD[1]	Fusion to GAL4-BD[2]	Intensity of blue colony colour[3]	β-galactosidase Activity (Miller Units)[4]
$MinD_{Ng}$[5]	$MinD_{Ng}$	+++	8.75 ± 0.29
$MinD_{Ng}$	$MinE_{Ng}$	++	2.83 ± 0.41
$MinD_{Ng}$	$MinC_{Ec}$[6]	++++	215.53 ± 141.50
$MinD_{Ng\text{-}K3E}$	$MinD_{Ng\text{-}K3E}$	+++	6.22 ± 0.03
$MinD_{Ng\text{-}K3E}$	$MinD_{Ng}$	++	2.00 ± 0.05
$MinD_{Ng\text{-}K3E}$	$MinE_{Ng}$	++	2.96 ± 0.13
$MinD_{Ng\text{-}K3E}$	$MinC_{Ec}$	++++	282.34 ± 10.38
$MinD_{Ng\text{-}K3I}$	$MinD_{Ng\text{-}K3I}$	++	2.38 ± 0.01
$MinD_{Ng\text{-}K3I}$	$MinD_{Ng}$	++	1.30 ± 0.01
$MinD_{Ng\text{-}K3I}$	$MinE_{Ng}$	+	0.31 ± 0.11
$MinD_{Ng\text{-}K3I}$	$MinC_{Ec}$	++++	63.23 ± 4.79
$MinD_{Ng\text{-}K3A}$	$MinD_{Ng\text{-}K3A}$	+/-	0.21 ± 0.01
$MinD_{Ng\text{-}K3A}$	$MinD_{Ng}$	++	5.62 ± 0.59
$MinD_{Ng\text{-}K3A}$	$MinE_{Ng}$	+	0.56 ± 0.01
$MinD_{Ng\text{-}K3A}$	$MinC_{Ec}$	+++	47.20 ± 3.69
$MinD_{Ng\text{-}I4Q}$	$MinD_{Ng\text{-}I4Q}$	++	3.53 ± 0.01
$MinD_{Ng\text{-}I4Q}$	$MinD_{Ng}$	++	10.88 ± 0.56
$MinD_{Ng\text{-}I4Q}$	$MinE_{Ng}$	++	2.43 ± 0.30
$MinD_{Ng\text{-}I4Q}$	$MinC_{Ec}$	++++	63.07 ± 6.67
$MinD_{Ng\text{-}I5E}$	$MinD_{Ng\text{-}I5E}$	-	0.25 ± 0.01
$MinD_{Ng\text{-}I5E}$	$MinD_{Ng}$	-	0.21 ± 0.01
$MinD_{Ng\text{-}I5E}$	$MinE_{Ng}$	-	0.11 ± 0.01
$MinD_{Ng\text{-}I5E}$	$MinC_{Ec}$	+	0.38 ± 0.01
$MinD_{Ng\text{-}I5A}$	$MinD_{Ng\text{-}I5A}$	++	3.87 ± 0.13
$MinD_{Ng\text{-}I5A}$	$MinD_{Ng}$	++	1.47 ± 0.42
$MinD_{Ng\text{-}I5A}$	$MinE_{Ng}$	+	1.23 ± 0.38
$MinD_{Ng\text{-}I5A}$	$MinC_{Ec}$	+++	50.09 ± 1.25

[1] GAL4-activation domain

[2] GAL4-DNA binding domain

[3] Yeast colony colour intensity indicating strength of interaction, ranging from dark blue (++++) to faint blue (+); (-) = white colonies; (+/-) = indicates a combination of faint blue and white colonies

[4] One unit equals the amount of β-galactosidase which hydrolyzes 1 μmol of ONPG per minute per cell

[5] *N. gonorrhoeae* MinD

[6] *E. coli* MinC

should be used to detect whether GAL4- $MinD_{Ng\text{-}I5E}$ fusions are expressed in the yeast; however, it is recognized that the yeast two-hybrid system used in this study has inherently low expression levels of GAL-4 fusion genes (Clontech). Furthermore, the Dillon laboratory has not been able to detect GAL4-fusions in the yeast reporter strain SFY526 (Ramirez-Arcos *et al.*, in press). However, since $MinD_{Ng\text{-}I5E}$ did have a weak interaction with $MinC_{Ec}$, it suggests that the mutant $MinD_{Ng}$ was still expressed stably to some degree in the yeast reporter strain. Overall, these results suggest residues at the extreme N-terminus of $MinD_{Ng}$ are involved in $MinD_{Ng}$ interaction with all other Min proteins.

Deletion of $MinD_{Ng}$ N-terminal residues affects dynamic localization of GFP-$MinD_{Ng}$ fusions. GFP-fusions to N-terminal deletion derivatives of $MinD_{Ng}$ were constructed to determine whether this region of $MinD_{Ng}$ is implicated in dynamic localization of the protein. Initial studies of GFP-$MinD_{Ng\text{-}4aaNT}$ and GFP-$MinD_{Ng\text{-}19aaNT}$ were conducted in *E. coli* WM1032 ($\Delta minCDE_{Ec}$) (Table 2.1), in collaboration with Dr. W. Margolin, University of Texas Medical School. GFP-$MinD_{Ng\text{-}K16Q}$ was used as a negative control. In all cases, the $minE_{Ng}$ gene was also provided immediately downstream of each plasmid-encoded mutant *gfp-*$minD_{Ng}$ gene to stimulate fusion protein movement.

E. coli WM1032 transformed with pJDE2 (GFP-$MinD_{Ng\text{-}4aaNT}$) and pJDE3 (GFP-$MinD_{Ng\text{-}19aaNT}$) (Figure 7.5 A, B) did not display any discernible intracellular fusion protein movement seen with wild-type GFP-$MinD_{Ng}$ (See Figure 4.5 A), and presented cytosolic fusion protein localization instead. This localization was similar to that observed with the negative control GFP-$MinD_{Ng\text{-}K16Q}$ (Figure 7.5 C).

Western blotting indicated the expression of GFP-$MinD_{Ng\text{-}K16Q}$ was similar to that of wild-type GFP-$MinD_{Ng}$ (Figure 7.5 D, lanes 1 and 2). GFP-$MinD_{Ng\text{-}4aaNT}$ and GFP-$MinD_{Ng\text{-}19aaNT}$ levels were slightly less, at 86% and 70% of the wild-type fusion protein level, respectively (Figure 7.5 D, lanes 3 and 4). Furthermore, immunoblotting showed that the levels of $MinE_{Ng}$ in all transformants were similar (Figure 7.5 E). These localization results suggested that deletion of only the first four N-

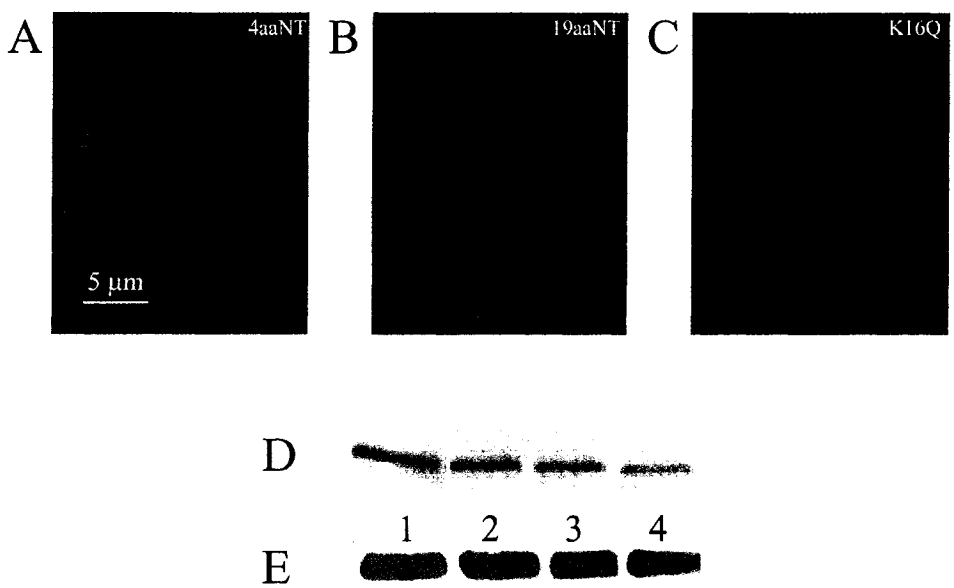

Figure 7.5. Localization of GFP-fusions to N-terminal $MinD_{Ng}$ deletion derivatives in *E. coli* WM1032. Examination of cells expressing (A) GFP-$MinD_{Ng\text{-}4aaNT}$, (B) GFP-$MinD_{Ng\text{-}19aaNT}$, and (C) GFP-$MinD_{Ng\text{-}K16Q}$. In all cases, no evidence of intracellular fusion protein movement is seen and fluorescent signal appears distributed throughout the cytoplasm. Bar in (A) indicates 5 μm and all images are at the same magnification. (D and E) Western blotting verifies expression of GFP-$MinD_{Ng}$ and $MinE_{Ng}$ in *E. coli* WM1032 ($\Delta minCDE_{Ec}$). (D) Anti-$MinD_{Ng}$ antisera detects wild-type GFP-$MinD_{Ng}$ (lane 1), GFP-$MinD_{Ng\text{-}K16Q}$ (lane 2), GFP-$MinD_{Ng\text{-}4aaNT}$ (lane 3), and GFP-$MinD_{Ng\text{-}19aaNT}$ (lane 4) in *E. coli* WM1032 cells transformed with pSR15 (*gfp-*$minD_{Ng}$, $minE_{Ng}$), pJDE1 (*gfp-*$minD_{Ng\text{-}K16Q}$, $minE_{Ng}$), pJDE2 (*gfp-*$minD_{Ng\text{-}4aaNT}$, $minE_{Ng}$), and pJDE3 (*gfp-*$minD_{Ng\text{-}19aaNT}$, $minE_{Ng}$), respectively. (E) Anti-$MinE_{Ng}$ antisera detects $MinE_{Ng}$ in cell extracts of *E. coli* WM1032 transformed with pSR15 (lane 1), pJDE1 (lane 2), pJDE2 (lane 3), and pJDE3 (lane 4).

terminal amino acid residues of $MinD_{Ng}$ is sufficient to disrupt the intracellular movement and membrane association of GFP-$MinD_{Ng}$.

More sophisticated localization studies were conducted with GFP-$MinD_{Ng\text{-}2aaNT}$ and GFP-$MinD_{Ng\text{-}3aaNT}$ fusions using an advanced microscope system acquired by our laboratory. These experiments were conducted in *E. coli* PB114, which also lacks its native *minCDE* gene cluster, similar to *E. coli* WM1032 (Table 2.1). $MinE_{Ng}$ was encoded on the same plasmid as each GFP-$MinD_{Ng}$ fusion to induce *in vivo* movement.

Positive control cells expressing wild-type GFP-$MinD_{Ng}$ displayed dynamic intracellular fusion protein movement (Figure 7.6 A). Wild-type GFP-$MinD_{Ng}$ oscillation required an average of 33.2 ± 5.8 seconds (Table 7.4). GFP-$MinD_{Ng\text{-}2aaNT}$ displayed similar pole-to-pole movement as wild-type GFP-$MinD_{Ng}$ (Figure 7.6 C), with an average oscillation cycle of 32.5 ± 5.2 seconds that was not significantly different from the positive control (Table 7.4).

At first glance, GFP-$MinD_{Ng\text{-}3aaNT}$ did not appear to move in *E. coli* PB114 cells, with much of the fluorescent signal distributed throughout the cytoplasm. However, closer inspection revealed faint oscillatory signals shifting from one end of the cell to the other (Figure 7.6 E, arrows), amidst the increased cytosolic fluorescence relative to wild-type GFP-$MinD_{Ng}$ and GFP-$MinD_{Ng\text{-}2aaNT}$. The increased tendency to remain distributed in the cytoplasm made visualizing clear pole-to-pole movement of GFP-$MinD_{Ng\text{-}3aaNT}$ more difficult (Figure 7.6 E). Interestingly, the average oscillation time of this GFP-$MinD_{Ng\text{-}3aaNT}$ (19.8 ± 3.8 seconds) was significantly faster than GFP fusions to both wild-type and $MinD_{Ng\text{-}2aaNT}$ ($p<0.001$) (Table 7.4).

E. coli GFP-MinD has been shown to localize in a MinE-dependent manner within a membrane-associated coiled array (Shih *et al.*, 2003). GFP-$MinD_{Ng}$ localizes similarly in a $MinE_{Ng}$-dependent manner within an *E. coli* background (Chapter 4, Chapter 6). As with wild-type GFP-$MinD_{Ng}$ (Figure 7.6 B), GFP-$MinD_{Ng\text{-}2aaNT}$ was localized in what appeared to be a coiled array (Figure 7.6 D), with increased fluorescence within specific segments of the array that contributed to the

Figure 7.6. Localization of wild-type and N-terminal deletion derivatives of $MinD_{Ng}$ in *E. coli* PB114. Oscillation cycles (from one pole to the other, and back) of GFP-$MinD_{Ng}$ fusions were measured in *E. coli* rods. (A) Distinct pole-to-pole movement of wild-type GFP-$MinD_{Ng}$ in *E. coli*. Leftmost panel shows DIC image. Remaining panels show GFP-$MinD_{Ng}$ localization. One cycle of fusion protein movement required 30 seconds in this cell. Note the U-shaped fluorescent signal of the fusion protein alternately lining each cell pole region (arrows). Scale bar in (A) indicates 5 μm and all other images are at similar magnification. (B) GFP-$MinD_{Ng}$ localizes in longer *E. coli* cells as regularly spaced bands. Each band contains fusion protein arranged within a coil (arrows). (C) GFP-$MinD_{Ng\text{-}2aaNT}$ undergoes pole-to-pole oscillation. The time required for the fusion protein to complete one oscillatory cycle is 30 seconds (arrows). (D) GFP-$MinD_{Ng\text{-}2aaNT}$ can localize within segments of a coiled array (arrows). (E) GFP-$MinD_{Ng\text{-}3aaNT}$ can also undergo pole-to-pole oscillation (arrows), with one cycle requiring 15 seconds in the cell shown. Note that much of the fusion protein signal is found distributed throughout the cytosol. (F) Raw image of *E. coli* PB114 expressing GFP-$MinD_{Ng\text{-}3aaNT}$. Note the near uniform cytosolic localization of the protein. (F') Image enhancement of previous figure reveals presence of GFP-$MinD_{Ng\text{-}3aaNT}$ localizing within coil-like structure (arrows). (G) Western blot using anti-$MinD_{Ng}$ antisera to detect GFP-$MinD_{Ng}$ proteins in *E. coli* PB114: Lane 1, cell extract from untransformed *E. coli* PB114; lane 2, wild-type GFP-$MinD_{Ng}$ (pSR15); lane 3, GFP-$MinD_{Ng\text{-}2aaNT}$ (pSIA16); and lane 4, GFP-$MinD_{Ng\text{-}3aaNT}$ (pSIA17). (H) Western blot using anti-$MinE_{Ng}$ antisera to detect $MinE_{Ng}$ in *E. coli* PB114 transformed with: Lane 1, no plasmid; lane 2, pSR15; lane 3, pSIA16; and lane 4, pSIA17.

Table 7.4. Dynamic localization characteristics of GFP-fusions to $MinD_{Ng}$ N-terminal mutants

GFP-fusion	Dynamic movement[a]	Average oscillation cycle (seconds)	Ability to localize in coiled array[b]	Propensity to remain in cytoplasm[c]
Wild-type $MinD_{Ng}$	Yes	33.2 ± 5.8 (n=30)[d]	++++	+
$MinD_{Ng\text{-}2aaNT}$[e]	Yes	32.5 ± 5.2 (n=30)	++++	+
$MinD_{Ng\text{-}3aaNT}$	Yes	19.8 ± 3.8 (n=30)[f]	+	++++
$MinD_{Ng\text{-}K3E}$	Yes	25.8 ± 5.7 (n=30)[f]	++++	+
$MinD_{Ng\text{-}K3I}$	Yes	20.5 ± 3.9 (n=30)[f]	+++	++
$MinD_{Ng\text{-}I4Q}$	Yes	19.9 ± 3.1 (n=30)[f]	++	+++
$MinD_{Ng\text{-}I5A}$	Yes	ND[g]	+	++++
$MinD_{Ng\text{-}I5E}$	No	None	-	+++++
$MinD_{Ng\text{-}K16Q}$	No	None	-	+++++

[a] Dynamic movement of GFP-fusions in *E. coli* PB114 as determined by pole-to-pole oscillation in 2.0-2.5 μm long cells, or discernible fluorescent signal movement in longer cells.

[b] As determined by the ability of fusion protein to localize distinctly to intracellular coiled arrays, easily distinguishable from cytosolic fluorescent signals. All observations compared to wild-type $MinD_{Ng}$, set at (++++). An inability to localize within a coiled array is denoted by (-).

[c] In comparison to negative control GFP-$MinD_{Ng\text{-}K16Q}$, which remains wholly cytoplasmic and is set at (+++++) value. In contrast, wild-type GFP-$MinD_{Ng}$ is recruited to the membrane at cell poles and to a coiled array; hence its propensity to remain cytosolic is set at (+).

[d] n = number of cells observed to obtain average oscillation cycle

[e] NT denotes N-terminal truncation [e.g. 2aaNT = deletion of first 2 amino acids (codons) from N-terminus]. In place of the removed codons is a start codon.

[f] Average oscillation cycle calculated to be significantly faster than wild-type, as determined by the unpaired Student's *t*-test ($p<0.001$).

[g] ND, not determined. Due to excessive background fluorescent signal from GFP-$MinD_{Ng\text{-}I5A}$ localized throughout the cytoplasm, clearly distinguishable pole-to-pole oscillation could not be determined; however, oscillatory patterns were observed in longer cells in these samples.

dynamic 'zebra-stripe' banding patterns typical of GFP-MinD proteins in elongated *E. coli* cells (See Figure 4.6 E, F). As before (Chapters 4 and 6), GFP-$MinD_{Ng}$-decorated coiled arrays were easier to visualize in *E. coli* cells that were ≥ 5 μm in length.

Despite the increased cytosolic localization of GFP-$MinD_{Ng\text{-}3aaNT}$ (Figure 7.6 F), image enhancement revealed that a small proportion of fusion protein could also localize in what appeared to be segments of a helical array (Figure 7.6 F', arrows). Hence, despite a tendency to localize mainly in the cytosol, GFP-$MinD_{Ng\text{-}3aaNT}$ is still able to localize within a coil, likely permitting the faint oscillation patterns observed. As expected, the negative control GFP-$MinD_{Ng\text{-}K16Q}$ was distributed uniformly throughout the cytoplasm, without any evidence of localizing within a spiral array (see Figure 4.6 D).

Western blotting using anti-$MinD_{Ng}$ antisera (Figure 7.6 G) verified the overexpression of wild-type GFP-$MinD_{Ng}$ (lane 2), GFP-$MinD_{Ng\text{-}2aaNT}$ (lane 3) and GFP-$MinD_{Ng\text{-}3aaNT}$ (lane 4) in *E. coli* PB114 transformants, relative to untransformed cells (lane 1). Densitometric analysis indicated that GFP-$MinD_{Ng\text{-}2aaNT}$ and GFP-$MinD_{Ng\text{-}3aaNT}$ levels were at ~92% and ~86% of wild-type GFP-$MinD_{Ng}$, respectively. Western blotting detected similar levels of $MinE_{Ng}$ in all *E. coli* PB114 transformants used in these studies (Figure 7.6 H; lanes 2, 3, and 4), in comparison to the untransformed cell extract (lane 1).

These studies indicate that removal of the first three amino acids of $MinD_{Ng}$ affects the dynamic localization of the protein by producing a faster oscillation rate and an increased propensity to remain in the cytosol, in comparison to wild-type protein.

Mutation of $MinD_{Ng}$ N-terminal residues affects dynamic localization of GFP-$MinD_{Ng}$ fusions.

Similar to GFP-fusions to N-terminal deletion derivatives of $MinD_{Ng}$, localization of GFP-fusions to $MinD_{Ng}$ bearing K3E, K3I, I4Q, I5A, or I5E mutations was examined in *E. coli* PB114 (Table 2.1). From yeast two-hybrid assays, $MinD_{Ng\text{-}K3E}$ interacted with the other Min proteins in a

similar manner as wild-type $MinD_{Ng}$. As expected, GFP-$MinD_{Ng\text{-}K3E}$ displayed clear pole-to-pole movement in *E. coli* PB114 rods, characterized by its distinct localization along the inner cell periphery at either cell pole as the fusion oscillated (Figure 7.7 A), similar to wild-type GFP-$MinD_{Ng}$ (Figure 7.6 A). However, the average oscillation cycle of GFP-$MinD_{Ng\text{-}K3E}$ required only 25.8 ± 5.7 seconds, significantly faster than the wild-type control ($p<0.001$) (Table 7.4). Similar to wild-type GFP-$MinD_{Ng}$, GFP-$MinD_{Ng\text{-}K3E}$ also localized as a coiled array, with dynamic fluorescent bands resulting from fusion protein accumulation along evenly spaced segments of the coil (Figure 7.7 B, arrows).

GFP-$MinD_{Ng\text{-}K3I}$ also displayed pole-to-pole movement (Figure 7.7 C). However, like GFP-$MinD_{Ng\text{-}K3E}$, the fusion had a significantly faster oscillation cycle compared to the wild-type fusion, with an average oscillation cycle of only 20.5 ± 3.9 seconds ($p<0.001$) (Table 7.4). Furthermore, while it was clear that pole-to-pole oscillation was occuring, a slightly greater fraction of GFP-$MinD_{Ng\text{-}K3I}$ appeared to be distributed in the cytosol at any particular time (Figure 7.7 C, D), in comparison to wild-type GFP-$MinD_{Ng}$ (Figure 7.6 A, B) and to GFP-$MinD_{Ng\text{-}K3E}$ (Figure 7.7 A, B). This increased cytosolic fluorescence also made it difficult to visualize any intracellular GFP-$MinD_{Ng\text{-}K3I}$ within coiled arrays; however, fluorescent banding patterns within cells suggested the presence of this array (Figure 7.7 D). Image enhancement confirmed that GFP-$MinD_{Ng\text{-}K3I}$ could still localize within a membrane-associated coiled array (Figure 7.7 D'), despite an apparently increased propensity to remain cytosolic (Table 7.4).

The localization of GFP-$MinD_{Ng\text{-}I4Q}$ proved to be even more preferentially distributed in the cytosol than GFP-$MinD_{Ng\text{-}K3I}$. From fluorescent images, it was apparent that a significant portion of GFP-$MinD_{Ng\text{-}I4Q}$ did not localize to membrane sites at the cell poles, but remained distributed in the cytoplasm instead (Figure 7.7 E). While pole-to-pole movement of GFP-$MinD_{Ng\text{-}I4Q}$ could still be discerned (Figure 7.7 E), it required an average oscillation period of 19.9 ± 3.1 seconds, significantly faster the wild-type control ($p<0.001$) (Table 7.4). In addition, the average oscillation cycle of GFP-

Figure 7.7. Localization of N-terminal mutants of $MinD_{Ng}$ fused to GFP in *E. coli* PB114. (A) Distinct pole-to-pole movement of GFP-$MinD_{Ng\text{-}K3E}$ in *E. coli*. Here, the fusion protein required 25 seconds to complete one cycle of oscillation. Note the U-shaped fluorescent signal of the fusion protein alternately lining each cell pole region. Bar in (A) represents 5 μm and all figures are at the same magnification. (B) GFP-$MinD_{Ng\text{-}K3E}$ localizes in longer *E. coli* cells as regularly spaced bands. Each band consists of fusion protein arranged within a coiled segment (arrows). (C) GFP-$MinD_{Ng\text{-}K3I}$ also undergoes pole-to-pole oscillation (arrows); however, more of the fusion protein signal is also found distributed throughout the cytosol. The time required for the fusion protein to complete one oscillatory cycle in the cell shown is 20 seconds. (D) Raw image of *E. coli* PB114 expressing GFP-$MinD_{Ng\text{-}K3I}$. Note the increased cytosolic localization of GFP-$MinD_{Ng\text{-}K3I}$ relative to GFP-$MinD_{Ng\text{-}K3E}$ (B). (D') Image enhancement of (D) reveals GFP-$MinD_{Ng\text{-}K3I}$ localizing within segments of a coiled array (arrows). (E) GFP-$MinD_{Ng\text{-}I4Q}$ can move from pole-to-pole (arrows); however, much of the fusion protein is found distributed throughout the cytoplasm. The time required for GFP-$MinD_{Ng\text{-}I4Q}$ to complete one oscillatory cycle in the indicated cell is 15 seconds (arrows). (F) Raw image of elongated *E. coli* PB114 expressing GFP-$MinD_{Ng\text{-}I4Q}$. Note the near uniform cytosolic localization of the protein. (F') Image enhancement of previous image shows evidence of GFP-$MinD_{Ng\text{-}I4Q}$ still localizing along a coiled array (arrows). (G) GFP-$MinD_{Ng\text{-}I5A}$ is mostly localized to the cytosol. (G') Image enhancement of previous image shows GFP-$MinD_{Ng\text{-}I5A}$ retains the ability to localize as coils. (H) GFP-$MinD_{Ng\text{-}I5E}$ is uniformly distributed throughout the cytoplasm. I) Western blot using anti-$MinD_{Ng}$ antisera to detect GFP-$MinD_{Ng}$ fusions in *E. coli* PB114: Lane 1, wild-type GFP-$MinD_{Ng}$ (pSR15); lane 2, GFP-$MinD_{Ng\text{-}K3E}$ (pSIA18); lane 3, $MinD_{Ng\text{-}K3I}$ (pJS30); lane 4, GFP-$MinD_{Ng\text{-}I4Q}$ (pJS18); lane 5, GFP-$MinD_{Ng\text{-}I5E}$ (pJS29); lane 6, GFP-$MinD_{Ng\text{-}I5A}$ (pJS19); and lane 7, untransformed *E. coli* cell extract. (J) Western blotting using anti-$MinE_{Ng}$ antisera to detect $MinE_{Ng}$ in *E. coli* transformed with: Lane 1, no plasmid; lane 2, pSR15; lane 3, pSIA18; lane 4, pJS30; lane 5, pJS18; lane 6, pJS29; lane 7, pJS19.

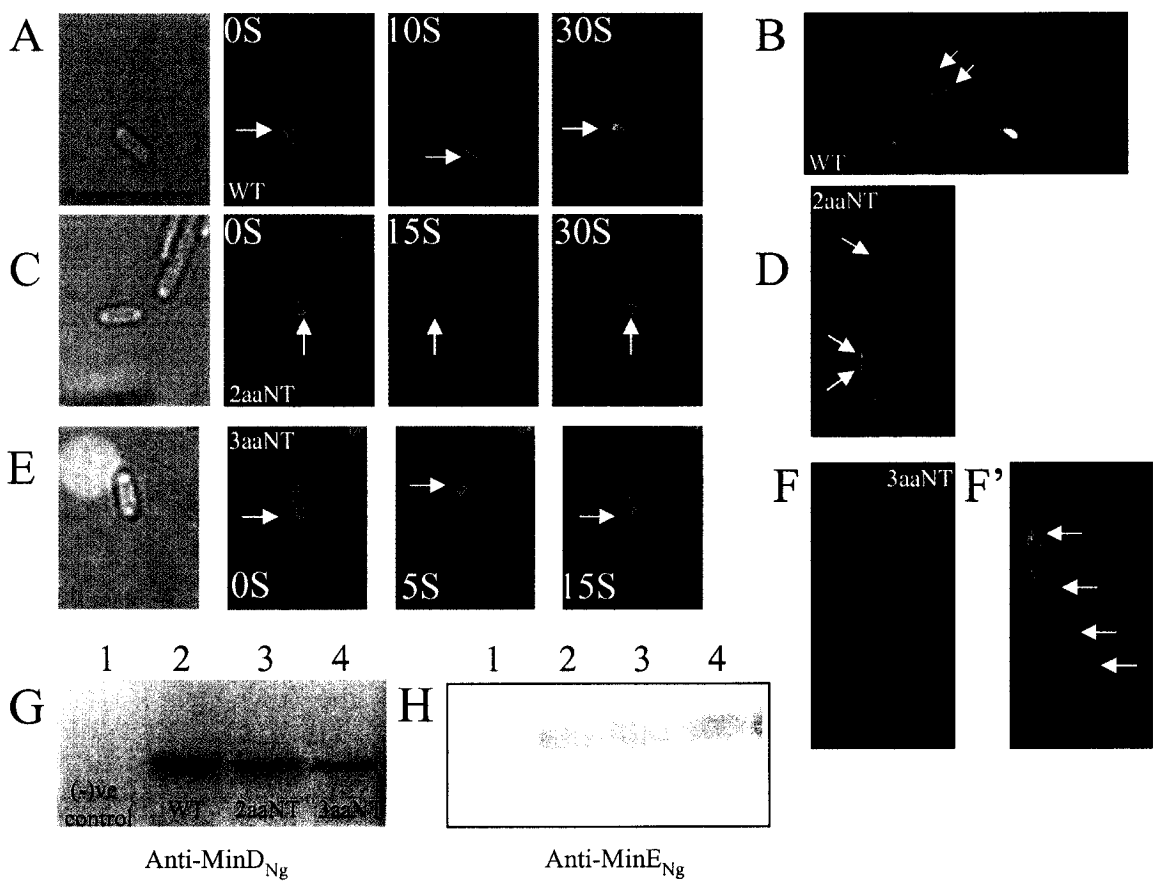
A
0S
10S
30S
WT
B
WT
C
0S
15S
30S
2aaNT
D
2aaNT
E
3aaNT
0S
5S
15S
F
3aaNT
F'
1 2 3 4
G
(-)ve control
WT
2aaNT
3aaNT
Anti-MinD$_{Ng}$
1 2 3 4
H
Anti-MinE$_{Ng}$

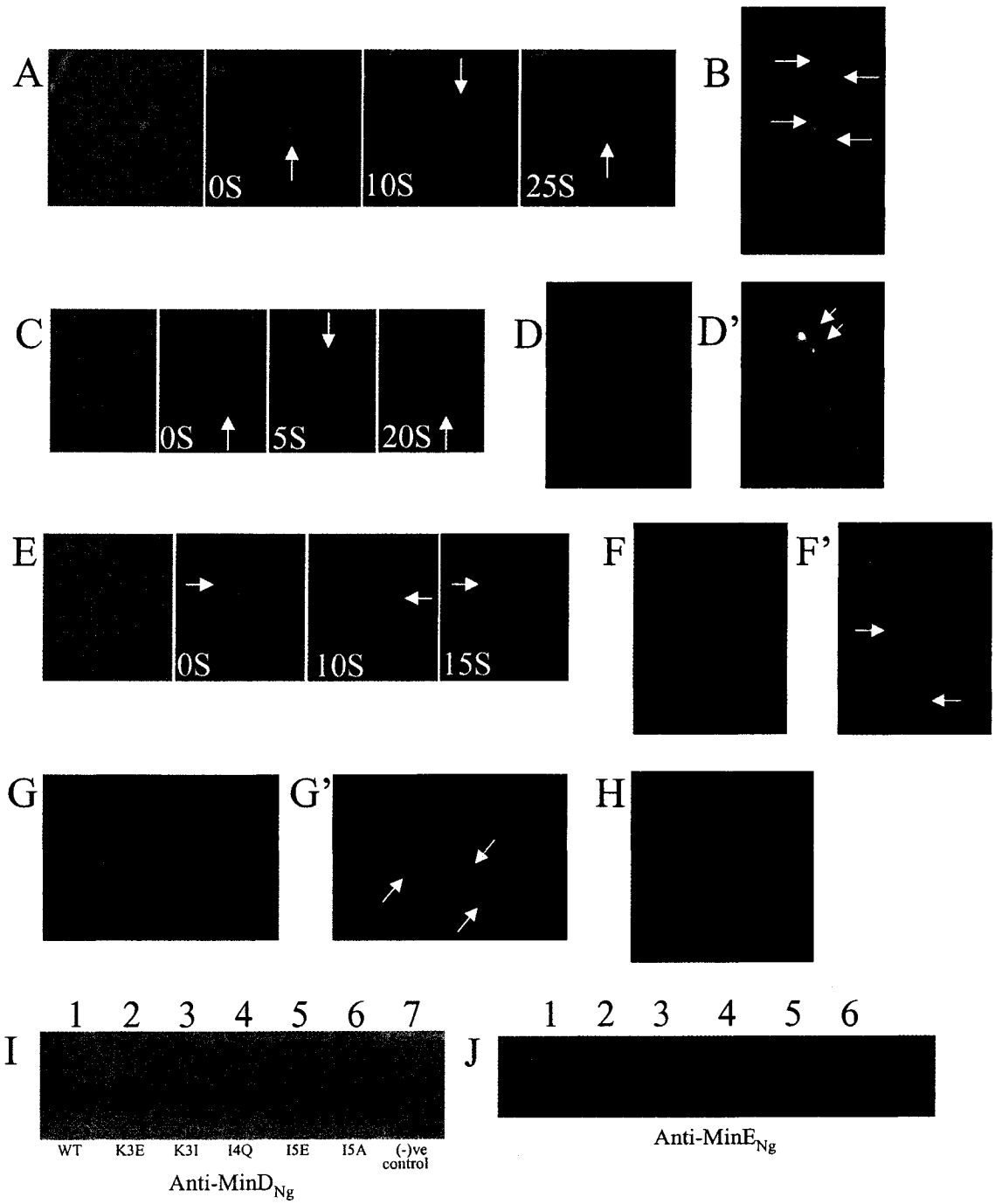
A
0S
10S
25S
B
C
0S
5S
20S
D
D'
E
0S
10S
15S
F
F'
G
G'
H
1 2 3 4 5 6 7
I
WT
K3E
K3I
I4Q
I5E
I5A
(-)ve control
Anti-MinD$_{Ng}$
1 2 3 4 5 6
J
Anti-MinE$_{Ng}$

$MinD_{Ng\text{-}I4Q}$ was significantly faster than that of GFP-$MinD_{Ng\text{-}K3E}$ ($p<0.001$), but not of GFP-$MinD_{Ng\text{-}K3I}$ (Table 7.4). Image enhancement revealed that GFP-$MinD_{Ng\text{-}I4Q}$ could also localize within a helical array (Figure 7.7 F and F'; arrows), despite its increased distribution in the cytosol.

GFP-$MinD_{Ng\text{-}I5A}$ tended to remain almost entirely in the cytoplasm. While faint evidence of dynamic fusion protein movement in bands could be discerned in longer filamentous *E. coli* PB114 cells (Table 7.4), it was not possible to clearly measure pole-to-pole movement in *E. coli* rods due to the increased cytosolic fluorescent signal. However, evidence of GFP-$MinD_{Ng\text{-}I5A}$ localizing as a coiled array (Figure 7.7 G') was obtained from enhancement of raw images of filamentous cells (Figure 7.7 G). The final mutant, GFP-$MinD_{Ng\text{-}I5E}$, appeared to be wholly distributed in the cytosol, presenting uniform fluorescence throughout the cell with no evidence of dynamic movement or helical array formation (Figure 7.7 H) (Table 7.4).

Western blotting confirmed that similar levels of GFP-$MinD_{Ng}$ fusions were found in each *E. coli* PB114 transformant used in these studies (Figure 7.7 I). In addition, immunoblotting showed similar levels of $MinE_{Ng}$ expressed from each plasmid used in the localization studies (Figure 7.7 J).

Hence, as residues from the third to the fifth position of $MinD_{Ng}$ are sequentially targeted for mutation, there is a decrease in the time required for GFP-$MinD_{Ng}$ to oscillate from pole-to-pole in *E. coli*. As a result, oscillation periods were as follows: wild-type GFP-$MinD_{Ng}$ > GFP-$MinD_{Ng\text{-}K3E}$ > GFP-$MinD_{Ng\text{-}K3I}$ = GFP-$MinD_{Ng\text{-}I4Q}$. Interestingly, this is accompanied by an increased tendency of each succesive GFP-$MinD_{Ng}$ mutant to remain in the cytosol, such that I5A and I5E mutations conferred near-complete and complete tendencies to localize in the cytoplasm, respectively.

N-terminal mutation derivatives of $MinD_{Ng}$ exhibit increased basal ATPase activity that is not affected by $MinE_{Ng}$.

MinE-induced stimulation of MinD ATPase activity is believed to be a key factor regulating the dynamic localization of Min proteins (Hu *et al.*, 2001; Hu *et al.*, 2002; Lackner *et al.*, 2003). To elucidate a possible biochemical explanation for the altered *in vivo* dynamism of some of the N-

terminal $MinD_{Ng}$ mutants, ATPase stimulation assays were conducted on purified $MinD_{Ng\text{-}3aaNT}$ and $MinD_{Ng\text{-}I5E}$. These mutants were selected to gain insight into why N-terminal mutations to MinD appear to confer increased cytosolic distribution ($MinD_{Ng\text{-}3aaNT}$ and $MinD_{Ng\text{-}I5E}$) or faster oscillation rates ($MinD_{Ng\text{-}3aaNT}$). $MinD_{Ng\text{-}K16Q}$ served as a negative control in these experiments, since this mutant exhibited little ATPase activity, even in the presence of $MinE_{Ng}$ and phospholipids (Chapter 6).

Functionality of each C-terminal His-tagged $MinD_{Ng}$ protein was first monitored in the *E. coli* expression strain C41 (DE3) (Table 2.1). As shown previously (Chapter 6), the short C-terminal 6XHis-tag did not affect the ability of wild-type $MinD_{Ng}$ to inhibit cell division in the *E. coli* expression strain (Figure 7.8 A). As expected, overexpression of the negative control protein, C-terminal His-tagged $MinD_{Ng\text{-}K16Q}$, did not alter the typical short rod morphology of this *E. coli* strain (See Figure 6.4 E). Finally, cells expressing C-terminal His-tagged $MinD_{Ng\text{-}3aaNT}$ and $MinD_{Ng\text{-}I5E}$ presented minicell phenotypes (Figure 7.8 C and D), similar to the expression of corresponding untagged proteins in *E. coli* PB103 (Figures 7.2 D and 7.3 H). Therefore, the cell morphologies induced by each His-tagged $MinD_{Ng}$ protein were consistent with those caused by equivalent untagged proteins. While $MinD_{Ng\text{-}3aaNT}$ could be readily purified from induced cultures (Figure 7.8 E), a large fraction of $MinD_{Ng\text{-}I5E}$ was found in insoluble *E. coli* fractions (Figure 7.8 F, lane 1). However, there remained sufficient $MinD_{Ng\text{-}I5E}$ in soluble fractions (lane 2) to be purified by nickel affinity chromatography (lane 3, arrow).

As in Chapter 6, artificial phosphatidylglycerol (PG) vesicles were made and used for the ATPase assays. Purified wild-type $MinD_{Ng}$, $MinD_{Ng\text{-}3aaNT}$, $MinD_{Ng\text{-}I5E}$, $MinD_{Ng\text{-}K16Q}$, and $MinE_{Ng}$, were incubated in the presence of ATP and PG vesicles to measure the release of inorganic phosphate (P_i) from hydrolyzed ATP. In the absence of $MinE_{Ng}$, wild-type $MinD_{Ng}$ incubated with phospholipid vesicles and ATP displayed a low level of basal enymatic activity (Figure 7.9). Addition of $MinE_{Ng}$ increased the amount of P_i released from wild-type $MinD_{Ng}$, up to three times the basal level after 90

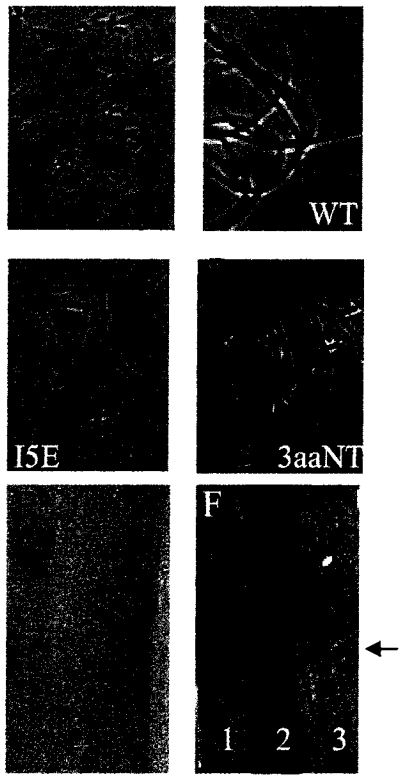

Figure 7.8. Effects of expressing C-terminal His-tagged $MinD_{Ng}$ proteins in *E. coli* C41 (DE3). (A) Cells transformed with the negative control vector pET30a have a short rod morphology. (B) Cells transformed with pSC9 ($minD_{Ng}$-His) display a filamentous phenotype. (C and D) Cells transformed with pJS33 ($minD_{Ng\text{-}I5E}$-His) or pJS34 ($minD_{Ng\text{-}3aaNT}$-His) show a minicell phenotype. Scale bar in (A) represents 10 μm and all figures are at the same magnification. (E) Purification of $MinD_{Ng\text{-}3aaNT}$-His from induced *E. coli* cultures. Lane 1, 5 mM wash buffer eluate; lane 2, 60 mM imidazole wash buffer eluate; lane 3, 1 M imidazole elution. (F) Lane 1: insoluble fraction of *E. coli* C41 (DE3) expressing $MinD_{Ng\text{-}I5A}$-His (pJS33). Lane 2: soluble fraction of pJS33 transformants. Lane 3: Eluted $MinD_{Ng\text{-}I5A}$-His from nickel affinity chromotography (arrow).

minutes (Figure 7.9). In contrast, the $MinD_{Ng\text{-}K16Q}$ negative control exhibited little ATPase activity irrespective of the presence or absence of $MinE_{Ng}$ (Figure 7.9).

Interestingly, in the absence of $MinE_{Ng}$, both $MinD_{Ng\text{-}3aaNT}$ and $MinD_{Ng\text{-}I5E}$ incubated with PG vesicles and ATP exhibited markedly greater ATPase activities than the basal wild-type $MinD_{Ng}$ reaction (Figure 7.9). After 45 minutes, wild-type $MinD_{Ng}$ had not released any measurable amount of P_i in the absence of $MinE_{Ng}$. However, at the same timepoint, both $MinD_{Ng\text{-}3aaNT}$ and $MinD_{Ng\text{-}I5E}$ had already released significantly more P_i (>350 pmol), despite the lack of $MinE_{Ng}$ (Figure 7.9). By the end of the assay, both mutants released approximately twice as much P_i as wild-type (Figure 7.9). Strikingly, the addition of $MinE_{Ng}$ did not result in any significant increase in the ATPase activities of $MinD_{Ng\text{-}3aaNT}$ and $MinD_{Ng\text{-}I5E}$ over the period of the assay (Figure 7.9).

Therefore, mutations to the N-terminus of $MinD_{Ng}$ that decreased dynamic oscillatory periods and/or promoted cytosolic localization *in vivo* also conferred $MinE_{Ng}$-independent hyper-ATPase activity to $MinD_{Ng}$ in the presence of phospholipids, which was not further stimulated by the addition of $MinE_{Ng}$. These studies indicate there are determinants within the extreme N-terminus of $MinD_{Ng}$ involved in regulating the dynamic localization and intrinsic enzymatic activity of the protein.

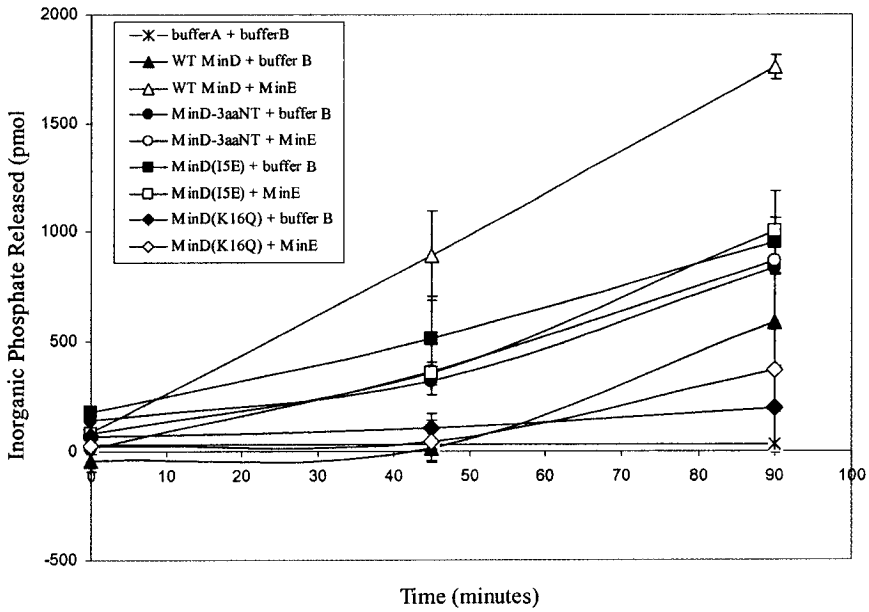

Figure 7.9. $MinD_{Ng}$ ATPase stimulation assays using $MinD_{Ng}$, $MinD_{Ng\text{-}I5E}$, $MinD_{Ng\text{-}3aaNT}$, and $MinD_{Ng\text{-}K16Q}$. Equal amounts of purified $MinD_{Ng}$, $MinD_{Ng\text{-}I5E}$, $MinD_{Ng\text{-}3aaNT}$, and $MinD_{Ng\text{-}K16Q}$ were incubated with PG vesicles and 1 mM ATP. The ATPase activities of each were tested in the presence or absence of $MinE_{Ng}$ over a 90 minute period. Inorganic phosphate released due to ATP hydrolysis was monitored using a malachite green based method. Buffer A is $MinD_{Ng}$ storage buffer, Buffer B is $MinE_{Ng}$ storage buffer.

7.4. DISCUSSION

The coordinated intracellular movement of MinD is essential for maintaining proper septum placement in bacteria (Raskin and de Boer, 1999a; Rowland *et al.*, 2000). To achieve this, MinD must bind reversibly to specific membrane and/or membrane associated targets (Hu *et al.*, 2002; Lackner *et al.,* 2003; Szeto *et al*, 2003, Mileykovskaya *et al.*, 2003, Shih *et al.*, 2003). Several studies have now highlighted the role of the extreme C-terminus of MinD in membrane targeting (Szeto *et al.*, 2002; Hu *et al.*, 2003; Szeto *et al*, 2003; Zhou and Lutkenhaus, 2003). However, little is known about the function(s) of the N-terminus of MinD which, based on MinD sequence alignments, exhibits higher overall conservation than the C-terminus (Szeto *et al.*, 2001). Interestingly, this study showed that mutation or deletion of residues at the extreme N-terminus of MinD affected protein dynamism and interactions with other Min proteins.

To date, the only factors shown to affect MinD oscillation frequency *in vivo* are mutations within MinE or changes in intracellular MinD/MinE ratios (Raskin and de Boer, 1999a; Hu and Lutkenhaus, 2001). Inadequate stimulation of *E. coli* MinD ATPase activity by $MinE_{Ec}$ mutants has been shown to extend the oscillation period of GFP-$MinD_{Ec}$ (Hu and Lutkenhaus, 2001). In support of this, $MinE_{Ng}$ mutants with impaired $MinD_{Ng}$-$MinE_{Ng}$ interaction will induce slower oscillation cycles of GFP-$MinD_{Ng}$ (N. F. Eng and J. R. Dillon, unpublished data). In contrast, the mutant GFP-$MinD_{Ng}$ proteins in the present study had faster oscillation rates, despite the presence of wild-type $MinE_{Ng}$. Furthermore, yeast two-hybrid studies showed $MinD_{Ng}$ bearing 3aaNT, K3A, and K3I mutations all had significantly diminished abilities to interact with wild-type $MinE_{Ng}$. Hence, the rapid oscillation cycles of these GFP-$MinD_{Ng}$ variants were likely due to determinants within $MinD_{Ng}$ itself.

The oscillation frequency of MinD is also inversely related to intracellular MinD/MinE ratios (Raskin and de Boer, 1999a). An increased ratio results in extended oscillation cycles while a decreased ratio is proposed to have the opposite effect (Raskin and de Boer, 1999a). In this study, the intracellular levels of all GFP-$MinD_{Ng}$ variants (except for GFP-$MinD_{Ng\text{-}3aaNT}$), and of their co-expressed $MinE_{Ng}$, were the same. Despite this, the average oscillation cycles of several N-terminal $MinD_{Ng}$ mutants were significantly faster than wild-type. In addition, oscillation cycle times between some mutants were also different (e.g GFP-$MinD_{Ng\text{-}I4Q}$ had a significantly faster oscillation cycle than GFP-$MinD_{Ng\text{-}K3E}$). Therefore, it appears that the decreased oscillation periods of the $MinD_{Ng}$ mutants were not due to gross changes in MinD/MinE ratios, but rather due to changes intrinsic to $MinD_{Ng}$, and independent of $MinE_{Ng}$. Since $MinD_{Ng\text{-}3aaNT}$ had significantly diminished interaction with $MinE_{Ng}$, it remains possible that the effects of this deletion on GFP-$MinD_{Ng\text{-}3aaNT}$ were $MinE_{Ng}$-independent as well.

The observed changes in the dynamism of N-terminal $MinD_{Ng}$ mutants were not likely due to diminished interaction with $MinE_{Ng}$ for several reasons. Firstly, $MinD_{Ng}$ mutants that retained similar interaction with $MinE_{Ng}$ as wild-type $MinD_{Ng}$ (e.g. K3E and I4Q mutants) still had faster oscillation rates than the control, indicating the phenotypes observed were independent of $MinE_{Ng}$. Secondly, it has been demonstrated that diminished and/or abrogated interaction with mutant MinE will cause GFP-$MinD_{Ec}$ (Ma *et al.*, 2003) or GFP-$MinD_{Ng}$ (N.F. Eng and J.R. Dillon, unpublished results) to oscillate slower and remain for an extended period at one cell pole, presumably due to inefficient stimulation of MinD ATPase. However, it is clear from our studies that the $MinD_{Ng}$ mutants with decreased interaction with $MinE_{Ng}$ had significantly faster oscillation than wild-type and decreased

propensities to remain associated with the membrane. Thirdly, the increased ATPase activity of two of the mutants, $MinD_{Ng\text{-}3aaNT}$ and $MinD_{Ng\text{-}I5A}$, was not affected by the presence $MinE_{Ng}$. Finally, studies by others have revealed evidence that the MinE binding site on MinD is within the α-7 helix of MinD, which is not in proximity to the MinD N-terminus (G. King, University of Connecticut Health Centre, personal communication). Hence, the phenotypes of the mutant $MinD_{Ng}$ proteins were likely MinE-independent.

While several N-terminal deletion and point mutation mutants of $MinD_{Ng}$ had significantly diminished interaction with MinC, this could not possibly have contributed to the faster oscillation and increased cytosolic localization of these GFP-$MinD_{Ng}$ variants. Firstly, all localization studies were conduced in an *E. coli* system devoid of any MinC. Secondly, it is well established that GFP-MinD localization is independent of MinC (Raskin and de Boer, 1999a). These studies do indicate that the extreme N-terminus of $MinD_{Ng}$ contains determinants that are involved in, but not entirely responsible for, interaction with the MinC division inhibitor. In support of this, previous yeast two-hybrid studies have indicated that residues within the α-7 helix of $MinD_{Ec}$ (e.g. E146 and D152), which are not in proximity to the extreme N-terminus, may play a more direct role in binding MinC (Hayashi *et al.*, 2001). Despite interacting as strongly with $MinC_{Ec}$ as some of the other $MinD_{Ng}$ mutants, the greater tendencies of $MinD_{Ng\text{-}3aaNT}$ and $MinD_{Ng\text{-}I5A}$ to remain and/or return to the cytosol, in comparison to the other mutants, may have prevented them from recruiting sufficient $MinC_{Ec}$ to the membrane *in vivo*. As a result, expression of these two mutant $MinD_{Ng}$ proteins did not induce total cell division arrest in wild-type *E. coli,* unlike the other mutant $MinD_{Ng}$ proteins.

This study demonstrated that, despite the absence of $MinE_{Ng}$, $MinD_{Ng\text{-}3aaNT}$ and $MinD_{Ng\text{-}I5E}$ each had significantly greater $MinE_{Ng}$-independent ATPase activities than wild-type protein. Such hyper-ATPase activity in these, and the remaining N-terminal mutants, could account for their faster oscillation cycles and/or increased cytosolic distribution relative to wild-type $MinD_{Ng}$. Interestingly, both GFP-$MinD_{Ng\text{-}I5E}$ and the negative control GFP-$MinD_{Ng\text{-}K16Q}$ were found entirely in the cytosol. However, since $MinD_{Ng\text{-}I5E}$ had increased ATPase activity, in contrast to the low activity of $MinD_{Ng\text{-}K16Q}$, it suggests that their common intracellular localization pattern was due to separate factors. While a K16Q mutation to MinD is proposed to render the protein insensitive to the effects of ATP-binding (Hu *et al.*, 2002), it is conceivable that increased intrinsic ATPase activity of $MinD_{Ng\text{-}I5E}$ would prevent sufficient stable MinD-ATP to localize effectively along the membrane *in vivo*.

Under normal circumstances, the MinE-induced ATPase activity of MinD has been proposed to be the rate-limiting step for GFP-MinD oscillation (Hu and Lutkenhaus, 2001). However, as a result of increased intrinsic ATPase activity at the membrane, it is possible that GFP-$MinD_{Ng\text{-}3aaNT}$ and GFP-$MinD_{Ng\text{-}I5E}$ were more prone to dissociate from their membrane targets regardless of $MinE_{Ng}$. In effect, GFP-fusions to N-terminal $MinD_{Ng}$ mutants would be released sooner into the cytosol than wild-type GFP-$MinD_{Ng}$, allowing them to migrate towards the opposite cell pole and to produce faster oscillation cycles, which was observed. This would account for the positive correlation observed between the relative amount of each GFP-$MinD_{Ng}$ residing in the cytoplasm and its rate of protein oscillation. In contrast, wild-type $MinD_{Ng}$ would require sufficient $MinE_{Ng}$ recruitment and stimulation prior to commencing a cycle of oscillation *in vivo*. This delay would result in a more stable

$MinD_{Ng}$ membrane association and longer oscillation cycles than the N-terminal mutants. The diminished and lost interactions of $MinE_{Ng}$ with $MinD_{Ng\text{-}3aaNT}$ or $MinD_{Ng\text{-}I5E}$, respectively, would have also contributed to the inability of $MinE_{Ng}$ to further stimulate their *in vitro* ATPase activities.

MinD oscillation and ATPase activity are intimately linked and require MinD self-association (Hu and Lutkenhaus, 2001; Hu *et al.*, 2003; Lutkenhaus and Sundaramoorthy, 2003). Hence, the faster oscillation cycles and increased ATPase activities of the $MinD_{Ng}$ mutants in this study indicate they still possess significant functional self-association, despite their decreased affinities to homodimerize, as detected by the yeast two-hybrid system. Results from the *in vitro* ATPase assays also provide an explanation for this decreased self-affinity. While ATP-binding induces MinD dimerization, the hydrolysis of ATP should lead to the dissociation of MinD dimers as well (Hu *et al.*, 2002; Hu *et al.*, 2003). Hence, while still able to interact in the yeast reporter strain, hyper-ATPase activity of N-terminal $MinD_{Ng}$ mutants within yeast may have destabilized the self-association of these proteins, resulting in the diminished strengths of interaction observed.

Interestingly, each of the $MinD_{Ng}$ mutants displaying tendencies to localize cytoplasmically (3aaNT, K3I, I4Q, I5A, or I5E mutations) had less than half the strength of self-interaction of wild-type protein, based on β-galactosidase activities. In contrast, $MinD_{Ng\text{-}2aaNT}$ and $MinD_{Ng\text{-}K3E}$ each retained at least half of the strength of self-interaction of wild-type $MinD_{Ng}$, and were localized clearly along the membrane. Therefore, it is possible that a certain threshold of self-binding affinity must be achieved prior to the commitment of MinD to bind membrane targets.

The changes in the dynamic localization characteristics of the N-terminal $MinD_{Ng}$ mutants were not likely due to inefficiencies in ATP-binding, but rather due to the effects of MinE-independent hyper-ATPase activities. In support of this, examination of Archaeal MinD crystal structures show that the extreme N-terminus of MinD does not contain residues that directly participate in nucleotide binding (Hayashi *et al.*, 2001; Sakai *et al.*, 2001). In addition, the N-terminal $MinD_{Ng}$ mutants which exhibited faster intracellular oscillation, as well as increased ATPase activities, would first require ATP-binding. Moreover, MinC-MinD interaction appears to require ATP (Hu *et al.*, 2003; Lackner *et al.*, 2003), and almost all of the $MinD_{Ng}$ N-terminal mutants could still interact with MinC and could induce total cell division arrest in *E. coli*.

These studies also support the notion that a basic, MinD-containing, helical scaffold is required for any degree of intracellular MinD protein oscillation. It should be noted that each GFP-$MinD_{Ng}$ mutant that displayed oscillation, no matter how faint, could still localize within coil-like arrays. The ability of each $MinD_{Ng}$ variant to form these arrays corresponded with its ability to interact with $MinE_{Ng}$, even if this interaction was severely diminished (e.g. $MinD_{Ng\text{-}I5A}$). This is in support of a proposal that MinE may serve as a cross-linker for MinD filaments, in addition to its role in inducing MinD disassembly from the membrane (Suefuji *et al.*, 2002). Hence, these studies indicate that some (even minimal) interaction with MinE, must be maintained in order to form MinD-containing coiled arrays that direct protein oscillation *in vivo*.

What role might the N-terminus of $MinD_{Ng}$ play in the functionality of the protein? It is possible that the N-terminus of $MinD_{Ng}$ may be involved in controlling intrinsic ATPase activity. Using the solved structure of MinD from *Archaeoglobus fulgidus* as a representative structure (Figure 7.10), residues of the extreme N-terminus (yellow residues, aa 1-5) form one end of a buried β-strand

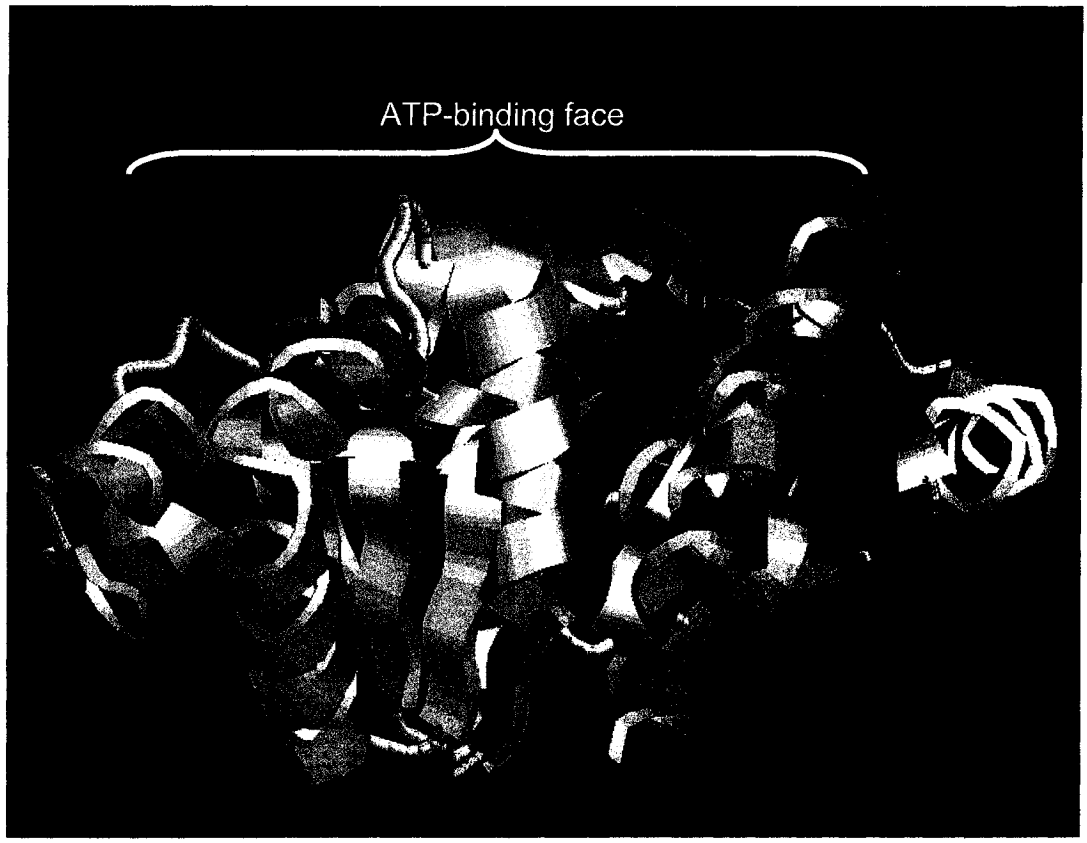

Figure 7.10. Structure of *Archaeoglobus fulgidus* MinD highlighting the N-terminus residues (Cordell and Löwe, 2001). Yellow residues indicate the extreme N-terminus amino acids at positions 1-5. Red residues (aa 6-9), in conjunction with yellow residues (1-5) form a β-strand that connects to the P-loop (Walker A ATP-binding motif, green residues). The general position of the ATP-binding face of MinD is indicated. Ribbon diagram generated with RasMol Molecular Graphics Visualization Tool (Version 2.7.2.1).

(yellow and red residues) that connects directly to the P-loop (Walker A ATP-binding motif, green residues) which is found at the opposite side of the protein (Cordell and Löwe, 2001). Hence, it is possible that some of the effects of ATP-binding are transmitted from the ATP-binding face (Figure 7.10) through the N-terminus residues (yellow and red residues) to other regions of the protein in preparation for membrane association and/or ATP hydrolysis. Mutation of this N-terminus region may therefore render MinD more sensitive to the effects of ATP-binding, in contrast to the desensitization proposed with a K16Q mutation (Hu *et al.*, 2002), and result in increased intrinsic enzymatic activity.

There are several examples of ATPases in which the N-terminus is directly involved in regulating functionality. Sequential truncations to the first five residues of the chloroplast ATP synthase epsilon subunit resulted in significant increases in the ATPase activity of the holoenzyme (Shi *et al.*, 2001). Furthermore, deletion of the N-terminal 'A' domain of the transcriptional regulator XylR has been shown to lock the regulator in a fully active form (Fernandez *et al.*, 1995), which displays a strongly stimulated ATPase activity in the presence of DNA activation sequences (Perez-Martin and de Lorenzo, 1996). In addition, the N-terminal domain of the DmpR transcriptional activator has been shown to act as a repressor of its ATPase activity (Shingler and Pavel, 1995). Normally, DmpR ATPase activity is induced by binding of aromatic compounds (Shingler and Pavel, 1995), which draws an interesting comparison to the effects of MinE binding to MinD.

This study demonstrates that mutations or truncations within the first five residues of the conserved N-terminus of $MinD_{Ng}$ affect the movement and localization properties of the protein. Residues 6-9 of MinD are even more conserved than the first five, and it would be interesting to study their functional roles as well. Since the extreme N-terminus of MinD is highly conserved, its function is likely shared across MinD proteins from various organisms, particularly Gram-negative bacteria. Evidence is provided that the altered dynamism of these $MinD_{Ng}$ mutants may result from increased intrinsic basal ATPase activities. Further work, including *in vitro* membrane binding assays using

vesicles that closely approximate bacterial cell membranes, as well as combined structural and enzymatic studies, should prove useful in further elucidating the function of the MinD N-terminus. Since correct cell division site-selection is such an important event in the bacterial cell cycle, there should conceivably be several mechanisms and/or factors that regulate dynamic Min protein movement, including determinants within MinD itself that ensure its proper ATPase activity.

CHAPTER 8

General discussion, future considerations, and concluding statements

The study of Min proteins from rod-shaped organisms is well advanced. However, the discovery of *min* gene homologues in the coccus *N. gonorrhoeae* was intriguing (Ramirez-Arcos *et al.*, 2001a) and prompted our laboratory to initiate investigations into the function of Min proteins from coccal organisms. Using a variety of methods and assays, it was shown that $MinD_{Ng}$ functions as a cell division site determinant in the gonococcus, and is active across species as well. Despite differences in morphology and cell division patterns, both *N. gonorrhoeae* and the rod *E. coli* share similar proteins to achieve successful cell division. The tripartite Min system (MinC, MinD, and MinE), with its highly conserved MinD protein, therefore appears to be a relatively common cell division regulator in Gram-negative organisms. However, in contrast to the rod *E. coli*, it would appear that the Min system in gonoccocal cells must function in two dimensions to maintain the perpendicularly alternating division planes characteristic of *N. gonorrhoeae*.

Overall, these studies suggest a universality of MinD function, at least in Gram-negative organisms. Based on *in vivo* studies in *E. coli*, it is apparent that $MinD_{Ng}$ is active in this background, since it displayed several characteristics that have also been reported with *E. coli* MinD, including the induction of MinC-activated cell division arrest and MinE-dependent pole-to-pole oscillation along a coiled scaffold. These observations suggest that *N. gonorrhoeae* and *E. coli* MinD have more functional similarities than differences. The ability of GFP-$MinD_{Ng}$ to localize as coils in *E. coli* backgrounds suggests that the formation of such MinD helical arrays may be common in all Gram-negative organisms bearing a Min system, regardless of shape. For $MinD_{Ng}$, this ability was not entirely unexpected, since it shares significant identity (73%) with $MinD_{Ec}$, and comes from an organism that also contains MinC and MinE proteins. Of course, more subtle differences between each protein, such as slight differences in the C-terminal MTS region for example (KSFFKRLF in $MinD_{Ng}$ and KGFFKRLF in $MinD_{Ec}$), likely reflect evolutionary changes that accommodate corresponding changes in their respective host targets, including membrane, MinC, and MinE partners.

Interestingly, there is one species of *Neisseria*, *N. elongata*, which presents a rod-shaped morphology (Bovre and Hotten, 1970). While there is no available genome project for this organism, it should, more than likely, contain MinD, MinC, and MinE homologues, which would predictably behave as Min proteins in other rods, such as *E. coli*. It is also conceivable that MinD from the rod-shaped *N. elongata* would have an even *higher* identity to $MinD_{Ng}$ than to $MinD_{Ec}$, further blurring the line of distinction, if any, between 'coccal'- and 'rod'-derived MinD. However, further investigation of a potential *min* system in *N. elongata* must be done to confirm this.

From accumulated studies in *E. coli*, several models of cell division site selection have been generated and progressively modified (Hu and Lutkenhaus, 1999; Hu and Lutkenhaus, 2001; Margolin, 2001a; Lackner *et al.*, 2003; Shih *et al.*, 2003). By combining observations from the present study with *E. coli* Min protein models, a model for division site selection in Gram-negative round bacteria such as *N. gonorrhoeae* is proposed (Figure 8.1). Since GFP-$MinD_{Ng}$ was able to oscillate and to assemble/localize within coiled structures in rod-shaped and round *E. coli*, it is likely that $MinD_{Ng}$ undergoes similar behaviour within gonococcal cells. Nucleoid occlusion also influences cell division site placement (Woldringh, 1990: Yu and Margolin, 1999); therefore, the effect of bulk chromosomal DNA is also considered in this model, based on preliminary data obtained from nucleoid localization studies conducted in dividing gonococcal cells (see Appendix, Part D).

The model of cell division toporegulation in *N. gonorrhoeae* is similar to that of *E. coli*, as both require the localization of Min proteins along a helical scaffold. In *N. gonorrhoeae,* this basic Min protein array, which includes $MinD_{Ng}$, is proposed to coil along the longest available axis of the cell (Figure 8.1 A, red arrowheads), similar to that observed in both round and rod-shaped *E. coli* (Chapter 4). In fact, *N. gonorrhoeae* cells have been shown to elongate during their growth cycle, resulting in a *slight* longitudinal axis (Westling-Häggström *et al.*, 1977); hence, it could be argued that gonococcal cells resemble extremely short rods prior to cytokinesis. Transmission electron microscopy in the present study also verified that gonococcal cells are not perfectly round, and can present a long axis (Figures 3.4 A and 3.9 E). Interestingly, the Min protein scaffold in *E. coli* does

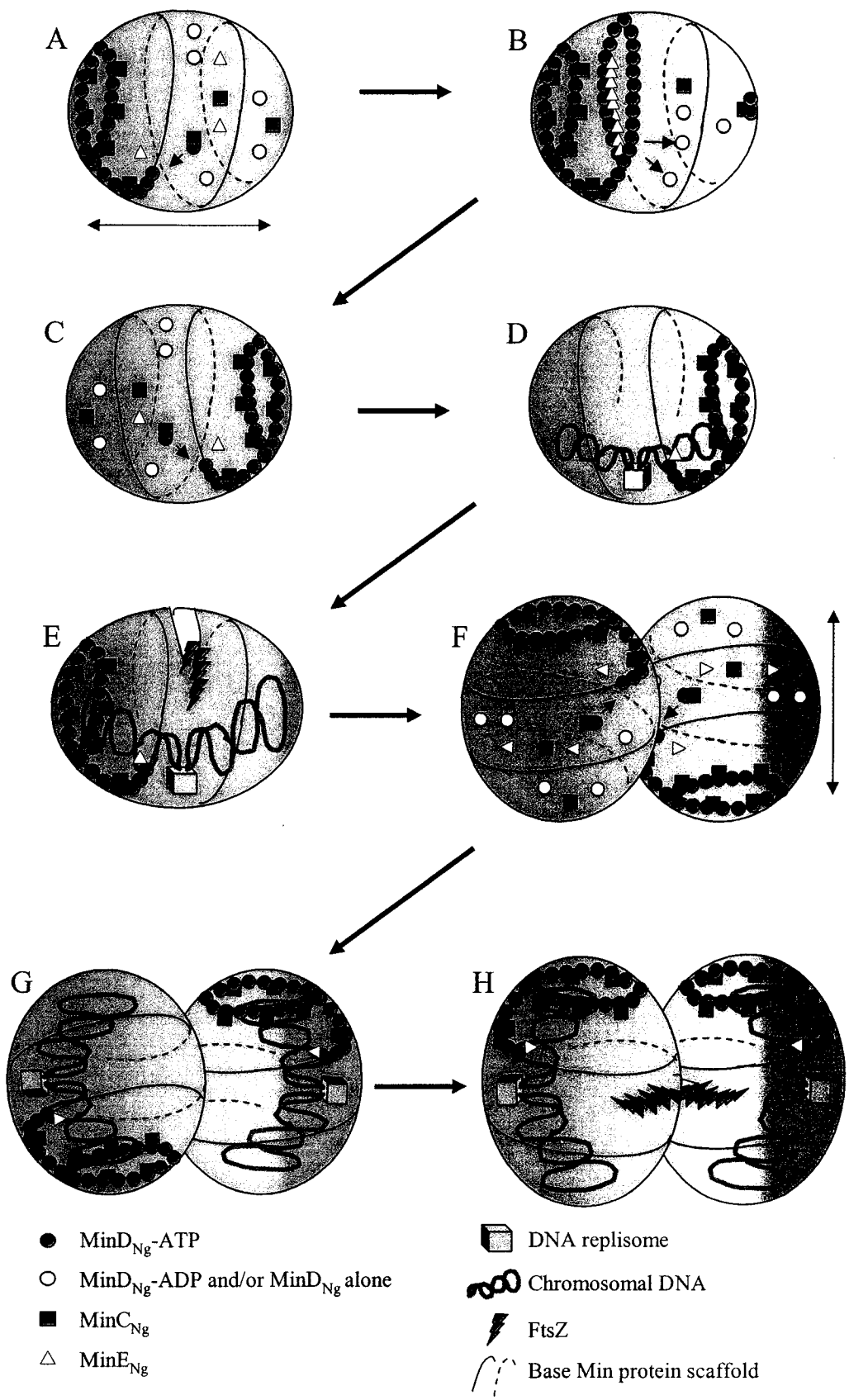
A
B
C
D
E
F
G
H
MinD$_{Ng}$-ATP
MinD$_{Ng}$-ADP and/or MinD$_{Ng}$ alone
MinC$_{Ng}$
MinE$_{Ng}$
DNA replisome
Chromosomal DNA
FtsZ
Base Min protein scaffold

not appear to be associated with other helical cytoskeletal structures, such as MreB arrays, which are involved in maintaining bacterial shape (Shih *et al.*, 2003). Hence, it is tempting to speculate that the coiling orientation of Min protein arrays is *dependent* upon cell shape which, in turn, is dictated by cell growth.

Upon binding ATP, $MinD_{Ng}$ dimerizes and gains membrane affinity. Accumulation of $MinD_{Ng}$-ATP subunits (green circles) along the helical array at one half of the cell commences, forming a '$MinD_{Ng}$ zone', which recruits the $MinC_{Ng}$ division inhibitor (red squares) to that region as well (Figure 8.1A). $MinE_{Ng}$ would also be required for the localization of $MinD_{Ng}$ within a coil, possibly acting as a crosslinker (Suefuji *et al.*, 2003). The extent of the $MinD_{Ng}$ zone is restricted to one cell half, as accumulated $MinE_{Ng}$ near the middle of the cell ($MinE_{Ng}$ ring-like structure; triangles) induces the dissocation of $MinC_{Ng}$ from $MinD_{Ng}$, and stimulates the ATPase activity and release of $MinD_{Ng}$ from the membrane/Min protein lattice (Figure 8.1 B). Cytoplasmic $MinD_{Ng}$-ADP (white circles) can diffuse towards the opposite end of the cell, where it re-initiates localization within a coil upon binding ATP (Figure 8.1 B, C). Hence, the continued oscillation of the $MinCD_{Ng}$ complex between opposite cell hemispheres should allow FtsZ assembly to commence at a midcell site (thunderbolts), which is relatively free of division inhibition (Figure 8.1 B-E).

Immunoelectron microscopy revealed that FtsZ initially accumulates specifically at a single invagination point in dividing gonococci. What role might the chromosome play in this process? Studies in *E. coli* and *B. subtilis* have shown that chromosomal DNA replication machinery (DNA replisome) is localized at midcell, suggesting that replicating chromosomes are threaded through a stationary replisome (Lemon and Grossman, 1998; Koppes *et al.*, 1999). Therefore, it is possible that such a fixed DNA replisome is also present in growing *N. gonorrhoeae* cells. In Figure 8.1 D, this replisome is depicted at the 'bottom' of the cell (orange box). Hence, the periodic oscillation of the $MinCD_{Ng}$ complex from 'left to right' hemispheres, coupled with the presence of a replicating chromosomal mass at the 'bottom' of the cell would result in cytokinetic inhibition at all sites, *except* at the location opposite of the replisome (i.e. the 'top' of the cell in Figure 8.1 E), where FtsZ

polymerization can initiate. Once DNA replication and chromosome segregation events approach termination, the effects of nucleoid occulsion at midcell are diminished and full septation can occur.

Upon completing the first division event, each cell in the resulting diplococcus experiences growth along a second dimension that is perpendicular to the first, producing a new longitudinal axis (Westling-Häggström *et al.*, 1977) (Figure 8.1 F, red arrowheads). A corresponding re-orientation of the Min protein coil would also occur, in order to direct Min protein subunit oscillations parallel to the nascent septum. This pattern of oscillation was observed in diplococcal *E. coli* cells expressing GFP-$MinD_{Ng}$ (this study) and GFP-$MinD_{Ec}$ (Corbin *et al.*, 2002). In addition, it is possible that the DNA replisome in each daughter cell attaches to a new intracellular site, directly opposite the nascent septum (Figure 8.1 G; also Appendix, Figure A.6 B, C), which would further restrict FtsZ polymerization to the junction point between two cells (Figure 8.1 H). Hence, the redirection of Min protein oscillation and the effects of bulk chromosomal DNA will result in cell division along a plane that is perpendicular to the first (Figure 8.1 H, thunderbolts).

Therefore, based on their septation patterns, the major difference between the *N. gonorrhoeae* and *E. coli* Min systems would seem to be the reorientation of Min protein oscillation in the coccal system. From the present study, it appears that the direction of MinD oscillation corresponds to the longitudinal direction of its winding coil. It is possible that the 'permanent' MinCDE coiled array proposed to exist in rod-shaped bacteria (Shih *et al.*, 2003) may not be as 'fixed' in coccal backgrounds, thus allowing the disassembly and/or reorientation of the array along a second dimension in cells such as *N. gonorrhoeae.* Interestingly, *E. coli* GFP-MinD also undergoes a perpendicular shift in oscillation direction in dividing round cells (Corbin *et al.*, 2002); hence, the reorientation of GFP-$MinD_{Ng}$ in round cells was not due to $MinD_{Ng}$ regions that are specifically adapted for coccal cell systems. Again, it is interesting to propose that the coiling of the Min protein array is under the influence of the longest available cell axis created by cell growth.

There is evidence that lipid domains within the bacterial membrane can also influence the assembly of MinD *in vivo*. In *E. coli* lacking the zwitterionic phospholipid phosphatidylethanolamine,

and containing only anionic phospholipids cardiolipin and phosphatidylglycerol, GFP-$MinD_{Ec}$ assembled into dynamic foci rather than its characteristic bands, despite the presence of MinE (Mileykovskaya *et al.*, 2003). Therefore, since lipid composition seems to affect Min protein assembly *in vivo*, it is possible that rearrangements in lipid domains within actively dividing coccal bacteria can also contribute to reorienting Min protein oscillation.

Future studies to investigate the formation of Min protein coiled arrays in dividing cocci should prove very interesting, particularly during the transition from oscillating along one dimension to the other. These studies should shed light onto whether the MinCDE helical arrays are disassembled and re-assembled along new axes, or whether the coiled array is maintained, but rotated to accommodate the second oscillation direction. Such investigations could be achieved by live cell imaging of dividing round *E. coli* cells expressing GFP-fusions to $MinD_{Ng}$ or to $MinD_{Ec}$. In addition, colocalization studies of FtsZ and nucleoids should increase our knowledge of the effects of nucleoid occlusion on multi-septating bacteria such as *N. gonorrhoeae*. Furthermore, studies to address the mechanisms that induce the direction of cell growth in relation to nascent septa should be of particular interest, especially when combined with Min coil localization.

Several questions still need to be addressed in the model of *N. gonorrhoeae* cell division. The challenges of genetically manipulating and localizing proteins in *N. gonorrhoeae* limited the $MinD_{Ng}$ studies that could be performed in its native organism. While it is highly likely that the Min proteins exhibit dynamic localization and assembly in *N. gonorrhoeae*, *in vivo* localization studies using GFP-fusions should be performed to verify this. Cloning of these fusions into the gonococcal shuttle vector, or their integration into the gonococcal chromosome, should facilitate these studies. However, gonococci are prone to cell autolysis and are extremely fastidious; hence, *in vivo* localization studies may prove to be very difficult.

MinD is a complex protein which must perform a variety of activities in order to properly influence cell division site placement. These include binding ATP, dimerization and polymerization,

interaction with membrane and/or coiled array targets, recruitment of MinC, binding to MinE and having its ATPase activity stimulated, and dissociation from the membrane (Raskin and de Boer, 1999a; Hu and Lutkenhaus, 2001; Hu *et al.*, 2002; Hu and Lutkenhaus, 2003; Hu *et al.*, 2003, Lackner *et al.*, 2003, Szeto *et al.*, 2003; this study). With all these different functions, it is not surprising that bacterial MinD studies show that regions involved in mediating these different functions are distributed throughout the protein. By mapping these regions onto the solved crystal structure of Archaeal MinD (Figure 8.2; *A. fulgidus* MinD; Cordell and Löwe, 2001) the distribution of functional sites is more evident. While the actual structure and position of the C-terminal MTS of MinD is not known, it is predicted to form an amphipathic helix (Szeto *et al.*, 2002); hence, an α-helix was manually inserted in Figure 8.2 A to complete the protein structure.

Although each MinD region shown in Figure 8.2 has been assigned a 'main' role, it remains difficult to designate any clear-cut regions of function, except perhaps the MTS. For example, while residues within the α-7 helix are implicated in MinC interaction (Hayashi *et al.*, 2002) (Figure 8.2; purple residues in yellow helix), their effects on MinE-binding, dimerization, ATPase activity, and protein dynamism are unexplored. In addition, while the switch I and II sites may play a role in mediating MinC interaction (Figure 8.2, blue and green residues), they also affect MinE-induced ATPase activity of MinD, and their role in affecting MinD dynamic behaviour is not known (Zhou and Lutkenhaus, 2004). Furthermore, the K16Q mutation is of key importance in almost every facet of MinD function (Hu *et al.*, 2002; this study). Hence, it appears that many aspects of MinD function are intimately linked with one another, and that assigning certain regions with a single function should be carefully considered.

The results from the present study further identify new functional regions in bacterial MinD (Figure 8.2). Each region was characterized by a battery of assays in order to better address their specific, as well as global, roles in MinD function. Interestingly, the 'loop' and extreme N-terminal regions identified in this study have almost opposite effects. In terms of MinD dynamics, loop region

8.2. Functional regions identified in MinD proteins from Gram-negative bacteria mapped onto the crystal structure of MinD from the Archaea *A. fulgidus* ($MinD_{Pf}$). (A) Residues and regions identified to have functional significance in $MinD_{Ng}$ and $MinD_{Ec}$ are indicated by arrows pointing to corresponding sites in the $MinD_{Pf}$ crystal structure (Cordell and Löwe, 2001). Unless indicated, amino acid designations correspond to the $MinD_{Pf}$ protein. Red helix represents the C-terminal membrane targeting sequence; however, its exact position and structure are currently not known and was therefore manually inserted into the figure to present a complete protein. Yellow helix, and the purple residues within, shows the α-7 helix, containing residues involved in binding to MinC, based on yeast two hybrid studies (Hayashi *et al.*, 2001) and as proposed by molecular modeling by our laboratory (Ramirez-Arcos *et al.*, in press). Single red residue represents K16 of the Walker A-ATP binding motif found. Blue and green residues indicate location of switch I and II sites, respectively, that appear to be required for interaction with MinC (Zhou and Lutkenhaus, 2004). 'Loop' region, identified in the present study, is shown in cyan and is implicated in conferring to MinD the ability to respond to MinE binding. N-terminal residues (orange) are involved in affecting the dynamics of MinD association with the membrane and/or Min coiled array, as well as interactions with other Min proteins (this study). The proposed dimerization interface is shown along the protein face indicated by the bracket. (B) represents a 90° downward rotation of (A). The proposed C-terminal MTS is not shown in (B).

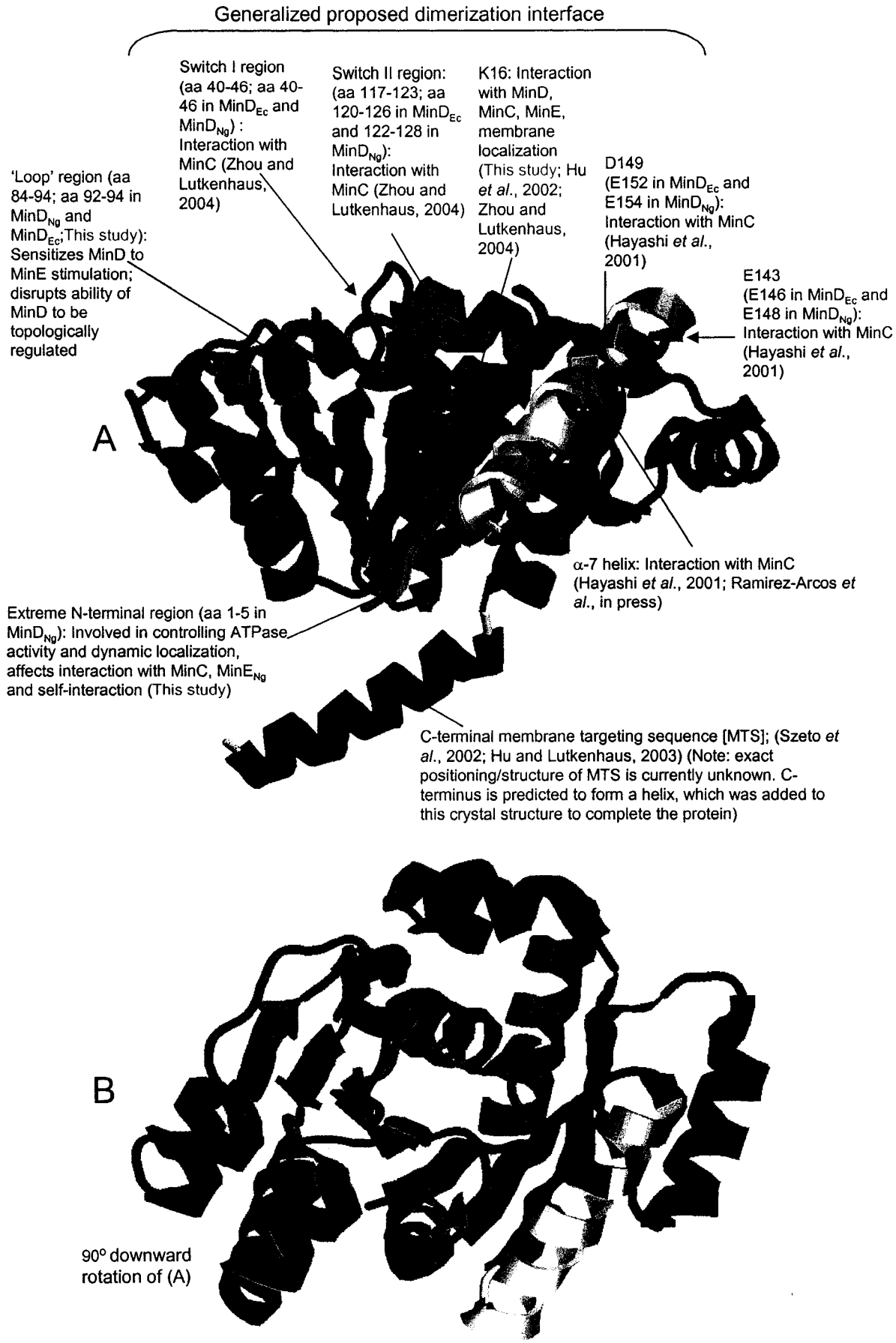
Generalized proposed dimerization interface
Switch I region (aa 40-46; aa 40-46 in $MinD_{Ec}$ and $MinD_{Ng}$) : Interaction with MinC (Zhou and Lutkenhaus, 2004)
Switch II region: (aa 117-123; aa 120-126 in $MinD_{Ec}$ and 122-128 in $MinD_{Ng}$): Interaction with MinC (Zhou and Lutkenhaus, 2004)
K16: Interaction with MinD, MinC, MinE, membrane localization (This study; Hu *et al.*, 2002; Zhou and Lutkenhaus, 2004)
D149 (E152 in $MinD_{Ec}$ and E154 in $MinD_{Ng}$): Interaction with MinC (Hayashi *et al.*, 2001)
'Loop' region (aa 84-94; aa 92-94 in $MinD_{Ng}$ and $MinD_{Ec}$;This study): Sensitizes MinD to MinE stimulation; disrupts ability of MinD to be topologically regulated
E143 (E146 in $MinD_{Ec}$ and E148 in $MinD_{Ng}$): Interaction with MinC (Hayashi *et al.*, 2001)
A
α-7 helix: Interaction with MinC (Hayashi *et al.*, 2001; Ramirez-Arcos *et al.*, in press)
Extreme N-terminal region (aa 1-5 in $MinD_{Ng}$): Involved in controlling ATPase activity and dynamic localization, affects interaction with MinC, $MinE_{Ng}$ and self-interaction (This study)
C-terminal membrane targeting sequence [MTS]; (Szeto *et al.*, 2002; Hu and Lutkenhaus, 2003) (Note: exact positioning/structure of MTS is currently unknown. C-terminus is predicted to form a helix, which was added to this crystal structure to complete the protein)
B
90° downward rotation of (A)

mutants lost the ability to oscillate clearly from pole-to-pole, and localized throughout a membrane-associated coil. In contrast, N-terminal MinD mutants experienced faster oscillation cycles, accompanied by increased tendencies to localize in the cytosol. Furthermore, while loop region mutations did not eliminate $MinD_{Ng}$ interaction with any other Min proteins, N-terminal mutations did diminish or abolish such interactions. Finally, while $MinD_{Ng\text{-}loop}$ exhibited low ATPase activity, even in the presence of $MinE_{Ng}$, N-terminal $MinD_{Ng}$ mutants displayed MinE-independent ATPase activity. Hence, it is interesting to propose that these two separate regions may be involved in fine-tuning the dynamic properties of MinD through opposing effects. As such, MinD proteins would contain determinants within themselves that help autoregulate their activity, since correct cell division site placement is so vital for proper cell development.

In terms of $MinD_{Ng}$ itself, there are many interesting avenues of research that may be further pursued. Optimization of $MinD_{Ng}$ membrane binding assays are underway (Appendix) and should provide an additional useful functional assay for studying $MinD_{Ng}$ mutant activity. Furthermore, our laboratory has initiated NMR structural studies of $MinD_{Ng}$. While there are several solved structures of Archaeal MinD proteins, there is, to date, no evidence that any of them are involved in cell division regulation, particularly since these organisms lack the other *min* genes. Hence, structural information from a bacterial MinD protein should be extremely useful to those studying in this field.

Aside from additional standard mutational analyses of other regions in MinD, another attractive project would be to extend $MinD_{Ng}$ studies (and Min proteins in general) to examine their role in bacterial pathogenicity. Such studies would be *unique* to the Min protein field. Both *N. gonorrhoeae* $minC_{Ng}$ (Ramirez-Arcos *et al.*, 2001a) and $minD_{Ng}$ (this study) mutants exhibit decreased cell viability, and preliminary *in vitro* studies with collaborators at the University of Iowa have shown that these mutants are severely attenuated in adhesion and invasion of host epithelial cells (Dillon *et al.*, unpublised results). Future studies combining molecular and cellular biology may even lead to unique Min protein target sites for the development of novel antimicrobials.

It is noted that a BLAST search of the human genome reveals two human proteins that have some identity to $MinD_{Ng}$. One protein, E2F transcription protein 3, has 27% identity and 54% similarity to $MinD_{Ng}$ over a region corresponding to residues 49-120 of the bacterial protein. Interestingly, this region does not include the switch I and II sites of MinD, which one might expect to be conserved among various proteins in different organisms. Instead, the similarity encompasses a region between both switch sites, which contains the identified MinD 'loop' region in this study. Another human protein, identified as a sperm protein, has 20% identity and 43% similarity to $MinD_{Ng}$ residues 103-228, which contains the switch II site and α-7 helix. Since these human proteins share homologous regions with MinD, the bacterial protein may not be suitable for antimicrobial targeting. However, by focusing on truly MinD-*specific* residues/regions which are not shared with human proteins, this issue could be circumvented.

Environmental factors from the host may also contribute to Min expression in *N. gonorrhoeae* and could also be an interesting focus for research. The *min* genes of *N. gonorrhoeae* are part of a large gene cluster containing several other genes that seem to be unrelated to the act of cell division, including those involved in transcriptional regulation (e.g. *rpoA* and *oxyR*) and translation (e.g. structural ribosomal genes) (Ramirez Arcos *et al.*, 2001a). This is in contrast to the three *E. coli min* genes which seem to form an independent transcriptional unit themselves (Ramirez-Arcos *et al.*, 2001a). Our laboratory has previously shown that the activity of promoter regions identified upstream of each min_{Ng} gene is influenced by factors that resemble the host genitourinary environment, including anaerobic conditions and the presence of urea (Ramirez-Arcos *et al.*, 2001b). It is possible that the remaining genes residing in the 17 kb cluster with $minCDE_{Ng}$ are also involved, in part, in regulating gonococcal *min* gene expression under different host environmental conditions. For example, *oxyR*, located downstream of $minCDE_{Ng}$, encodes a transcriptional regulator that acts as a repressor of catalase expression. In the presence of hydrogen peroxide, catalase production is induced through OxyR-mediated derepression (Tseng *et al.*, 2003). Hence, it would be interesting to determine whether the expression of $minCDE_{Ng}$ genes is affected by OxyR and/or hydrogen peroxide.

This is the first study of MinD from a coccal bacterium. The construction of *minD*$_{Ng}$ knockout and K16Q point mutation strains, as well as MinC$_{Ng}$-MinD$_{Ng}$ overexpression studies, demonstrated that MinD$_{Ng}$ is required to maintain the characteristic division pattern of *N. gonorrhoeae*. In addition, MinD$_{Ng}$ was shown to be active in *E. coli* backgrounds, being able to influence cell division and to exhibit intracellular dynamism and coil assembly in this organism. The use of *E. coli* as an indicator for MinD$_{Ng}$ function greatly facilitated this study, since genetic manipulation, protein expression studies, and GFP-MinD$_{Ng}$ localization could be readily conducted. Using various genetic and biochemical techniques, interactions between MinD$_{Ng}$ and the other Min proteins were identified. Significantly, this study was the first to observe the self-association of bacterial MinD, now considered a key property of the protein that allows for its dynamic assembly. Finally, the use of structural homology modeling and protein sequence alignments, coupled with mutational analyses, identified several regions in MinD$_{Ng}$ that are involved in maintaining function, including an exposed polar region implicated in sensitizing MinD$_{Ng}$ to MinE binding/stimulation, and the extreme N-terminus of the protein that affects intrinsic MinD$_{Ng}$ ATPase activity and general dynamism.

While found in many bacteria, Min protein-containing systems are not universal. With the numerous morphologies and septation patterns encountered in bacteria, it is not surprising that several other mechanisms have likely evolved to correctly localize septation planes in other microorganisms. For example, some bacteria, including Gram-positive cocci, seem to be devoid of any *min* genes, and their mechanisms of regulating cytokinesis are entirely unknown. Hence, while the Min proteins provide one solution for proper cell division site selection, the rich diversity in bacteria should ensure no shortage in studies that address alternative mechanisms for splitting heirs.

REFERENCES

Addinall, S., Cao, C., and Lutkenhaus, J. (1997). Temperature shift experiments with an *ftsZ*84(Ts) strain reveal rapid dynamics of FtsZ localization and indicate that the Z ring is required throughout septation and cannot reoccupy division sites once constriction has initiated. J.Bacteriol.. *179*, 4277-4284.

Addinall, S., Cao, C., and Lutkenhaus, J. (1997). FtsN, a late recruit to the septum in *Escherichia coli.* Mol. Micro. *25*, 303-309.

Addinall, S.G. and Holland, B. (2002). The tubulin ancestor, FtsZ, draughtsman, designer and driving force for bacterial cytokinesis. J. Mol. Biol. *318*, 219-236.

Arvidson, C.G., Powers, T., Walter, P., and So, M. (1999). *Neisseria gonorrhoeae* PilA is an FtsY homolog. J. Bacteriol. *181*, 731-739.

Aussel, L., Barre, F.X., Aroyo, M., Stasiak, A., Stasiak, A.Z., and Sherratt, D. (2002). FtsK Is a DNA motor protein that activates chromosome dimer resolution by switching the catalytic state of the XerC and XerD recombinases. Cell *108*, 195-205.

Autret, S. and Errington, J. (2003). A role for division-site-selection protein MinD in regulation of internucleoid jumping of Soj (ParA) protein in *Bacillus subtilis*. Mol. Microbiol. *47*, 159-169.

Ayala ,J.A., Garrido, T., de Pedro, M.A., and Vicente, M. (1994). Molecular biology of bacterial septation. In Bacterial Cell Wall, J.M. Ghuysen and R. Hakenbeck, eds. (Amsterdam: Elsevier), pp. 73-102.

Begg, K.J., Spratt, B.G., and Donachie, W.D. (1986). Interaction between membrane proteins PBP3 and rodA is required for normal cell shape and division in *Escherichia coli.* J. Bacteriol. *167*, 1004-1008.

Begg, K.J. and Donachie, W.D. (1998). Division planes alternate in spherical cells of *Escherichia coli.* J. Bacteriol. *180*, 2564-2567.

Ben Yehuda, S., Rudner, D.Z., and Losick, R. (2003). RacA, a bacterial protein that anchors chromosomes to the cell poles. Science *299*, 532-536.

Beveridge, T.J., Popkin, T.J., and Cole, R.M. (1994). Electron Microscopy. In Methods for General and Molecular Microbiology, P. Gerhardt, R.G.E. Murray, W.A. Woods, and N.R. Krieg, eds. (Washington, D.C.: American Society for Microbiology Press), pp. 44-70.

Bi, E. and Lutkenhaus ,J. (1991). FtsZ ring structure associated with division in *Escherichia coli.* Nature *354*, 161-164.

Bignell, C. and Thomas, C.M. (2001). The bacterial ParA-ParB partitioning proteins. J. Biotechnol. *91*, 1-34.

Bovre, K. and Holten, E. (1970). *Neisseria elongata* sp. nov., a rod-shaped member of the genus *Neisseria*. Re-evaluation of cell shape as a criterion in classification. J. Gen. Microbiol. *60*, 67-75.

Bramhill, D. (1997). Bacterial cell division. Annu. Rev. Cell Dev. Biol. 395-424.

Britton, R.A., Lin, D.C., and Grossman, A.D. (1998). Characterization of a prokaryotic SMC protein involved in chromosome partitioning. Genes Dev. *12*, 1254-1259.

Buddelmeijer, N., Judson, N., Boyd, D., Mekalanos ,J.J., and Beckwith, J. (2002). YgbQ, a cell division protein in *Escherichia coli* and *Vibrio cholerae*, localizes in codependent fashion with FtsL to the division site. Proc. Natl. Acad. Sci. USA *99*, 6316-6321.

Carson, M.J., Barondess J., and Beckwith, J. (1991). The FtsQ protein of *Escherichia coli*: membrane topology, abundance, and cell division phenotypes due to overproduction and insertion mutations. J. Bacteriol. *173*, 2187-2195.

Cha, J. and Stewart, G. (1997). The *divIVA* minicell locus of *B.subtilis*. J. Bacteriol. *179*, 1671-1683.

Chen, J.C., Weiss, D.S., Ghigo, J.M., and Beckwith, J. (1999). Septal localization of FtsQ, an essential cell division protein in *Escherichia coli.* J. Bacteriol. *181*, 521-530.

Chen, J.C. and Beckwith, J. (2001). FtsQ, FtsL and FtsI require FtsK, but not FtsN, for co-localization with FtsZ during *Escherichia coli* cell division. Mol. Microbiol. *42*, 395-413.

CLONTECH Laboratories, Inc. (1999). Clontech Yeast Protocols Handbook., BD Biosciences (Palo Alto, CA).

Corbin, B.D., Yu, X.C., and Margolin, W. (2002). Exploring intracellular space: function of the Min system in round- shaped *Escherichia coli.* EMBO J. *21*, 1998-2008.

Cordell, S.C. and Löwe, J. (2001). Crystal structure of the bacterial cell division regulator MinD. FEBS Lett. *492*, 160-165.

Cordell, S.C., Anderson, R.E., and Löwe, J. (2001). Crystal structure of the bacterial cell division inhibitor MinC. EMBO J. *20* , 2454-2461.

Costa C.S. and Anton, D.N. (1999). Conditional lethality of cell shape mutations of *Salmonella typhimurium*: *rodA* and *mre* mutants are lethal on solid but not in liquid medium. Curr. Microbiol. *38*, 137-142.

Dai, K. and Lutkenhaus, J. (1992). The proper ratio of FtsZ to FtsA is required for cell division to occur in *Escherichia coli*. J. Bacteriol. *174*, 6145-6151.

Daniel, R.A., Williams, A.M., and Errington J. (1996). A complex four-gene operon containing essential cell division gene *pbpB* in *Bacillus subtilis*. J. Bacteriol. *178*, 2343-2350.

Davie, E., Sydnor, K., and Rothfield, L.I. (1984). Genetic basis of minicell formation in *Escherichia coli* K-12. J. Bacteriol. *158*, 1202-1203.

de Boer, P., Crossley, R., and Rothfield, L. (1988). Isolation and properties of *minB*, a complex genetic locus involved in correct placement of the division site in *Escherichia coli* . J. Bacteriol. *170*, 2106-2112.

de Boer ,P. and Crossley, R. (1989). A division inhibitor and a topological specificity factor coded for by the minicell locus determine proper placement of the division septum in *Escherichia coli*. Cell *56*, 641-649.

de Boer, P., Crossley, R.E., Hand, A.R., and Rothfield, L. (1991). The MinD protein is a membrane ATPase required for the correct placement of the *Escherichia coli* division site. EMBO J. *10*, 4371-4380.

de Boer, P., Crossley R., and Rothfield, L. (1992). Roles of MinC and MinD in the site-specific septation block mediated by the MinCDE system of *Escherichia coli*. J. Bacteriol. *174* , 63-70.

de Pedro, M.A., Donachie, W.D., Holtje, J.V., and Schwarz, H. (2001). Constitutive septal murein synthesis in *Escherichia coli* with impaired activity of the morphogenetic proteins RodA and penicillin-binding protein 2. J. Bacteriol. *183*, 4115-4126.

Dehio, C., Gray-Owen, S.D., and Meyer, T.F. (2000). Host cell invasion by pathogenic *Neisseriae*. Subcell. Biochem *33*, 61-96.

den Blaauwen, T., Buddelmeijer, N., Aarsman, M.E., Hameete, C.M., and Nanninga, N. (1999). Timing of FtsZ assembly in *Escherichia coli*. J. Bacteriol. *181*, 5167-5175.

Donachie,W. (1993). The cell cycle of *Escherichia coli*. Annu. Rev. Microbiol. 199-230.

Draper, G.C., McLennan, N., Begg, K., Masters, M., and Donachie, W.D. (1998). Only the N-terminal domain of FtsK functions in cell division. J. Bacteriol. *180*, 4621-4627.

Draper, G.C. and Gober, J.W. (2002). Bacterial chromosome segregation. Annu. Rev. Microbiol. *56*, 567-597.

Edwards, D. and Errington, J. (1997). The *Bacillus subtilis* DivIVA protein targets to the division septum and controls the site specificity of cell division. Mol. Microbiol. *25*, 905-915.

El Karoui, M., Errington, J. (2001). Isolation and characterization of topological specificity mutants of *minD* in *Bacillus subtilis*. Mol. Microbiol. *42*, 1211-1221.

Erickson, H.P. (2001). Cytoskeleton. Evolution in bacteria. Nature *413*, 30.

Errington, J. (2001). Septation and chromosome segregation during sporulation in Bacillus subtilis. Curr. Opin. Microbiol. *4*, 660-666.

Errington, J., Daniel, R.A., and Scheffers, D.J. (2003). Cytokinesis in bacteria. Microbiol. Mol. Biol. Rev. *67*, 52-65.

Fernandez, S., de Lorenzo, V., and Perez-Martin, J. (1995). Activation of the transcriptional regulator XylR of *Pseudomonas putid*a by release of repression between functional domains. Mol. Microbiol. *16*, 205-213.

Feucht, A., Lucet ,I., Yudkin, M.D., and Errington, J. (2001). Cytological and biochemical characterization of the FtsA cell division protein of *Bacillus subtilis*. Mol. Microbiol. *40*, 115-125.

Fitz-James, P. (1964). Thin sections of dividing *Neisseria gonorrhoeae*. J. Bacteriol. *87*, 1477-1482.

Fleischmann, R.D., Adams, M.D., White, O., Clayton, R.A., Kirkness, E.F., Kerlavage, A.R., Bult, C.J., Tomb, J.F., Dougherty, B.A., Merrick, J.M., *et al.* (1995). Whole-genome random sequencing and assembly of Haemophilus influenzae Rd. Science *269*, 496-512.

Fox, K.K. and Knapp, J.S. (1999). Antimicrobial resistance in *Neisseria gonorrhoeae*. Curr. Opin. Urol. *9*, 65-70.

Francis, F., Ramirez-Arcos, S., Salimnia, H., Victor, C., and Dillon, J.R. (2000). Organization and transcription of the division cell wall (*dcw*) cluster in *Neisseria gonorrhoeae*. Gene *251*, 141-151.

Fu, X., Shih, Y.-L., Zhang, Y., and Rothfield, L.I. (2001). The MinE ring required for proper placement of the division site is a mobile structure that changes its cellular location during the *Escherichia coli* division cycle. Proc. Natl. Acad. Sci. USA *98*, 980-985.

Fusseneggar, M., Kahrs, A., Facius, D., and Meyer, T. (1996). Tetrapac (*tpc*), a novel genotype of *Neisseria gonorrhoeae* affecting epithelial cell invasion, natural transformation competence and cell separation. Mol. Microbiol. *19*, 1357-1372.

Gerdes, K., Moller-Jensen, J., and Bugge, J.R. (2000). Plasmid and chromosome partitioning: surprises from phylogeny. Mol. Microbiol. *37*, 455-466.

Ghigo, J-M. and Beckwith, J. (2000). Cell division in *Escherichia coli*: role of FtsL domains in septal localization, function, and oligomerization. J.Bacteriol. *182*, 116-129. 2000.

Gill, D.R. and Salmond, G.P. (1987). The *Escherichia coli* cell division proteins FtsY, FtsE and FtsX are inner membrane-associated. Mol. Gen. Genet. *210*, 504-508.

Goffin, C. and Ghuysen, J.M. (1998). Multimodular penicillin-binding proteins: an enigmatic family of orthologs and paralogs. Microbiol. Mol. Biol. Rev. *62*, 1079-1093.

Goodman, S.D. and Scocca, J.J. (1988). Identification and arrangement of the DNA sequences recognized in specific transformation of *Neisseria gonorrhoeae*. Proc. Natl. Acad. Sci. USA *85*, 6982-6986.

Gordon, G.S., Sitnikov, D., Webb, C.D., Teleman, A., Straight, A., Losick, R., Murray, A.W., and Wright, A. (1997). Chromosome and low copy plasmid segregation in *E. coli*: visual evidence for distinct mechanisms. Cell *90*, 1113-1121.

Gordon, G.S. and Wright, A. (2000). DNA segregation in bacteria. Annu. Rev. Microbiol. *54*, 681-708.

Graumann, P.L., Losick, R., and Strunnikov, A.V. (1998). Subcellular localization of *Bacillus subtilis* SMC, a protein involved in chromosome condensation and segregation. J. Bacteriol. *180*, 5749-5755.

Greco, V. 2004. Functional Analysis of the Role of Conserved Glycine Residues and N-terminus Motifs in the Cell Division Inhibitor MinC from *Neisseria gonorrhoeae*. M.Sc. Thesis. Dept. Biochemistry, Microbiology, and Immunology, University of Ottawa.

Gueiros-Filho, F.J. and Losick, R. (2002). A widely conserved bacterial cell division protein that promotes assembly of the tubulin-like protein FtsZ. Genes Dev. *16*, 2544-2556.

Gullbrand, B. and Nordström, K. (2000). FtsZ ring formation without subsequent cell division after replication runout in *Escherichia coli*. Mol. Microbiol. *36*, 1349-1359.

Guzman, L., Barondess, J., and Beckwith, J. (1992). FtsL, an essential cytoplasmic membrane protein involved in cell division in *Escherichia coli*. J. Bacteriol. *174*, 7717-7728.

Hagman, K.E., Pan, W., Spratt, B.G., Balthazar, J.T., Judd, R.C., and Shafer, W.M. (1995). Resistance of *Neisseria gonorrhoeae* to antimicrobial hydrophobic agents is modulated by the *mtrRCDE* efflux system. Microbiology *141 (Pt 3)*, 611-622.

Hale, C. and de Boer, P. (1997). Direct binding of FtsZ to ZipA, an essential component of the septal ring structure that mediates cell division in *E. coli*. Cell *88*, 175-185.

Hale, C. and de Boer, P. (1999). Recruitment of ZipA to the septal ring of *Escherichia coli* is dependent on FtsZ and independent of FtsA. J. Bacteriol. *181*, 167-176.

Hale, C.A., Rhee, A.C., and de Boer, P.A. (2000). ZipA-induced bundling of FtsZ polymers mediated by an interaction between C-terminal domains. J. Bacteriol. *182*, 5153-5166.

Hale, C.A., Meinhardt, H., and de Boer, P.A. (2001). Dynamic localization cycle of the cell division regulator MinE in *Escherichia coli*. EMBO J. *20*, 1563-1572.

Haney, S.A., Glasfeld, E., Hale, C., Keeney, D., He, Z., and de Boer, P. (2001). Genetic analysis of the *Escherichia coli* FtsZ-ZipA interaction in the yeast two-hybrid system. Characterization of FtsZ residues essential for the interactions with ZipA and with FtsA. J. Biol. Chem. *276*, 11980-11987.

Harder, K.W., Owen, P., Wong, L.K., Aebersold, R., Clark-Lewis, I., and Jirik, F.R. (1994). Characterization and kinetic analysis of the intracellular domain of human protein tyrosine phosphatase beta (HPTP beta) using synthetic phosphopeptides. Biochem. J. 298 *(Pt 2)*, 395-401.

Harry, E.J. and Lewis, P.J. (2003). Early targeting of Min proteins to the cell poles in germinated spores of *Bacillus subtilis*: evidence for division apparatus-independent recruitment of Min proteins to the division site. Mol. Microbiol. *47*, 37-48.

Hasan, M.N., Hagedoorn, P.L., and Hagen, W.R. (2002). *Pyrococcus furiosus* ferredoxin is a functional dimer. FEBS Lett. *531*, 335-338.

Hayashi, I., Oyama, T., and Morikawa, K. (2001). Structural and functional studies of MinD ATPase: implications for the molecular recognition of the bacterial cell division apparatus. EMBO J. *20*, 1819-1828.

Hebert, G.A., Pelham, P.L., and Pittman, B. (1973). Determination of the optimal ammonium sulfate concentration for the fractionation of rabbit, sheep, horse, and goat antisera. Appl. Microbiol. *25*, 26-36.

Hendricks, E.C., Szerlong, H., Hill, T., and Kuempel, P. (2000). Cell division, guillotining of dimer chromosomes and SOS induction in resolution mutants (*dif, xerC* and *xerD*) of *Escherichia coli*. Mol. Microbiol. *36*, 973-981.

Henriques, A.O., de Lencastre, H., and Piggot, P.J. (1992). A *Bacillus subtilis* morphogene cluster that includes *spoVE* is homologous to the *mra* region of *Escherichia coli*. Biochimie *74*, 735-748.

Hiraga, S., Ogura, T., Niki, H., Ichinose, C., and Mori, H. (1990). Positioning of replicated chromosomes in *Escherichia coli*. J. Bacteriol. *172*, 31-39.

Holmes, K.K. (1994). Human ecology and behavior and sexually transmitted bacterial infections. Proc. Natl. Acad. Sci. USA *91*, 2448-2455.

Holtje, J. (1998). Growth of the stress-bearing and shape-maintaining murein sacculus of *Escherichia coli*. Microbiol. Mol. Biol. Rev. *62*, 181-203.

Horn, C., Bremer, E., and Schmitt, L. (2003). Nucleotide dependent monomer/dimer equilibrium of OpuAA, the nucleotide-binding protein of the osmotically regulated ABC transporter OpuA from *Bacillus subtilis*. J. Mol. Biol. *334*, 403-419.

Howard, B.J. (1994). *Neisseria*. In Clinical and Pathogenic Microbiology, B.J. Howard, J. Klass, S.J. Rubin, A.S. Weissfeld, and R.C. Tilton, eds. (St. Louis, MO: The C.V. Mosby Company).

Howard, M., Rutenberg, A.D., and de Vet, S. (2001). Dynamic compartmentalization of bacteria: accurate division in *E. coli*. Phys. Rev. Lett. *87*, 278102.

Hu, Z., Mukherjee, A., Pichoff, S., and Lutkenhaus, J. (1999). The MinC component of the division site selection system in *Escherichia coli* interacts with FtsZ to prevent polymerization. Proc. Natl. Acad. Sci. USA *96*, 14819-14824.

Hu, Z. and Lutkenhaus, J. (1999). Topological regulation of cell division in *Escherichia coli* involves rapid pole to pole oscillation of the division inhibitor MinC under the control of MinD and MinE. Mol. Microbiol. *34*, 82-90.

Hu, Z. and Lutkenhaus, J. (2000). Analysis of MinC reveals two independent domains involved in interaction with MinD and FtsZ. J.Bacteriol. 182, 3965-3971.

Hu, Z. and Lutkenhaus, J. (2001). Topological regulation of cell division in *E. coli*: spatiotemporal oscillation of MinD requires stimulation of its ATPase by MinE and phospholipid. Mol. Cell *7*, 1337-1343.

Hu, Z., Gogol, E.P., and Lutkenhaus, J. (2002). Dynamic assembly of MinD on phospholipid vesicles regulated by ATP and MinE. Proc. Natl. Acad. Sci. USA. *99*, 6761-6766.

Hu, Z., Saez, C., and Lutkenhaus, J. (2003). Recruitment of MinC, an inhibitor of Z-Ring formation, to the membrane in *Escherichia coli*: role of MinD and MinE. J. Bacteriol. *185*, 196-203.

Hu, Z. and Lutkenhaus, J. (2003). A conserved sequence at the C-terminus of MinD is required for binding to the membrane and targeting MinC to the septum. Mol. Microbiol. *47*, 345-355.

Huang, J., Cao, C., and Lutkenhaus, J. (1996). Interaction between FtsZ and inhibitors of cell division. J. Bacteriol. *178*, 5080-5085.

Jacob, F., Brenner, S., and Cuzin, F. (1963). On the regulation of DNA replication in bacteria. Cold Spring Harbour Symp Quant. Biol. *23*, 329-348.

Janik, A., Juni, E., and Heym, G.A. (1976). Genetic Transformation as a tool for detection of *Neisseria gonorrhoeae*. J. Clin. Microbiol. *4*, 71-81.

Johnson, J.E., Lackner L.L., and de Boer, P.A. (2002). Targeting of (D)MinC/MinD and (D)MinC/DicB complexes to septal rings in *Escherichia coli* suggests a multistep mechanism for MinC-mediated destruction of nascent FtsZ rings. J. Bacteriol. *184*, 2951-2962.

Johnson, M.L., Correia, J.J., Yphantis, D.A., and Halvorson, H.R. (1981). Analysis of data from the analytical ultracentrifuge by nonlinear least-squares techniques. Biophys. J. *36*, 575-588.

Juni, E. and Heym, G.A. (1977). Simple method for distinguishing gonococcal colony types. J. Clin. Microbiol. *6*, 511-517.

Kellogg Jr., D.S., Peacock Jr., W.L., Deacon, W.E., Brown, L., and Pirkle, D.I. (1963). *Neisseria gonorrhoeae* I. Virulence gentically linked to clonal variation. J. Bacteriol. *85*, 1274-1279.

King, G.F., Rowland, S.L., Pan, B., Mackay, J.P., Mullen, G.P., and Rothfield, L.I. (1999). The dimerization and topological specificity functions of MinE reside in a structurally autonomous C-terminal domain. Mol. Microbiol. *31*, 1161-1169.

King, G.F., Shih, Y.L., Maciejewski, M.W., Bains, N.P., Pan, B., Rowland, S.L., Mullen, G.P., and Rothfield, L.I. (2000). Structural basis for the topological specificity function of MinE. Nat. Struct. Biol. *7*, 1013-1017.

Kline, K.A., Sechman, E.V., Skaar, E.P., and Seifert, H.S. (2003). Recombination, repair and replication in the pathogenic *Neisseriae*: the 3 R's of molecular genetics of two human-specific bacterial pathogens. Mol. Microbiol. *50*, 3-13.

Koch, A.L. (1985). How bacteria grow and divide in spite of internal hydrostatic pressure. Can. J. Microbiol. *31*, 1071-1084.

Koelle, M. Affinity Purification of Antibodies. 1998. http://130.15.90.245/methods/Antibody%20Purification.doc

Koonin, E.V. (1993). A superfamily of ATPases with diverse functions containing either classical or deviant ATP-binding motif. J. Mol. Biol. *229*, 1165-1174.

Koppelman, C.M., Aarsman, M.E., Postmus, J., Pas, E., Muijsers, A.O., Scheffers, D.J., Nanninga, N., den Blaauwen, T. (2004). R174 of *Escherichia coli* FtsZ is involved in membrane interaction and protofilament bundling, and is essential for cell division. Mol. Microbiol. *51*, 645-657.

Koppes, L.J., Woldringh, C.L., and Nanninga, N. (1999). *Escherichia coli* contains a DNA replication compartment in the cell center. Biochimie *81*, 803-810.

Korch, C., Hagblom, P., Ohman, H., Goransson, M., and Normark, S. (1985). Cryptic plasmid of *Neisseria gonorrhoeae*: complete nucleotide sequence and genetic organization. J. Bacteriol. *163*, 430-438.

Kruse, K. (2002). A dynamic model for detemining the middle of *Escherichia coli*. Biophys. J. *82*, 618-627.

Kuempel, P.L., Henson, J.M., Dircks, L., Tecklenburg, M., and Lim, D.F. (1991). *dif*, a *recA*-independent recombination site in the terminus region of the chromosome of *Escherichia coli*. New Biol. *3*, 799-811.

Lackner, L.L., Raskin, D.M., and de Boer, P.A. (2003). ATP-dependent interactions between *Escherichia coli* Min proteins and the phospholipid membrane *in vitro*. J. Bacteriol. *185*, 735-749.

Lara, B. and Ayala, J.A. (2002). Topological characterization of the essential *Escherichia coli* cell division protein FtsW. FEMS Microbiol. Lett. *216*, 23-32.

Laue, T.M., Shah, B.D., Ridgeway, T.M., and Pelletier, S.L. (1991). Computer-aided interpretation of analytical sedimentation data for proteins. In Analytical ultracentirfugation in biochemistry and polymer science, S.E. Harding, A.J. Rowe, and J.C. Horton, eds. (Cambridge, UK: Royal Society of Chemistry), pp. 90-125.

Lee, S. and Price, C.W. (1993). The *minCD* locus of *Bacillus subtilis* lacks the *minE* determinant that provides topological specificity to cell division. Mol. Microbiol. *7*, 601-610.

Lemon, K.P. and Grossman, A.D. (1998). Localization of bacterial DNA polymerase: evidence for a factory model of replication. Science *282*, 1516-1519.

Lemon, K.P. and Grossman, A.D. (2000). Movement of replicating DNA through a stationary replisome. Mol. Cell *6*, 1321-1330.

Lemon, K.P. and Grossman, A.D. (2001). The extrusion-capture model for chromosome partitioning in bacteria. Genes Dev. *15*, 2031-2041.

Levin, P.A., Margolis, P.S., Setlow, P., Losick, R., and Sun, D. (1992). Identification of *Bacillus subtilis* genes for septum placement and shape determination. J. Bacteriol. *174*, 6717-6728.

Levin, P.A., Kurtser, I.G., and Grossman, A.D. (1999). Identification and characterization of a negative regulator of FtsZ ring formation in *Bacillus subtilis*. Proc. Natl. Acad. Sci. USA *96*, 9642-9647.

Lewis, P.J. and Errington, J. (1997). Direct evidence for active segregation of *oriC* regions of the *Bacillus subtilis* chromosome and co-localization with the SpoOJ partitioning protein. Mol. Microbiol. *25*, 945-954.

Lin, Z. and Mallavia, L.P. (1998). Membrane association of active plasmid partitioning protein A in *Escherichia coli*. J. Biol. Chem. *273*, 11302-11312.

Liu, G., Draper, G.C., and Donachie, W.D. (1998). FtsK is a bifunctional protein involved in cell division and chromosome localization in *Escherichia coli*. Mol. Microbiol. *29*, 893-903.

Liu, Z., Mukherjee, A., and Lutkenhaus, J. (1999). Recruitment of ZipA to the division site by interaction with FtsZ. Mol. Microbiol. *31*, 1853-1861.

Löwe, J. and Amos, L. (1998). Crystal structure of the bacterial cell-division protein FtsZ. Nature *391*, 203-206.

Löwe, J. and Amos, L.A. (1999). Tubulin-like protofilaments in Ca2+-induced FtsZ sheets. EMBO J. *18*, 2364-2371.

Lu, C., Stricker, J., and Erickson, H.P. (1998). FtsZ from *Escherichia coli*, *Azotobacter vinelandii*, and *Thermotoga maritima*--quantitation, GTP hydrolysis, and assembly. Cell Motil. Cytoskeleton *40*, 71-86.

Lu, C., Reedy, M., and Erickson, H.P. (2000). Straight and curved conformations of FtsZ are regulated by GTP hydrolysis. J. Bacteriol. *182*, 164-170.

Luirink, J., Hagen-Jongman, C.M., van der Weijden, C.C., Oudega, B., High, S., Dobberstein, B., and Kusters, R. (1994). An alternative protein targeting pathway in *Escherichia coli*: studies on the role of FtsY. EMBO J. *13*, 2289-2296.

Lutkenhaus, J. and Mukherjee, A. (1996). Cell Division. In *Escherchia coli* and *Salmonella* cellular and Molecular Biology, F.C. Neidhardt, R. Curtis III, J.L. Ingraham, E.C.C. Lin, K.B. Low, B. Magasanik, W.S. Reznikoff, M. Riley, M. Schaechter, and H.E. Umbarger, eds. (Washington, D.C.: ASM Press), pp. 1615-1626.

Lutkenhaus, J. and Addinall, S. (1997). Bacterial cell division and the Z ring. Annu. Rev. Biochem. *66*, 93-116.

Lutkenhaus, J. and Sundaramoorthy, M. (2003). MinD and role of the deviant Walker A motif, dimerization and membrane binding in oscillation. Mol. Microbiol. *48*, 295-303.

Ma, L.Y., King, G., and Rothfield, L. (2003). Mapping the MinE site involved in interaction with the MinD division site selection protein of *Escherichia coli*. J. Bacteriol. *185*, 4948-4955.

Ma, X., Ehrhardt, D., and Margolin, W. (1996). Colocalization of cell division proteins FtsZ and FtsA to cytoskeletal structures in living *Escherichia coli* cells by using green fluorescent protein. Proc. Natl. Acad. Sci. USA *93*, 12998-12003.

Maness, M.J. and Sparling, P.F. (1973). Multiple antibiotic resistance due to a single mutation in *Neisseria gonorrhoeae*. J. Infect. Dis. *128*, 321-330.

Margolin, W. (2001a). Spatial regulation of cytokinesis in bacteria. Curr. Opin. Microbiol. *4*, 647-652.

Margolin, W. (2001b). Bacterial cell division: A moving MinE sweeper boggles the MinD. Curr. Biol. *11*, R395-R398.

Margolin, W. (2003). Bacterial division: the fellowship of the ring. Curr. Biol. *13*, R16-R18.

Marinus, M.G. (1973). Location of DNA methylation genes on the *Escherichia coli* K-12 genetic map. Mol. Gen. Genet. *127*, 47-55.

Marston, A., Thomaides, H., Edwards, D., Sharpe, M., and Errington, J. (1998). Polar localization of the MinD protein of *Bacillus subtilis* and its role in selection of the mid-cell division site. Genes and Development *12*, 3419-3430.

Marston, A.L. and Errington, J. (1999a). Dynamic movement of the ParA-like Soj protein of *B. subtilis* and its dual role in nucleoid organization and developmental regulation. Mol. Cell *4*, 673-682.

Marston, A.L. and Errington, J. (1999b). Selection of the midcell division site in *Bacillus subtilis* through MinD-dependent polar localization and activation of MinC. Mol. Microbiol. *33*, 84-96.

Massidda, O., Anderluzzi, D., Friedli, L., and Feger, G. (1998). Unconventional organization of the division and cell wall gene cluster of *Streptococcus pneumoniae*. Microbiology *144 (Pt 11)*, 3069-3078.

Meinhardt, H. and de Boer, P.A. (2001). Pattern formation in *Escherichia coli*: a model for the pole-to-pole oscillations of Min proteins and the localization of the division site. Proc. Natl. Acad. Sci. U. S. A *98*, 14202-14207.

Melby, T.E., Ciampaglio, C.N., Briscoe G., and Erickson, H.P. (1998). The symmetrical structure of structural maintenance of chromosomes (SMC) and MukB proteins: long, antiparallel coiled coils, folded at a flexible hinge. J. Cell Biol. *142*, 1595-1604.

Mengin-Lecreulx, D., Ayala, J., Bouhss, A., Van Heijenhoort, J., Parquet, C., and Hara, H. (1998). Contribution of the P_{mra} promoter to expression of genes in the *Escherichia coli mra* cluster of cell envelope biosynthesis and cell division genes. J. of Bacter. *180*, 4406-4412.

Merz, A.J. and So, M. (2000). Interactions of pathogenic *Neisseriae* with epithelial cell membranes. Annu. Rev. Cell Dev. Biol. *16*, 423-457.

Mileykovskaya, E., Fishov, I., Fu, X., Corbin, B.D., Margolin, W., and Dowhan, W. (2003). Effects of phospholipid composition on MinD-membrane interactions *in vitro* and *in vivo*. J. Biol. Chem. *278*, 22193-22198.

Miroux, B. and Walker, J.E. (1996). Over-production of proteins in *Escherichia coli*: mutant hosts that allow synthesis of some membrane proteins and globular proteins at high levels. J. Mol. Biol. *260*, 289-298.

Morse, S.A., Johnson, S.R., Biddle, J.W., and Roberts, M.C. (1986). High-level tetracycline resistance in *Neisseria gonorrhoeae* is result of acquisition of streptococcal *tetM* determinant. Antimicrob. Agents Chemother. *30*, 664-670.

Mukherjee, A. and Lutkenhaus, J. (1998). Dynamic assembly of FtsZ regulated by GTP hydrolysis. EMBO J. *17*, 462-469.

Mulder, E. and Woldringh, C.L. (1989). Actively replicating nucleoids influence positioning of division sites in *Escherichia coli* filaments forming cells lacking DNA. J. Bacteriol. *8*, 4303-4314.

Nanninga, N. (1998). Morphogenesis of *Escherichia coli*. Microbiol. Mol. Biol. Rev. *62*, 110-129.

Nanninga, N. (2001). Cytokinesis in prokaryotes and eukaryotes: common principles and different solutions. Microbiol. Mol. Biol. Rev. *65*, 319-333.

Niki, H., Jaffe, A., Imamura, R., Ogura, T., and Hiraga, S. (1991). The new gene *mukB* codes for a 177 kd protein with coiled-coil domains involved in chromosome partitioning of *E. coli*. EMBO J. *10*, 183-193.

Niki, H., Imamura, R., Kitaoka, M., Yamanaka, K., Ogura, T., and Hiraga, S. (1992). *E.coli* MukB protein involved in chromosome partition forms a homodimer with a rod-and-hinge structure having DNA binding and ATP/GTP binding activities. EMBO J. *11*, 5101-5109.

Novagen, Inc. (1995). pET System Manual. Novagen, Inc. (Madison, WI).

Ohashi, T., Hale, C.A., de Boer, P.A., and Erickson, H.P. (2002). Structural evidence that the P/Q domain of ZipA is an unstructured, flexible tether between the membrane and the C-terminal FtsZ-binding domain. J. Bacteriol. *184*, 4313-4315.

Pagotto, F.J., Salimnia, H., Totten, P.A., and Dillon, J.R. (2000). Stable shuttle vectors for *Neisseria gonorrhoeae, Haemophilus spp.* and other bacteria based on a single origin of replication. Gene *244*, 13-19.

Perez-Martin, J. and de Lorenzo, V. (1996). *In vitro* activities of an N-terminal truncated form of XylR, a sigma 54-dependent transcriptional activator of *Pseudomonas putida*. J. Mol. Biol. *258*, 575-587.

Picard, F.J. and Dillon, J.R. (1989). Biochemical and genetic studies with arginine and proline auxotrophs of *Neisseria gonorrhoeae*. Can. J. Microbiol. *35*, 1069-1075.

Pichoff, S., Vollrath, B., Touriol, C., and Bouché, J. (1995). Deletion analysis of gene *minE* which encodes the topological specificity factor of cell division in *Escherichia coli*. Mol. Microbiol. *18*, 321-329.

Pichoff, S. and Lutkenhaus, J. (2002). Unique and overlapping roles for ZipA and FtsA in septal ring assembly in Escherichia coli. EMBO J. *21*, 685-693.

Pucci, M.J., Thanassi, J.A., Discotto, L.F., Kessler, R.E., and Dougherty, T.J. (1997). Identification and characterization of cell wall-cell division gene clusters in pathogenic gram-positive cocci. J. Bacteriol. *179*, 5632-5635.

Qiagen (1997). The QIA*expressionist*. (Mississauga, ON: Qiagen Inc.).

Quisel, J.D., Lin, D.C., and Grossman, A.D. (1999). Control of development by altered localization of a transcription factor in *B. subtilis*. Mol. Cell *4*, 665-672.

Raetz, C.R. (1978). Enzymology, genetics, and regulation of membrane phospholipid synthesis in *Escherichia coli*. Microbiol. Rev. *42*, 614-659.

Rahman, M.M., Kolli, V.S., Kahler, C.M., Shih, G., Stephens, D.S., and Carlson, R.W. (2000). The membrane phospholipids of *Neisseria meningitidis* and *Neisseria gonorrhoeae* as characterized by fast atom bombardment mass spectrometry. Microbiology *146 (Pt 8)*, 1901-1911.

Ramirez-Arcos, S., Szeto, J., Beveridge, T.J., Victor, C., Francis, F., and Dillon, J.R. (2001a). Deletion of the cell division inhibitor MinC results in lysis of *Neisseria gonorrhoeae*. Microbiology *147*, 225-237.

Ramirez-Arcos, S., Salimnia, H., Bergevin, I., Paradis, M., and Dillon, J.R. (2001b). Expression of *Neisseria gonorrhoeae* cell division genes *ftsZ, ftsE* and *minD* is influenced by environmental conditions. Res. Microbiol. *152*, 781-791.

Ramirez-Arcos, S., Szeto, J., Dillon, J.R., and Margolin, W. (2002). Conservation of dynamic localization among MinD and MinE orthologues: oscillation of *Neisseria gonorrhoeae* proteins in *Escherichia coli.* Mol. Microbiol. *46*, 493-504.

Ramirez-Arcos, S., Greco, V., Douglas, H., Tessier, D., Fan, D, Szeto, J., Wang, J., and Dillon, J. R. (2004). Conserved glycines in the C-terminus of MinC proteins are implicated in their functionality as a cell division inhibitor. J.Bacteriol. In press.

Raskin, D.M. and de Boer, P.A.J. (1997). The MinE ring: an FtsZ-independent cell structure required for selection of the correct division site in *E.coli.* Cell *91*, 685-694.

Raskin, D.M. and de Boer, P.A.J. (1999a). Rapid pole-to-pole oscillation of a protein required for directing division to the middle of *Escherichia coli.* Proc. Natl. Acad. Sci. USA *96*, 4971-4976.

Raskin, D.M. and de Boer, P.A.J. (1999b). MinDE-dependent pole-to-pole oscillation of division inhibitor MinC in *Escherichia coli.* J. Bacteriol. *181*, 6419-6424.

RayChaudhuri, D. (1999). ZipA is a MAP-Tau homolog and is essential for structural integrity of the cytokinetic FtsZ ring during bacterial cell division. EMBO J. *18*, 2372-2383.

Regamey, A., Harry, E.J., and Wake, R.G. (2000). Mid-cell Z ring assembly in the absence of entry into the elongation phase of the round of replication in bacteria: co-ordinating chromosome replication with cell division. Mol. Microbiol. *38*, 423-434.

Roberts, M., Piot, P., and Falkow, S. (1979). The ecology of gonococcal plasmids. J. Gen. Microbiol. *114*, 491-494.

Roberts, M.C. and Knapp, J.S. (1988). Host range of the conjugative 25.2-megadalton tetracycline resistance plasmid from *Neisseria gonorrhoeae* and related species. Antimicrob. Agents Chemother. *32*, 488-491.

Roe, B.A., Lin, S.P., Song, L., Yuan, X., Clifton, S., Ducey, T., Lewis, L., and Dyer, D.W. (2000). Gonococcal Genome Sequencing Project (Funded by USPHS/ NIH grant # AI 38399). University of Oklahoma.

Rowland, S.L., Fu, X., Sayed, M.A., Zhang, Y., Cook, W.R., and Rothfield, L.I. (2000). Membrane redistribution of the *Escherichia coli* MinD protein induced by MinE. J. Bacteriol. *182*, 613-619.

Sakai, N., Yao, M., Itou, H., Watanabe, N., Yumoto, F., Tanokura, M., and Tanaka, I. (2001). The three-dimensional structure of septum site-determining protein MinD from *Pyrococcus horikoshii* OT3 in complex with Mg-ADP. Structure. (Camb.) *9*, 817-826.

Salimnia, H., Radia, A., Bernatchez, S., and Dillon, J.R. (2000). Characterization of the *ftsZ* cell division gene of *Neisseria gonorrhoeae*: expression and localization in *E. coli* and *N. gonorrhoeae.* Arch. Microbiol. *173*, 10-20.

Sambrook, J., Fritschand, E.F., and Maniatis, T. (1989). Molecular cloning. A laboratory manual., N. Ford, C. Nolan,, and M. Ferguson, eds. (Cold Spring Harbour, New York: Cold Spring Harbour Laboratory Press).

Sanchez, M., Valencia, A., Ferrandiz, M., Sander, C., and Vicente, M. (1994). Correlation between the structure and biochemical activities of FtsA, an essential cell division protein of the actin family. EMBO J. *13*, 4919-4925.

Sarandopoulos, S. and Davies, J.K. (1993). Genetic organization and evolution of the cryptic plasmid of *Neisseria gonorrhoeae*. Plasmid *29*, 206-221.

Schindelin, H., Kisker, C., Schlessman, J.L., Howard, J.B., and Rees, D.C. (1997). Structure of ADP x AIF4(-)-stabilized nitrogenase complex and its implications for signal transduction. Nature *387*, 370-376.

Schlessman, J.L., Woo, D., Joshua-Tor, L., Howard, J.B., and Rees, D.C. (1998). Conformational variability in structures of the nitrogenase iron proteins from *Azotobacter vinelandii* and *Clostridium pasteurianum*. J. Mol. Biol. *280*, 669-685.

Seifert, H.S. and So, M. (1991). Genetic systems in pathogenic *Neisseriae*. Methods Enzymol. *204*, 342-357.

Senff, L.M., Wegener, W.S., Brooks, G.F., Finnerty, W.R., and Makula, R.A. (1976). Phospholipid composition and phospholipase A activity of *Neisseria gonorrhoeae*. J. Bacteriol. *127*, 874-880.

Shafer, W.M., Balthazar, J.T., Hagman, K.E., and Morse, S.A. (1995). Missense mutations that alter the DNA-binding domain of the MtrR protein occur frequently in rectal isolates of *Neisseria gonorrhoeae* that are resistant to faecal lipids. Microbiology *141 (Pt 4)*, 907-911.

Sharp, M.D. and Pogliano, K. (2002a). Role of cell-specific SpoIIIE assembly in polarity of DNA transfer. Science *295*, 137-139.

Sharp, M.D. and Pogliano, K. (2002b). MinCD-dependent regulation of the polarity of SpoIIIE assembly and DNA transfer. EMBO J. *21*, 6267-6274.

Sharpe, M.E. and Errington, J. (1998). A fixed distance for separation of newly replicated copies of oriC in Bacillus subtilis: implications for co-ordination of chromosome segregation and cell division. Mol. Microbiol. *28*, 981-990.

Shi, X.B., Wei, J.M., and Shen, Y.K. (2001). Effects of sequential deletions of residues from the N- or C-terminus on the functions of epsilon subunit of the chloroplast ATP synthase. Biochemistry *40*, 10825-10831.

Shih, Y.L., Fu, X., King, G.F., Le, T., and Rothfield, L. (2002). Division site placement in *E.coli*: mutations that prevent formation of the MinE ring lead to loss of the normal midcell arrest of growth of polar MinD membrane domains. EMBO J. *21*, 3347-3357.

Shih, Y.L., Le, T., and Rothfield, L. (2003). Division site selection in *Escherichia coli* involves dynamic redistribution of Min proteins within coiled structures that extend between the two cell poles. Proc. Natl. Acad. Sci. USA *100*, 7865-7870.

Shingler, V. and Pavel, H. (1995). Direct regulation of the ATPase activity of the transcriptional activator DmpR by aromatic compounds. Mol. Microbiol. *17*, 505-513.

Snyder, L.A., Saunders, N.J., and Shafer, W.M. (2001). A putatively phase variable gene (*dca*) required for natural competence in *Neisseria gonorrhoeae* but not *Neisseria meningitidis* is located within the division cell wall (*dcw*) gene cluster. J. Bacteriol. *183*, 1233-1241.

Snyder, L.A., Shafer, W.M., and Saunders, N.J. (2003). Divergence and transcriptional analysis of the division cell wall (*dcw*) gene cluster in *Neisseria spp*. Mol. Microbiol. *47*, 431-442.

Sparling, P.F., Elkins, C., Wyrick, P.B., and Cohen, M.S. (1994). Vaccines for bacterial sexually transmitted infections: a realistic goal? Proc. Natl. Acad. Sci. USA *91*, 2456-2463.

Stephens, R.S., Kalman, S., Lammel, C., Fan, J., Marathe, R., Aravind, L., Mitchell, W., Olinger, L., Tatusov, R.L., Zhao, Q., Koonin, E.V., and Davis, R.W. (1998). Genome sequence of an obligate intracellular pathogen of humans: *Chlamydia trachomatis*. Science *282*, 754-759.

Stricker, J., Maddox, P., Salmon, E.D., and Erickson, H.P. (2002). Rapid assembly dynamics of the *Escherichia coli* FtsZ-ring demonstrated by fluorescence recovery after photobleaching. Proc. Natl. Acad. Sci. USA *99*, 3171-3175.

Sud, I.J. and Feingold, D.S. (1975). Phospholipids and fatty acids of *Neisseria gonorrhoeae*. J. Bacteriol. *124*, 713-717.

Suefuji, K., Valluzzi, R., and RayChaudhuri, D. (2002). Dynamic assembly of MinD into filament bundles modulated by ATP, phospholipids, and MinE. Proc. Natl. Acad. Sci. USA *99*, 16776-16781.

Sun, Q. and Margolin, W. (1998). FtsZ dynamics during the division cycle of live *Escherichia coli* cells. J. Bacteriol. *180*, 2050-2056.

Sun, Q. and Margolin, W. (2001). Influence of the nucleoid on placement of FtsZ and MinE rings in *Escherichia coli*. J. Bacteriol. *183*, 1413-1422.

Szeto, J., Ramirez-Arcos, S., Raymond, C., Hicks, L.D., Kay, C.M., and Dillon, J.R. (2001a). Gonococcal MinD affects cell division in *Neisseria gonorrhoeae* and *Escherichia coli* and exhibits a novel self-interaction. J. Bacteriol. *183*, 6253-6264.

Szeto, T.H., Rowland, S.L., and King, G.F. (2001b). The dimerization function of MinC resides in a structurally autonomous C-terminal domain. J. Bacteriol. *183*, 6684-6687.

Szeto, T.H., Rowland, S.L., Rothfield, L.I., and King, G.F. (2002). Membrane localization of MinD is mediated by a C-terminal motif that is conserved across eubacteria, archaea, and chloroplasts. Proc. Natl. Acad. Sci. USA *99*, 15693-15698.

Szeto, T.H., Rowland, S.L., Habrukowich, C.L., and King, G.F. (2003). The MinD membrane targeting sequence is a transplantable lipid-binding helix. J. Biol. Chem. *278*, 40050-40056.

Tseng, H.J., McEwan, A.G., Apicella, M.A., and Jennings, M.P. (2003). OxyR acts as a repressor of catalase expression in *Neisseria gonorrhoeae*. Infect. Immun. *71*, 550-556.

Vale, R.D. (1996). Switches, latches, and amplifiers: common themes of G proteins and molecular motors. J. Cell Biol. *135*, 291-302.

van den Ent, F. and Löwe, J. (2000). Crystal structure of the cell division protein FtsA from *Thermotoga maritima*. EMBO J. *19*, 5300-5307.

Varley, A. and Stewart, G. (1992). The *divIVB* region of the *Bacillus subtilis* chromosome encoded homologs of *E.coli* septum placement (MinCD) and Cell shape (MreBCD) determinants. J. Bacteriol. *174*, 6729-6742.

Veal, W.L., Yellen, A., Balthazar, J.T., Pan, W., Spratt, B.G., and Shafer, W.M. (1998). Loss-of-function mutations in the *mtr* efflux system of *Neisseria gonorrhoeae*. Microbiology *144 (Pt 3)*, 621-627.

Vicente, M., Gomez, M., and Ayala, J. (1998). Regulation of transcription of cell division genes in the *Escherichia coli dcw* cluster. Cell. Mol. Life Sci. *54*, 317-324.

Wang, H.C. and Gayda, R.C. (1990). High-level expression of the FtsA protein inhibits cell septation in *Escherichia coli* K-12. J. Bacteriol. *172*, 4736-4740.

Wang, L. and Lutkenhaus, J. (1998). FtsK is an essential cell division protein that is localized to the septum and induced as part of the SOS response. Mol. Microbiol. *29*, 731-740.

Ward, J. and Lutkenhaus, J. (1985). Overproduction of FtsZ induces minicell formation in *E. coli*. Cell *42*, 941-949.

Wasserheit, J.N. (1992). Epidemiological synergy. Interrelationships between human immunodeficiency virus infection and other sexually transmitted diseases. Sex Transm. Dis. *19*, 61-77.

Weaver, K.E. (2000). Enterococcal genetics. In Gram-positive pathogens, V.A. Fischetti, R.P. Novick, J.J. Ferretti, D.A. Portnoy, and J.I. Rood, eds. (Washington, D.C.: ASM Press), pp. 259-271.

Webb, C.D., Teleman, A., Gordon, S., Straight, A., Belmont, A., Lin, D.C., Grossman, A.D., Wright, A., and Losick, R. (1997). Bipolar localization of the replication origin regions of chromosomes in vegetative and sporulating cells of *B. subtilis*. Cell *88*, 667-674.

Webb, C.D., Graumann, P.L., Kahana, J.A., Teleman, A.A., Silver, P.A., and Losick, R. (1998). Use of time-lapse microscopy to visualize rapid movement of the replication origin region of the chromosome during the cell cycle in *Bacillus subtilis*. Mol. Microbiol. *28*, 883-892.

Weiss, D.S., Chen, J.C., Ghigo, J.M., Boyd, D., and Beckwith, J. (1999). Localization of FtsI (PBP3) to the septal ring requires its membrane anchor, the Z ring, FtsA, FtsQ, and FtsL. J. Bacteriol. *181*, 508-520.

West, S.E. and Clark, V.L. (1989). Genetic loci and linkage associations in *Neisseria gonorrhoeae* and *Neisseria meningitidis*. Clin. Microbiol. Rev. *2 Suppl*, S92-103.

Westling-Häggström, B., Elmros, T., Normark, S., and Winblad, B. (1977). Growth pattern and cell division in *Neisseria gonorrhoeae*. J. Bacteriol. *29*, 333-342.

Woldringh, C.L., Mulder, E., Valkenburg ,J.A., Wientjes, F.B., Zaritsky, A., and Nanninga, N. (1990). Role of the nucleoid in the toporegulation of division. Res. Microbiol. *141*, 39-49.

Woldringh, C.L., Mulder, E., Huls, P.G., and Vischer, N. (1991). Toporegulation of bacterial division according to the nucleoid occlusion model. Res. Microbiol. *142*, 309-320.

Woldringh, C.L. (2002). The role of co-transcriptional translation and protein translocation (transertion) in bacterial chromosome segregation. Mol. Microbiol. *45*, 17-29.

Woodbury, R.L., Hardy, S.J., and Randall, L.L. (2002). Complex behavior in solution of homodimeric SecA. Protein Sci. *11*, 875-882.

World Health Organization. (1995). Global Programme on AIDS. An Overview of Selected Curable Sexually Transmitted Diseases.

Yu, X. and Margolin, W. (1999). FtsZ ring clusters in *min* and partition mutants: role of both the Min system and the nucleoid in regulating FtsZ ring localization. Mol. Microbiol. *32*, 315-326.

Yu, X.C., Sun,Q., and Margolin, W. (2001). FtsZ rings in *mukB* mutants with or without the Min system. Biochimie *83*, 125-129.

Zaritsky, A. and Woldringh, C.L. (2003). Localizing cell division in spherical *Escherichia coli* by nucleoid occlusion. FEMS Microbiol. Lett. *226*, 209-214.

Zhao, C., de Boer, P., and Rothfield, L. (1995). Proper placement of the *Escherichia coli* division site requires two functions that are associated with different domains of the MinE protein. Proc. Natl. Acad. Sci. USA *92*, 4313-4317.

Zhou, H. and Lutkenhaus, J. (2003). Membrane binding by MinD involves insertion of hydrophobic residues within the C-terminal amphipathic helix into the bilayer. J. Bacteriol. *185*, 4326-4335.

Zhou, H. and Lutkenhaus, J. (2004). The switch I and II regions of MinD are required for binding and activating MinC. J. Bacteriol. *186*, 1546-1555.

CONTRIBUTION OF COLLABORATORS

The author would like to thank past and present members of the Dillon laboratory for their technical help in various apects of this project. Dr. Sandra Ramirez-Arcos constructed plasmids pSR15, pSR3, pSRBD-C and pSRAD-C and provided much useful insight throughout this study. In addition, Dr. Ramirez-Arcos initiated GFP-localization studies. Nelson Eng provided purified $MinE_{Ng}$ and assisted with ATPase assays and GFP-localization studies. Sudeep Acharya constructed many of the plasmids (designated with pSIA-) used in the studies of the $MinD_{Ng}$ N-terminus while he was under my direct supervision, and contributed to both MinD 'loop' region and N-terminus experiments. Sheila Costford generated the *N. gonorrhoeae* mutant strain SCD-1 and constructed pSC9 and pSC10 plasmids as an Honour's student under my supervision. Claude Raymond constructed the modified gonococcal shuttle vector and all its derivatives, while Mylène Theriault constructed plasmids designated with the pMJ- prefix, with both students under my direct supervision. Hui Li constructed pHLCN and purified soluble $MinC_{Ng}$. Dr. P. Anderson, University of Ottawa, provided access to size-exclusion chromatography equipment and Marc Rigden provided technical assistance with standardizing gel-filtration conditions. Polyclonal mouse anti-$MinE_{Ng}$ antisera was prepared by Dr. J. Webb, University of Ottawa. Peter Rippstein, Ottawa Hospital, Civic Campus, performed immunolocalization studies of $MinD_{Ng}$. He also immunogold labeled $FtsZ_{Ng}$ in gonococcal cells and provided me with access to the electron microscope at the Laboratory Pathology facilities, Ottawa Hospital, to visualize $FtsZ_{Ng}$ localization, as well as to examine *N. gonorrhoeae* SCD-1 morphology. Dr. P. Thibault, Institute of Biological Sciences, National Research Council of Canada, provided MALDI-TOF mass spectrometry analysis of His-$MinD_{Ng}$.

The author would also like to thank collaborators from other universities. Dr. T. Beveridge and Diane Moyles, University of Guelph, performed electron microscopy on *N. gonorrhoeae* strain CJSD1 and control cells. Dr. C. Kay and Leslie Hicks, University of Alberta, performed analytical ultracentrifugation analyses on purified $MinD_{Ng}$. Initial GFP-$MinD_{Ng}$ localization studies were done

in collaboration with Dr. W. Margolin, University of Texas Medical School. Far-UV circular dichroism was conducted by Dr. J. Wang and D. Fan, Southern Illinois University.

APPENDICES: Additional experiments

The following chapter details some studies performed in addition to the main body of work. Each study contains a brief description on its purpose and why they were not investigated further in this project. Results and Discussion are combined for each respective section. Table A.1 describes all plasmids used in the Appendix.

A. INVESTIGATION OF THE $MinD_{Ng}$ C-TERMINUS

Similar to the N-terminal studies performed on $MinD_{Ng}$ (Chapter 7), the C-terminus was also subjected to truncation to determine the effects on protein function and interactions. However, as it was reported that the C-terminus of MinD proteins contains a membrane targeting sequence (Szeto *et al.*, 2002; Hu and Lutkenhaus, 2003), these studies were not pursued further, and experiments were re-directed towards investigating the $MinD_{Ng}$ N-terminus.

MATERIALS AND MATERIALS

Construction of C-terminal truncations to *minD*$_{Ng}$. C-terminal truncations (CT) to *minD*$_{Ng}$ were made to remove the last 21 and 38 amino acids from $MinD_{Ng}$ ($MinD_{Ng\text{-}21aaCT}$ and $MinD_{Ng\text{-}38aaCT}$) to determine the effects on protein functionality . Primers minD10B or minD9B, each encoding a stop codon, were used with primer minD1 (Table 2.2) to amplify truncated *minD*$_{Ng}$ from *N. gonorrhoeae* CH811 (Table 2.1) chromosomal DNA. PCR amplicons were digested with *Eco*RI and *Bam*HI and ligated into similarly digested pUC18 as above to form pMJ4 (*minD*$_{Ng\text{-}21aaCT}$), and pMJ2 (*minD*$_{Ng\text{-}38aaCT}$) (Table A.1). These plasmids, as well as pUC18 (negative control) and pSR3 (positive control; previously constructed in Chapter 4) (Table A.1) were transformed in wild-type *E. coli* PB103 for morphology studies as outlined in Chapters 2 and 4.

Construction of yeast two-hybrid plasmids encoding GAL4 fusions to C-terminal truncated *minD*$_{Ng}$. C-terminal truncated *minD*$_{Ng}$ genes, encoding $MinD_{Ng\text{-}21aaCT}$, $MinD_{Ng\text{-}38aaCT}$, $MinD_{Ng\text{-}83aaCT}$,

Table A.1. Plasmids used in this study

Plasmids	Relevant genotype	Source or reference
Plasmids for expression studies		
pUC18	P_{lac} (Amp^R)	Amersham
pSR3	pUC18; P_{lac}::*minD*$_{Ng}$ (Amp^R)	Chapter 4, this study
pMJ4	pUC18; P_{lac}::*minD*$_{Ng\text{-}21aaCT}$ (Amp^R)	This study
pMJ2	pUC18; P_{lac}::*minD*$_{Ng\text{-}38aaCT}$ (Amp^R)	This study
Yeast two-hybrid plasmids		
pGAD424	P_{ADH1}[a]::*gal4*(AD)[1] (Amp^R)	Clontech
pGBT9	P_{ADH1}::*gal4*(BD)[2] (Amp^R)	Clontech
pGADminD	pGAD424; P_{ADH1}::*gal4*(AD)-*minD*$_{Ng}$ (Amp^R)	Chapter 5, this study
pGBT9minD	pGBT9; P_{ADH1}::*gal4*(BD)-*minD*$_{Ng}$ (Amp^R)	Chapter 5, this study
pGBT9minE	pGBT9; P_{ADH1}::*gal4*(BD)-*minE*$_{Ng}$ (Amp^R)	Chapter 5, this study
pSRBD-C	pGBT9; P_{ADH1}::*gal4*(BD)-*minC*$_{Ec}$ (Amp^R)	Chapter 5, this study
pJminD10	pGAD424; P_{ADH1}::*gal4*(AD)-*minD*$_{Ng\text{-}21aaCT}$[3] (Amp^R)	This study
pJminD11	pGAD424; P_{ADH1}::*gal4*(AD)-*minD*$_{Ng\text{-}38aaCT}$ (Amp^R)	This study
pJminD2	pGAD424; P_{ADH1}::*gal4*(AD)-*minD*$_{Ng\text{-}83aCT}$ (Amp^R)	This study
pJminD1	pGAD424; P_{ADH1}::*gal4*(AD)-*minD*$_{Ng\text{-}237aaCT}$ (Amp^R)	This study
pJminD6	pGBT9; P_{ADH1}::*gal4*(BD)-*minD*$_{Ng\text{-}21aaCT}$ (Amp^R)	This study
pJminD7	pGBT9; P_{ADH1}::*gal4*(BD)-*minD*$_{Ng\text{-}38aaCT}$ (Amp^R)	This study
pJminE5	pGBT9; P_{ADH1}::*gal4*(BD)-*minE*$_{Ng\text{-}5aaNT}$ (Amp^R)	This study
pJminE6	pGBT9; P_{ADH1}::*gal4*(BD)-*minE*$_{Ng\text{-}11aaNT}$ (Amp^R)	This study
pJminE3	pGBT9; P_{ADH1}::*gal4*(BD)-*minE*$_{Ng\text{-}26aaNT}$ (Amp^R)	This study
pJminE4	pGBT9; P_{ADH1}::*gal4*(BD)-*minE*$_{Ng\text{-}54aaNT}$ (Amp^R)	This study
pJminE7	pGBT9; P_{ADH1}::*gal4*(BD)-*minE*$_{Ng\text{-}4aaCT}$ (Amp^R)	This study
pJminE8	pGBT9; P_{ADH1}::*gal4*(BD)-*minE*$_{Ng\text{-}15aaCT}$ (Amp^R)	This study
pJminE2	pGBT9; P_{ADH1}::*gal4*(BD)-*minE*$_{Ng\text{-}30aaCT}$ (Amp^R)	This study
pJminE1	pGBT9; P_{ADH1}::*gal4*(BD)-*minE*$_{Ng\text{-}59aaCT}$ (Amp^R)	This study

[1] GAL4-activation domain
[2] GAL4 DNA-binding domain
[3] CT denotes C-terminal truncation (e.g. 21aaCT = deletion of the 21 amino acids from the C-terminus)

and $MinD_{Ng\text{-}237aaCT}$ were also generated using primer pairs minD1/minD9, minD1/minD10, minD1/minD4, and minD1/minD3 (Table 2.2). Each of these were cloned into the *Eco*RI and *Bam*HI sites of pGAD424 to produce fusions with GAL4-AD encoded on pJminD10 ($MinD_{Ng\text{-}21aaCT}$), pJminD11 ($MinD_{Ng\text{-}38aaCT}$), pJminD2 ($MinD_{Ng\text{-}83aaCT}$), and pJminD1 ($MinD_{Ng\text{-}237aaCT}$) (Table A.1). Similarly, plasmids pJminD6 ($MinD_{Ng\text{-}21aaCT}$) and pJminD7 ($MinD_{Ng\text{-}38aaCT}$) were also constructed, where truncated $MinD_{Ng}$ was in-frame with the GAL4-DNA BD encoded on pGBT9 (Table A.1). Yeast two-hybrid studies were carried out as described in Chapter 2.

RESULTS AND DISCUSSION

To determine whether the C-terminus of $MinD_{Ng}$ is involved in inducing cell division arrest, deletion derivatives of $minD_{Ng}$ were constructed to encode $MinD_{Ng}$ bearing 21 and 38 aa C-terminal deletions (CT). Wild-type *E. coli* PB103 transformed with pMJ4 ($minD_{Ng\text{-}21aaCT}$) and pMJ2 ($minD_{Ng\text{-}38aaCT}$) (Table A.1) retained the characteristic short rod morphology (Figure A.1 C, D) seen with pUC18 negative control transformants (Figure A.1 A). As expected, cells transformed with pSR3, encoding wild-type $MinD_{Ng}$ (Table A.1), were filamentous (Figure A.1 B), indicative of cell division arrest. Western blotting of cell extracts showed the overexpression of wild-type $MinD_{Ng}$ (Figure A.1 E, lane 2) and $MinD_{Ng\text{-}21aaCT}$ (lane 3) in comparison to the background levels of native *E. coli* PB103 MinD (lane 1). Overexpression of $MinD_{Ng\text{-}38aaCT}$ was not observed (Figure A.1 E, lane 4), such that only native *E. coli* MinD was detected in the pMJ2 ($minD_{Ng\text{-}38aaCT}$) transformants.

The yeast two-hybrid system was also employed to determine how deletions from the C-terminus of $MinD_{Ng}$ may affect interactions with other Min proteins. While unable to induce cell division inhibition in *E. coli*, $MinD_{Ng\text{-}21aaCT}$ could still interact with $MinC_{Ec}$ and with $MinE_{Ng}$; however, the apparent strength of interaction with $MinC_{Ec}$ (34.73 ± 3.77 Miller units) was considerably less than wild-type $MinD_{Ng}$ (141.01 ± 4.43 Miller units) (Table A.2). The interaction between $MinD_{Ng\text{-}21aaCT}$ and wild-type $MinD_{Ng}$ was abrogated (Table A.2). Further C-terminal deletions to $MinD_{Ng}$, including $MinD_{Ng\text{-}38aaCT}$, and the more drastic $MinD_{Ng\text{-}83aaCT}$ and $MinD_{Ng\text{-}238aaCT}$, resulted in

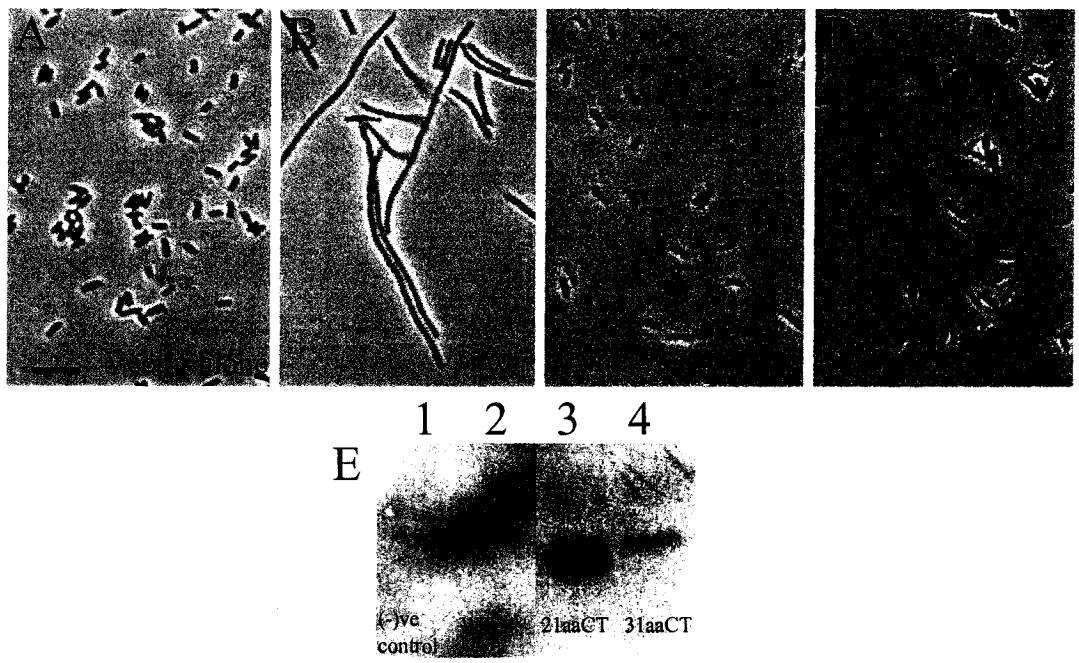

Figure A.1. Expression of C-terminal truncated $MinD_{Ng}$ derivatives in wild-type *E. coli* PB103. (A) Cells containing pUC18 display a short rod morphology. (B) Cells transformed with pSR3 wild-type $minD_{Ng}$are filamentous. Cells transformed with (C) pMJ4 ($minD_{Ng\text{-}21aaCT}$) and (D) pMJ2 ($minD_{Ng\text{-}38aaCT}$) retain short rod morphologies. (E) Western blotting using anti-$MinD_{Ng}$ antisera shows overexpression of wild-type $MinD_{Ng}$ (lane 2) and $MinD_{Ng\text{-}21aaCT}$ (lane 3) in comparison to the background levels of native *E. coli* PB103 MinD (lane 1). Overexpression of $MinD_{Ng\text{-}38aaCT}$ was not observed, and only native *E. coli* MinD was detected in pMJ2 ($minD_{Ng\text{-}38aaCT}$) transformants (lane 4). Scale bar in (A) indicates 10 μm, and all images are at the same magnificaiton.

Table A.2. Yeast two-hybrid assays to determine Min protein interactions with C-terminal deletion derivatives of $MinD_{Ng}$

Fusion to GAL4- AD[1]	Fusion to GAL4-DNA-BD[2]	Intensity of blue colony colour[3]	β-galactosidase Activity (Miller Units)[4]
$MinD_{Ng}$[5]	$MinC_{Ec}$[6]	+++	141.07 ± 4.43
$MinD_{Ng}$	$MinE_{Ng}$	++	8.70 ± 0.05
$MinD_{Ng}$	$MinD_{Ng}$	++	23.14 ± 7.33
$MinD_{Ng\text{-}21aaCT}$[7]	$MinC_{Ec}$	++	34.73 ± 3.77
$MinD_{Ng\text{-}21aaCT}$	$MinE_{Ng}$	++	12.21 ± 0.29
$MinD_{Ng\text{-}21aaCT}$	$MinD_{Ng}$	-	ND[8]
$MinD_{Ng}$	$MinD_{Ng\text{-}21aaCT}$	-	ND
$MinD_{Ng\text{-}38aaCT}$	$MinC_{Ec}$	-	0.04 ± 0.01
$MinD_{Ng\text{-}38aaCT}$	$MinE_{Ng}$	-	0.02 ± 0.01
$MinD_{Ng\text{-}38aaCT}$	$MinD_{Ng}$	-	ND
$MinD_{Ng}$	$MinD_{Ng\text{-}38aaCT}$	-	ND
$MinD_{Ng\text{-}83aaCT}$	$MinC_{Ec}$	-	ND
$MinD_{Ng\text{-}83aaCT}$	$MinE_{Ng}$	-	ND
$MinD_{Ng\text{-}83aaCT}$	$MinD_{Ng}$	-	ND
$MinD_{Ng\text{-}238aaCT}$	$MinC_{Ec}$	-	ND
$MinD_{Ng\text{-}238aaCT}$	$MinE_{Ng}$	-	ND
$MinD_{Ng\text{-}238aaCT}$	$MinD_{Ng}$	-	ND

[1] GAL4-activation domain
[2] GAL4-DNA binding domain
[3] Yeast colony colour intensity corresponding to strength of interaction: (+++) = dark blue; (++) = blue; (+) = faint blue; (-) = white colonies
[4] One unit equals the amount of β-galactosidase which hydrolyzes 1 μmol of ONPG per minute per cell
[5] *N. gonorrhoeae* MinD
[6] *E. coli* MinC
[7] 'CT' indicates C-terminal truncation (e.g. 21aaCT = 21 amino acid truncation from the C-terminus of $MinD_{Ng}$)
[8] 'ND' indicates β-galactosidase activity Not Determined

the loss of interaction with $MinC_{Ec}$, $MinE_{Ng}$, and $MinD_{Ng}$ (Table A.2). These results suggest the last 21 residues from the C-terminus of $MinD_{Ng}$ may play a role in its self-association; however, this region does not appear to be absolutely required for interaction with MinC and MinE.

These studies also indicate that removal of the last 21 residues from $MinD_{Ng}$ abrogates its ability to induce cell division arrest. It has now been demonstrated that the C-terminus of bacterial MinD proteins contains a relatively conserved membrane targeting sequence (MTS) (Szeto *et al.*, 2002; Hu and Lutkenhaus, 2003). Hence, deletion of the last 21 amino acids of $MinD_{Ng}$ will remove its MTS (KSFFKRLF; Figure 3.1, green bar), resulting in its inability to cause cell division arrest upon overexpression in wild-type *E. coli* by virtue of its disrupted membrane association.

Similarly, a 20 amino acid C-terminal deletion to *E. coli* MinD disrupted the ability of $MinD_{Ec}$ to activate MinC-dependent cell division arrest (Hu and Lutkenhaus, 2003). However, this $MinD_{Ec}$ truncation also lost interaction with MinC, and was therefore proposed to be misfolded (Hu and Lutkenhaus, 2003). In contrast, the $MinD_{Ng\text{-}21aaCT}$ derivative used in the present study retained interaction with both $MinC_{Ec}$ and $MinE_{Ng}$, suggesting its inactivity in wild-type *E. coli* was not due to misfolding, but rather to a direct result of MTS removal. Furthermore, since $MinD_{Ng\text{-}21aaCT}$ no longer interacted with wild-type $MinD_{Ng}$, as detected by yeast two-hybrid assays, it suggests that the regions responsible for self-interaction and for interaction with MinC/MinE do not have significant overlap. In addition, the loss of $MinD_{Ng\text{-}21aaCT}$ interaction with wild-type protein suggests that determinants within the C-terminus of $MinD_{Ng}$ may have a role in homodimerization; however, further studies, including a yeast two hybrid assay of $MinD_{Ng\text{-}21aaCT}$- $MinD_{Ng\text{-}21aaCT}$ should be initiated to address this issue.

B. *IN VITRO* $MinD_{Ng}$ LIPID VESICLE BINDING ASSAYS

Several groups have employed *in vitro* studies to investigate MinD membrane association (Hu *et al.*, 2002; Hu *et al.*, 2003; Lackner *et al.*, 2003; Mileyskovskaya *et al.*, 2003). In general, purified MinD proteins are incubated with artificial vesicles composed of phospholipids such as phosphatidycholine (PC), phosphatidylethanolamine (PE), phosphatidylglycerol (PG), cardiolipin (CL), or total *E. coli* membrane phospholipids, with the binding of protein to vesicles monitored by sedimentation assays (Hu *et al.*, 2002; Lackner *et al.*, 2003; Mileykovskaya, 2003). It has been shown that *E. coli* MinD-ATP binds preferentially to anionic phospholipids such as PG and CL (Mileykovskaya *et al.*, 2003), and can be induced to dissociate from lipid vesicles by $MinE_{Ec}$ (Hu *et al.*, 2002).

The following study was initiated to develop an additional *in vitro* functional assay for $MinD_{Ng}$, which would complement the MinD-ATPase stimulation assay developed in Chapter 6. While $MinD_{Ng}$ bound preferentially to PG over PE vesicles, and could be induced to dissociate from PG vesicles by $MinE_{Ng}$, there was also evidence of some non-specific binding. As further work must be done to standardize reaction conditions, these results are presented in the Appendix for future considerations.

MATERIALS AND METHODS

$MinD_{Ng}$ lipid vesicle binding assays. The ability of $MinD_{Ng}$ to bind to phospholipid vesicles was examined using a sedimentation based assay, modified from previous protocols (Hu *et al.*, 2002; Lackner *et al.*, 2003) Purified N- and C-terminal His-tagged $MinD_{Ng}$ proteins, as well as $MinE_{Ng}$, were obtained as outlined in Chapters 5 and 6, respectively.

Zwitterionic *E. coli* L-α-phosphatidylethanolamine (PE) and anionic 1,2-dioleoyl-sn-glycero-3-[phospho-rac-(1-glycerol)] (PG) (Avanti Polar Lipids, Inc.) vesicles were prepared for $MinD_{Ng}$-His vesicle binding studies. For PE vesicle formation, the method of Lackner *et al.* (2003) was modified

as follows. 0.5 ml of stock PE (supplied at 25 mg/ml in chloroform) was dispensed into a borosilicate glass tube and allowed to dry under a gentle stream of filtered air. Dried PE was resuspended in 1.25 ml of reaction buffer (RB; 25 mM Tris-Cl, 50 mM KCl, pH 7.5) to give a final lipid concentration of 10 mg/ml. The solution was incubated at 65°C with frequent vortexing and pipetting using a fine microtip. PE vesicles were prepared fresh prior to each experiment. Anionic PG vesicles were prepared according to the protocol detailed in Chapter 6 Materials and Methods.

Purified His-$MinD_{Ng}$, $MinD_{Ng}$-His, and $MinD_{Ng\text{-}K16Q}$-His were incubated with PG or PE vesicles, ATP, and $MinE_{Ng}$ to determine their associative properties with lipids. Prior to each experiment, protein concentrations were determined using the Bio-Rad protein assay kit and equalized as required by diluting in their respective dialysis buffers. In a typical 50 μl reaction, the following reagents were added in this order (final concentrations in brackets): reaction buffer (RB: reaction buffer, 25 mM Tris-Cl, 50 mM KCl, pH 7.5; volume added depending on other reagents to be included), $MinD_{Ng}$ protein (0.2-0.24 mg/ml), ATP (1mM), lipid vesicles (0.5 mg/ml), and $MgCl_2$ (1mM). Reactions were incubated at room temperature for five minutes and, if required, $MinE_{Ng}$ (0.5 mg/ml final concentration) was then added for an additional five minutes. The reactions were then centrifuged at high speed for one minute to pellet vesicles and any associated proteins. The supernatant was removed and the pellet was resuspended in 50 µl RB. Proteins within the supernatant and pellet fractions were analyzed by SDS-PAGE.

RESULTS AND DISCUSSION

In the presence of ATP, *E. coli* MinD has been shown to associate with artificial vesicles composed of PG, PE, CL, total *E. coli* membrane phospholipids, and various combinations of these components as well (Hu *et al.*, 2002; Lackner *et al.*, 2003; Mileykovskaya *et al.*, 2003). To determine membrane binding capabilities of $MinD_{Ng}$, purified N-terminal His-tagged $MinD_{Ng}$ (His-$MinD_{Ng}$) was incubated in the presence or absence of ATP and artificial vesicles composed of either the zwitterionic phospholipid PE, or the anionic phospholipid PG. Protein-vesicle complexes were subsequently isolated by sedimentation and analyzed by SDS-PAGE, similar to assays performed previously (Lackner *et al.*, 2003). Any $MinD_{Ng}$ protein remaining in the supernatant is presumed not associated with any lipid vesicles.

Prior to their use, the integrity of PE (Figure A.2 A) and PG (Figure A.2 B) vesicles was determined using phase contrast microscopy. Vesicle diameters ranged from ~3-10 μm (Figure A.2 A, B). When incubated with ATP and PE vesicles, the majority of His-$MinD_{Ng}$ was found in the supernatant fraction, indicating little association between $MinD_{Ng}$ and zwitterionic vesicles (Figure A.2 C; lanes 1, 2). However, incubation of His-$MinD_{Ng}$ with PG vesicles and ATP resulted in the majority of protein associated with lipids in the pellet fraction (Figure A.2 D; lanes 1, 2). This indicates that $MinD_{Ng}$ preferentially binds anionic phospholipid vesicles over zwitterionic ones. Even in the absence of ATP, a greater proportion of His-$MinD_{Ng}$ was still associated with PG in the pellet fraction (Figure A.2 D; lanes 5) compared to the supernatant (lane 6). In the absence of vesicles, His-$MinD_{Ng}$ was found almost exclusively in the supernatant fraction (Figure A.2 D; lanes 3, 4).

His-$MinD_{Ng}$ could also be induced to dissociate from PG vesicles by $MinE_{Ng}$. Addition of $MinE_{Ng}$ to a reaction containing His-$MinD_{Ng}$ and PG resulted in a greater proportion of His-$MinD_{Ng}$ appearing in the supernatant fraction (Figure A.2 D; lanes 7, 8) as compared to a similar reaction without $MinE_{Ng}$ (Figure A.2 D; lanes 1, 2).

C-terminal His-tagged $MinD_{Ng}$ ($MinD_{Ng}$-His) was also assayed for vesicle binding. When incubated with PE vesicles and ATP, almost all $MinD_{Ng}$-His was found in the supernatant fraction

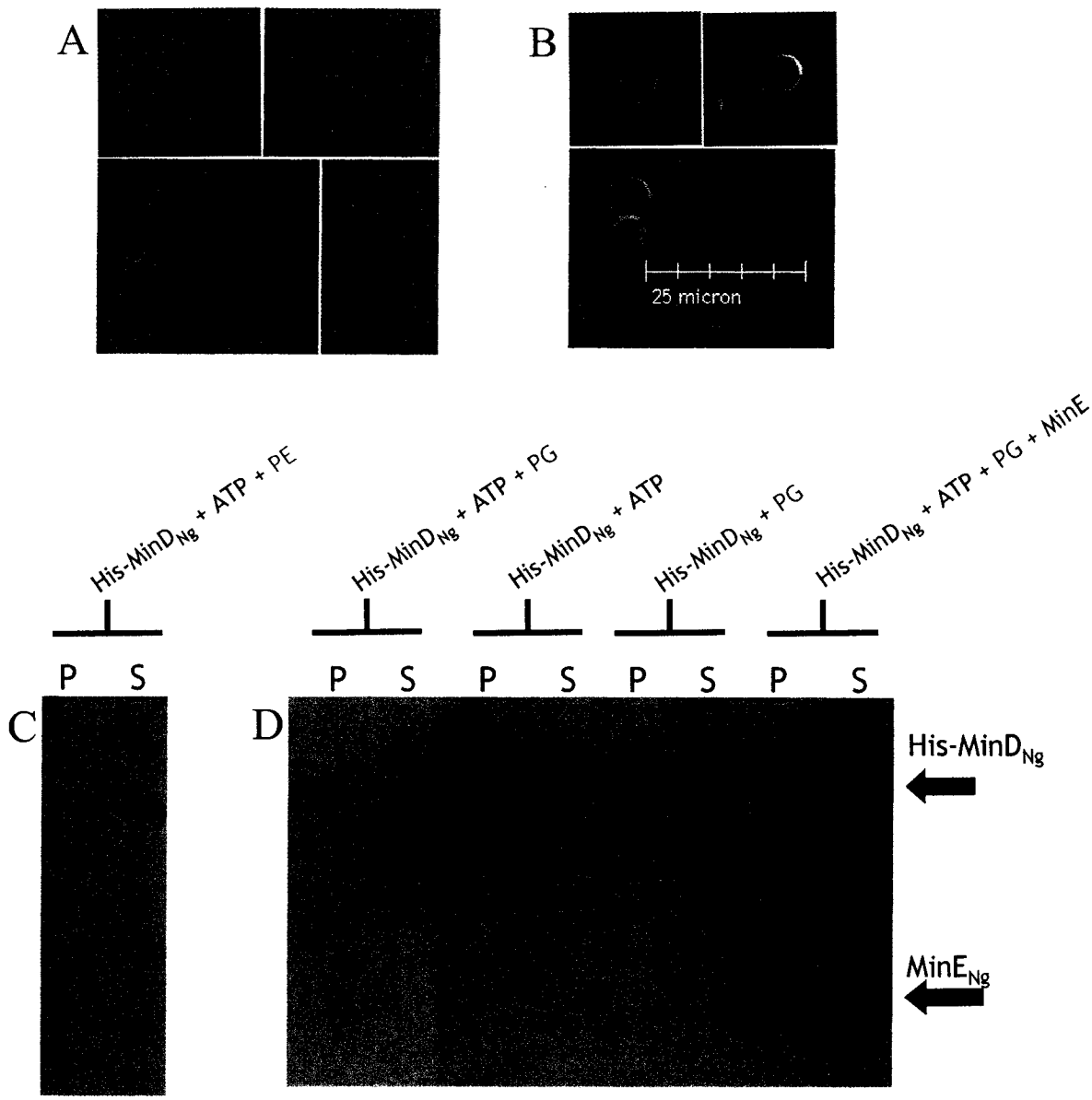

Figure A.2. Vesicle binding studies using N-terminal His-tagged MinD$_{Ng}$ (His-MinD$_{Ng}$). Pellet fractions denoted by 'P' and supernatant fractions denoted by 'S'. (A) Zwitterionic PE vesicles observed under phase contrast microscopy. All panels are at the same magnification (B) Anionic PG vesicles observed under phase contrast microscopy. All panels are at the same magnification. (C) Vesicle sedimentation assay conducted with His-MinD$_{Ng}$, ATP, and PE vesicles. (D) Vesicle sedimentation studies conducted with His-MinD$_{Ng}$ and PG vesicles. Lanes 1,2: ATP and PG included. Lanes 3,4: only ATP included. Lanes 5,6: only PG included. Lanes 7,8: ATP, PG, and MinE$_{Ng}$ included. All reactions carried out in presence of 1 mM $MgCl_2$.

(Figure A.3; lanes 7, 8), indicating a low affinity for zwitterionic phospholipid vesicles. In contrast, $MinD_{Ng}$-His was found in the pellet fraction when incubated with PG vesicles and ATP (Figure A.3; lanes 5, 6). When ATP was omitted, the majority of $MinD_{Ng}$-His was still associated with PG vesicles (Figure A.3; lanes 3, 4), behaving similarly as His-$MinD_{Ng}$ in the absence of ATP (Figure A.2 D; lanes 5, 6). In the absence of PG vesicles, $MinD_{Ng}$-His was found almost entirely in the supernatant fraction (Figure A.3; lanes 1, 2).

As with N-terminal His-tagged $MinD_{Ng}$, $MinD_{Ng}$-His could also be induced by $MinE_{Ng}$ to dissociate from PG vesicles (Figure A.4). This ability was concentration dependent, as increasing $MinE_{Ng}$ concentration resulted in greater amounts of $MinD_{Ng}$-His dislodged from the PG vesicles. As a result, increased $MinD_{Ng}$-His was observed in supernatant fractions (Figure A.4; lanes 2, 4, 6, 8), with corresponding decreases in $MinD_{Ng}$-His levels in pellet fractions (Figure A.4; lanes 1, 3, 5, 7). In contrast, $MinE_{Ng}$ storage buffer could not induce the dissociation of $MinD_{Ng}$-His from PG vesicles. Hence, the ability to remove of $MinD_{Ng}$-His from lipid vesicles is specific to $MinE_{Ng}$.

Surprisingly, the negative control $MinD_{Ng\text{-}K16Q}$-His protein could also associate with PG vesicles in the presence or absence of ATP (Figure A.5; lanes 1, 2 and 5, 6). This result was unexpected, since GFP-$MinD_{Ng\text{-}K16Q}$ was observed to localize to the cytoplasm when expressed in *E. coli* (Chapter 4). Furthermore, studies using purified *E. coli* $MinD_{K16Q}$ and total *E. coli* phospholipid vesicles have indicated a lack of association between the two (Hu *et al.*, 2002). Interestingly, in parallel experiments, the addition of $MinE_{Ng}$ could induce a greater dissociation of $MinD_{Ng\text{-}K16Q}$-His from PG vesicles (Figure A.5; lanes 7, 8) than wild-type $MinD_{Ng}$-His (Figure A.5; lanes 9, 10). While 57% and 43% of wild-type $MinD_{Ng}$-His was distributed in the pellet and supernatant fractions, respectively, $MinD_{Ng\text{-}K16Q}$-His was distributed almost equally in both fractions (49% and 51%).

Overall, these studies show that purified $MinD_{Ng}$ proteins display a preference to bind anionic vesicles over zwitterionic ones. This supports observations using purified *E. coli* MinD, as well as *E. coli* and *B. subtilis* MinD MTS peptides (Szeto *et al.*, 2003; Mileykovskaya *et al.*, 2003). The MTS of MinD is proposed to form an amphipathic helix that lies parallel to the inner cell membrane surface.

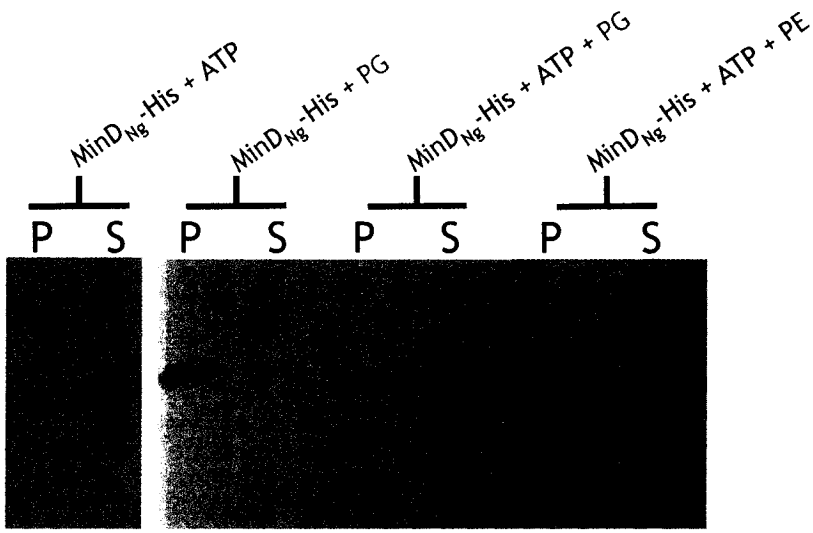

Figure A.3. Vesicle binding studies using C-terminal His-tagged MinD$_{Ng}$ (MinD$_{Ng}$-His). Pellet fractions denoted by 'P' and supernatant fractions denoted by 'S'. Sedimentation studies conducted with MinD$_{Ng}$-His and: ATP (lanes 1, 2); PG (lanes 3, 4); ATP and PG (lanes 5, 6); and ATP with PE (lanes 7, 8). All reactions carried out in presence of 1 mM $MgCl_2$.

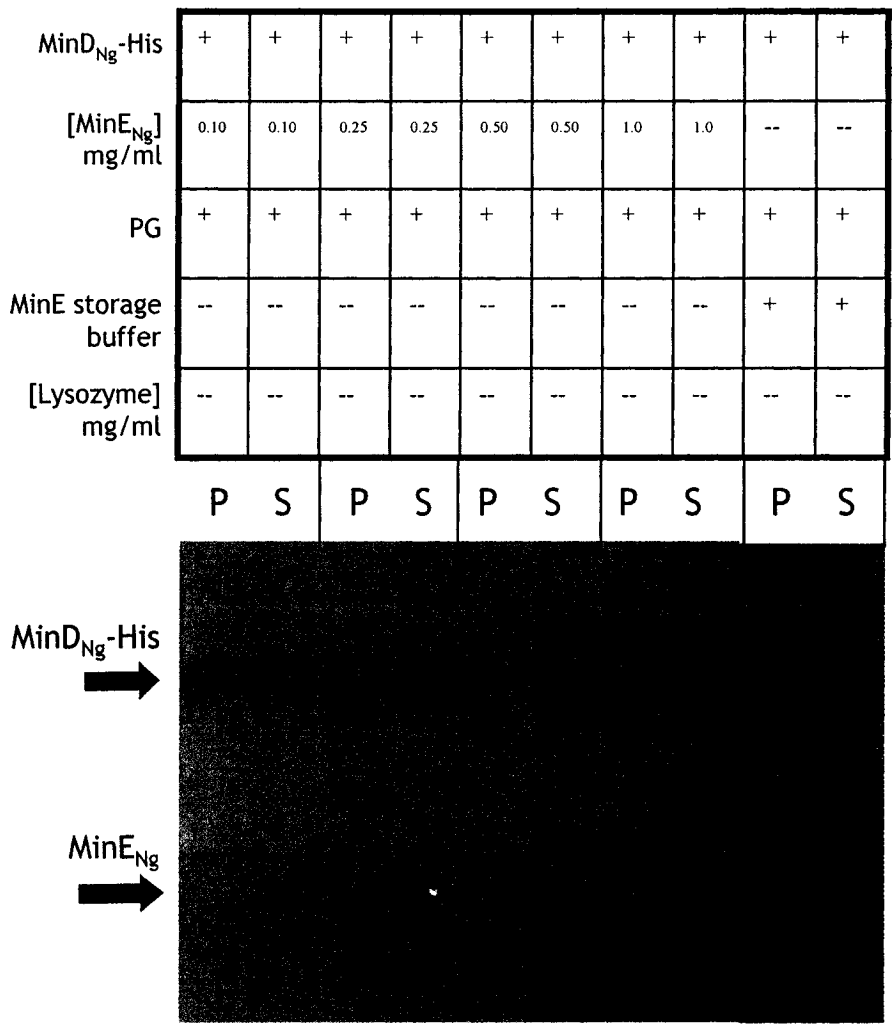

Figure A.4. MinE$_{Ng}$-induced dissociation of MinD$_{Ng}$-His from PG vesicles. Lanes 1-8: MinD$_{Ng}$ bound to PG vesicles was incubated with increasing quantities of MinE$_{Ng}$. Note the corresponding decrease in the amount of MinD$_{Ng}$ found in the pellet fraction (P; lanes 1, 3, 5, and 7) and the increase in MinD$_{Ng}$-His appearing in the supernatant (S; lanes 2, 4, 6, 8). Lanes 9 and 10 show that MinE$_{Ng}$ storage buffer is unable to induce dissociation of MinD$_{Ng}$ from PG vesicles. All reactions carried out in presence of 1 mM $MgCl_2$.

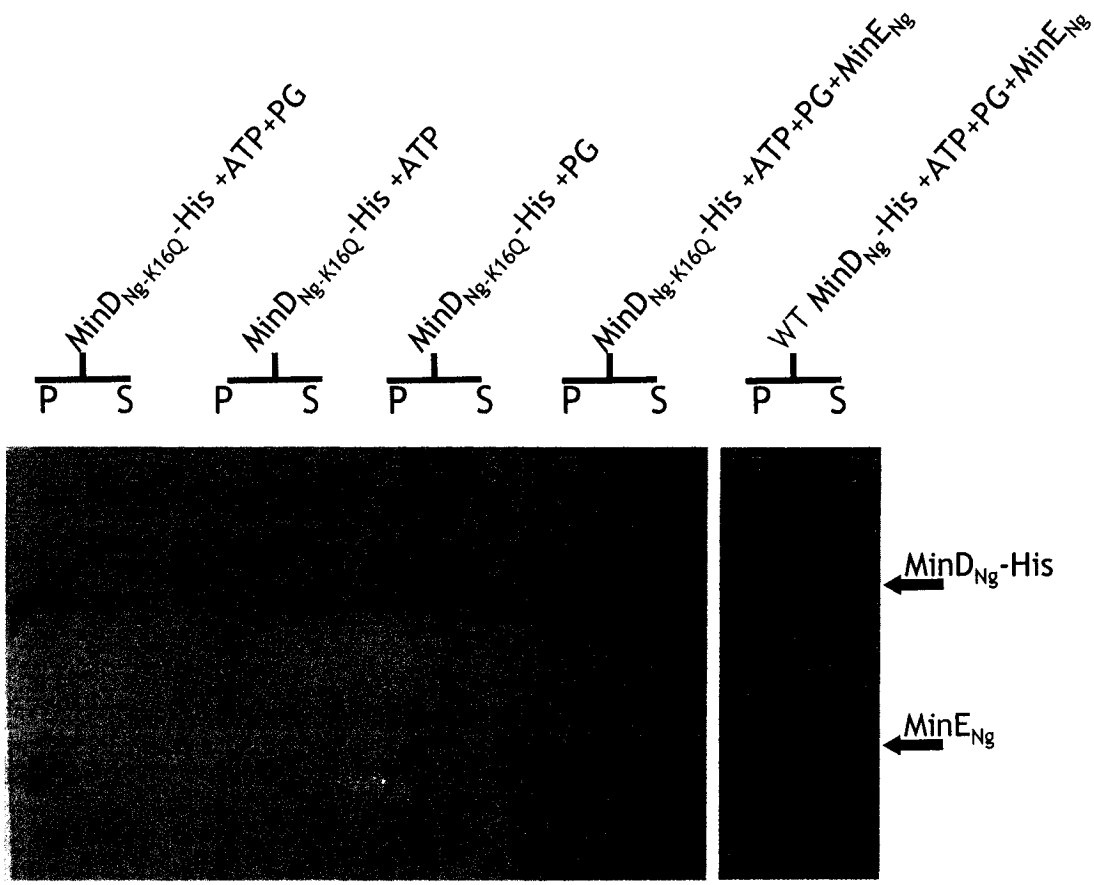

Figure A.5. Vesicle binding studies using MinD$_{Ng-K16Q}$-His and wild-type MinD$_{Ng}$-His. Pellet fractions denoted by 'P' and supernatant fractions denoted by 'S'. Sedimentation studies conducted with MinD$_{Ng-K16Q}$-His and: ATP and PG (lanes 1, 2); ATP only (lanes 3, 4); PG only (lanes 5, 6); and ATP, PG, and MinE$_{Ng}$ (lanes 7, 8). Lanes 9 and 10 are equivalent to lanes 7 and 8, except wild-type MinD$_{Ng}$ was used. All reactions carried out in presence of 1 mM $MgCl_2$.

In doing so, the hydrophobic face of the helix interacts with lipid acyl chains, while the positively charged face interacts with polar lipid headgroups (Szeto *et al.*, 2002). Examination of the $MinD_{Ng}$ MTS (KSFFKRLF) shows that it is very similar to the MTS of $MinD_{Ec}$ (KGFLKRLF) (Figure 3.1, green bar), with both containing positively charged residues that, when arraged in a helix, would be predicted to preferentially interact with negatively charged lipid headgroups (Szeto *et al.*, 2002), such as those found in PG vesicles used in this study.

Why $MinD_{Ng\text{-}K16Q}$-His associates with PG vesicles is unclear. It is possible that the C-terminal His-tag common to both $MinD_{Ng\text{-}K16Q}$-His and $MinD_{Ng}$-His contributed to non-specific binding with anionic phospholipids, resulting in the ATP-*independent* association of each protein to the vesicles. However, it is noted that His-$MinD_{Ng}$, bearing a tag-*free* C-terminus, also associated specifically with PG vesicles in the absence of ATP. Therefore, it is unlikely that a C-terminal 6XHis tag is reponsible for ATP-independent $MinD_{Ng}$ membrane binding.

Gonococcal and *E. coli* cell membranes are not naturally composed of pure PG (each containing approximately 20% PG) (Raetz, 1978; Senff *et al.*, 1976; Sud and Feingold, 1976; Rahman *et al.*, 2000). Hence, it is possible that the excessive concentration of anionic phospholipid may have accounted for some ATP-independent binding of purified $MinD_{Ng}$ and $MinD_{Ng\text{-}K16Q}$ to PG vesicles used in this study. In support of this, studies using vesicles composed of increasing concentrations of another anionic phospholipid, cardiolipin, have also demonstrated a corresponding increase in ATP-independent association of *E. coli* MinD with the vesicles (Mileykovskaya *et al.*, 2003). Further studies using vesicles that better represent the gonococcal cell membrane should be investigated to in order to optimize conditions for $MinD_{Ng}$ vesicle binding assays.

Despite this, it is clear that the PG vesicles made in this study can be used successfully for $MinE_{Ng}$-induced ATPase stimulation assays of $MinD_{Ng}$ (Chapter 6). Wild-type $MinD_{Ng}$ ATPase is stimulated in the presence of these vesicles and $MinE_{Ng}$, similar to *E. coli* MinD (Hu *et al.*, 2002), while the negative control $MinD_{Ng\text{-}K16Q}$ was not (Chapter 6).

C. PRELIMINARY STUDIES ELUCIDATING REGIONS IN $MinE_{Ng}$ RESPONSIBLE FOR INTERACTION WITH $MinD_{Ng}$

$MinE_{Ng}$ has been shown to interact with $MinD_{Ng}$ in this study using the yeast two-hybrid system (Chapter 5) and is required to stimulate GFP-$MinD_{Ng}$ oscillation and its localization within coiled arrays (Chapter 4). A recent study using *E. coli* MinE has implicated specific residues within the N-terminus (aa 1-31) of the protein to be involved in binding to $MinD_{Ec}$ (Ma *et al.*, 2003). These residues are all located along the same face of an α-helix, and are proposed to interact with a corresponding helical region in MinD (King *et al.*, 1999). Mutation of residues from positions 15 to 30 along this particular α-helix face were shown to disrupt $MinE_{Ec}$ interaction with $MinD_{Ec}$ (Ma *et al.*, 2003). To determine what region of $MinE_{Ng}$ binds to $MinD_{Ng}$, N- and C-terminal truncations to $MinE_{Ng}$ were constructed for use in yeast two-hybrid assays.

MATERIALS AND METHODS

Construction of GAL4-BD fusions to $MinE_{Ng}$ N- and C-terminal deletion derivatives. Truncations to $minE_{Ng}$ were made and cloned into the yeast two-hybrid vector pGBT9 (Table A.1) to determine $MinE_{Ng}$ regions (full length of 87 aa) that interact with $MinD_{Ng}$. Deletions to the 5' end of $minE_{Ng}$ were made using primer pairs JSminE7/minE2, JSminE8/minE2, minE5/minE2, and minE6/minE2 (Table 2.2). PCR amplicons were digested with *Eco*RI and *Bam*HI and ligated into similarly digested pGBT9 produced plasmids pJminE5 ($MinE_{Ng\text{-}5aaNT}$), pJminE6 ($MinE_{Ng\text{-}11aaNT}$), pJminE3 ($MinE_{Ng\text{-}26aaNT}$), and pJminE4 ($MinE_{Ng\text{-}54aaNT}$), respectively ('NT' denotes N-terminal truncation) (Table A.1). Deletions to the 3' end of $minE_{Ng}$ were also made using primer pairs minE1/JSminE9, minE1/JSminE10, minE1/minE3, and minE1/minE4 (Table 2.2), and ligated into pGBT9 as above. The resulting plasmids were pJminE7 ($MinE_{Ng\text{-}4aaCT}$), pJminE8 ($MinE_{Ng\text{-}15aaCT}$), pJminE2 ($MinE_{Ng\text{-}30aaCT}$), and pJminE1 ($MinE_{Ng\text{-}59aaCT}$), respectively ('CT' denotes C-terminal truncation) (Table A.1). The integrity of all GAL4 fusions was verified by DNA sequencing.

RESULTS AND DISCUSSION

MinE interacts with MinD to stimulate MinD ATPase activity and intracellular movement (Chapter 4, 5, and 6, this study; Huang *et al.*, 1996; Raskin and de Boer, 1999a; Rowland *et al.*, 2000; Hu and Lutkenhaus, 2001). Preliminary yeast two-hybrid studies were initiated using N- and C-terminal deletion derivatives of $MinE_{Ng}$ in order to begin elucidating potential interacting regions with $MinD_{Ng}$. Severe truncation derivatives to either the N- or the C-terminus of $MinE_{Ng}$ were constructed, and included $MinE_{Ng\text{-}26aaNT}$, $MinE_{Ng\text{-}54aaNT}$, $MinE_{Ng\text{-}30aaCT}$, and $MinE_{Ng\text{-}59aaCT}$. All of these deletions abrogated $MinE_{Ng}$ interaction with $MinD_{Ng}$ (Table A.3). However, less drastic deletions, including removal of the first 5 or 11 N-terminal residues ($MinE_{Ng\text{-}5aaNT}$ and $MinE_{Ng\text{-}11aaNT}$), or the last 4 or 15 residues ($MinE_{Ng\text{-}4aaCT}$ and $MinE_{Ng\text{-}15aaCT}$) of $MinE_{Ng}$ did not eliminate its interaction with $MinD_{Ng}$ (Table A.3).

These studies suggest that residues found at the extreme N- and C-termini of $MinE_{Ng}$ are not implicated in its interaction with $MinD_{Ng}$, and that region(s) involved in binding to $MinD_{Ng}$ are located within residues 12-72 of $MinE_{Ng}$. The N-terminus of *E. coli* MinE (aa 6-35) is predicted to form an α-helix that interacts with $MinD_{Ec}$ (Ma *et al.*, 2003). Since the N-terminus of $MinE_{Ng}$ (aa 1-35) has 31% identity and 57% similarity to that of $MinE_{Ec}$, it is possible that gonococcal MinE also contains a similar N-terminal α-helix. Mutations within residues 15-30 that are proposed to lie along the same face of this helix can disrupt $MinE_{Ec}$ binding to $MinD_{Ec}$. Hence, deletion of the first 11 residues in $MinE_{Ng\text{-}11aaNT}$ would not likely disturb $MinD_{Ng}$ binding, while more severe N-terminal truncations would, as seen in the present study. Comprehensive studies with $MinE_{Ng}$ are currently being conducted by another doctoral student in the Dillon laboratory.

Table A.3. Yeast two-hybrid analysis of the interactions of $MinE_{Ng}$ deletion derivatives with wild-type $MinD_{Ng}$

Fusion to GAL4-BD[1]	Fusion to GAL4-DNA-AD[2]	Intensity of blue colony colour[3]
$MinE_{Ng}$[5]	$MinD_{Ng}$[6]	++
$MinE_{Ng\text{-}5aaNT}$	$MinD_{Ng}$	++
$MinE_{Ng\text{-}11aaNT}$	$MinD_{Ng}$	++
$MinE_{Ng\text{-}26aaNT}$	$MinD_{Ng}$	-
$MinE_{Ng\text{-}54aaNT}$	$MinD_{Ng}$	-
$MinE_{Ng\text{-}4aaCT}$	$MinD_{Ng}$	++
$MinE_{Ng\text{-}15aaCT}$	$MinD_{Ng}$	++
$MinE_{Ng\text{-}30aaCT}$	$MinD_{Ng}$	-
$MinE_{Ng\text{-}59aaCT}$	$MinD_{Ng}$	-

[1] GAL4-DNA binding domain
[2] GAL4-activation domain
[3] Colour intensity corresponding to strength of interaction: (++) denotes blue; (+) denotes light blue; (-) denotes white colonies
[5] *N. gonorrhoeae* MinE
[6] *N. gonorrhoeae* MinD

D. NUCLEOID LOCALIZATION IN DIVIDING *N. gonorrhoeae* CELLS

The nucleoid appears to have a role in toporegulating cell division site placement (Woldringh, 1990). To determine what information can be obtained about the role that the nucleoid may have specifying the alternating division planes in gonococci, DAPI staining was employed to visualize chromosomes in dividing *N. gonorrhoeae*. These experiments are preliminary, but they do indicate that the nucleoids in dividing gonococci are arranged such that they would accommodate the typical division pattern of these cells. However, due to the small size of *N. gonorrhoeae*, microscopy and image collection techniques should be standardized to better elucidate the effects of nucleoid occlusion on gonococcal cell division. Hence, results are presented in the Appendix to provide considerations for future study.

MATERIALS AND METHODS

Nucleoid localization in *N. gonorrhoeae* cells using DAPI staining. To determine the position of the bulk chromosomal mass in dividing *N. gonorrhoeae* CH811 cells (Table 2.1), DAPI (4' 6-diamidino-2-phenylindole-2HCl) (Molecular Probes) staining was used. A log phase culture of *N. gonorrhoeae* CH811 was fixed, adhered to polylysine coated coverslips, and stained with DAPI as outlined in Chapter 7 Materials and Methods. Fluorescence microscopy was performed on an Olympus BX50 fluorescent microscope (Dr. Douglas Franks, Department of Pathology, University of Ottawa) equipped with a CCD Monichron camera and Northern Eclipse software.

RESULTS AND DISCUSSION

In addition to the Min system, the nucleoid itself is proposed to have a role in determining the positioning of bacterial division sites, supposedly by interfering with FtsZ polymerization through nucleoid 'occlusion' (Woldringh, 1990). In *N. gonorrhoeae*, the first round of cell division is initiated by a single invagination point at one side of the cell (Figure 1.7 B), while a second cell division event begins at the junction between two connected daughter cells (Figure 1.7 C). Both of these events involve the localization of FtsZ to the leading edge of cell envelope constrictions (Figure 3.9 A, B, and E).

To determine whether the nucleoid influences the positioning of cytokinetic constrictions in dividing *N. gonorrhoeae*, DAPI staining was employed to localize bulk chromosomal material in these cells. While difficult to draw conclusions regarding the influence of the nucleoid, if any, on gonococcal cell division, fluorescence microscopy did reveal that the general localization of chromosomal material was consistent with the cell division pattern observed in *N. gonorrhoeae.* While individual cocci each presented a single circular DAPI signal (Figure A.6 A), each cell comprising a *diplococcal* arrangement typically exhibited a curved 'C'-shaped chromosomal mass (Figure A.6 B, C). These curved chromosomal masses were distributed such that the junction between two cells was devoid of any DNA material (Figure A.6 C, arrow). This is consistent with leaving the junction free for FtsZ accumulation (as observed in Figure 3.9 E), in preparation for division along a plane that is perpendicular to the first. Some diplococci also displayed evidence of four nucleoid bodies, with each cell containing two DAPI stained chromosomes (Figure A.6 D, arrows). In these instances, the nucleoids were consistently arranged such that they would NOT block the second plane of division (Figure A.6 D', dotted line). Cytokinesis along this second dimension would then result in four cells, each having its own nucleoid.

Overall, these studies show that the nucleoid in *N. gonorrhoeae* is arranged in patterns that are consistent with accomodating the nature of cytokinesis in this organism. Future studies to localize

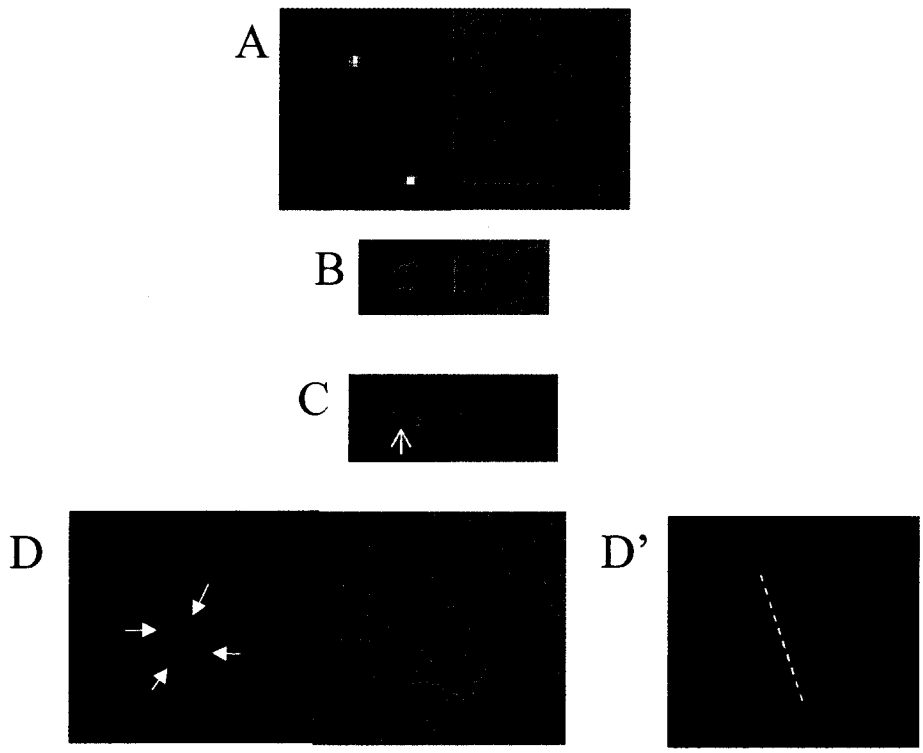

Figure A.6. Localization of DAPI stained nucleoids in wild-type *N. gonorrhoeae* CH811 cells. In all images, fluorescent nucleoids are presented in the left panel, and the corresponding phase contrast image is shown on the right. (A) Individual cocci, each containing a single, circular DAPI fluorescent signal. (B, C) Diplococci contain nucleoids that localize in a crescent shaped arrangement in each cell. Arrow in (C) indicates DNA-free zone in the middle of the junction point between each cell comprising a diplococcus. (D) Diplococcus showing four DAPI-stained chromosomal masses (arrows). Each cell contains two distinct DAPI signals. (D') The arrangement of the four nucleoids in (D) is consistent with allowing cell division to proceed along a plane (dotted line) that is perpendicular to the first. Scale bar in (A) indicates 5 μm, and all images are at the same magnification.

both nucleoid and FtsZ should further enlighten details regarding alternating cell division planes that are characterisitic of *N. gonorrhoeae*.

CURRICULUM VITAE

Education

1999-Present **Ph.D. Microbiology and Immunology**
Department of Biochemistry, Microbiology, and Immunology
University of Ottawa, Ottawa, Ontario
Thesis title- **Splitting heirs: A study of the cell division site determinant MinD from the coccus *Neisseria gonorrhoeae***

1994-1998 **B.Sc.Honours Biology-Biotechnology**
Department of Biology
University of Ottawa, Ottawa, Ontario
Thesis title- **The role of integration host factor binding sites in gonococcal ß-lactamase producing plasmid replication**

Honours and Distinctions

Canadian Association of Gastroenterology (CAG)/Canadian Institutes of Health Research (CIHR)/Solvay Fellowship (2004-2005)

Canadian Institutes of Health Research (CIHR) Doctoral Research Award (2002-2005)

Winner at the 2001 Canadian Society of Microbiologists Student Award Symposium Presentations

Natural Sciences and Engineering Research Council (NSERC) PGS B Award (2000-2002)

University of Ottawa Strategic Areas of Development Award (1999-2000, 2000-2001)

Natural Sciences and Engineering Research Council (NSERC) PGS A Award (1998-2000)

University of Ottawa Undergraduate Summer Research Award (1997)

University of Ottawa Merit Scholarship (1996-1997, 1997-1998)

Canada Scholarship (1994-1998)

University of Ottawa Admission Scholarship (1994)

Professional associations

Canadian Society of Microbiologists
American Society of Microbiology
Canadian Association of Gastroenterology

University activities

09/1999-12/1999 09/2000-12/2000 09/2001-12/2001	Teaching assistant for General Microbiology course Department of Biology, University of Ottawa
10/1998-11/1998	Teaching assistant for Medical Microbiology Laboratory Faculty of Medicine, University of Ottawa
05/1998-08/1998	Research assistant for Dr. Jo-Anne R. Dillon Department of Biochemistry, Microbiology, and Immunology, University of Ottawa
01/1998-04/1998	Teaching assistant for undergraduate Molecular Biology course, Department of Biology, University of Ottawa
05/1997-08/1997	Research assistant for Dr. Linda Bonen Department of Biology, University of Ottawa

Supervision of undergraduate students

09/2002-04/2003	Sudeep Acharya, 4th year undergraduate Honours student Biopharmaceuticals Program, University of Ottawa
09/2001-04/2002	Sheila Costford, 4th year undergraduate Honours student Department of Biochemistry, University of Ottawa
05/2001-08/2001	Mylène Thériault, undergraduate summer student Department of Biology, University of Ottawa
01/2001-04/2001	Yulia Artemenko, undergraduate volunteer student Department of Biochemistry, University of Ottawa
05/2000-08/2000	Claude Raymond, undergraduate summer student Department of Biology, University of Ottawa

Publications in refereed journals

Ramirez-Arcos, S., **J. Szeto**, T.J. Beveridge, C. Victor, F. Francis, and J.R. Dillon. 2001. Deletion of the cell division inhibitor MinC results in lysis of *Neisseria gonorrhoeae*. Microbiology. 147:225-237.

Szeto, J., S. Ramirez-Arcos, C. Raymond, L.D. Hicks, C.M. Kay, and J.R. Dillon. 2001. Gonococcal MinD affects cell division in *Neisseria gonorrhoeae* and *Escherichia coli* and exhibits a novel self-interaction. Journal of Bacteriology. 183: 6253-6264.

Ramirez-Arcos,S., **J. Szeto**, J.R. Dillon, and W. Margolin. 2002. Conservation of dynamic localization among MinD and MinE orthologs: oscillation of *Neisseria gonorrhoeae* proteins in *Escherichia coli*. Molecular Microbiology. 46:493-504.

Ramirez-Arcos, S., V. Greco, H. Douglas, D. Tessier, D. Fan, **J. Szeto**, J.Wang, and J. R. Dillon. Journal of Bacteriology, in press. Control # JB01521-03. Conserved glycines in the C-terminus of MinC proteins are implicated in their functionality as a cell division inhibitor.

Submitted publications

Szeto, J., N.F. Eng, S.Acharya, M.D. Rigden, and J.R.Dillon. A distinct region in the cell division site-determinant MinD is implicated in sensitizing the protein to MinE stimulation. Submitted to Research in Microbiology.

Szeto, J., S.Acharya, N.F. Eng, and J.R.Dillon. The N-terminus of MinD contains determinants which affect its dynamic localization and enzymatic activity. Submitted to Journal of Bacteriology.

Number of manuscripts reviewed at the request of scientific journals: 1

Patent applications

Provisional patent applied for:
"Blocking cell-division as a therapeutic treatment of pathogenic bacteria".

Joint inventors: Dr. Jo-Anne R. Dillon, Dr. Sandra Ramirez-Arcos, Dr. Hossein Salimnia, and Jason Szeto.
Application filed May 26, 2000 in Canada (Ref #08-882835CA) and United States of America (Serial# Ref #08-882757US).

Published conference abstracts

Ramirez-Arcos, S., **J. Szeto**, and J.R. Dillon. 1999. Expression and interaction of the *minCDE* genes of *Neisseria gonorrhoeae*. 99th General Meeting of the American Society of Microbiology. Chicago, Illinois. May 30-June 3, 1999.

Szeto, J., S. Ramirez-Arcos, T. Beveridge, and J.R. Dillon. 2000. MinD from *Neisseria gonorrhoeae* causes aberrant cell division in bacteria. Annual General Meeting of the Canadian Bacterial Diseases Network. Canmore, Alberta. May 6-9, 2000.

Ramirez-Arcos, S., H. Li, **J. Szeto**, T. Beveridge, P. Anderson, P. Thibault, A. Ridsdale, and J.R. Dillon. 2000. Cell division inhibitor MinC: a new candidate as an alternative target to treat bacterial infectious diseases. Annual General Meeting of the Canadian Bacterial Diseases Network. Canmore, Alberta. May 6-9, 2000.

Szeto, J., S. Ramirez-Arcos, H. Li, and J.R. Dillon. 2000. MinD is implicated in maintaining proper cell division in Gram negative cocci. 12th International Pathogenic Neisseria conference. Galveston, Texas. November 12-17, 2000.

Ramirez-Arcos, **J. Szeto**, T.J. Beveridge, A. Ridsdale, and J.R. Dillon. 2000. Overexpression or deletion of the cell division inhibitor MinC from *Neisseria gonorrhoeae* causes Gram negative cocci to lyse. 12th International Pathogenic Neisseria conference. Galveston, Texas. November 12-17, 2000.

Szeto, J., S.R.M. Costford, S. Ramirez-Arcos, W. Margolin, and J.R. Dillon. 2002. Motifs in gonococcal MinD essential for structure and function. American Society of Microbiology Conference on Prokaryotic Development. Quebec City, Quebec. July 10-14, 2002.

Conference oral presentations

Szeto, J., S. Ramirez-Arcos, L. Hicks, C.M. Kay, and J.R. Dillon. 2001. Choosing division planes in cocci: A split decision. MinD is involved in proper gonococcal cell division and exhibits self-interaction. 51st Annual Meeting of the Canadian Society of Microbiologists. Winner at Student Award Symposium. Waterloo, Ontario. June 10-13, 2001.